Technische Universität München

Max-Planck-Institut für extraterrestrische Physik

Optical Novae as Supersoft X-ray Sources in the Andromeda Galaxy

Martin Henze

Vollständiger Abdruck der von der Fakultät für Physik der Technischen Universität München zur Erlangung des akademischen Grades eines

Doktors der Naturwissenschaften

genehmigten Dissertation.

Vorsitzender: Univ.-Prof. Dr. A. Ibarra
Prüfer der Dissertation:
1. Hon.-Prof. Dr. G. Hasinger
2. Univ.-Prof. Dr. L. Oberauer

Die Dissertation wurde am 15.12.2010 bei der Technischen Universität München eingereicht und durch die Fakultät für Physik am 17.02.2011 angenommen.

TECHNISCHE UNIVERSITÄT MÜNCHEN

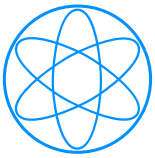

Optical Novae as Supersoft X-ray Sources in the Andromeda Galaxy

Dissertation von
Martin Henze
15. Dezember 2010

MAX-PLANCK-GESELLSCHAFT

MAX-PLANCK-INSTITUT
FÜR
EXTRATERRESTRISCHE PHYSIK

Optical Novae as Supersoft X-ray Sources in the Andromeda Galaxy

Optical novae are a subclass of variable stars that display a strong, eruptive increase in their optical luminosity and are sometimes observed as supersoft X-ray sources (SSSs). The physical process responsible for this behaviour is a thermonuclear runaway in an accreted hydrogen envelope on top of a white dwarf in a cataclysmic binary system. This dissertation describes the results from the first dedicated monitoring campaigns for SSS states of optical novae in the central region of the Andromeda galaxy (M 31) with the X-ray telescopes XMM-Newton and *Chandra* . I present the first analysis of the X-ray properties of the nova population in M 31 based on a statistically significant sample. Peculiar objects from this sample are discussed in detail.

Optische Novae als superweiche Röntgenquellen in der Andromedagalaxie

Bei optischen Novae handelt es sich um variable Sterne, deren Helligkeit im Optischen während eines singulären Ausbruchs stark zunimmt und die teilweise auch als Röntgenquellen mit extrem weichem Spektrum beobachtet werden. Die physikalische Ursache für dieses Verhalten ist eine thermonukleare Explosion auf der Oberfläche eines Weißen Zwergs in einem engen Doppelsternsystem. Meine Dissertation beschreibt Beobachtungen der Andromeda-Galaxie (M 31) mit den Röntgenteleskopen XMM-Newton und *Chandra* , die erstmals speziell auf die Entdeckung von Novae in Röntgenbereich ausgelegt waren. Das Ziel meiner Arbeit war die erste Untersuchung der Röntgeneigenschaften der Nova-Population in M 31 auf Basis einer statistisch signifikanten Stichprobe. Diese Dissertation stellt die Ergebnisse der Populationsstudie vor und geht näher auf ungewöhnliche Einzelquellen ein.

Contents

Chapter 1

Introduction

1.1 Classical Novae

Classical novae (CNe) originate from thermonuclear explosions on the surface of white dwarfs (WDs) in cataclysmic binary systems. This section describes the physics of the nova phenomenon, its optical and X-ray properties, and highlights the special role of the Andromeda galaxy (M 31) in nova research.

1.1.1 Physics of Classical Novae

The host systems of CNe constitute a subclass of cataclysmic variables (CVs), which are close interacting binary star systems (Bode & Evans 2008). The primary component in a CV is a WD. WDs are the final evolutionary stages of stars with initial masses of $\lesssim 8..10\ M_{\odot}$ (see e.g. Truran & Livio 1986, and references therein). The secondary component is typically a main-sequence star or a red giant star, which fills its gravitational Roche-lobe (Bode & Evans 2008). This leads to the transfer of matter from the secondary to the WD. If the magnetic field of the WD is not strong, in contrast to AM Her or polar systems, this matter forms an accretion disk around the WD due to conservation of angular momentum. Friction induced energy loss in the accretion disk then causes the matter to settle on the WD's surface. These processes cause the luminosity of the CV to vary significantly. The variability manifests itself in different observational characteristics for different subtypes of CVs, dependent on the masses and separation of the binary stars and the magnetic field of the WD (see Warner 1995, for an extensive review on CVs).

In the case of CNe, the transferred hydrogen-rich matter eventually accumulates on the surface of the WD until hydrogen ignition starts a thermonuclear runaway in the degenerate matter of the WD envelope. The resulting expansion of the hot envelope (see Fig. 1.1) causes the optical brightness of the WD to rise by ~ 12 magnitudes within a few days, and mass to be ejected at high velocities (see Hernanz 2005; Warner 1995, and references therein).

1.1.2 Optical properties and classification

Novae stand out among the plethora of variable star types due to distinctive observational characteristics, although it should be noted that no two novae show exactly the same properties (Bode & Evans 2008).

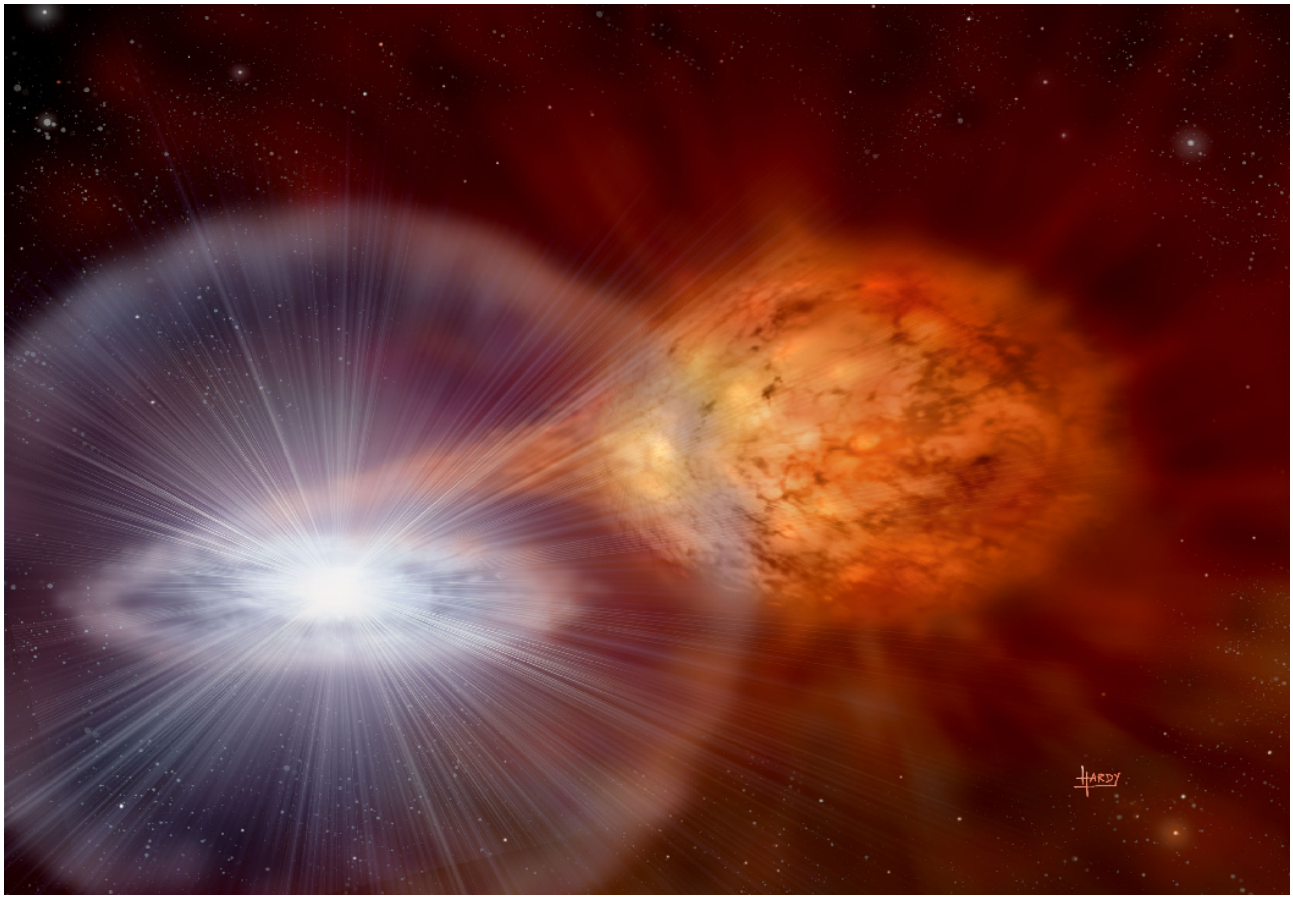

Figure 1.1: Artist's impression of a nova occurring on a WD (left) in a close binary system (Credits: Mark A. Garlick, http://www.space-art.co.uk).

The *light curve* of a star describes the evolution of its luminosity over time. Optical light curves of CNe reflect the singular nature of the explosive outburst by showing a rapid rise of the star's luminosity to the maximum within days. This is followed by a slower decline on time scales of weeks to years back to the pre-outburst luminosity. A schematic nova light curve is shown in Fig. 1.2. Observed nova light curves from the optical monitoring of M 31 are given in Appendix C.

Based on the speed of the optical decline, light curves of CNe can be categorised into *speed classes*, according to the scheme of Payne-Gaposchkin (1964). More precisely, measuring the time the nova luminosity needs to decline by two magnitudes from maximum light, the so-called t_2 *time*, allows the classification the nova as very fast ($t_2 < 10$ days), fast (11 – 25), moderately fast (26 – 80), slow (81 – 150), or very slow (151 – 250) (Bode & Evans 2008).

Recently, Strope et al. (2010) introduced a new classification system for nova light curves based on a catalogue of 93 light curves of Galactic novae. This system utilises the shape of the light curve to distinguish seven basic classes, the prototypes of which are shown in Fig. 1.3 (figure 2 from Strope et al. 2010). In the context of this classification scheme a further specification of the light curve can be given using its t_3 *time*, which is defined in a similar way as the t_2 time described above.

While an optical light curve with outburst-like features already gives hints of the underlying nova phenomenon, an optical *spectrum* allows to classify a nova candidate as a CN. The strongest emission lines in nova spectra are Balmer lines of hydrogen (Williams 1992). Indeed, surveys for novae have made use of the fact that novae are bright sources in observations taken with Hα filter, where they are

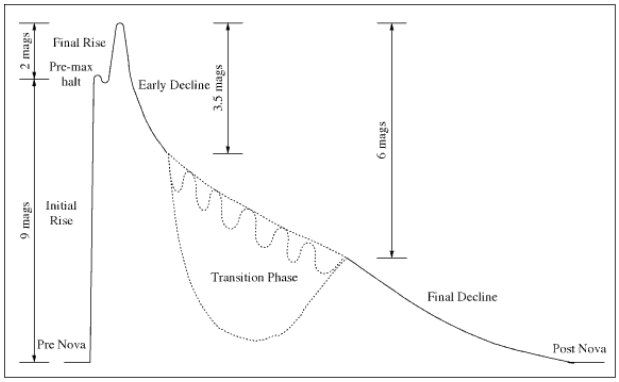

Figure 1.2: Schematic nova light curve, taken from Bode & Evans (2008). Displayed is the evolution of the optical magnitude of the nova (ordinate) over the time (abscissa).

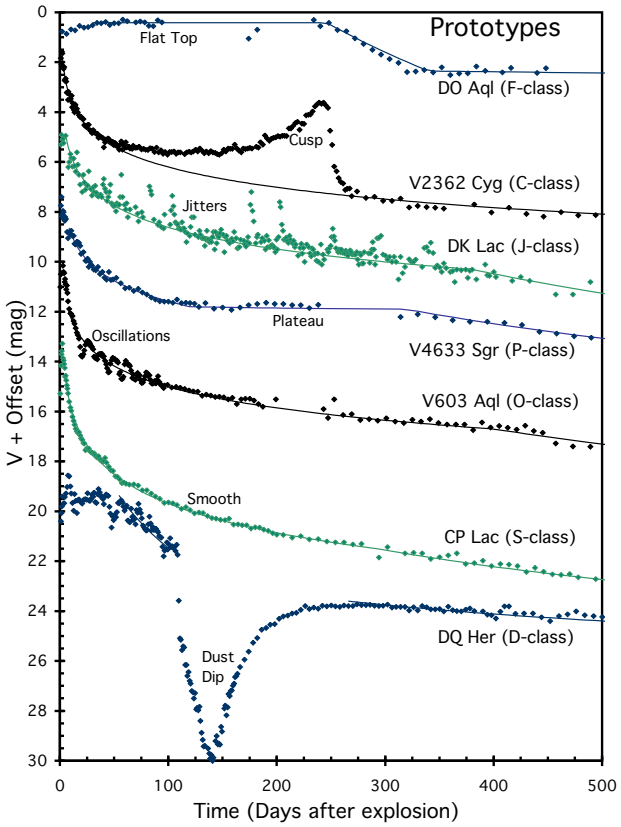

Figure 1.3: Nova light curve classes from Strope et al. (2010).

also visible for a longer time than in broad band observations, since the pioneering work of Ciardullo et al. (1987) on M 31 novae. The detection of a nova candidate in photometric Hα observations can be used as a criterion to confirm this candidate as a nova (see e.g. Henze et al. 2008i). Measuring the broadening of the Balmer lines, in particular the strong Hα line, further allows us to estimate the *expansion velocity* of the nova ejected envelope.

The strongest non-Balmer emission lines vary from nova to nova. Williams (1992) developed a classification scheme that distinguishes two main types of CNe. Novae with prominent Fe II lines in the optical spectrum (*Fe II novae*) evolve more slowly with lower expansion velocities and lower levels of ionisation. On the other hand, novae with stronger lines of He and N (*He/N novae*) have large expansion velocities and a rapid spectral evolution. There are a few novae that do not fit into one of the two classes. These *hybrid novae* evolve from a Fe II-type to a He/N-type spectrum or show the features of both classes simultaneously (Williams 1992).

1.1.3 X-ray properties - classical novae as supersoft X-ray sources

After the optical nova outburst, a fraction of the hot envelope can remain in steady hydrogen burning on the surface of the WD (Starrfield et al. 1974; Sala & Hernanz 2005). This powers a supersoft X-ray source (SSS) that can be observed directly, once the ejected envelope becomes sufficiently transparent (Starrfield 1989; Krautter 2002). The term *turn on of the SSS* is defined in this work from an observational point of view as the time when the SSS becomes visible to us, due to the decreasing

opacity of the ejected material. This is not the same as the actual turn on of the stable H-burning on the WD surface shortly after the explosion. The *turn-off of the SSS*, on the other hand, does not suffer from extinction effects and clearly marks the actual turn-off of the H-burning in the WD envelope and the disappearance of the SSS.

The class of SSSs was first characterised on the basis of ROSAT observations (Trümper et al. 1991; Greiner et al. 1991). These sources show extremely soft X-ray spectra with little or no emission at energies above 1 keV, that can be described by equivalent blackbody temperatures of ∼15-80 eV (see Kahabka & van den Heuvel 1997, and references therein). The standard model to explain the SSS characteristics involves a hydrogen-burning WD which is powered by accretion (van den Heuvel et al. 1992). Steady hydrogen burning occurs for mass-accretion rates of $\sim 10^{-7}\ M_{\odot}\ \mathrm{yr}^{-1}$ (canonical SSS), whereas for lower accretion rates unstable hydrogen shell flashes trigger nova outbursts (for a recent review see Kato 2010).

It is well known that blackbody fits to SSS spectra are *not* the physically correct model for a WD atmosphere. These fits produce in general too high values of N_{H} and too low temperatures, resulting in overestimated luminosities (see e.g. Greiner et al. 1991; Kahabka & van den Heuvel 1997, and references therein). A more realistic approach would be to use stellar atmosphere models that assume non-local thermodynamic equilibrium (NLTE) (see e.g. van Rossum & Ness 2010, and references therein). These models are still in development. They have been tested on bright Galactic CNe with promising results for static atmospheres (see e.g. Nelson et al. 2008b) and expanding atmospheres (see e.g. Petz et al. 2005). Detailed WD atmosphere models are needed to interpret high spectral resolution observations (taken e.g. with X-ray grating spectrometers). However, these models involve a large number of parameters for a physically realistic description of post-nova atmospheres. To adjust these parameters, high-quality X-ray spectra (with high photon statistic and energy resolution) are essential. For Galactic novae such data are achievable using the grating spectrometers on board XMM-Newton and *Chandra*. Supersoft X-ray sources in M 31 (distance 780 kpc; Holland 1998; Stanek & Garnavich 1998) are not bright enough to be observed with X-ray grating spectrometers. Furthermore, in the M 31 central region the source density is too high and the diffuse emission too strong to successfully apply grating spectroscopy for individual sources with the currently available instruments. Due to the low resolution and relatively low signal-to-noise ratio of the XMM-Newton EPIC PN spectra analysed in this work, I decided to apply blackbody fits. In this way, I use the blackbody temperature as a first order parametrisation of the spectrum and can directly compare my results with the earlier works of Pietsch et al. (2005a, hereafter PFF2005) and Pietsch et al. (2007g, hereafter PHS2007), who used the same method, while keeping in mind the biases outlined above.

The duration of the SSS phase in CNe is related to the mass of accreted H-rich matter that is *not* ejected in the nova outburst and on the mass of the WD. More massive WDs have a stronger surface gravity. Theoretical models predict that they need less accreted matter to initiate the thermonuclear runaway (José & Hernanz 1998) and that they eject a smaller fraction of the accreted matter during the nova outburst (Yaron et al. 2005) compared to less massive WDs. Indeed, observations have found less massive ($\sim 2{\times}10^{-5}\ M_{\odot}$) ejecta associated with the brightest, very fast declining novae. For slow novae the mass of the ejecta is about 10 times larger (Della Valle et al. 2002). In general, more massive WDs reach higher luminosities (Yaron et al. 2005) and retain less mass after the explosion, although this also depends on the accretion rate. Thus, the duration of the SSS state is inversely related to the mass of the WD, for a given hydrogen-mass fraction in the remaining envelope. On the other hand, the larger the hydrogen content, the longer the duration of the SSS state for a given WD mass (see Tuchman & Truran 1998; Sala & Hernanz 2005; Hachisu & Kato 2006).

In turn, the transparency requirement mentioned above implies that the turn-on time is determined

by the fraction of mass ejected in the outburst. X-ray observations therefore provide important clues to the physics of the nova outburst and might help to answer the key question of whether a WD accumulates matter over time to become a potential progenitor for a type Ia supernova (SN-Ia). The duration of the SSS state provides the only direct indicator of the post-outburst envelope mass in CNe. For massive WDs, the expected SSS duration is very short (< 100 d) (Tuchman & Truran 1998; Sala & Hernanz 2005). Several novae with short SSS states have been found in this work (see Chap. 4).

1.1.4 Recurrent novae

Recurrent novae (RNe) are classified by being observed to have had more than one recorded nova outburst. These objects are very good candidates for SN-Ia progenitors in the single degenerate scenario, in which a carbon-oxygen (CO) WD accretes matter from a non-degenerate companion (Whelan & Iben 1973; Nomoto 1982), as RNe are believed to contain WDs with masses close to the Chandrasekhar limit ($\sim$ 1.4 $M_{\odot}$). Alternatively, two WDs that merge can cause a SN-Ia if one of them is a CO WD (= double degenerate scenario; Webbink 1984; Iben & Tutukov 1984). However, because nova outbursts occur on accreting WDs, only the single degenerate scenario is important in the context of this work. Optical surveys show that RNe are rare relative to the observed SN-Ia rate (Della Valle & Livio 1996). The missing RNe might be explained by gaps in optical surveys. In this way, a fraction of RNe would only have been classified as CNe. Interesting cases are CNe with very short SSS phases because they indicate a high WD mass. These objects are potentially capable of frequent outbursts as in RNe.

One of the best studied Galactic RNe is RS Oph, which underwent its last outburst in 2006 (Nelson et al. 2008b; Ness et al. 2007b). X-ray observations documented a rapid decline in supersoft emission at $\sim$ 90 days after the optical outburst and a duration of the SSS phase of $\sim$ 60 days (Osborne et al. 2006a; Hachisu et al. 2007). From theoretical models, Hachisu et al. (2007) estimated a WD mass of $(1.35 \pm 0.01)M_{\odot}$.

I discuss the X-ray properties of two apparent RNe in M 31 in Chap. 6.2.1.

1.1.5 Novae in M 31

Due to its proximity to the Galaxy and its moderate Galactic foreground absorption ($N_{\rm H} \sim 6.7 \times 10^{20}$ cm^{-2}, Stark et al. 1992), M 31 is a unique target for CN surveys which started with the seminal work of Hubble (1929) (see also Shafter & Irby 2001; Henze et al. 2008e, and references therein). However, nova monitoring programs for M 31 that include fast data analysis and therefore provide the possibility to conduct follow-up optical spectroscopy (see e.g. Hatzidimitriou et al. 2007), which allows to confirm CNe and to classify them within the system of Williams (1992), were only recently established.

There have been about 850 novae discovered in M 31 as of August 2010. This number is more than a factor of two higher than for our Galaxy (about 400 known novae). Considering only the last ten years (2000-2009), the average observed nova rate was even higher by a factor of about three for M 31 ($\sim$ 22 yr^{-1}) than it was for the Galaxy ($\sim$ 7 yr^{-1}). I have indicated all novae discovered between 2000 and 2009 in M 31 on a three colour optical image of the whole galaxy (courtesy of Thüringer Landessternwarte Tautenburg (TLS), Germany; Fig. 1.4). From a 5 year Hα survey for novae in M 31 (Shafter & Irby 2001) extrapolated an overall nova rate of $\sim$ 37 yr^{-1}. Darnley et al. (2006) estimated even higher nova rates of $\sim$ 65 yr^{-1} for the entire galaxy and 35^{+16}_{-12} yr^{-1} for the bulge.

Our group maintains catalogues for optical novae in M 31[1] and other Local Group galaxies which are updated regularly (for a description of the catalogue see PHS2007).

The advantages and disadvantages of X-ray surveys for CNe in M 31 compared to Galactic surveys (e.g. Ness et al. 2007a; Orio et al. 2001) are similar to those of optical surveys. In our galaxy, the investigation of the whole nova population is hampered by the large area (namely the whole sky) to be monitored and by our unfavourable position close to the Galactic Plane. For M 31 on the other hand, a much smaller area has to be surveyed. As Ness et al. (2007a) pointed out, the detectability of a SSS is highly dependent on its foreground absorption which attenuates the supersoft X-rays much stronger than harder photons. Therefore only nearby SSSs can be detected in the Galactic Plane because of the absorption by the interstellar medium (ISM). Observing SSSs in M 31 is much easier due to the low Galactic foreground absorption.

Galactic novae and SSSs can of course be studied in much greater detail than is possible for M 31 objects, simply because of their proximity. But they have to be observed individually. Furthermore, determining the actual distance to a Galactic CN is not trivial. Observations of M 31 on the other hand, yield light curves of many CNe simultaneously and all of these objects are effectively at the same distance. Therefore, while Galactic sources are the ideal targets to examine the SSS emission of individual novae in detail, observations of M 31 allow us to study the "big picture" and provide insight into the CN population of a large spiral galaxy.

1.1.6 Nova population studies

The idea of two distinct optical nova populations was first presented by Duerbeck (1990) and Della Valle et al. (1992), based on data on Galactic novae. They suggested that fast novae ($t_2 \leq 12$ days) are mainly associated with the disk of the Galaxy or are concentrated at low heights above the Galactic plane, whereas slower novae are mostly present in the bulge region of the Galaxy or at greater heights above the Galactic plane. Another argument in favour of this idea came from Della Valle & Livio (1998), who showed that there are systematic spectroscopic differences in the optical between Galactic bulge and disk novae. They found that novae that could be classified as Fe II novae in the system of Williams (1992) tended to be associated with the bulge of the Galaxy, whereas He/N novae mostly belonged to the Galactic disk. The He/N novae are often observed to also display strong Ne lines, which may point to relatively massive ONe WDs in the binary systems (see e.g. Shafter & Quimby 2007). ONe WDs are believed to be initially more massive than CO WDs (José & Hernanz 1998) and to have more massive progenitors. Therefore, a correlation of these objects with the younger stellar population of the Galactic disk seems plausible.

So far, M 31 has played a key role in nova population studies (see e.g. Ciardullo et al. 1987; Capaccioli et al. 1989; Shafter & Irby 2001). There is an on-going controversy about the presence of two distinct nova populations and, if present, which of the two populations dominates the nova rate in M 31 and the Galaxy (for an early overview see Hatano et al. 1997). In this work, for the first time the differences between M 31 bulge and disk novae are studied in the X-ray regime.

1.1.7 Novae and supersoft X-ray sources in globular star clusters

Globular clusters (GCs) are spherical, gravitationally bound concentrations of typically several 10^5 stars. These systems are found in the halos of galaxies and they mostly consist of old stars (age > 10 Gyr). Novae in GCs are rarely detected. Prior to 2007, there were just two known sources that likely

[1] http://www.mpe.mpg.de/~m31novae/opt/m31/index.php

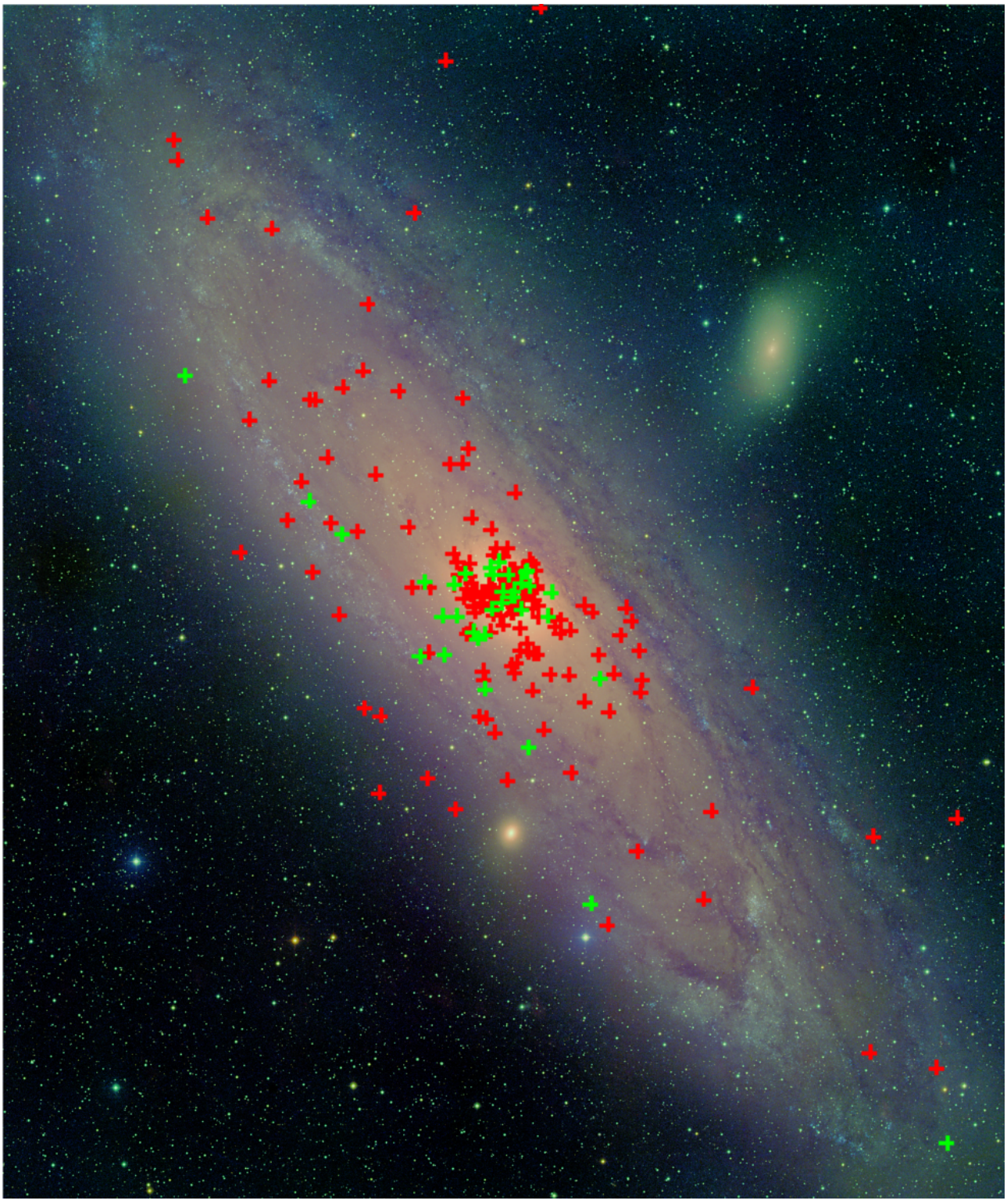

Figure 1.4: Distribution of optical nova candidates in M31 discovered between 2000 and 2009(**red**). Marked with **green** are the novae that have SSS counterparts. The background image is an *UBV* photo plates colour composite, courtesy of Thüringer Landessternwarte Tautenburg (TLS), Germany. The field size is 1.7 deg $\times$ 2.0 deg. North is up and east is left.

fitted this definition. One of them was seen in the Galactic GC M 80 whereas the second nova was found in a GC of the galaxy M 87 (see Shara et al. 2004, and references therein). According to Shara et al. (2004) a third candidate (nova 1938 in the galactic GC M 14) is less likely to be a GC nova. More recently, Shafter & Quimby (2007) reported the very first nova found in a M 31 GC.

Almost all optical surveys for CNe in M 31 that were previously conducted, searched for suddenly appearing objects that have not been visible before and fade back to invisibility in days to weeks. This condition is certainly not fulfilled by CNe in relatively bright GCs. In this case, the optical background light of the GC itself considerably complicates the photometric discovery of a nova outburst.

Independent from their connection to CNe, SSSs in GCs are rare objects, too. Prior to this work there was just one SSS known in a GC at all: the transient 1E 1339.8+2837 in the Galactic GC M 3 (NGC 5272) (Dotani et al. 1999; Verbunt et al. 1995). 1E 1339.8+2837, first discovered with the Einstein satellite and found to have a hard X-ray spectrum and a low luminosity of 4×10^{33} erg s^{-1} (Hertz & Grindlay 1983), showed a very soft high-luminosity state during 1991-92 when observed with ROSAT (Dotani et al. 1999). Dotani et al. (1999) give for 1E 1339.8+2837 a blackbody temperature of $kT \sim 36$ eV and a luminosity of $\sim 10^{35}$ erg s^{-1}, which is significantly lower than the observed peak luminosities of typical nova SSSs ($\sim 10^{37..38}$ erg s^{-1}). They discuss this object as a cataclysmic variable (CV) system that may be a dwarf nova including a massive WD. The CV interpretation is supported by Edmonds et al. (2004) who used Hubble Space Telescope observations to discover an optical counterpart to 1E 1339.8+2837. They suggest that magnetically channelled accretion could explain the peculiarities of 1E 1339.8+2837.

In this work I report the discovery of the first two SSSs in M 31 GCs and discuss their connection to optical novae (see Chap. 5).

1.1.8 The naming convention for novae in M 31

Recently, PHS2007 together with the Central Bureau for Astronomical Telegrams (CBAT) introduced a homogeneous naming scheme for all optical novae and nova candidates in M 31. According to the CBAT webpage[2], "the designation scheme is M31N YYYY-MMx, where YYYY is the year and MM is the 2-digit month of discovery, and 'x' is a lower-case letter (a, b, c, etc.) representing the order of discovery within that month". This means, that e.g. nova M31N 2007-12b was the second nova (candidate) that had been discovered in December 2007. Throughout the dissertation this naming convention is used to refer to individual novae in M 31.

1.2 The XMM-Newton, *Chandra* and *Swift* X-ray observatories

Due to the fact that the Earth's atmosphere is opaque for X-ray radiation, X-ray emission from stellar objects has to be observed from satellites in space. The X-ray imaging telescopes on these satellites operate on the principle of grazing incidence reflection. This is necessary because high energy X-ray photons would be absorbed, transmitted or scattered rather than reflected by (spheroid or paraboloid) mirrors used in optical astronomy. Most X-ray imaging telescopes are constructed as so-called Wolter telescopes, introduced by Wolter (1952), that combine two grazing incidence mirrors into a system that is free of both spherical aberration and coma. X-ray astronomy utilises mainly Wolter I systems, which consist of a paraboloid and a confocal hyperboloid, because they can be nested to increase the

[2] http://www.cfa.harvard.edu/iau/CBAT_M31.html

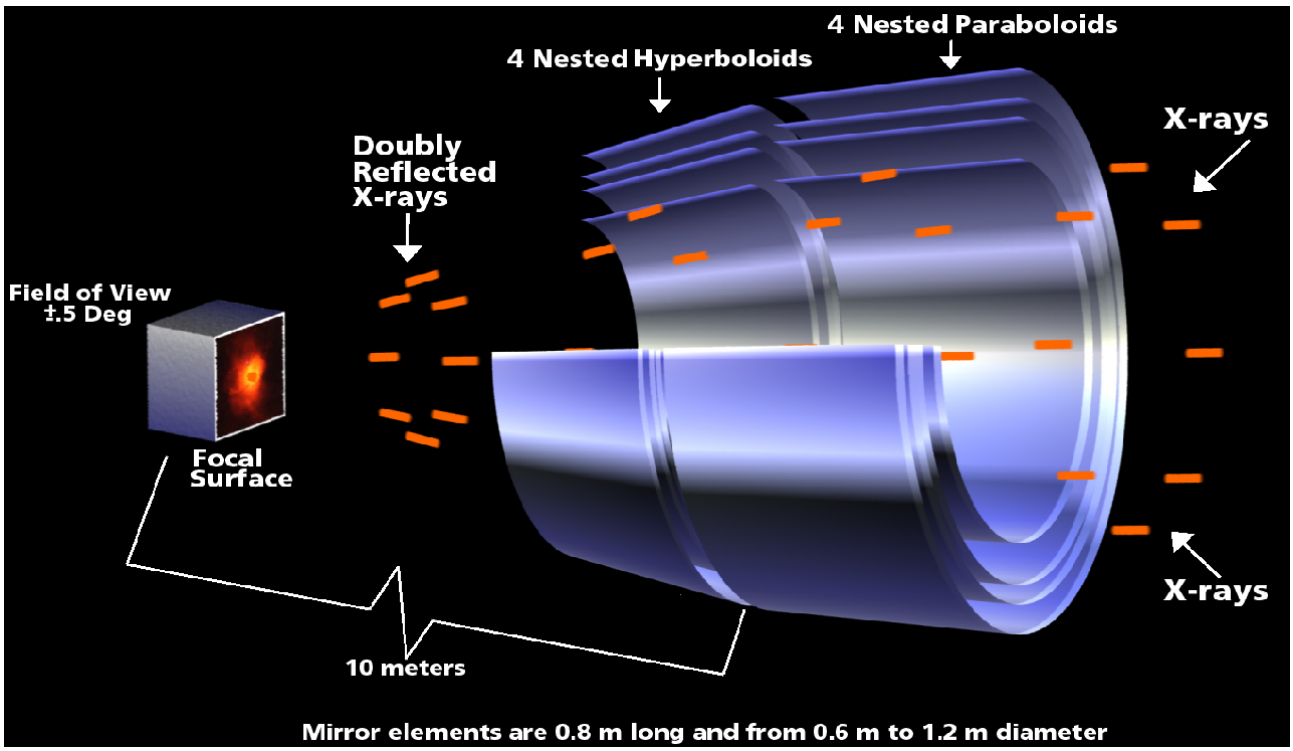

Figure 1.5: Working principle of an X-ray telescope Wolter I type mirror by the example of the *Chandra* mirror system (see Chap. 1.2.2). Image provided by NASA.

effective aperture areas. Figure 1.5 shows the principle of a Wolter I telescope by the example of the *Chandra* mirror system (see Chap. 1.2.2).

This dissertation is based on X-ray observations that were obtained with the X-ray satellites XMM-Newton (Jansen et al. 2001), *Chandra* (Weisskopf et al. 2002) and *Swift* (Gehrels et al. 2004). This section introduces the three observatories and describes their main properties.

1.2.1 The XMM-Newton observatory

The X-ray Multi-Mirror Mission observatory (XMM-Newton)[3] is a cornerstone mission of the European Space Agencys (ESA) Horizon 2000 programme (Jansen et al. 2001). The satellite was launched on December 10th 1999 to an highly eccentric orbit (perigee of 7000 km and apogee of 114 000 km) with an orbital period of about 48 hours.

XMM-Newton is equipped with three independent X-ray mirror modules each of which consists of 58 Wolter I mirrors (maximum diameter of 70 cm and focal length of 7.5 m) nested in a coaxial and confocal configuration (Aschenbach et al. 2000). The following X-ray detectors are located on the telescope's focal plane (see Fig. 1.6): the European Photon Imaging Camera (EPIC) PN-CCD camera (Strüder et al. 2001), two EPIC MOS imaging detectors (Turner et al. 2001) and two readout cameras for the Reflection Grating Spectrometer (RGS; den Herder et al. 2001). The X-ray instruments are supplemented by the Optical/UV Monitor Telescope (OM; Mason et al. 2001), a Ritchey-Chrétien telescope with a 0.3 m primary mirror, which extends the spectral coverage of the observatory into the ultraviolet (UV) and optical range.

[3] http://xmm.esac.esa.int/

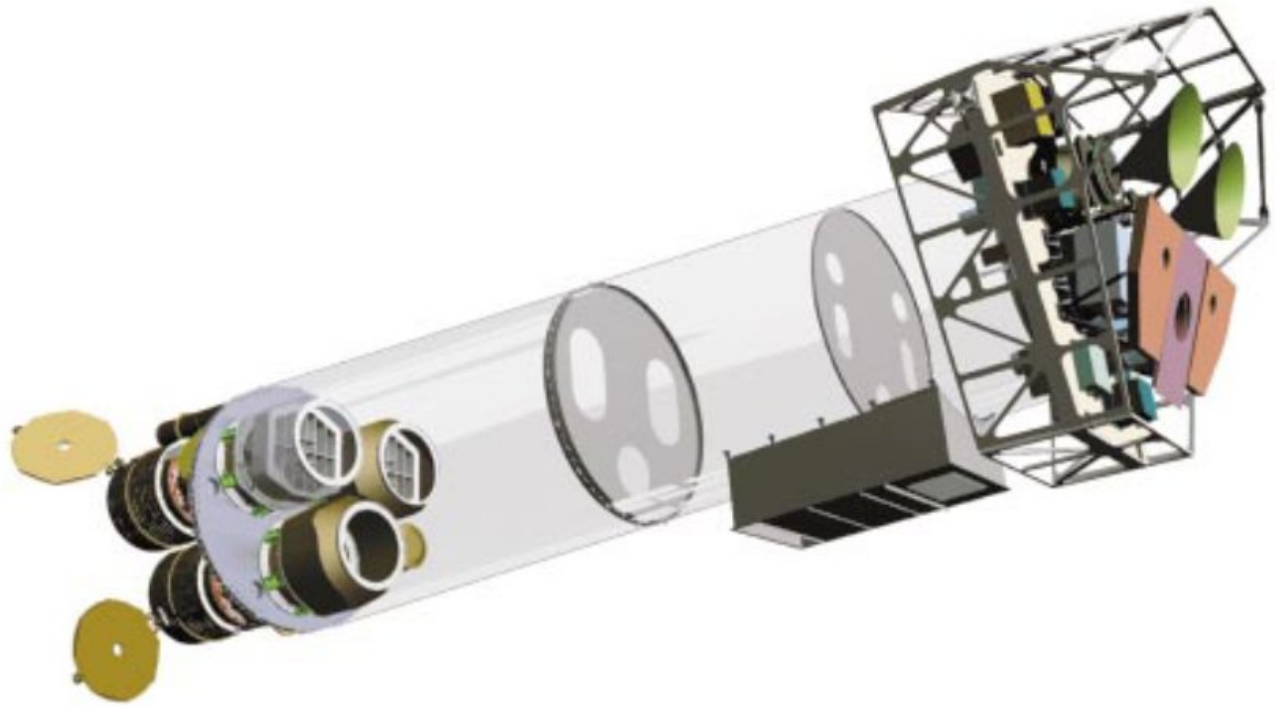

Figure 1.6: "Open" view of the XMM-Newton telescope. Mirrors are on the left and the instrument platform with all the radiators is visible on the right. Picture and description from Jansen et al. (2001).

One of the main strengths of XMM-Newton is the unprecedentedly large effective area of the three mirror modules of ~ 2000 cm^2 at 1 keV (see the XMM-Newton Users Handbook[4]) because it allows the collection of a large number of source photons. The three EPIC detectors have the following characteristics, which are important for the scientific goals of this work: (i) a field of view of about half a degree in diameter that allows to cover the central region of M 31 in a single observation, (ii) a point spread function of $\sim 5''$ (FWHM) which means that except for the very centre of M 31 individual sources can be resolved, and (iii) the capability of low resolution spectroscopy that was used to classify objects as SSSs based on their spectrum or hardness ratio (= "X-ray colour").

The XMM-Newton telescope allows high-resolution X-ray grating spectroscopy with the RGS. Unfortunately, for this work the RGS was not useful because of the high source density in the M 31 central region and the relative faintness of SSSs in M 31. The OM was used to derive UV magnitudes for several novae (see Chap. 3.2).

1.2.2 The *Chandra* observatory

The *Chandra* X-ray observatory[5] is a NASA facility that was launched on July 23rd 1999. It is operating in a highly elliptical orbit (perigee of 10 000 km and apogee of 140 000 km) with a period of 63.5 hours (Weisskopf et al. 2002).

Chandra's telescope system, the High-Resolution Mirror Assembly (HRMA), is made of a nested set of four Wolter I grazing-incidence X-ray mirror pairs, with the largest having a diameter of 1.2 m, and a focal length of 10 m. The telescope is equipped with two focal plane instruments, the High-

[4] http://xmm.esac.esa.int/external/xmm_user_support/documentation/uhb/index.html
[5] http://cxc.harvard.edu/

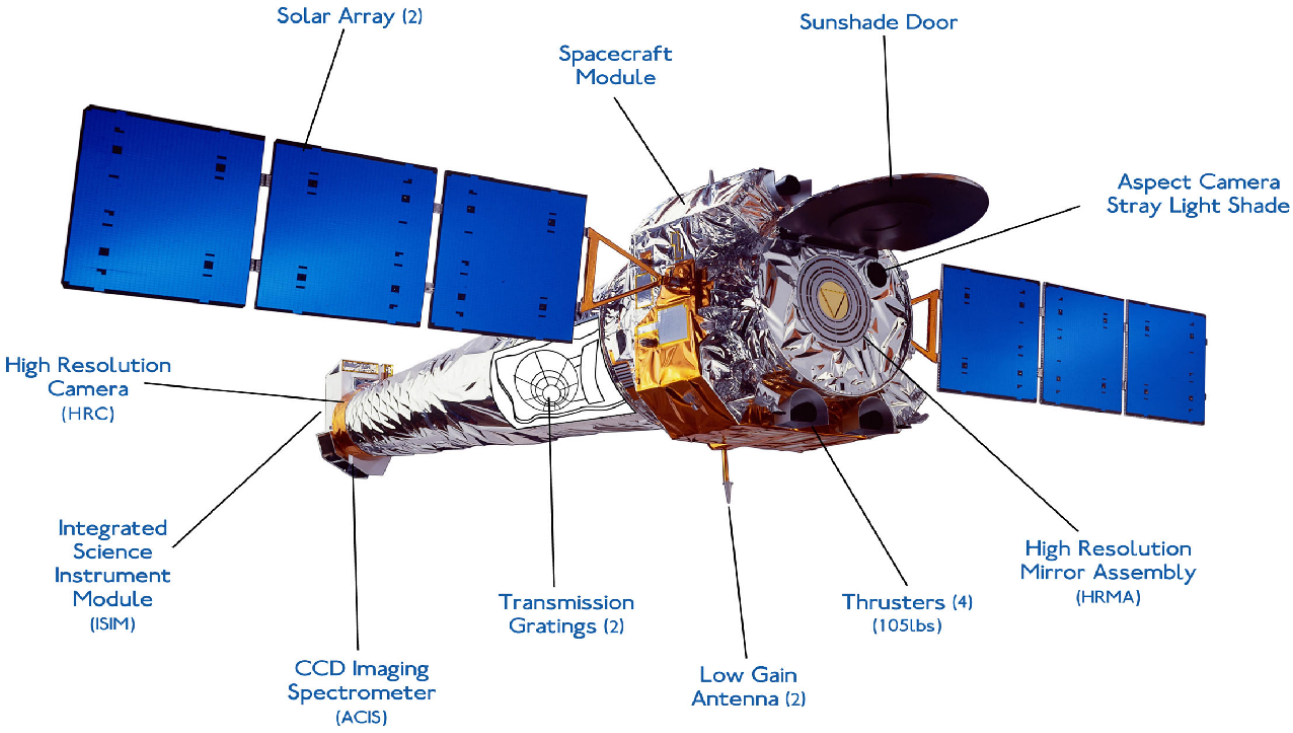

Figure 1.7: View of the *Chandra* X-ray observatory with annotations. Image provided by NASA.

Resolution Camera (HRC; Murray et al. 2000) and the Advanced CCD Imaging Spectrometer (ACIS; Garmire et al. 2003). Both instruments provide an imaging detector (HRC-I/ACIS-I) as well as a spectroscopy detector (HRC-S/ACIS-S) (Weisskopf et al. 2002). The two spectroscopy detectors were designed in particular to be combined with the two transmission gratings of the observatory: the Low-Energy Transmission Grating (LETG; Brinkman et al. 2000) and the High-Energy Transmission Grating (HETG; Canizares et al. 2005). Figure 1.7 shows a view of *Chandra* .

In this work HRC-I monitoring observations are reduced and analysed in detail while archival ACIS-I observations are only used to check for the presence of known sources. The HRC-I detector was used for the monitoring of SSSs in M 31 because the combination of HRMA and HRC-I provides the best spatial resolution (on-axis point spread function FWHM of $\sim 0\farcs5$) and largest field of view ($\sim 31'$) (Weisskopf et al. 2002). Furthermore, it provides a good response in the soft X-ray regime.

It is *Chandra*'s outstanding imaging quality which allows the resolution of even the very centre of M 31 into individual sources (see Fig. 4.3). Unfortunately, the spectral resolution of the *Chandra* HRC-I is very limited and only crude hardness-ratios can be inferred from the recorded photon energy distribution (see "The Chandra Proposers Observatory Guide"[6]).

1.2.3 The *Swift* observatory

The *Swift* satellite is a part of NASA's medium explorer program and was launched into a low-Earth orbit on November 20th 2004[7]. It is a multi-wavelength observatory that was designed particularly for gamma-ray burst (GRB) astronomy and rapid-response observations (Gehrels et al. 2004). *Swift* carries the following instruments: the Burst Alert Telescope (BAT, energy range 15 – 150 keV; Barthelmy

[6] http://cxc.harvard.edu/proposer/POG/html/index.html; chapter 7.6
[7] http://heasarc.nasa.gov/docs/swift/swiftsc.html

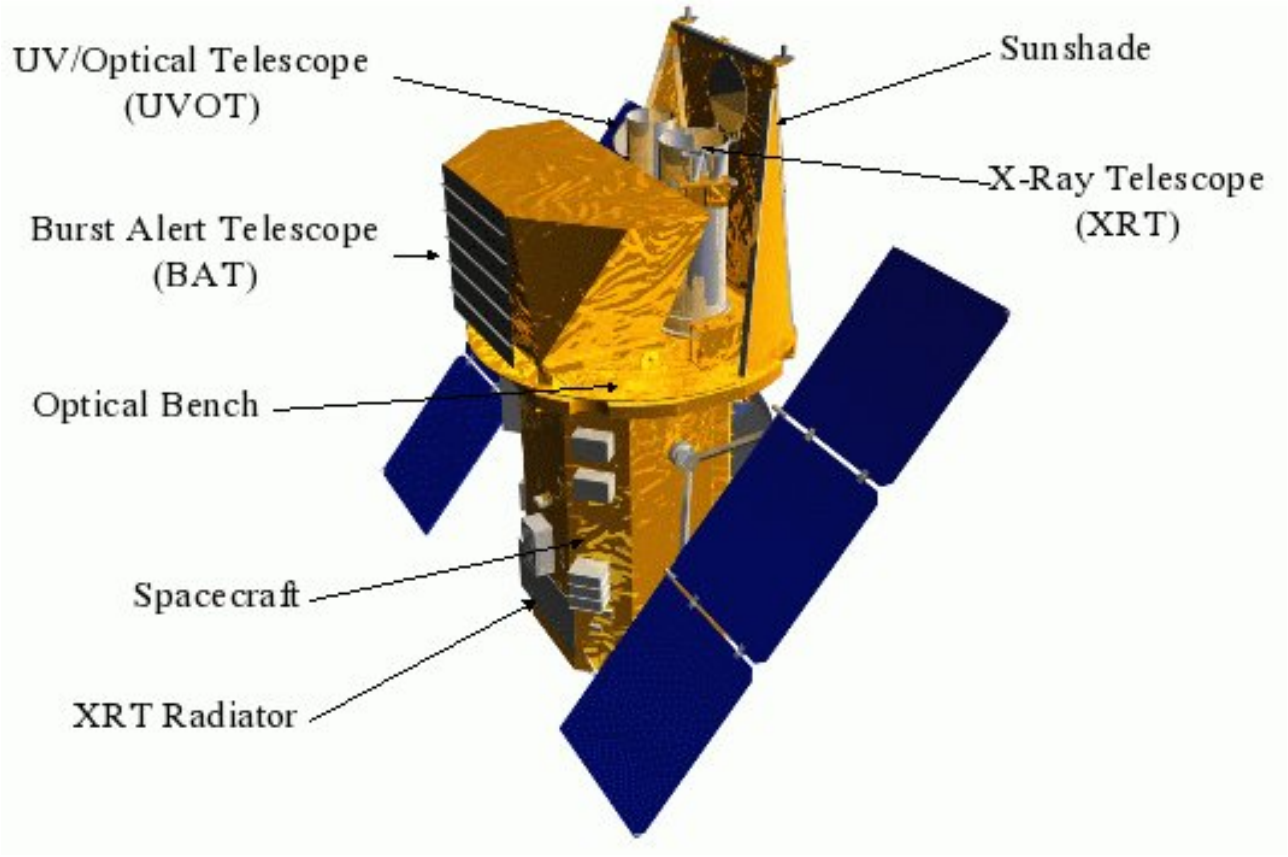

Figure 1.8: View of the *Swift* observatory with annotations. Image provided by the UK Swift Science Data Centre.

et al. 2005), the X-Ray Telescope (XRT, 0.2 – 10.0 keV; Burrows et al. 2005) and the Ultraviolet/Optical Telescope (UVOT; Roming et al. 2005). The design of the latter instrument was based on the XMM-Newton OM. An overview of the spacecraft is shown in Fig. 1.8[8].

The main strength of the *Swift* observatory is its ability to respond swiftly to science triggers, making it the ideal instrument for fast follow-up observations of newly discovered sources. In the context of this work, *Swift* observing time was requested successfully for so-called Target of Opportunity (ToO) observations of particularly interesting sources with both the XRT and the UVOT.

The XRT is an X-ray imaging spectrometer equipped with a Wolter I telescope with 3.5 m focal length that consists of 12 nested concentric mirror shells, the largest having a diameter of 30 cm. With its 23.′6 field of view (Burrows et al. 2005) the XRT was used to characterise and classify individual SSSs (see e.g. Chap. 5).

The UVOT, a modified RitcheyChrétien optical configuration with a 30 cm primary mirror and a 17′ field of view (similar to the XMM-Newton OM), was utilised to record UV light curves of novae discovered in the M 31 central region.

During the course of my work, both the serendipitous discovery and the follow-up of X-ray and optical transient sources in M 31 with *Swift* accounted for a significant scientific output in addition to the main monitoring project (see e.g. Chaps. 3.2 and Appendix A).

[8] http://www.swift.ac.uk/

1.3 Dissertation aims and outline

The subjects of this dissertation are the first dedicated monitoring campaigns for SSS states of optical novae in the central region of M 31 (see also Henze et al. 2010c,d). It is following the works of PFF2005 and PHS2007, who analysed archival X-ray data of novae in this region. PFF2005 found that optical novae constitute the major class of SSSs in the M 31 central region and PHS2007 discovered that the fraction of novae detected as SSSs was higher than previously estimated (> 30%). PHS2007 further reported a significant percentage of novae with short (< 100 days) SSS states.

At the time of writing all observational input for theoretical nova models involving X-rays had come from Galactic novae (see e.g. Hernanz 2005; Hachisu & Kato 2006; Krautter 2008, and related work of the same authors). Important progress had been made in recent years in studying individual Galactic novae in great detail, with the most prominent example being the RN RS Oph (see e.g. Ness et al. 2007b; Hachisu et al. 2007; Nelson et al. 2008b). However, a global study of the X-ray properties of the entire nova population of a galaxy was still missing, mainly because of an insufficient database. As outlined above, in contrast to our own Galaxy, M 31 is a much better subject for such a population study. In the context of optical properties of novae, observations of M 31 have resulted in major progress of nova population studies (see e.g. Ciardullo et al. 1987; Capaccioli et al. 1989; Tomaney & Shafter 1992; Sharov 1993; Hatano et al. 1997; Shafter & Irby 2001).

The aim of this work was to gather sufficient information about the SSS phase of many optical novae in the central area of M 31. This was successfully accomplished and I could create a data base that allowed for the first time the study of SSS novae with statistical means. I conducted the statistical analysis in this work and present several new relations between optical and X-ray parameters as well as an X-ray view on nova populations and a statistical approach to the question how many novae are expected to be seen as SSSs.

This dissertation is structured as follows. Chapter 2 describes the X-ray and optical observational data my work was based on, and the reduction and analysis methods I used. The results from this analysis are presented in Chaps. 3 and 4 for the X-ray and optical monitorings, respectively. A special highlight is the subject of Chap. 5: the very first SSSs found in M 31 GCs. I discuss my results in Chap. 6 for individual sources as well as for the entire population of nova SSSs in M 31. Finally, Chap. 7 contains a summary of my dissertation and the conclusions that can be drawn from the results I presented. Supplementary information is given in Appendix A, B and C.

Chapter 2

Observations and data analysis

2.1 Observations

The X-ray data used in this dissertation were obtained mainly in a joint XMM-Newton/*Chandra* monitoring program (PI: W. Pietsch)[1]. The fields of view of the X-ray telescopes cover the central region of the galaxy, including its bulge, for which Darnley et al. (2006) derived an optical nova rate of 35^{+16}_{-12} yr^{-1}. The aim of the project was to simultaneously monitor the SSS state of many optical novae in the central region of M 31.

This work is based on data from the first three monitoring campaigns of the project. For two particularly interesting X-ray sources in M 31 GCs the data set was supplemented by two observations from the XMM-Newton M 31 large survey project[2], by one XMM-Newton Target of Opportunity (ToO) observation as well as by several *Swift* XRT ToO observations. Details of these observations are given in Chap. 5 together with the X-ray light curves of both sources. Archival *Chandra* ACIS and *Swift* XRT observations of the M 31 central region were used to determine additional information for individual novae.

The X-ray monitoring was complemented by a regular optical monitoring of the M 31 central region using small telescopes. Additionally, several individual novae were detected as UV sources in various *Swift* UVOT observations of M 31.

Below, I describe the X-ray, optical and UV observations used in this dissertation.

2.1.1 The XMM-Newton/*Chandra* monitoring of the M 31 central region

In the first monitoring campaign the M 31 central region was observed with five XMM-Newton EPIC and four *Chandra* HRC-I observations between June 2006 and March 2007. Individual observations were separated by about 30 days. This campaign is designated as "2006/7" in the remainder of this work. The second and the third campaign consisted of five 20 ks XMM-Newton EPIC observations following five 20 ks *Chandra* HRC-I observations each from November to February 2007/8 and 2008/9 respectively. In the third campaign, the fifth *Chandra* observation was split in two parts of 10 ks duration each and two additional 20 ks HRC-I observations were performed in February 2009 after the XMM-Newton observations using MPE *Chandra* guaranteed time. The observations in the second and third campaign had a 10-day spacing. The monitoring strategy was changed after the

[1] http://www.mpe.mpg.de/~m31novae/xray/index.php

[2] XMM-Newton Large Program: The X-ray source population of the Andromeda galaxy M 31; PI: W. Pietsch see http://www.mpe.mpg.de/xray/research/normal_galaxies/m31/lp.php

first campaign to account for a significant percentage of CNe in M 31 with short SSS phases found in PHS2007. Henceforth, the second and third campaign are designated as “2007/8” and “2008/9”, respectively.

The dates, observation identifications (ObsIDs) and dead-time corrected exposure times of the individual observations are given in Table 2.1. XMM-Newton EPIC colour images of the field are shown in Figs. 4.1 (2006/7) and 4.2 (2007/8 and 2008/9). X-ray sources in the inner 2 arcminutes of M 31 can only be resolved in *Chandra* observations. Stacked images from all *Chandra* observations of the individual campaigns are shown in Figs. 4.3 (2006/7) and 4.4 (2007/8 and 2008/9).

Table 2.1: Observations of the 2006/7, 2007/8 and 2008/9 M 31 monitoring campaigns.

Telescope/Instrument	ObsID	Exposure Time[a] [ks]				Start Date[b]	JD[b]	Offset[c]	
		PN	MOS1	MOS2	HRC-I	[UT]	2 450 000+	RA [″]	Dec [″]
2006/7									
Chandra HRC-I	7283				19.9	2006-06-05.29	3891.79	0.2	0.4
XMM-Newton EPIC	0405320501	10.8	13.0	13.5		2006-07-02.61	3919.11	2.1	1.8
XMM-Newton EPIC	0405320601	9.8	16.3	12.0		2006-08-09.51	3957.02	1.6	1.6
Chandra HRC-I	7284				20.0	2006-09-30.89	4009.39	-0.3	0.4
Chandra HRC-I	7285				18.5	2006-11-13.30	4052.80	-0.4	0.0
XMM-Newton EPIC	0405320701	12.3	15.4	15.4		2006-12-31.60	4101.10	0.8	0.9
XMM-Newton EPIC	0405320801	9.9	13.2	13.4		2007-01-16.49	4116.99	0.0	0.5
XMM-Newton EPIC	0405320901	12.5	16.3	16.3		2007-02-05.15	4136.66	-0.4	2.0
Chandra HRC-I	7286				18.7	2007-03-11.61	4171.11	-0.3	-0.1
2007/8									
Chandra HRC-I	8526				19.9	2007-11-07.63	4412.14	-0.3	0.3
Chandra HRC-I	8527				20.0	2007-11-17.76	4422.26	-0.3	0.3
Chandra HRC-I	8528				20.0	2007-11-28.79	4433.29	-0.2	0.2
Chandra HRC-I	8529				18.9	2007-12-07.57	4442.07	-0.3	0.1
Chandra HRC-I	8530				19.9	2007-12-17.49	4451.99	-0.3	0.1
XMM-Newton EPIC	0505720201	22.3	26.9	26.9		2007-12-29.57	4464.07	0.0	0.1
XMM-Newton EPIC	0505720301	20.4	26.4	26.4		2008-01-08.29	4473.79	0.0	0.1
XMM-Newton EPIC	0505720401	17.2	21.2	20.9		2008-01-18.63	4484.13	-0.3	0.1
XMM-Newton EPIC	0505720501	9.9	15.6	14.9		2008-01-27.94	4493.44	0.0	0.0
XMM-Newton EPIC	0505720601	15.1	20.7	20.7		2008-02-07.20	4503.75	0.0	0.3
2008/9									
Chandra HRC-I	9825				20.2	2008-11-08.34	4778.84	-0.3	0.2
Chandra HRC-I	9826				19.9	2008-11-17.14	4787.64	-0.4	0.3
Chandra HRC-I	9827				20.0	2008-11-28.24	4798.74	-0.3	0.3
Chandra HRC-I	9828				20.0	2008-12-07.41	4807.91	-0.4	0.1
Chandra HRC-I	9829				10.1	2008-12-18.02	4818.52	-0.5	0.0
Chandra HRC-I	10838				10.0	2008-12-18.49	4818.99	-0.4	0.1
XMM-Newton EPIC	0551690201	15.6	21.2	21.2		2008-12-30.14	4830.64	-0.1	0.1
XMM-Newton EPIC	0551690301	16.3	20.9	20.9		2009-01-09.26	4840.76	0.1	0.1
XMM-Newton EPIC	0551690401	6.1	9.9	10.0		2009-01-15.90	4847.40	0.1	0.0
XMM-Newton EPIC	0551690501	13.6	19.5	18.7		2009-01-27.31	4858.81	0.1	0.3
XMM-Newton EPIC	0551690601	12.7	5.5	5.5		2009-02-04.56	4867.06	-0.2	-0.1
Chandra HRC-I	10683				19.9	2009-02-16.90	4879.40	-0.5	0.1
Chandra HRC-I	10684				18.7	2009-02-26.17	4888.67	-0.5	0.1

Notes: [a]: Dead-time corrected; for XMM-Newton EPIC after screening for high background.
[b]: Start date of observations; for XMM-Newton EPIC the PN start date was used.
[c]: Offset of the image coordinates to the catalogue by Kaaret (2002).

2.1.2 Archival X-ray observations of the M 31 central region

During the time of the three monitoring campaigns, several additional observations of the M 31 central region had been conducted with *Chandra* ACIS-I and *Swift* XRT. Details of these observations are given in Tables 2.2, 2.3 and 2.4. In 2006/7 only two of the CN counterparts detected in our monitoring data were visible in these archival data: Nova M31N 2004-05b can be seen as a faint object in both *Swift* observations, whereas M31N 2005-02a is detected with about seven counts in the 23 ks *Chandra* ACIS-I observation 7064.

From the beginning of the 2007/8 campaign until the end of the 2008/9 campaign there were twelve observations with *Chandra* ACIS-I and 62 observations with the *Swift* XRT that included the M 31 central region. All these observations were checked for further information on the novae found in the monitoring. In the ACIS-I data (see Table 2.3) none of the novae was detected. In the *Swift* XRT observations (see Table 2.4) the novae M31N 2007-06b, M31N 2007-11a and M31N 2007-12b are detected. Unfortunately, there were no *Swift* non-detections of SSS counterparts that could provide additional constraints on their turn-on or turn-off time. The main reasons for this are (a) the temporal distribution of the observations, (b) the smaller field of view of the *Swift* XRT compared to XMM-Newton EPIC and *Chandra* HRC and (c) the fact that many observations were not pointed directly at the M 31 centre (see Table 2.4).

Table 2.2: Archival *Chandra* ACIS-I and *Swift* XRT observations of the M 31 central region during the 2006/7 campaign.

Telescope/Instrument	ObsID	$t^{a}_{\rm exp}$ [ks]	Start Date [UT]
Chandra ACIS-I	7136	4.0	2006-01-06.84
Chandra ACIS-I	7137	4.0	2006-05-26.18
Chandra ACIS-I	7138	4.1	2006-06-09.68
Chandra ACIS-I	7139	4.0	2006-07-31.02
Swift XRT	00030802001	5.9	2006-09-01.75
Swift XRT	00030804001	5.9	2006-09-11.73
Chandra ACIS-I	7140	4.1	2006-09-24.76
Chandra ACIS-I	7064	23.2	2006-12-04.88
Chandra ACIS-I	8183	4.0	2007-01-14.86
Chandra ACIS-I	8184	4.1	2007-02-14.08
Chandra ACIS-I	8185	4.0	2007-03-10.25

Notes: [a]: Dead-time corrected exposure time.

Table 2.3: Archival *Chandra* ACIS-I observations of the M 31 central region during the 2007/8 and 2008/9 campaigns.

ObsID	Exposure Time[a] [ks]	Start Date [UT]
8195	4.0	2007-09-26.63
8186	4.1	2007-11-03.18
8187	3.8	2007-11-27.15
9520	4.0	2007-12-29.70
9529	4.1	2008-05-31.47
9522	4.0	2008-07-15.70
9523	4.1	2008-09-01.32
9524	4.1	2008-10-13.15
9521	4.0	2008-11-27.72
10551	4.0	2009-01-09.98
10552	4.0	2009-02-07.44
10553	4.1	2009-03-11.59

Notes: [a]: Dead-time corrected.

Table 2.4: Archival *Swift* XRT observations near the M 31 central region during the 2007/8 and 2008/9 campaigns.

ObsID	Exp. time [ks]	Start Date [UT]	Distance[a] [arcmin]
00031017001	1.9	2007-11-18.39	14.8
00031017002	5.3	2007-11-19.26	15.4
00031028001	1.1	2007-11-24.20	2.9
00031028002	4.6	2007-11-24.20	2.9
00031027001	7.3	2007-11-24.33	13.7
00031028003	0.02	2007-11-27.01	3.2
00031028004	1.9	2007-11-27.01	3.8
00031028006	4.7	2007-11-30.02	2.6
00031027002	1.0	2007-12-02.64	13.1
00031028008	1.7	2007-12-02.97	2.6
00031027003	3.7	2007-12-03.24	14.1
00031017003	3.1	2007-12-13.01	16.6
00031017004	3.0	2007-12-14.02	15.9
00031017005	3.2	2007-12-15.02	16.4
00031027004	3.9	2007-12-16.77	14.5
00031017006	2.2	2007-12-20.24	16.4
00031017007	2.1	2007-12-22.38	16.6
00031017008	2.3	2007-12-24.32	16.3
00031027005	4.0	2007-12-30.01	15.9
00031017009	2.3	2007-12-30.15	16.6
00031017010	2.0	2008-01-03.43	17.6
00031017011	1.9	2008-01-06.24	15.9
00031017012	1.7	2008-01-09.99	16.9
00031027006	4.0	2008-01-13.74	15.2
00037717001	1.5	2008-05-26.04	29.2
00037718001	4.8	2008-05-26.29	11.6
00037719001	4.9	2008-05-26.70	2.3
00037720001	2.2	2008-05-26.96	13.8
00037721001	4.5	2008-05-28.11	27.7
00037720002	3.0	2008-05-28.84	15.6
00037725001	0.1	2008-07-04.51	16.9
00037724001	3.5	2008-07-04.60	23.3
00037711001	0.5	2008-07-06.13	24.9
00037712001	0.2	2008-07-06.53	14
00037713001	4.4	2008-07-06.80	15.5
00037714001	4.1	2008-07-07.07	25
00037725002	2.5	2008-07-09.41	14.3
00037717002	2.5	2008-07-09.62	26.3

Table 2.4: continued.

ObsID	Exp. time [ks]	Start Date [UT]	Distance[a] [arcmin]
00037712002	4.1	2008-07-20.45	13.4
00037711002	3.8	2008-07-20.79	25
00037726002	4.8	2008-07-22.06	14.5
00037727002	1.7	2008-07-24.20	25.7
00037727003	1.1	2008-07-26.48	26.3
00031255001	6.1	2008-08-21.30	2.4
00031255002	2.5	2008-08-28.67	2.6
00031255003	2.3	2008-09-04.22	1.5
00031255004	4.9	2008-09-06.59	2.9
00031255005	5.8	2008-09-11.47	0.8
00031255006	4.7	2008-09-25.50	2.1
00031255008	2.1	2008-10-14.73	1.2
00031255009	2.5	2008-10-15.14	1.6
00031255010	6.0	2008-10-21.63	1
00031255011	4.4	2008-10-28.65	1.2
00031283001	1.2	2008-12-07.07	1.5
00031283002	1.0	2008-12-08.14	1.9
00031283003	0.9	2008-12-09.01	1.9
00031283004	1.1	2008-12-10.08	2.2
00031283005	0.3	2008-12-11.02	2
00031283006	0.4	2008-12-12.02	2.3
00031283007	1.0	2008-12-13.22	1.8
00031283008	1.0	2008-12-14.03	2.7
00031283009	1.0	2008-12-15.17	1.7

Notes: [a]: Pointing distance from M 31 centre.

2.1.3 Optical monitoring of the M 31 central region

In order to complement the X-ray observations, our group is conducting an optical monitoring for CNe in the M 31 central region. This is because novae have to be found (in the optical) before they can be studied (in X-rays). The optical monitoring is carried out in collaboration with several observatories using small optical telescopes (35 – 130 cm). The field of view covered in the optical observations is comparable to the field of view of our M 31 monitoring in X-rays (see Fig. 2.1).

The temporal coverage of the optical monitoring from October 2007 until August 2010 is shown in Fig. 2.2. This data set was the result of more than 400 individual observing runs. One observing run was carried out per night. The three gaps in the monitoring coverage in Fig. 2.2 correspond to the time of the year when M 31 is not observable (approximately March till May). Additional to the broad band (R) monitoring, Hα images were obtained with the Super-LOTIS telescope (70 Å filter) and at Skinakas Observatory (75 Å filter) in order to confirm nova candidates by their Hα emission, as described in Chap.1.1.2.

In the following, I briefly describe the individual optical telescopes and hosting observatories. Typical limiting magnitudes given below refer to an average of ten stacked individual images with exposure time of about 60s, respectively. For the individual telescopes I note the number of observing runs that were contributed to the overall data set and the mean frequency of observing nights during the periods indicated in Fig. 2.2. The results of the optical monitoring are given in Chap. 3.1.

Super-LOTIS (Livermore Optical Transient Imaging System, Williams et al. 2008) is a robotic 60 cm telescope equipped with an E2V CCD (2kx2k) located at Steward Observatory, Kitt Peak, Arizona, USA. Using four Super-LOTIS fields (field of view: $17' \times 17'$) allowed us to cover an area of $\sim 34' \times 34'$ centred on the core of M 31 (see Fig. 2.1). The pixel scale is 0.496″/pixel and the typical limiting magnitude is 19 mag in the Johnson R filter. With about 300 observing runs the Super-LOTIS telescope produced the clear majority of the optical data. On average M 31 was observed every third night for the time spans indicated in Fig. 2.2.

The *Skinakas Observatory*, Crete (Greece), operates a 1.3 m Ritchey-Chrétien f/7.5 telescope that is equipped with an Andor DZ436-BV CCD Camera (with a Marconi 2k x 2k chip with 13.5 μm square pixels). The field of view of the telescope is $11' \times 11'$, with a pixel scale of 0.28″/pixel. Similar to the Super-LOTIS monitoring strategy, four Skinakas fields cover $\sim 22' \times 22'$ around the M 31 center (see Fig. 2.1). The typical limiting magnitude in the R band is 19.5 mag. With this telescope there were about 50 observing runs performed that were on average separated by 4 nights.

At the *Athens University Observatory*, Greece, data were obtained using a 40 cm Cassegrain telescope with a focal reducer (F/5.1) equipped with a 2184 x 1472 pixel ST-10XME CCD camera (pixel size 6.8 microns square). Four fields cover $\sim 52' \times 35'$ around the M 31 center (0.71″/pixel). The typical limiting magnitude without filter is 18.0 mag. This telescope contributed about 60 observing runs that were taken on average on every third night during the times shown in Fig. 2.2.

The *Observatori Astronomic del Montsec*, owned by the Consorci del Montsec and operated by the Institut d'Estudis Espacials de Catalunya, contributes observations with the Joan Oro telescope, a 80 cm Ritchey-Chrétien F/9.6 telescope using a Finger Lakes PL4240-1-BI CCD Camera (with a Class 1 Basic Broadband coated 2k x 2k chip with 13.5 microns sq. pixels). Also with this telescope four fields are used that altogether cover an area of $\sim 25' \times 25'$ around the M 31 centre with a pixel scale of 0.33″/pixel and a typical R magnitude of 19.0 mag. The Montsec observatory so far only observed M 31 during three nights in June/July 2009. These observations are only included in the overall coverage in Fig. 2.2 but not indicated separately.

PIRATE is a 0.35-m f/11 Schmidt-Cassegrain telescope (+ SBIG STL-1001E CCD camera) located at Costitx, Mallorca (Spain), which is hosted by the Observatori Astronomic de Mallorca and

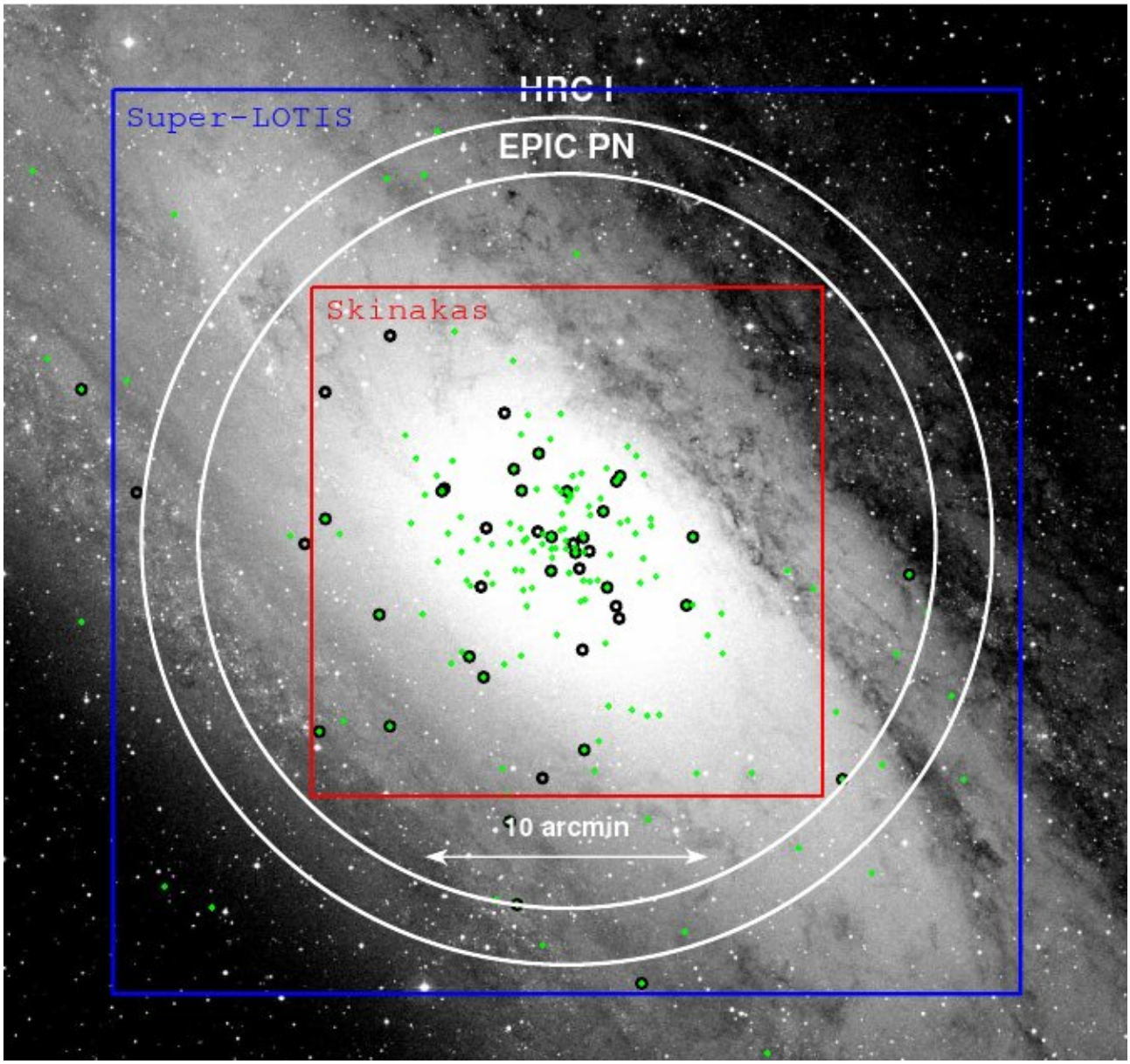

Figure 2.1: Optical DSS1 image of the central region of M 31 with superimposed fields of view of *Chandra* and XMM-Newton (white circles) and two optical telescopes (red: Skinakas observatory, blue: Super-LOTIS), respectively. Optical novae with outburst after 2000 are indicated as green dots. Black circles mark novae that have been detected as X-ray sources.

operated by the Open University[3]. The pixel size of the images is 1.209″/pixel. The field of view of 22′ diameter allowed us to cover an area of $\sim 44' \times 44'$ using a mosaic of four pointings. The typical limiting magnitude without a filter is 18.5 mag. There were 10 observations carried out with PIRATE, that were separated by about a week.

The *Observatorio Astronomico de La Sagra*, Spain, operates a 0.45m f/2.8 reflector equipped with a SBIG STL-11000M CCD Camera (3008 pixels x 2674 pixels each 9 x 9 micron square). It covers a area of $\sim 98' \times 65'$ with a pixel scale of 0.71″/pixel and an unfiltered limiting magnitude of 18.0. Three

[3]http://pirate.open.ac.uk/

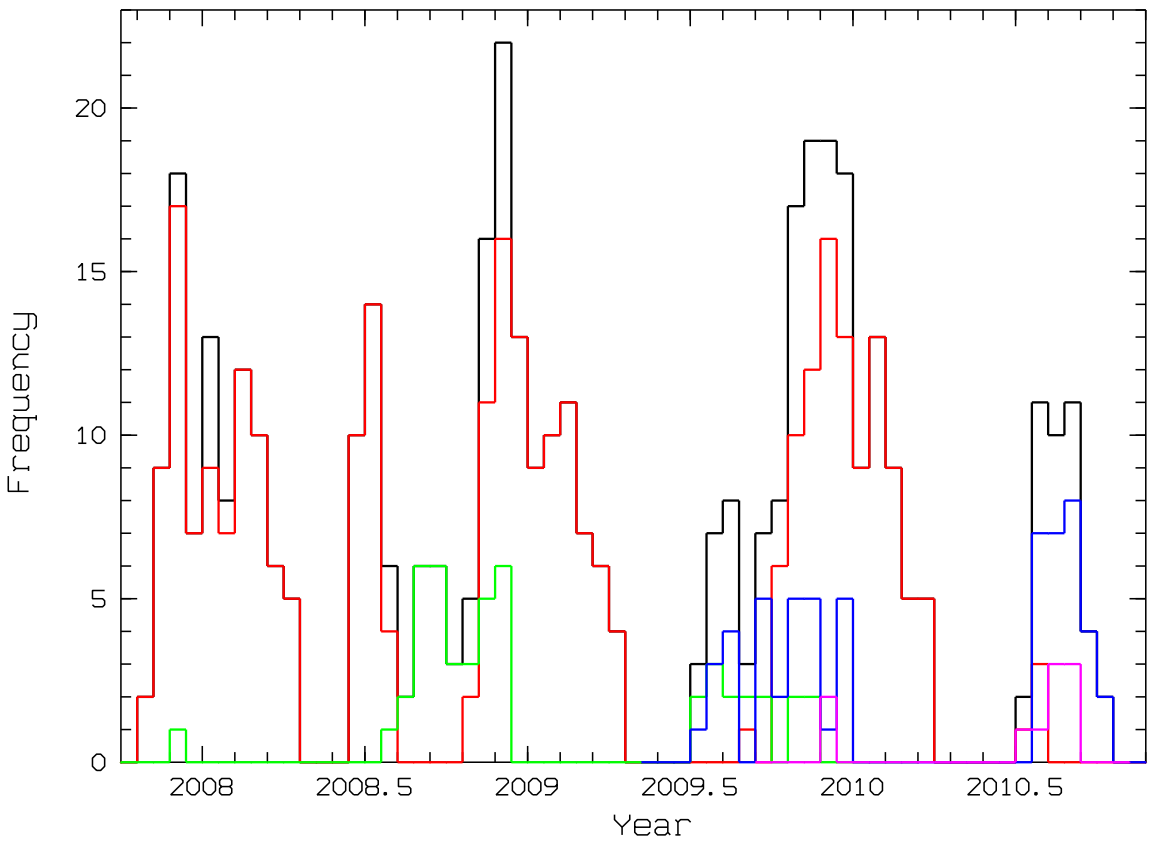

Figure 2.2: Temporal coverage of the optical monitoring. Bin size: 0.05 yr. Black: all observations, red: Super-LOTIS, green: Skinakas observatory, blue: Athens University observatory, magenta: OAM PIRATE.

fields were used to cover the main part of M 31 along the major axis of the galaxy. This telescope only contributed 5 observing nights during December 2007 and January 2008. The observing runs were on average separated by 3 days and are not included individually in Fig. 2.2.

2.1.4 Ultraviolet observations of novae with *Swift*

Several individual novae were found in *Swift* UVOT observations of M 31 which were performed by different groups and for various reasons. I describe the analysis of the *Swift* UVOT data in Chap. 2.2.4 and list the novae that were found in Chap. 3.2.

2.2 Data analysis

Unlike optical telescopes, that integrate photons over a certain time to generate a detectable signal, the X-ray telescopes used in this dissertation record a separate signal from every individual photon they detect. This detection is called an *event* and is characterised by its two-dimensional position on the detector, energy and time of arrival. Groups of events (e.g. all events from one observation) are usually stored in so-called *event files*. Therefore, it is possible to extract very specific information about individual sources from an event file (e.g. X-ray spectra or light curves) or to exclude times

of high X-ray background during an observations from the analysis in order to increase the source detection sensitivity. Furthermore, retaining the individual events preserves the Poisson statistics nature of the data.

In the following, I describe the data analysis procedures that I applied to the XMM-Newton, *Chandra* and *Swift* data and to the optical images.

2.2.1 Instrument specific X-ray data processing

XMM-Newton data

In the XMM-Newton observations of the monitoring campaigns, the EPIC PN and MOS instruments were operated in the full frame mode, using the entire CCD chip area. The thin filter was used for PN and the medium filter for MOS. The XMM-Newton data processing and analysis was carried out with the instrument specific software package XMMSAS v9.0 (XMM-Newton Science Analysis System; Gabriel et al. 2004)[4]. While source detection was performed on the EPIC PN and MOS images simultaneously, only PN data was used for extracting source spectra, due to the better sensitivity of PN in the soft energy band.

For XMM-Newton source detection, periods with high X-ray background radiation were removed from the observation. The EPIC PN data were processed first with the XMMSAS task `epreject`, which corrects shifts in the energy scale of specific pixels which were caused by high-energy particles hitting the detector during the calculation of the offset map at the beginning of each observation. Additionally, the PN data were carefully screened in order to exclude bad pixels and bad columns in individual CCDs. From the screened PN, MOS1 and MOS2 event files images were created for the energy bands 0.2 – 0.5, 0.5 – 1.0, 1.0 – 2.0, 2.0 – 4.5, and 4.5 – 12.0 keV. These images were binned to a pixel size of $2'' \times 2''$. For EPIC PN, single and double-pixel events (PATTERN ≤ 4) were selected for image creation for all bands except for the 0.2 – 0.5 keV band, where only single-pixel events were used (PATTERN = 0). For EPIC MOS, single to quadruple-pixel events (PATTERN ≤ 12) were used.

For each of the individual images background maps were created using the XMMSAS tasks `eboxdetect` (in "local" mode) and `esplinemap`. In its local detection mode `eboxdetect` performs a sliding box detection on the image, where source counts are accumulated from a small box and the background counts are estimated locally from a larger surrounding box. Count errors were estimated using Poissonian statistics for source and background regions. For each source likelihoods $L = -ln(p)$ were computed, where p is the probability of a Poissonian random fluctuation of the counts in the detection cell which would have resulted in at least the observed number of source counts. The preliminary source list, created with `eboxdetect`, was used as input for `esplinemap`. This task derived a spline background map from the non-source regions of the image.

The final source detection was carried out simultaneously on all 15 images (5 energy bands per detector) of the observation. In this second run, `eboxdetect` took the background from the background maps determined by `esplinemap`. This resulted in an improved detection sensitivity as compared to the local detection step. The output source list was used as input for the task `emldetect` which performed maximum likelihood multi-source point spread function (PSF) fitting. The detection algorithm is described in detail in Cruddace et al. (1988). The output of `emldetect` was a source list for all detected objects in the observation.

[4] http://xmm.esac.esa.int/external/xmm_data_analysis/

Chandra **data**

The *Chandra* HRC-I observations were reduced with the CIAO v4.2 software package (Chandra Interactive Analysis of Observations; Fruscione et al. 2006)[5] and with adapted versions of XMMSAS tools for source detection, starting from the pre-processed level 2 event files. Times of high background were removed as for XMM-Newton.

The adaptation of the XMMSAS detection tasks mainly accounts for the differences between the XMM-Newton and HRC-I detectors. It is based on software scripts developed for analysing the *Chandra* ACIS-I observations of the COSMOS survey with customized XMMSAS tools (see Elvis et al. 2009). I modified these scripts to take into account the larger field of view, PSF characteristics and angular resolution of the HRC-I detector. In particular, the fact that the *Chandra* PSF is significantly degrading with increasing off-axis angle did not allow XMMSAS tasks to process the entire field of view as a whole in high resolution with satisfactorily results. In order to account for this effect, I produced five images that covered the central 200″, 400″, 800″, 1400″ regions and the full field of view with a resolution of 1, 2, 4, 10, and 16 HRC pixels ($0\farcs13 \times 0\farcs13$), respectively. Furthermore, I created a *Chandra* HRC-I PSF map that can be used by the XMMSAS tools. This map describes the PSF in dependence on the detector position of the source and was based on the ACIS-I PSF map used in the COSMOS survey.

Background maps for the images with different resolution were created using adapted versions of the XMMSAS tools `eboxdetect` and `esplinemap` in a similar way as described above for XMM-Newton. The source detection was carried out with the CIAO tool `wavedetect` on the individual images. This task performs a Mexican-Hat Wavelet source detection, which correlates the image with wavelets of different scales and then searches the results for significant correlations. An adapted version of the XMMSAS tool `emldetect` was used to estimate background-corrected and exposure-corrected fluxes and count rates for the detected sources. Finally, the individual detection lists were merged in order to create a source list for the entire observation.

Some novae were only detected or resolved in *Chandra* HRC-I observations. For these objects I computed hardness ratios following the procedure outlined in the "The Chandra Proposers Observatory Guide"[6], from count rates in the bands S, M, and H (channels 1:100, 100:140, and 140:255). Additionally, I applied to these novae the method of PHS2007 and made use of some of the *Chandra* ACIS-I observations mentioned above, if they were taken close on time to HRC-I detections. Assuming that the novae did not change X-ray brightness and spectrum between these observations, it can be investigated if the corresponding X-ray source had a soft spectrum by comparing ACIS-I count rates or upper limits with HRC-I count rates. I justify this assumption for the individual novae it is applied to in Chap. 4. While hard or moderately hard spectra lead to conversion factors (ACIS-I/HRC-I) above one, typical supersoft spectra, as found in novae, show conversion factors below 0.5.

Swift **data**

The *Swift* XRT data were analysed using the HEAsoft XIMAGE package (version 4.4). Exposure maps were created with the XRT software task `xrtexpomap`, which takes into account the vignetting and several known bad pixels and columns of the XRT detector. Exposure map corrected count rates were estimated using the `sosta` command (source statistics). This task estimates source counts in a box that corresponds to 66% of the encircled energy function (EEF) and background from a region surrounding the source, outside the 98% EEF boundary. It takes also into account the XRT PSF.

[5] http://cxc.harvard.edu/ciao/

[6] http://cxc.harvard.edu/proposer/POG/html/index.html; chapter 7.6

Table 2.5: Energy conversion factors (ECF = (count rate)/flux) for blackbody models with different temperatures, including a Galactic foreground absorption of 6.7×10^{20} cm^{-2}, for XMM-Newton EPIC PN/MOS, *Chandra* HRC-I/ACIS-I and *Swift* XRT.

Telescope/ Detector	Band [keV]	20 eV	30 eV	40 eV	50 eV	60 eV	70 eV	80 eV	90 eV
		(10^{10} ct cm^2 erg^{-1})							
EPIC PN	0.2–0.5	1.12	3.28	6.69	10.8	14.9	18.7	22.2	25.3
	0.5–1.0	113	58.9	53.1	52.1	52.7	53.8	55.1	56.3
EPIC MOS	0.2–0.5	0.07	0.33	0.86	1.60	2.31	3.02	3.66	4.22
	0.5–1.0	15.7	6.62	6.89	7.40	7.98	8.60	9.23	9.81
HRC-I	0.2–10.0	0.40	0.66	1.19	1.94	2.85	3.85	4.90	5.92
ACIS-I	0.2–1.0	0.00348	0.0149	0.0593	0.159	0.327	0.570	0.884	1.26
XRT	0.2–1.0	0.0916	0.183	0.316	0.488	0.685	0.893	1.10	1.30

2.2.2 General X-ray data analysis procedures

For XMM-Newton and *Chandra* source detection, low likelihood thresholds of 6 and 3, respectively, were chosen in order to be able to detect faint sources that might be present in more than one observation. Consequently, these low-likelihood sources (detection likelihood < 10) were only accepted as candidate nova counterparts if they showed up in more than one observation. However, this only led to the rejection of two candidate nova counterparts (M31N 2007-03a and M31N 2007-08c) which were solely detected in *Chandra* observation 8526 (see Table 2.1) with likelihoods of about 6.

I derived intrinsic luminosities and 3σ upper limits for nova counterparts starting from the list of detected sources. Nova counterparts only showed emission in the two energy bands below 1 keV. Therefore, for XMM-Newton I derived their count rates and fluxes or upper limits from the 0.2 – 0.5 and 0.5 – 1.0 keV count rates, which I than added to get the 0.2 – 1.0 keV band values. For *Chandra* HRC-I all luminosities are given in the full 0.2 – 10.0 keV band.

For estimating count rate upper limits for non-detected X-ray counterparts of novae, I added the nova positions to the `eboxdetect` list of the observation. The new list was used as input for `emldetect` (with the parameters fixed position and likelihood threshold of zero) to derive the observed count rate, or an upper limit, for all objects in the list.

In order to compare the results to the earlier work of PHS2007, I computed the luminosities given in all tables assuming a typical 50 eV blackbody spectrum with Galactic foreground absorption ($N_{\rm H} \sim 6.7 \times 10^{20}$ cm^{-2}). Table 2.5 gives energy conversion factors (ECF = (count rate)/flux) for a range of blackbody temperatures and the different instruments, clearly showing that the ECFs depend strongly on the temperature of the spectrum. Therefore, apparent discrepancies in the X-ray luminosities of individual novae between XMM-Newton, *Chandra* and *Swift* might be due to deviations of the actual X-ray spectra from the assumed 50 eV blackbody spectrum.

For every SSS nova counterpart where I was able to extract a spectrum, the individual best-fit parameters and the resulting luminosities are given in Chap. 4. Note, that some of these luminosities exceed the Eddington limit for even a very massive WD with $M_{WD} \gtrsim 1.3 M_\odot$ ($L_{\rm Edd} \sim 1.7 \times 10^{38}$). This is due to the general effect of overestimated luminosities in blackbody models and the fact that additional absorption in M 31 would drastically change the observed count rate (see also PHS2007), in particular for very soft X-ray sources. All luminosities assume a distance to M 31 of 780 kpc.

To improve the astrometric accuracy of the measurements I applied a pointing offset correction using the X-ray source catalogue of Kaaret (2002). This catalogue was calibrated astrometrically using six coincidences with the Two Micron All Sky Survey (2MASS, Cutri et al. 2003). According to Kaaret (2002) the average displacement between the X-ray and 2MASS sources is $0\farcs15$. The offset corrections are given in Table 2.1.

I correlated the astrometrically calibrated objects from each observation with the updated catalogue of optical novae in M 31 by PHS2007 [7]. X-ray sources were identified as candidate counterparts of CNe if their positions matched within a certain search radius. This search radius was determined by the positional error of the CN as given in the catalogue and the 3σ error of the X-ray sources in the individual observation. I decided to constrain the search for X-ray counterparts to CNe with outbursts after 1995, in order to suppress spurious identifications, since the positions of earlier CNe are often not as well determined. This argument also holds for potential RNe. In addition, one would expect the start of the SSS phase to occur later than 10 years after the nova outburst only under extreme conditions (low WD mass and core material with close to solar abundance, see Hachisu & Kato 2006). The candidate counterparts found automatically were all inspected visually. I rejected candidates that turned out to be mis-identifications of known persistent hard sources in the field.

In order to increase the signal-to-noise ratio of low luminosity sources, I decided to merge the XMM-Newton event files from the monitoring campaign for each detector (EPIC PN, MOS1, MOS2). First, the individual images were projected into a common coordinate system, defined by the catalogue of Kaaret (2002), using the offsets given in Table 2.1. These offsets were corrected in the attitude file of the observation. This attitude file was used by the XMMSAS command `attcalc` to shift the pixel coordinates of the event files accordingly. Images for the three detectors and five energy bands given above were created for every observation (see Table 2.1) from the WCS corrected event files. For each energy band and detector the single images from the individual observations were added up to one merged image, based on the pixel coordinates re-computed with `attcalc`. Background map creation and object detection on the merged images was done analogously to the individual observations. Furthermore, the attitude corrected EPIC PN event files were stacked using the XMMSAS task `merge`, in order to extract spectra of low luminosity CN counterparts. XMM-Newton EPIC colour images created from the merged images for the three campaigns are presented in Figs. 4.1 and 4.2.

For *Chandra* HRC-I data I applied a similar strategy. The position offsets to the reference catalogue (see Table 2.1) were computed and applied to correct the aspect solution file with the CIAO task `wcs_update`. I used the updated aspect solution to re-project the level 2 event file coordinates to the catalogue system (CIAO procedure `reproject_events`). Images and exposure maps for each observation were created and merged using image manipulation tasks from HEASARCs software package FTOOLS (Blackburn 1995)[8]. Figures 4.3 and 4.4 show the merged images of the very centre of M 31 for the three campaign. The merged data were processed as described above for the individual observations.

I conducted a general search for SSSs in the XMM-Newton monitoring data, following the approach adopted by Pietsch et al. (2005b) and using hardness ratios computed from count rates in energy bands 1 to 3 (0.2–0.5 keV, 0.5–1.0 keV, 1.0–2.0 keV) to classify a source. These authors defined hardness ratios and errors as

$$HR_i = \frac{B_{i+1} - B_i}{B_{i+1} + B_i} \qquad \text{and} \qquad EHR_i = 2\frac{\sqrt{(B_{i+1}EB_i)^2 + (B_iEB_{i+1})^2}}{(B_{i+1} + B_i)^2}\ , \tag{2.1}$$

[7] http://www.mpe.mpg.de/~m31novae/opt/m31/index.php
[8] http://heasarc.gsfc.nasa.gov/ftools/

where B_i and EB_i denote count rates and corresponding errors in band i as derived by `emldetect`. PFF2005 also used these hardness ratios and classified sources as SSSs if they fulfilled the conditions $HR1 < 0.0$ and $HR2 - EHR2 < -0.4$. In this work, I used the same criteria.

If possible, I classified X-ray counterparts of CNe as SSSs according to their XMM-Newton EPIC PN spectra. I performed spectral analysis using XSPEC v12.3.1. In spectral models the Tübingen-Boulder ISM absorption model (`TBabs` in XSPEC) was used together with the photoelectric absorption cross-sections from Balucinska-Church & McCammon (1992) and ISM abundances from Wilms et al. (2000). In all cases, the statistical confidence ranges of spectral parameters are 90% unless stated otherwise. For nova counterparts that were only detected in *Chandra* HRC-I observations I computed hardness ratios as outlined above.

Short-term X-ray light curves were extracted for all nova counterparts in each individual observation using the image selection tools `evselect` (XMMSAS) or `dmextract` (CIAO). I always applied a barycentre correction using `barycen` (XMMSAS) or `axbary` (CIAO). These tasks convert times expressed in the local satellite frame to Barycentric Dynamical Time (TDB) whose spatial origin lies at the solar system barycentre. Further correction of XMM-Newton EPIC PN source light curves was done using the XMMSAS task `epiclccorr`, which takes into account effects like bad pixels, chip gaps, vignetting, quantum efficiency or the PSF. For further analysis of the light curves I used the XRONOS tasks of the FTOOLS package. I performed the statistical analysis described in Chap. 6 using the *R* software environment[9].

2.2.3 Optical data reduction and analysis

In order to shorten the time span between the optical observation and a possible discovery of a CN, the raw images and the necessary calibration data are send from the observatory to one of our FTP servers immediately after the end of the observing run. The reduction of these data is done entirely in our group.

The raw images are corrected for effects of dark current and flat field inhomogeneities of the CCD detector using the calibration images. All individual corrected images are then stacked using a median algorithm. This reduction step increases the limiting magnitude of the resulting median image significantly with respect to an individual image. Furthermore, image defects that are only present in a single image (e.g. traces of cosmic particles) are efficiently removed in this way. Some observatories perform the monitoring with dithering pointings (e.g. the Skinakas observatory), in which case the median stacking also removes effects caused by stationary bad pixels of the CCD detector. Both image correction and stacking are carried out with the MaximDL software[10]. The median images are calibrated astrometrically using the Visual PinPoint[11] or Astrometrica[12] software.

In the framework of my dissertation I created an automatic search routine for nova candidates on the stacked images. This routine was based on my experience with optical image analysis I acquired during my diploma thesis, which dealt with the analysis of digitised archival photo plates (see also, Henze et al. 2008e). The routine takes as input the median images created in the previous step. It makes use of the Source Extractor package (Bertin & Arnouts 1996) for object detection, background correction and relative photometry. The photometric calibration was done using the M 31 part of the Local Group Galaxies Survey (LGGS, Massey et al. 2006). Furthermore, the routine searches several optical catalogues of M 31 in order to identify objects that are not present in these catalogues and

[9] http://www.r-project.org
[10] http://www.cyanogen.com/maxim_main.php
[11] http://pinpoint.dc3.com/
[12] http://www.astrometrica.at/

might therefore be nova candidates. These selected objects have to be inspected by eye and compared to reference images. The routine therefore is capable of replacing time-consuming manual blinking of entire optical images with the examination of a number of suggested sources. The vast majority of the nova candidates discovered in the optical monitoring (see Chap. 3.1) were detected by my routine.

The entire optical data analysis typically takes between one and two hours per daily data set and allows for a announcement of new nova candidates in less than a day after the observation. This enables fast follow-up spectroscopy and confirmation of nova candidates.

2.2.4 Analysis of *Swift* ultraviolet data

I analysed the *Swift* UVOT image mode data in the framework of HEAsoft procedures, starting from the pre-processed level 2 sky images. Individual pointings of the same observation were stacked with the help of the `uvotimsum` task. Aperture photometry for known novae in the field of view was performed on the stacked images using the tool `uvotsource`. Short-term light curves (i.e. one measurement for each pointing of an observation) for bright sources were created with the `uvotmaghist` task, in order to search for source variability. The novae that were found in UV are summarised in Chap. 3.2.

Chapter 3

Results of the optical and ultraviolet observations

In this chapter I summarise the results of the optical nova monitoring and of several *Swift* UVOT observations of the M 31 centre that were obtained during the time of the X-ray monitoring. The discoveries or confirmations of nova candidates were immediately published in more than 30 issues of the Astronomer's Telegram (ATel) between October 2007 and August 2010 and distributed by mail to optical observers, to allow spectroscopic optical follow-up observations while the novae were still bright.

3.1 Novae discovered and confirmed in the optical monitoring

The optical monitoring that is supplementing the X-ray observations led to the discovery of 25 nova candidates which were announced in 24 ATels. For 17 of these candidates optical spectra could be obtained, thereby allowing to confirm them as novae and to classify them within the system of Williams (1992). Table 3.1 summarises the discovered nova candidates, names the telescopes that were used, gives references to the individual ATels and notes the nova type if follow-up spectroscopy was carried out.

A highlight discovery was M31N 2008-08b: the first recurrent nova in M 31 with sub-arcsecond position agreement between the two outbursts. Following our discovery alert of the nova candidate in ATel #1654 (see Henze et al. 2008a), Di Mille et al. (2008b) were able to spectroscopically confirm that M31N 2008-08b is a He/N nova in M 31.

Furthermore, observations with a broad Hα filter resulted in the confirmation of 17 nova candidates (see Chap.1.1.2) which were announced in 6 ATels. In Table 3.2 I list these objects together with the observation dates, telescopes used and comments.

Table 3.1: Novae in M 31 discovered in the optical monitoring.

Name M31N	Date [UT]	Telescope	Reference	Spectrum
2007-10a	2007-10-06.10	Super-LOTIS	Pietsch et al. (2007d)	Fe II (Gal-Yam & Quimby 2007)
2007-10b	2007-10-13.26	Super-LOTIS	Burwitz et al. (2007b)	He/N Rau et al. (2007)
2007-11a	2007-11-02.28	Super-LOTIS	Pietsch et al. (2007e)	-
2007-11c	2007-11-13.27	Super-LOTIS	Burwitz et al. (2007a)	Fe II (Ciroi et al. 2007)
2007-12c	2007-12-13.76	La Sagra	Pietsch et al. (2007c)	Fe II (Rau & Cenko 2007)
2007-12d	2007-12-18.19	Super-LOTIS	Henze et al. (2007a)	He/N (Shafter 2007a)
2008-01a	2008-01-20.21	Super-LOTIS	Burwitz et al. (2008a)	-
2008-02a	2008-02-07.17	Super-LOTIS	Henze et al. (2008h)	-
2008-05c	2008-05-26.45	Super-LOTIS	Henze et al. (2008b)	Fe II (Rau et al. 2008)
2008-05d	2008-06-06.47	Super-LOTIS	Henze et al. (2008d)	-
2008-06a	2008-06-14.46	Super-LOTIS	Henze et al. (2008c)	-
2008-06b	2008-06-26.11	La Sagra	Burwitz et al. (2008b)	He/N (Reig et al. 2008)
2008-07a	2008-06-30.45	Skinakas/Super-LOTIS	Henze et al. (2008g)	Fe II (Barsukova et al. 2008)
2008-08a	2008-08-09.96	Skinakas	Henze et al. (2008a)	Fe II (Di Mille et al. 2008b)
2008-08b	2008-08-09.96	Skinakas	Henze et al. (2008a)	He/N (Di Mille et al. 2008b)
2008-10b	2008-10-18.91	Super-LOTIS	Henze et al. (2008f)	Fe II (Di Mille et al. 2008a)
2009-02b	2009-02-20.13	Super-LOTIS	Pietsch et al. (2009b)	-
2009-06b	2009-06-30.05	Athens/Montsec	Pietsch et al. (2009a)	-
2009-08a	2009-08-04.03	Skinakas	Pietsch et al. (2009d)	Fe II (Valeev et al. 2009)
2009-10c	2009-10-09.08	Skinakas	Podigachoski et al. (2009a)	Fe II (Fabrika et al. 2009)
2009-11c	2009-11-06.26	Super-LOTIS	Podigachoski et al. (2009b)	Fe II (Hornoch et al. 2009b)
2009-11d	2009-11-19.19	Super-LOTIS	Podigachoski et al. (2009c)	Fe II (Hornoch et al. 2009a)
2009-11e	2009-11-20.25	Super-LOTIS	Pietsch et al. (2009e)	Fe II (Hornoch & Pejcha 2009)
2010-01a	2010-01-11.13	PIRATE	Burwitz et al. (2010b)	Fe II (Hornoch et al. 2010)
2010-06c	2010-06-26.08	PIRATE	Burwitz et al. (2010a)	-

Table 3.2: Novae in M 31 confirmed by Hα observations.

Name M31N	Date [UT]	Telescope	Reference	Comments
2008-03b	2008-06-13.45	Super-LOTIS	Henze et al. (2008i)	
2008-05a	2008-06-13.48	Super-LOTIS	Henze et al. (2008i)	
2008-05b	2008-05-28.45	Super-LOTIS	Henze et al. (2008i)	
2008-05c	2008-05-28.43	Super-LOTIS	Henze et al. (2008i)	
2008-05d	2008-06-27.48	Super-LOTIS	Henze et al. (2008i)	
2008-06a	2008-06-27.46	Super-LOTIS	Henze et al. (2008i)	
2008-06b	2008-06-27.46	Super-LOTIS	Henze et al. (2008i)	
2008-07a	2009-08-04.04	Skinakas	Pietsch et al. (2009d)	
2008-10b	2008-06-30.45	Skinakas	Henze et al. (2008f)	
2009-02b	2009-08-04.06	Skinakas	Pietsch et al. (2009d)	
2008-05a	2009-08-04.07	Skinakas	Pietsch et al. (2009d)	
2008-05b	2009-08-04.06	Skinakas	Pietsch et al. (2009d)	
2009-08a	2009-08-13.03	Skinakas	Henze et al. (2009a)	
2009-08c	2009-08-13.05	Skinakas	Henze et al. (2009a)	
2009-08d	2009-08-13.08	Skinakas	Henze et al. (2009a)	
2009-10c	2009-10-09.08	Skinakas	Podigachoski et al. (2009a)	discovered in Hα
2009-11b	2009-10-02.10	Skinakas	Henze et al. (2009e)	peculiar object, RN candidate

3.2 *Swift* ultraviolet detections of novae

Using publicly available *Swift* UVOT observations, which partly were requested by our group, several novae in the M 31 central region could be detected as UV sources. In Table 3.3 I list all these novae and the corresponding ATels in which the detection was announced.

Additionally, three novae were detected in three XMM-Newton OM observations (with UV filter) in January/February 2010: M31N 2010-01a, M31N 2010-01b, and M31N 2010-01d, which was discovered in OM data (Pietsch & Henze 2010).

Table 3.3: Novae in M 31 detected in *Swift* UVOT data.

Name M31N	Date [UT]	Reference	Comments
2008-03b	2008-05-26.76	Immler et al. (2008)	
2008-05a	2008-05-26.76	Immler et al. (2008)	
2008-05b	2008-05-26.76	Immler et al. (2008)	
2008-05c	2008-05-26.76	Immler et al. (2008)	
2009-02b	2009-10-22.61	Henze et al. (2009c)	
2009-08a	2009-10-22.61	Henze et al. (2009c)	
2009-08e	2009-10-22.61	Henze et al. (2009c)	
2009-10b	2009-10-22.61	Henze et al. (2009c)	
2009-10c	2009-10-22.61	Henze et al. (2009c)	
2009-11b	2009-10-22.61	Henze et al. (2009e)	possible RN
2009-11e	2009-11-18.67	Pietsch et al. (2009e)	
2010-01a	2010-01-27.05	Pietsch & Henze (2010)	
2010-01d	2010-01-27.05	Pietsch & Henze (2010)	XMM-Newton OM discovery
2010-05a	2010-07-07.07	Henze et al. (2010b)	slow UV evolution
2010-06a	2010-07-07.07	Henze et al. (2010b)	
2010-06d	2010-06-24.02	Pietsch et al. (2010a)	discovered in UV
2010-07a	2010-07-07.07	Henze et al. (2010a)	strongly variable in UV

Chapter 4

Results of the X-ray monitoring

This chapter presents the results of the three X-ray monitoring campaigns of the M 31 central region with XMM-Newton and *Chandra* in 2006/7, 2007/8 and 2008/9 (see Table 2.1). I extensively describe the properties of the detected X-ray counterparts of novae in Chaps. 4.1 and 4.2. A catalogue of all M 31 novae with known X-ray counterparts is introduced in Chap. 4.3. Furthermore, I tabulate upper limits for non-detected X-ray counterparts of M 31 novae in Chap. 4.4 and describe non-nova SSSs found in the monitoring in Chap. 4.5.

In total, there were 21 X-ray counterparts of CNe in M 31 detected in the three monitoring campaigns this dissertation is based on. The positions of these objects are shown in merged images of XMM-Newton (Figs. 4.1 or 4.2) or *Chandra* (Figs. 4.3 or 4.4). X-ray measurements of all detected optical nova counterparts are given in Tables 4.1 and 4.2, whereas Tables 4.4, 4.5, 4.6 and 4.7 present X-ray upper limits for optical nova candidates that were not detected.

The Tables 4.1 – 4.7 contain the following information: the name, coordinates, and outburst date of the optical nova (taken from the online catalogue of PHS2007[1]), the distance between optical and X-ray source (if detected), the X-ray observation and its time lag with respect to the optical outburst, the unabsorbed X-ray luminosity or its upper limit, and comments. I give luminosities for the sources that were detected at least with a 2σ significance in the (0.2–10.0) keV band combining all EPIC instruments. Upper limits are 3σ, determined from the more sensitive EPIC PN camera (see PFF2005) if possible.

Four of the 21 X-ray counterparts (see Table 4.1) had been reported previously in PHS2007 and are still visible at the end of the 2008/9 campaign. Their analysis is described in detail in Chap. 4.1 (see also Table 4.1). They are discussed in Chap. 6.2.2. Seventeen sources were detected in the observations of the campaigns presented here for the first time (see Table 4.2 and detailed description in Chap. 4.2). The X-ray counterpart of M31N 2007-06b, the first nova in a M 31 globular cluster (Henze et al. 2009d), will be examined individually in Chap. 5.

Additionally, there were four SSSs without a nova counterpart detected in the XMM-Newton monitoring data. These sources are described in Chap. 4.5. They are designated in Figs. 4.1 and 4.2 and their light curves are given in Table 4.8.

[1] http://www.mpe.mpg.de/~m31novae/opt/m31/index.php

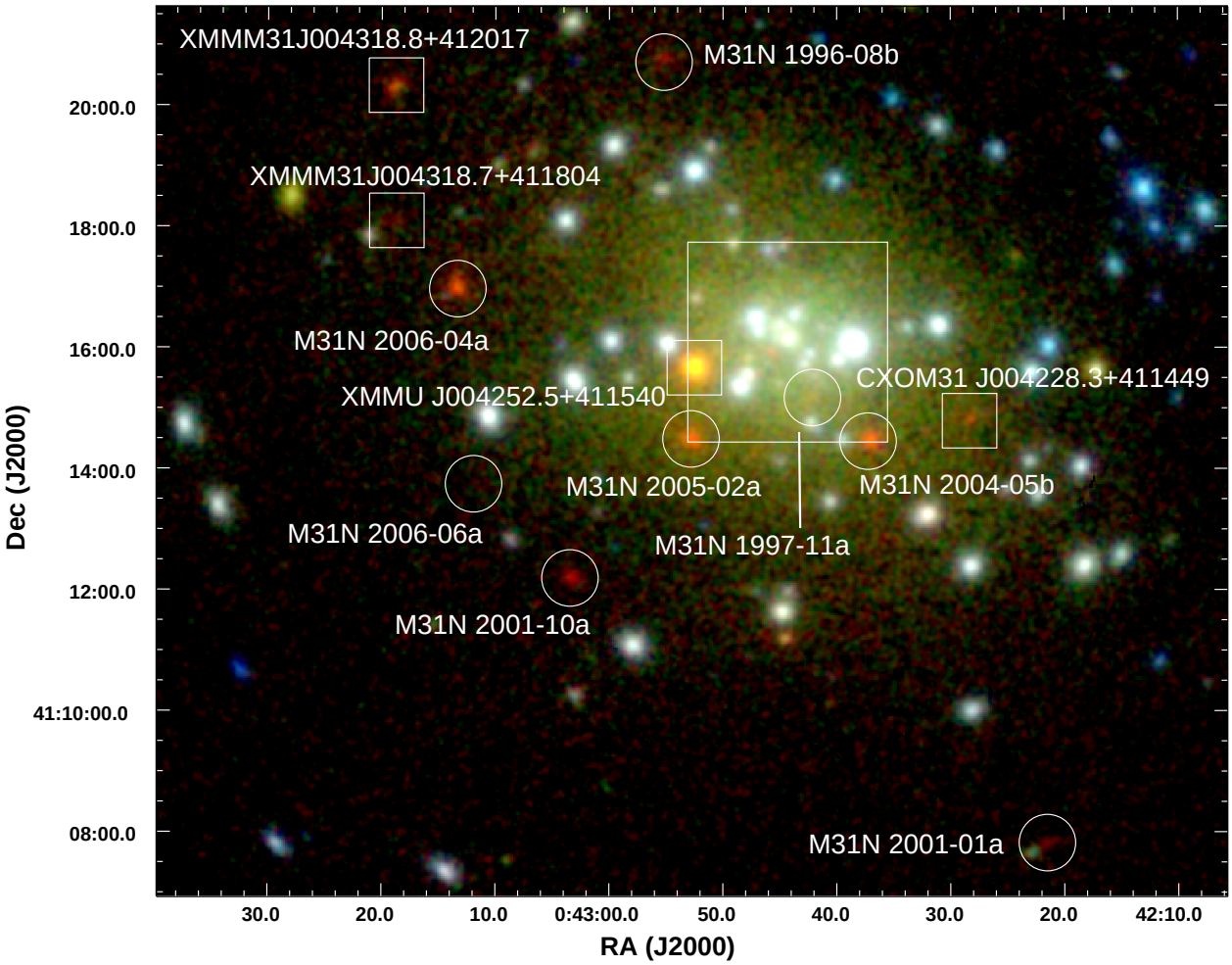

Figure 4.1: Logarithmically-scaled, three colour XMM-Newton EPIC image of the central area of M 31 combining PN, MOS1 and MOS2 data of all five observations of the 2006/7 campaign. Red, green and blue show the (0.2 – 0.5) keV, (0.5 – 1.0) keV and (1.0 – 2.0) keV bands. SSS show up in red. The data in each colour band were binned in 2″x 2″ pixels and smoothed using a Gaussian of FWHM 5″. The counterparts of optical novae detected in this campaign are marked with white circles. For M31N 1997-11a and M31N 2006-06a only the positions are designated, since they are not visible in this image but are detected in *Chandra* images. The four non-nova SSSs detected are marked with white boxes. The large white box includes the central region of M 31 which is shown as a *Chandra* composite in Fig. 4.3.

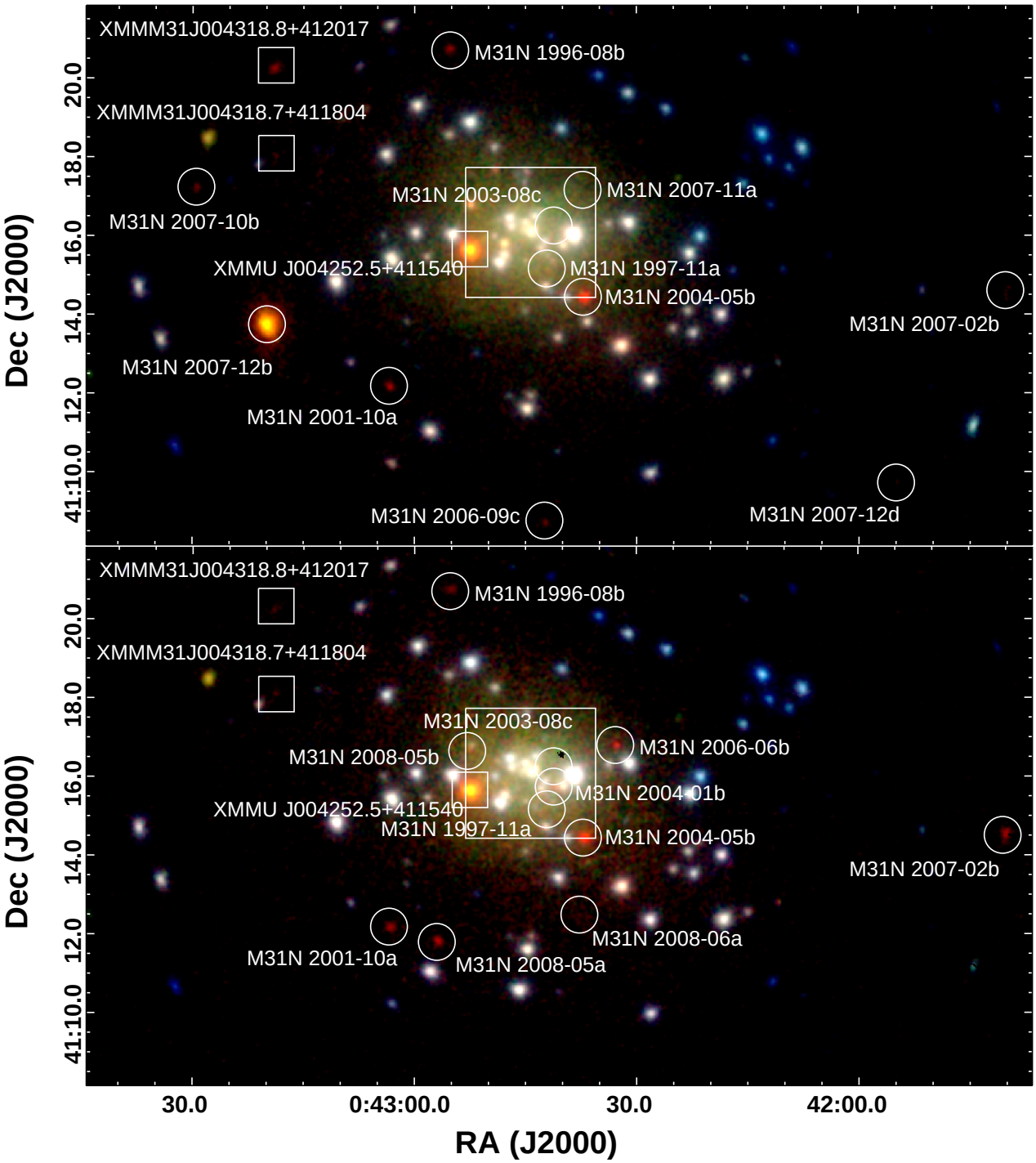

Figure 4.2: Same as Fig. 4.1 for the campaigns 2007/8 (**top panel**) and 2008/9 (**bottom panel**). For M31N 1997-11a, M31N 2003-08c, M31N 2004-01b, M31N 2007-11a, M31N 2008-05b and M31N 2008-06a only the positions are designated, since they are not visible in these images but are detected in *Chandra* images. The large white box includes the central region of M 31 which is shown as a *Chandra* composite in Fig. 4.4.

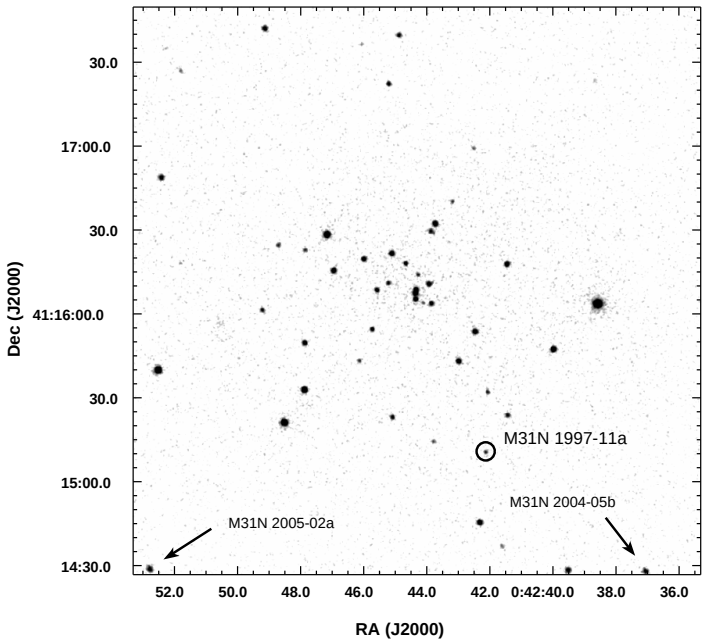

Figure 4.3: Logarithmically-scaled *Chandra* HRC-I image of the innermost $3\farcm3 \times 3\farcm3$ of M 31 combining all observations of the campaign. The image has not been binned (HRC electronic pixel size = $0\farcs13$) but has been smoothed with a Gaussian of FWHM $0\farcs5$. The X-ray counterpart of nova M31N 1997-11a is marked with a black circle. On the lower border of the field of view the X-ray counterparts of novae M31N 2005-02a and M31N 2004-05b can be seen.

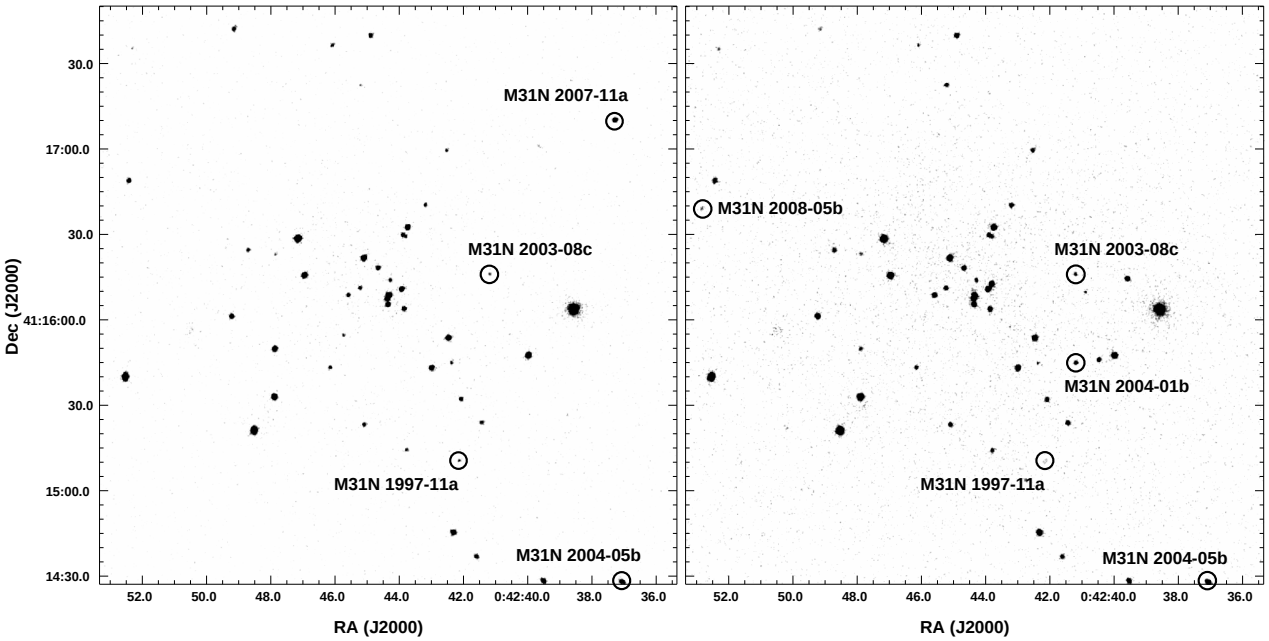

Figure 4.4: Same as Fig. 4.3 for 2007/8 (**left panel**) and 2008/9 (**right panel**). All X-ray counterparts of novae in the field are labelled and marked with black circles.

4.1 Nova counterparts known before this work

From the 14 SSS nova counterparts found by PHS2007, four sources are still visible in the 2006/7 monitoring: M31N 1996-08b, M31N 1997-11a, M31N 2001-10a, and M31N 2004-05b. All of them were visible throughout all three monitoring campaigns and are still detected in February 2009 (see Table 4.1).

Table 4.1: XMM-Newton, *Chandra* and *Swift* measurements of M 31 optical nova candidates known from PHS2007 and still detected here.

Optical nova candidate			X-ray measurements				
Name M31N	RA (h:m:s)[a] Dec (d:m:s)[a]	MJD[b] (d)	D[c] ($''$)	Observation[d] ID	Δt[e] (d)	L_X^f (10^{36} erg s^{-1})	Comment[g]
1996-08b	0:42:55.20	50307.0		7283 (HRC-I)	3584.3	< 6.9	SSS
	41:20:46.0		0.9	0405320501 (EPIC)	3611.6	3.0 ± 0.6	
			1.1	0405320601 (EPIC)	3649.5	2.7 ± 0.7	
				7284 (HRC-I)	3701.9	< 13.0	
				7285 (HRC-I)	3745.3	< 8.6	
				0405320701 (EPIC)	3793.6	< 2.8	
			0.1	0405320801 (EPIC)	3809.5	2.1 ± 0.8	
			1.0	0405320901 (EPIC)	3829.2	2.2 ± 0.5	
				7286 (HRC-I)	3863.6	< 3.7	
			0.8	mrg2 (HRC-I)	4104.6	4.1 ± 0.7	
			1.2	0505720201 (EPIC)	4156.6	2.5 ± 0.5	
			1.3	0505720301 (EPIC)	4166.3	2.4 ± 0.4	
			1.8	0505720401 (EPIC)	4176.6	2.5 ± 0.6	
			0.5	0505720501 (EPIC)	4185.9	2.4 ± 0.7	
			2.2	0505720601 (EPIC)	4196.2	2.8 ± 0.6	
			0.5	mrg3 (HRC-I)	4471.3	3.9 ± 0.6	
			2.3	0551690201 (EPIC)	4523.1	2.3 ± 0.5	
			2.3	0551690301 (EPIC)	4533.3	1.6 ± 0.5	
				0551690401 (EPIC)	4539.9	< 4.7	
				0551690501 (EPIC)	4551.3	< 3.9	
			1.2	0551690601 (EPIC)	4559.6	2.5 ± 1.3	
1997-11a	0:42:42.13	50753.0	0.4	7283 (HRC-I)	3138.3	9.5 ± 1.4	SSS-HR
	41:15:10.5		0.4	7284 (HRC-I)	3255.9	5.0 ± 1.0	
			0.5	7285 (HRC-I)	3299.3	7.8 ± 1.6	
			0.3	7286 (HRC-I)	3417.6	8.1 ± 1.3	
			0.3	8526 (HRC-I)	3658.6	3.5 ± 0.8	
			0.4	8527 (HRC-I)	3668.8	3.4 ± 0.8	
			0.4	8528 (HRC-I)	3679.8	2.3 ± 0.8	
			0.5	8529 (HRC-I)	3688.6	6.0 ± 1.4	
			0.5	8530 (HRC-I)	3698.5	3.0 ± 0.9	
			0.5	mrg3 (HRC-I)	4025.3	0.6 ± 0.2	

Table 4.1: continued.

Optical nova candidate			X-ray measurements				
Name M31N	RA (h:m:s)[a] Dec (d:m:s)[a]	MJD[b] (d)	D[c] ($''$)	Observation[d] ID	Δt[e] (d)	$L_{\rm X}^{f}$ (10^{36} erg s^{-1})	Comment[g]
2001-10a	0:43:03.31	52186.0		7283 (HRC-I)	1705.3	< 3.5	SSS
	41:12:11.5		3.2	0405320501 (EPIC)	1732.6	2.5 ± 0.6	
				0405320601 (EPIC)	1770.5	< 5.1	
			0.5	7284 (HRC-I)	1822.9	7.2 ± 1.5	
			0.6	7285 (HRC-I)	1866.3	11.8 ± 2.0	
			2.0	0405320701 (EPIC)	1914.6	3.9 ± 0.8	
			0.9	0405320801 (EPIC)	1930.5	3.5 ± 0.7	
				0405320901 (EPIC)	1950.2	< 5.2	
			0.9	7286 (HRC-I)	1984.6	7.4 ± 1.6	
			1.1	8526 (HRC-I)	2225.6	13.3 ± 2.2	
			1.0	8527 (HRC-I)	2235.8	10.4 ± 1.9	
			1.5	8528 (HRC-I)	2246.8	9.9 ± 1.9	
			1.9	8529 (HRC-I)	2255.6	9.8 ± 1.9	
				8530 (HRC-I)	2265.5	< 9.8	
			1.0	0505720201 (EPIC)	2277.6	2.6 ± 0.4	
				505720301 (EPIC)	2287.3	< 4.8	
			0.7	0505720401 (EPIC)	2297.6	2.7 ± 0.6	
			1.6	0505720501 (EPIC)	2306.9	3.4 ± 0.9	
			1.8	0505720601 (EPIC)	2317.2	3.6 ± 0.7	
			1.5	9825 (HRC-I)	2592.3	7.0 ± 1.8	
			2.1	9826 (HRC-I)	2601.1	8.1 ± 1.7	
			0.6	9827 (HRC-I)	2612.2	11.3 ± 2.2	
			0.3	9828 (HRC-I)	2621.4	10.8 ± 2.1	
			0.9	9829 (HRC-I)	2632.0	11.9 ± 3.4	
				10838 (HRC-I)	2632.5	< 20.4	
			0.7	0551690201 (EPIC)	2644.1	3.6 ± 0.6	
			1.7	0551690301 (EPIC)	2654.3	3.7 ± 0.7	
				0551690401 (EPIC)	2660.9	< 6.1	
				0551690501 (EPIC)	2672.3	< 4.0	
			1.1	0551690601 (EPIC)	2680.6	3.4 ± 0.9	
			1.4	10683 (HRC-I)	2692.9	7.3 ± 1.7	
				10684 (HRC-I)	2702.2	< 11.8	

Table 4.1: continued.

Optical nova candidate			X-ray measurements				
Name M31N	RA (h:m:s)[a] Dec (d:m:s)[a]	MJD[b] (d)	D[c] ($''$)	Observation[d] ID	Δt[e] (d)	L_X^f[f] (10^{36} erg s^{-1})	Comment[g]
2004-05b	0:42:37.04	53143.0		7283 (HRC-I)	748.3	< 2.5	SSS
	41:14:28.5		1.0	0405320501 (EPIC)	775.6	15.0 ± 1.8	
			1.3	0405320601 (EPIC)	813.5	6.0 ± 0.9	
				00030802001 (XRT)	836.7	3.9 ± 1.2	
				00030804001 (XRT)	846.7	6.0 ± 1.7	
			0.4	7284 (HRC-I)	865.9	25.6 ± 2.3	
			0.3	7285 (HRC-I)	909.3	20.8 ± 2.4	
			0.9	0405320701 (EPIC)	957.6	23.9 ± 1.3	
			1.6	0405320801 (EPIC)	973.5	19.2 ± 1.3	
			1.9	0405320901 (EPIC)	993.2	29.8 ± 1.4	
			0.7	7286 (HRC-I)	1027.6	45.8 ± 5.4	
			0.4	8526 (HRC-I)	1268.6	20.9 ± 2.3	
			0.4	8527 (HRC-I)	1278.8	47.9 ± 6.0	
			0.3	8528 (HRC-I)	1289.8	21.5 ± 2.6	
			0.3	8529 (HRC-I)	1298.6	24.8 ± 2.9	
			0.3	8530 (HRC-I)	1308.5	31.4 ± 3.4	
			1.4	0505720201 (EPIC)	1320.6	21.9 ± 0.9	
			1.2	0505720301 (EPIC)	1330.3	20.0 ± 0.9	
			1.1	0505720401 (EPIC)	1340.6	21.6 ± 1.0	
			1.2	0505720501 (EPIC)	1349.9	21.4 ± 1.3	
			1.0	0505720601 (EPIC)	1360.2	16.7 ± 1.0	
			0.3	9825 (HRC-I)	1635.3	19.5 ± 2.2	
			0.4	9826 (HRC-I)	1644.1	17.9 ± 2.2	
			0.4	9827 (HRC-I)	1655.2	25.4 ± 2.8	
			0.4	9828 (HRC-I)	1664.4	21.3 ± 2.6	
			0.4	9829 (HRC-I)	1675.0	19.9 ± 3.0	
			0.4	10838 (HRC-I)	1675.5	26.6 ± 3.9	
			1.2	0551690201 (EPIC)	1687.1	18.4 ± 1.0	
			0.8	0551690301 (EPIC)	1697.3	16.5 ± 1.0	
			0.6	0551690401 (EPIC)	1703.9	16.7 ± 1.9	
			1.2	0551690501 (EPIC)	1715.3	17.0 ± 1.0	
			0.6	0551690601 (EPIC)	1723.6	16.7 ± 1.2	
			0.7	10683 (HRC-I)	1735.9	33.9 ± 4.2	
			0.5	10684 (HRC-I)	1745.2	36.7 ± 4.6	

Notes: [a]: RA, Dec are given in J2000.0; [b]: Modified Julian Date of optical outburst; MJD = JD - 2 400 000.5; [c]: Distance in arcsec between optical and X-ray source; [d]: mrg1/2/3 (HRC-I/EPIC) indicates merged data of all HRC-I/EPIC observations during 2006/7, 2007/8 or 2008/9, mrg4 (HRC-I) indicate merged data of the *Chandra* observations 9829 and 10838 (taken on the same day) ; [e]: Time after observed start of optical outburst; [f]: unabsorbed luminosity in 0.2–10.0 keV band assuming a 50 eV blackbody spectrum with Galactic foreground absorption (luminosity errors are 1σ, upper limits are 3σ); [g]: SSS or SSS-HR indicate X-ray sources classified as supersoft based on XMM-Newton spectra or *Chandra* hardness ratios, respectively

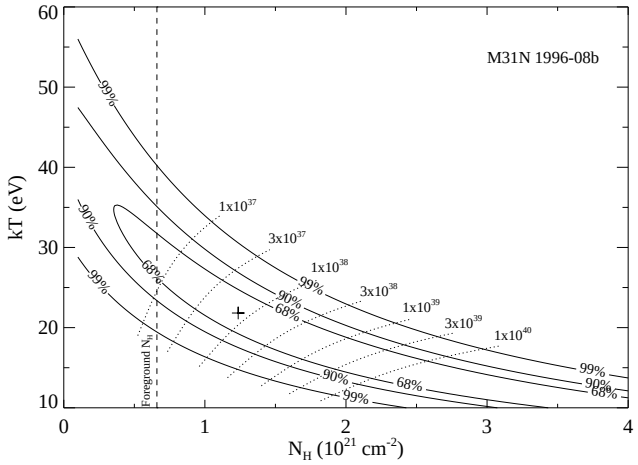

Figure 4.5: Column density ($N_{\rm H}$) - temperature (kT) contours inferred from the fit to the 2006/7 XMM-Newton EPIC PN spectra of M31N 1996-08b. Indicated are the formal best-fit parameters (**cross**), the lines of constant X-ray luminosity (0.2-10.0 keV, **dotted lines**), and the Galactic foreground absorption (**dashed line**).

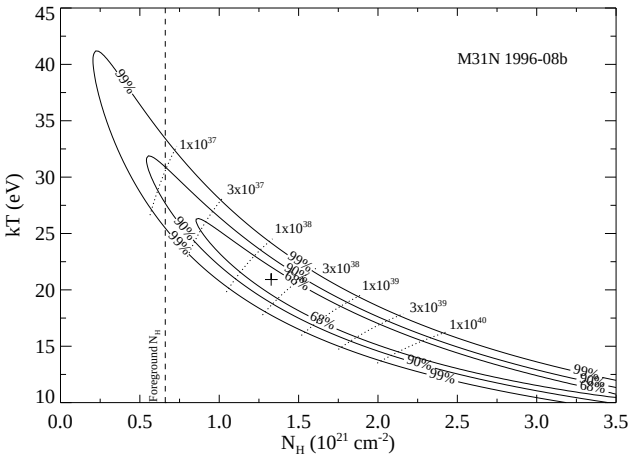

Figure 4.6: Same as Fig. 4.5 for merged spectra of 2007/8 and 2008/9.

M31N 1996-08b

The X-ray counterpart of this nova is still visible 12.5 years after the optical outburst, with an X-ray luminosity that agrees with the luminosity of the last detection in February 2005 (see PHS2007). Merging of all five XMM-Newton EPIC PN observations from 2006/7 allowed me to extract a spectrum of the X-ray source, which was previously only classified by PHS2007 based on hardness-ratios. This spectrum does not show emission above 0.7 keV. Therefore, the object is classified as a SSS. The nominal best-fit parameters (using the C statistic) for an absorbed blackbody model are an effective temperature $kT = 22^{+31}_{-15}$ eV and an absorption $N_{\rm H} = (1.2^{+1.8}_{-1.2}) \times 10^{21}$ cm^{-2}. This results in an unabsorbed 0.2–10.0 keV band luminosity of $L_x = 7.7{\times}10^{37}$ erg s^{-1} and a bolometric luminosity $L_{bol} = 4.4{\times}10^{39}$ erg s^{-1}. Confidence contours for absorption column density and blackbody temperature are shown in Fig. 4.5.

The spectral properties of the source did not change significantly in 2007/8 and 2008/9. In Fig. 4.6 I show the confidence contours of absorption column density and blackbody temperature for a combined spectral fit of all 2007/8 and 2008/9 spectra. Merging these data with the 2006/7 spectra described above, I derived a new best-fit effective temperature $kT = 21^{+8}_{-13}$ eV and an absorption $N_{\rm H} = (1.4^{+1.2}_{-0.8}) \times 10^{21}$ cm^{-2}. The best-fit values for both parameters are almost the same as for 2006/7 alone but the errors are significantly reduced. The X-ray brightness of the source, given in Table 4.1, did not change significantly over the course of the three monitoring campaigns. Discrepancies between XMM-Newton and *Chandra* luminosities are likely to arise due to the differences of the generic spectral model used to compute the luminosities in Table 4.1 and the actual source spectrum (see the energy conversion factors (ECFs) in Table 2.5).

M31N 1997-11a

The X-ray counterpart of this nova is only detected in the *Chandra* HRC-I observations. This is because the object is close to the centre of M 31, which causes source confusion in the XMM-Newton images. This source is still active 11.0 years after the optical outburst.

The X-ray luminosity in 2006/7 increased by about a factor of two with respect to the last detection in February 2005 (see PHS2007). HRC-I hardness ratios, as defined in Chap. 2.2.1, were computed as $\log(S/M) = -0.10 \pm 0.29$ and $\log(M/H) = 0.24 \pm 0.33$, indicating a SSS spectrum. The source was not detected in a 23 ks *Chandra* ACIS-I observation on 2006-12-04.88 UT (ObsID 7064, PI: S. Murray) with an upper limit of 3.2×10^{-4} ct s^{-1}. Compared with an average *Chandra* HRC-I count rate of about 1.4×10^{-3} ct s^{-1}, inferred from the merged HRC-I data of all four 2006/7 observations, this leads to an ACIS-I/HRC-I count rate factor (see Chap. 2.2.1) of about 0.23. Even if we assume a decrease in count rate by a factor of two from average during the ACIS-I observation, which is a stronger variability than the source light curve in Table 4.1 indicates, the ACIS-I/HRC-I factor would still be below 0.5. This is another strong indication of a supersoft spectrum. Therefore, *Chandra* data provide evidence to classify nova M31N 1997-11a as a SSS.

The X-ray light curve of the source showed a decline from an average $L_x = (7.6\pm0.8)\times10^{36}$ erg s^{-1} in 2006/7 through $L_x = (3.2 \pm 0.4)\times10^{36}$ erg s^{-1} in 2007/8 to $L_x = (0.6 \pm 0.2)\times10^{36}$ erg s^{-1} in 2008/9 (see Table 4.1). However, note the increase of luminosity by a factor of two during observation 8529 which is interrupting the overall decline. In the last campaign, 11.0 years after the optical outburst, the source is so faint that it is only detected in the merged *Chandra* data.

M31N 2001-10a

The X-ray counterpart of this nova is still detected 7.4 years after the optical outburst. The average luminosity of the X-ray source increased in 2006/7 by about a factor of two with respect to the average value of PHS2007, but the luminosities of the individual observations during 2006/7 (see Table 4.1) varied by about the same factor. Whereas PHS2007 did not have enough information to constrain the X-ray spectrum of this source, I was now able to classify it as a SSS based on merged EPIC PN spectra of the 2006/7 XMM-Newton observations. A blackbody fit gives best-fit parameters (C statistic) $kT = 14^{+15}_{-8}$ eV and $N_{\rm H} = (1.7^{+1.9}_{-1.7}) \times 10^{21}$ cm^{-2}, resulting in a nominal unabsorbed $L_x = 3.3\times10^{39}$ erg s^{-1} and $L_{bol} = 1.0\times10^{43}$ erg s^{-1}. Figure 4.7 shows the confidence contours for absorption column density and blackbody temperature.

The best-fit parameters for modelling the combined XMM-Newton 2007/8 and 2008/9 spectra are $kT = 14^{+5}_{-8}$ eV and $N_{\rm H} = (2.2 \pm 0.5) \times 10^{21}$ cm^{-2}. These values are not significantly different from the results for the 2006/7 spectra. The best fit $N_{\rm H}$ value is high and leads to X-ray luminosities exceeding the Eddington limit. This is illustrated in the confidence contour plot for the fitted parameters (Fig. 4.8). Fitting these spectra together with the 2006/7 spectra resulted in a slightly better constrained effective temperature of $kT = 14^{+4}_{-7}$ eV.

The X-ray luminosity averaged over the individual monitoring campaigns was constant within the errors at $L_x \sim 2.5\times10^{36}$ erg s^{-1} (XMM-Newton data). The X-ray light curve during the 2007/8 and 2008/9 campaigns did not vary significantly (see Table 4.1). Differences between XMM-Newton and *Chandra* luminosities are again due to the generic spectrum which I used for converting count rates to fluxes and which does not take into account the low source temperature.

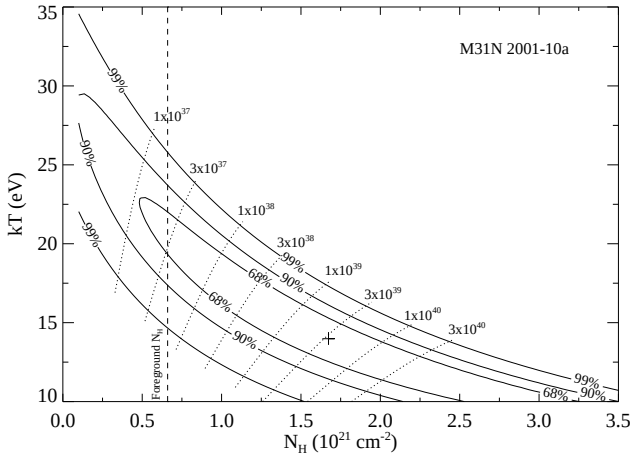

Figure 4.7: Same as Fig. 4.5 for M31N 2001-10a in 2006/7.

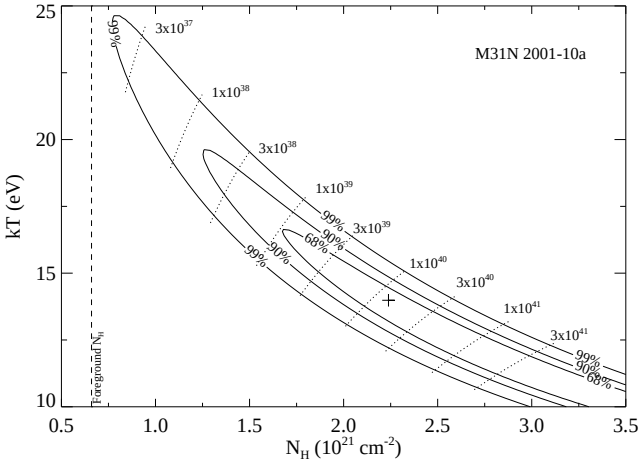

Figure 4.8: Same as Fig. 4.5 for M31N 2001-10a in 2007/8 and 2008/9.

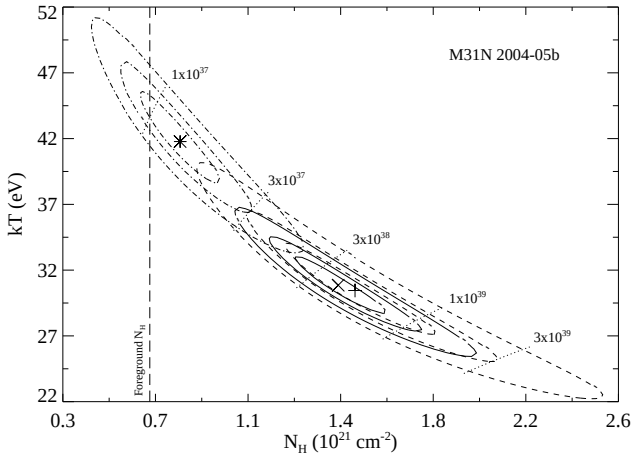

Figure 4.9: Comparison of column density ($N_{\rm H}$) - temperature (kT) contours inferred from the individual fits to the XMM-Newton EPIC PN spectra of M31N 2004-05b for 2006/7 (dashed lines), 2007/8 (solid lines) and 2008/9 (dash dotted lines). Best fit parameters are indicated with a plus sign (2006/7), a cross (2007/8) and an asterisk (2008/9). Further shown are the lines of constant X-ray luminosity (0.2-10.0 keV, dotted lines), and the Galactic foreground absorption (long dashed line).

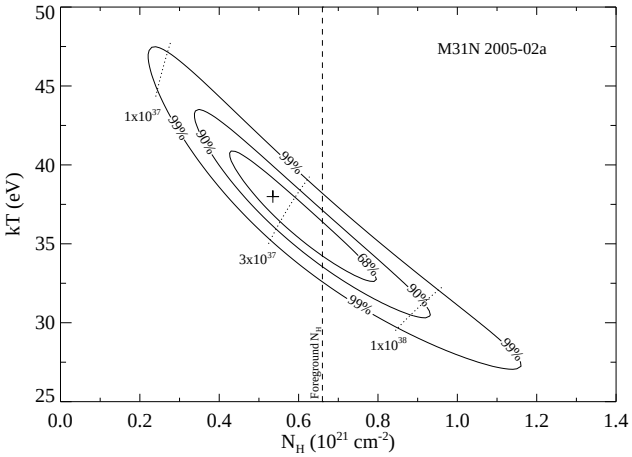

Figure 4.10: Same as Fig. 4.5 for M31N 2005-02a in 2006/7.

M31N 2004-05b

This nova is still detected 4.8 years after the optical outburst. In 2006/7 the average luminosity was slightly higher than in the last observation by PHS2007 in February 2005. It is the only nova counterpart discussed here that was detected in archival *Swift* XRT observations (see Table 2.2).

The X-ray light curve during the 2006/7 campaign showed strong variations by more than a factor of ten (see Table 4.1). For the first time it was possible to perform spectroscopy of this X-ray source, based on the XMM-Newton EPIC PN data of 2006/7. The resulting spectra can be fitted ($\chi^2_r = 1.2$, 44 d.o.f.) with an absorbed blackbody model with best-fit parameters $kT = 30^{+6}_{-5}$ eV and $N_{\rm H} = (1.5^{+0.5}_{-0.4}) \times 10^{21}$ cm^{-2}. Therefore, I classify this source as a SSS based on its PN spectrum. Derived unabsorbed luminosities are $L_x = 4.9{\times}10^{38}$ erg s^{-1} and $L_{bol} = 4.9{\times}10^{39}$ erg s^{-1}.

While the absorbed blackbody fit to the 2007/8 spectrum is still compatible within the errors with the 2006/7 fit, the best-fitting model for the 2008/9 spectrum deviates from the 2007/8 campaign at the 90% confidence level. This distinction is illustrated in Fig. 4.9 and does manifest itself in significantly different best-fit temperature and absorption: 2007/8: $kT = (31 \pm 4)$ eV, $N_{\rm H} = (1.4^{+0.3}_{-0.2}) \times 10^{21}$ cm^{-2}; 2008/9: $kT = (42 \pm 6)$ eV, $N_{\rm H} = (0.8^{+0.3}_{-0.2}) \times 10^{21}$ cm^{-2}. The X-ray light curve of M31N 2004-05b during 2007/8 (see Table 4.1) was relatively stable with a similar luminosity as measured in 2006/7. The 2008/9 luminosities might be slightly lower than those in 2007/8, but the effect is not significant and might be due to the spectral changes that the source is experiencing. Additionally, there was a strong increase in luminosity by a factor of about two in observation 8527, with respect to previous and subsequent observations (see Table 4.1).

4.2 New nova counterparts discovered in this work

During the three monitoring campaigns 17 new X-ray counterparts of novae in M 31 were detected for the first time. The observed light curves of these objects are given in Table 4.2 and plotted in Fig. 4.22 for novae with short turn-on times. All sources are described in detail in the following.

M31N 2001-01a

This nova candidate was discovered in the context of the Wendelstein Calar Alto Pixellensing Project (WeCAPP, Riffeser et al. (2001), see also PHS2007) on 2001-01-19. In X-rays, there is a faint counterpart existing (see Table 4.2), which was only found in the merged XMM-Newton data of 2006/7. It was not detected in any of the single XMM-Newton observations of 2006/7 or 2007/8 and also not in the merged data of 2007/8. I could not construct a source spectrum because of the low count rate and the existence of a neighbouring source (source 258 from Pietsch et al. 2005b). However, the hardness-ratios of the source allow us to classify it as a SSS based on the criterion given in Eq. 2.1 (Chap. 2.2).

I checked the merged *Chandra* HRC-I data used in PHS2007, which combines four archival 50 ks observations, and found the X-ray counterpart present as a very faint object ($L_x = (1.8 \pm 0.6) \times 10^{36}$ erg s^{-1}) with a detection significance of about 3σ. Of all the individual pointings the source is only detected with 2σ significance in observation 5925 (2004-12-06) at a similar luminosity as in the merged data. This observation was carried out 1387 days after the optical nova outburst. I assume this time as an upper limit for the turn-on time of the X-ray counterpart for Table 4.3. The turn-off time was estimated to 2426 ± 109 days which is between the last XMM-Newton observation of 2006/7 and the first XMM-Newton observation of 2007/8.

Table 4.2: M 31 optical novae with XMM-Newton and *Chandra* counterparts discovered in this work.

Optical nova candidate			X-ray measurements				
Name M31N	RA (h:m:s)[a] Dec (d:m:s)[a]	MJD[b] (d)	D^c ($''$)	Observation[d] ID	Δt^e (d)	L_X^f (10^{36} erg s^{-1})	Comment[g]
2001-01a	0:42:21.49	51928.8		mrg (HRC-I)	1962.5	< 7.3	SSS-HR
	41:07:47.4		2.5	mrg (EPIC)	1989.9	2.4 ± 0.5	
				mrg1 (HRC-I)	2482.9	< 1.5	
				mrg1 (EPIC)	2534.8	< 0.6	
2003-08c	0:42:41.20	52878.0		7286 (HRC-I)	1292.6	< 0.8	
	41:16:16.0			8526 (HRC-I)	1533.6	< 2.1	
			0.4	8527 (HRC-I)	1543.8	3.5 ± 0.7	
				8528 (HRC-I)	1554.8	< 3.3	
				8529 (HRC-I)	1563.6	2.6 ± 0.8	
			0.3	8530 (HRC-I)	1573.5	3.6 ± 0.8	
				mrg2 (EPIC)	1585.6	< 11.3	
				9825 (HRC-I)	1900.3	< 0.8	
			0.5	9826 (HRC-I)	1909.1	5.3 ± 1.1	
			0.3	9827 (HRC-I)	1920.2	4.7 ± 1.0	
			0.3	9828 (HRC-I)	1929.4	5.5 ± 1.1	
				9829 (HRC-I)	1940.0	< 6.2	
				10838 (HRC-I)	1940.5	< 5.0	
				mrg3 (EPIC)	1952.1	< 7.0	
				10683 (HRC-I)	2000.9	< 3.2	
			0.2	10684 (HRC-I)	2010.2	2.7 ± 0.8	
2004-01b	0:42:41.19	53005.8		8530 (HRC-I)	1445.7	< 1.6	
	41:15:45.0		0.4	9825 (HRC-I)	1772.6	5.0 ± 1.1	
			0.2	9826 (HRC-I)	1781.4	5.9 ± 1.2	
			0.4	9827 (HRC-I)	1792.5	5.1 ± 1.1	
			0.3	9828 (HRC-I)	1801.7	5.8 ± 1.3	
			0.4	9829 (HRC-I)	1812.3	5.7 ± 1.3	
			0.2	10838 (HRC-I)	1812.7	7.1 ± 1.5	
				mrg3 (EPIC)	1824.4	< 22.3	
			0.1	10683 (HRC-I)	1873.1	11.1 ± 1.6	
			0.1	10684 (HRC-I)	1882.4	8.7 ± 1.7	
2005-02a	0:42:52.79	53419.8	0.1	7283 (HRC-I)	471.5	13.2 ± 1.7	SSS
	41:14:28.9		0.1	405320501 (EPIC)	498.9	17.6 ± 1.2	
			0.4	405320601 (EPIC)	536.8	28.4 ± 1.6	
			0.4	7284 (HRC-I)	589.1	30.2 ± 2.8	
			0.4	7285 (HRC-I)	632.5	56.4 ± 4.9	
				7064 (ACIS-I)	654.2	18.9 ± 6.6	
			1.2	405320701 (EPIC)	680.9	20.3 ± 1.3	
			1.1	405320801 (EPIC)	696.7	18.6 ± 1.3	
			0.8	405320901 (EPIC)	716.4	8.9 ± 0.9	
			0.6	7286 (HRC-I)	750.9	23.3 ± 3.9	
				mrg2 (HRC-I)	991.9	< 0.5	
				mrg2 (EPIC)	1043.8	< 1.8	

Table 4.2: continued.

Optical nova candidate			X-ray measurements				
Name M31N	RA (h:m:s)[a] Dec (d:m:s)[a]	MJD[b] (d)	D^c ($''$)	Observation[d] ID	Δt^e (d)	L_X^f (10^{36} erg s^{-1})	Comment[g]
2006-04a	0:43:13.42	53851.2		7283 (HRC-I)	40.0	< 0.6	SSS,
	41:16:58.9			0405320501 (EPIC)	67.4	< 0.3	short-term
			1.0	0405320601 (EPIC)	105.3	48.9 ± 2.0	variable
				7284 (HRC-I)	157.6	< 2.0	
				7285 (HRC-I)	201.0	< 7.0	
				0405320701 (EPIC)	249.4	< 1.2	
				0405320801 (EPIC)	265.2	< 0.5	
				0405320901 (EPIC)	284.9	< 1.5	
				7286 (HRC-I)	319.4	< 1.7	
2006-06a	0:43:11.81	53877.0		7283 (HRC-I)	14.3	< 0.7	SSS
	41:13:44.7			0405320501 (EPIC)	41.6	< 1.4	candidate
				0405320601 (EPIC)	79.5	< 1.5	
			0.7	7284 (HRC-I)	131.9	7.5 ± 1.8	
			0.5	7285 (HRC-I)	175.3	10.3 ± 2.1	
				0405320701 (EPIC)	223.6	< 1.8	
				0405320801 (EPIC)	239.5	< 1.6	
				0405320901 (EPIC)	259.2	< 1.7	
				7286 (HRC-I)	293.6	< 6.2	
2006-06b	0:42:32.77	53869.0		0505720601 (EPIC)	634.2	< 1.8	
	41:16:49.2		0.4	9825 (HRC-I)	909.3	3.3 ± 0.7	
				9826 (HRC-I)	918.1	< 2.6	
			0.5	9827 (HRC-I)	929.2	1.9 ± 0.6	SSS
			0.3	9828 (HRC-I)	938.4	2.8 ± 0.6	
			0.1	9829 (HRC-I)	949.0	3.3 ± 1.2	
				10838 (HRC-I)	949.5	< 3.3	
			0.9	0551690201 (EPIC)	961.1	3.3 ± 0.5	
			0.3	0551690301 (EPIC)	971.3	2.9 ± 0.5	
				0551690401 (EPIC)	977.9	< 5.8	
			0.3	0551690501 (EPIC)	989.3	4.4 ± 0.6	
			0.8	0551690601 (EPIC)	997.6	4.0 ± 0.9	
			0.1	10683 (HRC-I)	1009.9	10.9 ± 1.7	
			0.2	10684 (HRC-I)	1019.2	7.2 ± 1.4	
2006-09c	0:42:42.38	53996.2		8526 (HRC-I)	415.4	< 4.5	SSS
	41:08:45.5			8527 (HRC-I)	425.5	4.2 ± 1.6	
				8528 (HRC-I)	436.5	5.1 ± 2.0	
				8529 (HRC-I)	445.3	< 5.3	
				8530 (HRC-I)	455.2	< 7.2	
			1.2	505720201 (EPIC)	467.3	2.5 ± 0.6	
			0.5	505720301 (EPIC)	477.0	1.6 ± 0.6	
			1.0	505720401 (EPIC)	487.4	2.8 ± 0.8	
				505720501 (EPIC)	496.7	< 2.7	
				505720601 (EPIC)	507.0	< 1.9	
				mrg3 (EPIC)	833.9	< 0.3	

Table 4.2: continued.

Optical nova candidate			X-ray measurements				
Name M31N	RA (h:m:s)[a] Dec (d:m:s)[a]	MJD[b] (d)	D^c ($''$)	Observation[d] ID	Δt^e (d)	L_X^f (10^{36} erg s^{-1})	Comment[g]
2007-02b	0:41:40.32	54134.8	1.0	0505720401 (EPIC)	348.9	1.8 ± 0.7	SSS
	41:14:33.5			0505720501 (EPIC)	358.2	< 5.6	
			0.5	0505720601 (EPIC)	368.5	6.2 ± 1.1	
			0.7	0551690201 (EPIC)	695.4	17.4 ± 5.3	
			1.3	0551690301 (EPIC)	705.5	17.5 ± 5.4	
			3.0	0551690401 (EPIC)	712.1	9.7 ± 3.0	
			0.2	0551690501 (EPIC)	723.6	9.7 ± 1.2	
			1.2	0551690601 (EPIC)	731.8	10.5 ± 1.8	
2007-06b	0:42:33.14	54270.0	9.4	8526 (HRC-I)	141.6	73.6 ± 16.6	SSS
	41:00:25.9		1.2	8527 (HRC-I)	151.8	72.4 ± 9.9	
			9.7	8528 (HRC-I)	162.8	80.9 ± 10.5	
			0.6	8529 (HRC-I)	171.6	88.0 ± 11.5	
			5.9	8530 (HRC-I)	181.5	96.7 ± 12.0	
				mrg3 (HRC-I)	508.3	< 14.5	
2007-10b	0:43:29.48	54386.2	1.2	8526 (HRC-I)	25.4	31.5 ± 4.4	SSS
	41:17:13.5		2.4	8527 (HRC-I)	35.5	24.2 ± 4.0	
			2.5	8528 (HRC-I)	46.5	16.7 ± 3.4	
				8529 (HRC-I)	55.3	< 10.1	
				8530 (HRC-I)	65.2	8.4 ± 3.0	
			1.8	0505720201 (EPIC)	77.3	5.0 ± 0.7	
			1.0	0505720301 (EPIC)	87.0	3.5 ± 0.7	
				0505720401 (EPIC)	97.4	< 2.3	
				0505720501 (EPIC)	106.7	< 2.1	
				0505720601 (EPIC)	117.0	< 0.6	
2007-11a	0:42:37.29	54406.2		8526 (HRC-I)	5.4	< 1.3	SSS-HR
	41:17:10.3		0.4	8527 (HRC-I)	15.5	65.5 ± 4.3	
			0.3	8528 (HRC-I)	26.5	16.1 ± 1.8	
			0.2	8529 (HRC-I)	35.3	17.7 ± 1.9	
			0.2	8530 (HRC-I)	45.2	11.2 ± 1.6	
				0505720201 (EPIC)	57.3	< 1.1	
				0505720301 (EPIC)	67.0	< 2.3	
				0505720401 (EPIC)	77.4	< 2.6	
				0505720501 (EPIC)	86.7	< 1.9	
				0505720601 (EPIC)	97.0	< 3.2	
2007-12b	0:43:19.94	54443.5		8530 (HRC-I)	8.0	< 3.5	SSS
	41:13:46.6			0505720201 (EPIC)	20.1	< 2.1	
			0.8	0505720301 (EPIC)	29.8	241.1 ± 3.1	
			0.8	0505720401 (EPIC)	40.1	335.8 ± 3.8	
			0.7	0505720501 (EPIC)	49.4	326.0 ± 5.2	
			0.6	0505720601 (EPIC)	59.8	222.5 ± 3.8	
				mrg3 (HRC-I)	334.8	< 1.3	
				mrg3 (EPIC)	386.6	< 0.2	

Table 4.2: continued.

Optical nova candidate			X-ray measurements				
Name M31N	RA (h:m:s)[a] Dec (d:m:s)[a]	MJD[b] (d)	D^c ($''$)	Observation[d] ID	Δt^e (d)	$L_{\rm X}^f$ (10^{36} erg s^{-1})	Comment[g]
2007-12d	0:41:54.96	54451.5		0505720201 (EPIC)	12.1	< 1.3	SSS-HR
	41:09:47.3		0.9	0505720301 (EPIC)	21.8	2.8 ± 0.8	
				0505720401 (EPIC)	32.1	< 1.6	
				0505720501 (EPIC)	41.4	< 0.5	
				0505720601 (EPIC)	51.8	< 1.3	
2008-05a	0:42:56.84	54600.8		9825 (HRC-I)	177.6	< 4.4	SSS
	41:11:52.4			9826 (HRC-I)	186.4	< 4.9	
			0.4	9827 (HRC-I)	197.5	7.3 ± 1.8	
				9828 (HRC-I)	206.7	3.5 ± 1.5	
				9829 (HRC-I)	217.3	< 5.7	
				10838 (HRC-I)	217.7	5.8 ± 2.5	
				0551690201 (EPIC)	229.4	< 1.9	
				0551690301 (EPIC)	239.5	< 3.3	
				0551690401 (EPIC)	246.1	< 4.2	
			0.6	0551690501 (EPIC)	257.6	3.5 ± 0.6	
			1.1	0551690601 (EPIC)	265.8	8.3 ± 1.3	
			0.4	10683 (HRC-I)	278.1	11.1 ± 1.9	
				10684 (HRC-I)	287.4	5.3 ± 1.8	
2008-05b	0:42:52.88	54608.8		9825 (HRC-I)	169.6	< 5.1	
	41:16:39.4			9826 (HRC-I)	178.4	< 5.5	
			1.4	9827 (HRC-I)	189.5	3.5 ± 0.9	
			1.0	9828 (HRC-I)	198.7	4.9 ± 1.3	
				mrg4 (HRC-I)	209.3	3.6 ± 1.1	
				mrg3 (EPIC)	221.4	< 3.2	
				10683 (HRC-I)	270.1	< 1.7	
				10684 (HRC-I)	279.4	< 2.3	
2008-06a	0:42:37.72	54631.5		9825 (HRC-I)	146.8	< 1.1	
	41:12:30.0			10838 (HRC-I)	187.0	< 2.8	
				0551690201 (EPIC)	198.6	< 0.2	
				0551690301 (EPIC)	208.8	< 3.3	
				0551690401 (EPIC)	215.4	< 1.6	
				0551690501 (EPIC)	226.8	< 1.6	
				0551690601 (EPIC)	235.1	< 2.3	
				10683 (HRC-I)	247.4	< 4.9	
			0.7	10684 (HRC-I)	256.7	3.2 ± 1.3	

Notes: As for Table 4.1.

M31N 2003-08c

The optical nova was discovered by Fiaschi et al. (2003) on 2003-10-16 and spectroscopically confirmed by di Mille et al. (2003). A faint ($L_x \sim 3.5 \times 10^{36}$ erg s^{-1}) X-ray counterpart first showed up in the *Chandra* observations of 2007/8 (see Table 4.2). Nothing was detected at this position in the last *Chandra* observations of 2006/7. Owing to the position of the source close to the M 31 centre, the XMM-Newton data suffered from source confusion and could only provide luminosity upper limits that are larger than the luminosities inferred from *Chandra*. For Table 4.3 I adopted as the turn-on time of the source the midpoint between the last observation from 2006/7 and the first *Chandra* observation in 2007/8. The luminosity of the object varied by at least a factor of two over the course of the 2007/8 and 2008/9 campaigns. The source was still detected in the last observation of 2008/9.

M31N 2004-01b

The optical nova candidate was discovered in the WeCAPP survey (Riffeser et al. 2001) on 2004-01-01 (see also PHS2007). An X-ray counterpart with an average luminosity $L_x = (6.1 \pm 0.5) \times 10^{36}$ erg s^{-1} was found in the *Chandra* data of 2008/9. This object was not detected in the *Chandra* data of the 2007/8 campaign with an upper limit of $L_x < 1.6 \times 10^{36}$ erg s^{-1} in observation 8530 (see Table 4.2). The turn-on time of the source given in Table 4.3 was assumed to be the midpoint between the observations 8530 and 9825. The source is situated close to the M 31 centre, therefore source confusion prevented detection with XMM-Newton. Towards the end of the 2008/9 campaign the luminosity of the source increased significantly up to $L_x = (11.1 \pm 1.6) \times 10^{36}$ erg s^{-1} in the second last *Chandra* observation.

M31N 2005-02a

This nova candidate was discovered in the WeCAPP survey (Riffeser et al. 2001) on 2005-02-18. An X-ray counterpart was detected in the first *Chandra* observation of 2006/7, 472 days after the optical outburst. The source was visible for the entire campaign, until 751 days after the optical outburst. It is the only nova counterpart discussed here that is visible in one of the archival *Chandra* ACIS-I observations listed in Table 2.2. The 23 ks observation 7064 contains about seven (supersoft) source counts, implying a luminosity compatible with the subsequent XMM-Newton observation (see Table 4.2).

The combined XMM-Newton EPIC PN spectra can be fitted ($\chi^2_r = 1.2$, 26 d.o.f.) with an absorbed blackbody model with best-fit parameters $kT = 38^{+6}_{-8}$ eV and $N_{\rm H} = (0.5^{+0.4}_{-0.2}) \times 10^{21}$ cm^{-2}. Therefore, I classify this source as a SSS based on its PN spectrum. Note that the formal best-fit $N_{\rm H}$ is smaller than the Galactic foreground absorption of $\sim 6.7 \times 10^{20}$ cm^{-2} (but still compatible with it within the errors). From the best-fit parameters I derive an unabsorbed luminosity for the 0.2–10.0 keV band of $L_x = 2.6 \times 10^{37}$ erg s^{-1} and a bolometric luminosity $L_{bol} = 1.2 \times 10^{38}$ erg s^{-1}. Confidence contours for absorption column density and blackbody temperature are shown in Fig. 4.10.

M31N 2006-04a

The optical nova candidate was detected independently in the context of our optical monitoring of M 31 (with the Bradford Robotic Telescope Galaxy at the Tenerife Observatory; see Pietsch et al. 2006b) and by Itagaki[2]. The discovery was on 2006-04-26, shortly after the M 31 visibility window opened again.

[2] see http://www.cfa.harvard.edu/iau/CBAT_M31.html#2006-04a

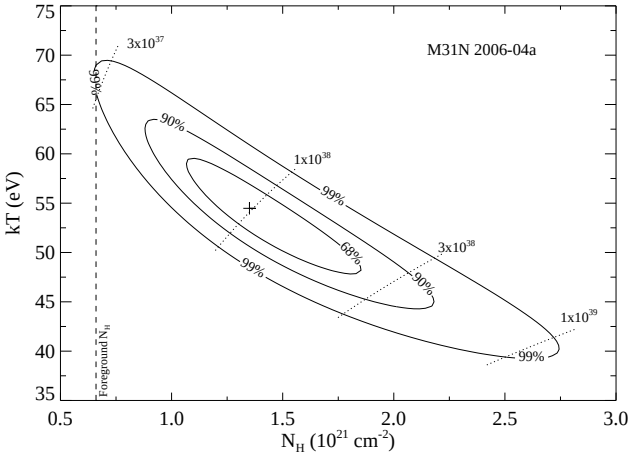

Figure 4.11: Same as Fig. 4.5 for M31N 2006-04a in 2006/7.

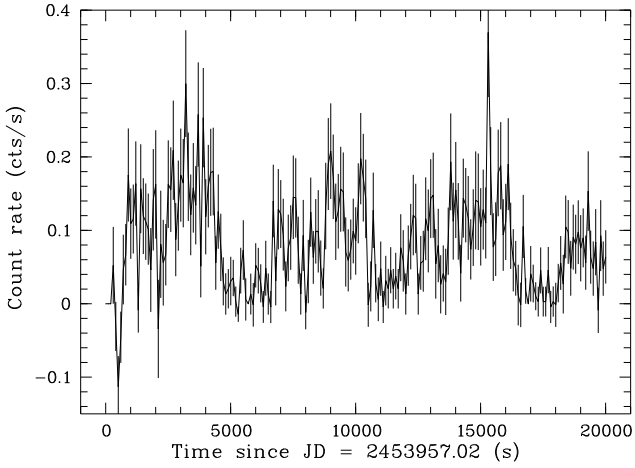

Figure 4.12: Exposure and barycentre corrected short-term X-ray light curve of M31N 2006-04a (0.2 – 1.0 keV, 100s binning) with superimposed count rate error bars.

The X-ray counterpart was only detected in a single XMM-Newton observation 105 days after the first optical detection (see Table 4.2). In the *Swift* observation 00030802001, 23 days later (128 days after outburst, see Table 2.2), the source was not detected, but its position was close to the edge of the XRT field of view. The field of view of the second *Swift* observation, 10 days later, was slightly shifted and did not contain the nova position at all. From 2 or 3 photons visible in the observation on day 128 I computed a luminosity upper limit of $2.5{\times}10^{37}$ erg s^{-1}, assuming a 50 eV blackbody spectrum with Galactic foreground absorption. As this is well above the luminosity detected from other novae in this work, the upper limit does not tell us if the SSS phase of the nova already ended at this day. I therefore decided not to include this measurement in my analysis. I show the X-ray light curve in Fig. 4.22.

The XMM-Newton EPIC PN spectrum of the source can be fitted (C statistic) with an absorbed blackbody with best-fit parameters $kT = 54^{+9}_{-10}$ eV and $N_{\rm H} = (1.3^{+0.8}_{-0.5}) \times 10^{21}$ cm^{-2}, allowing me to classify it as a SSS. This fit implies unabsorbed luminosities $L_x = 1.0{\times}10^{38}$ erg s^{-1} and $L_{bol} = 2.1{\times}10^{38}$ erg s^{-1}. Figure 4.11 shows the confidence contours for absorption column density and blackbody temperature.

The XMM-Newton EPIC PN light curve of M31N 2006-04a during observation 0405320601, presented in Fig. 4.12, shows variability. A frequency analysis of the light curve, which I performed by the means of a fast Fourier transformation (FFT) with the FTOOLS task `powspec`, yielded a significant peak in the power spectrum towards lower frequencies. Using the FTOOLS periodicity search algorithm `efsearch`, I determined a possible period of 5900 ± 900 s (1.6 ± 0.3 h). Note, that this is about one third of the duration of the entire observation (20 ks). I therefore cannot place stronger constraints on the suspected periodicity.

On the basis of the light curve I defined high- and low-luminosity states for nova M31N 2006-04a, with the border between the two regimes being at $\sim$ 0.15 cts s^{-1} (see Fig. 4.12). In Fig. 4.13 I show the confidence contour plot for individual absorbed blackbody fits to both states. The plot illustrates that the models differ at the 90% confidence level, which might indicate a variation in source temperature between the two states. However, the 99% confidence contours already overlap. The model-independent hardness ratio (0.2–0.5 vs. 0.5–0.8 keV band) supports a difference between

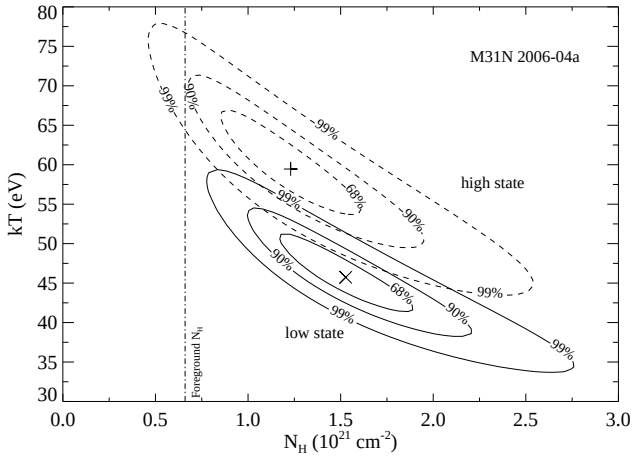

Figure 4.13: Same as Fig. 4.5 for the high- and low-luminosity states of M31N 2006-04a (**dashed** and **solid** lines) in 2006/7. Indicated are the formal best-fit parameters (**plus sign**/**cross** for high/low luminosity) and the Galactic foreground absorption (**dash-dotted line**).

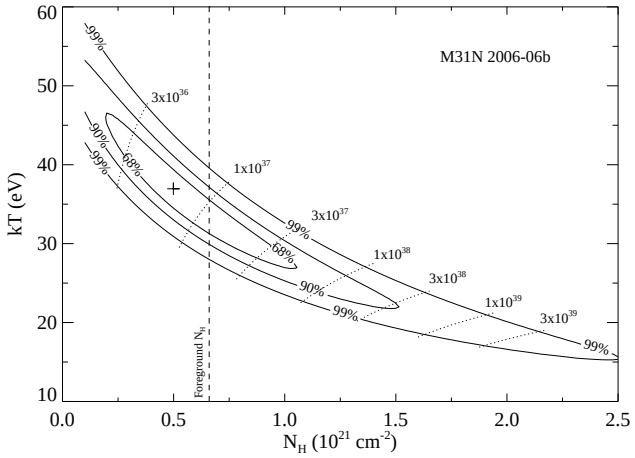

Figure 4.14: Same as Fig. 4.5 for M31N 2006-06b in 2008/9.

the two states only on the 68% level, therefore, this analysis does not provide strong evidence for an actually variable source temperature. This caveat holds more strongly because blackbody models are only a first approximation to SSS spectra. The variability of M31N 2006-04a could also have been caused by variable absorption features that are not taken into consideration in our models. An example for this kind of behaviour can be found in Ness et al. (2007b), who used a changing optical depth of the O I absorption edge to explain variability in the SSS counterpart of the Galactic nova RS Oph.

M31N 2006-06a

This nova candidate was discovered by Lang et al. (2006) on 2006-05-22 and classified as a Fe II nova by Pietsch et al. (2006a). An X-ray counterpart was found in *Chandra* observations of 2006/7 on day 140 and 175 after the optical outburst. The X-ray light curve is shown in Fig. 4.22. The source was not detected in a 4.1 ks *Chandra* ACIS-I observation on 2006-09-24.76 UT (ObsID 7140, PI: M. Garcia) with an upper limit of 1.1×10^{-3} ct s^{-1}. Assuming that the source did not change its X-ray spectrum and brightness between this observation, which is 126 days after the optical outburst, and the HRC-I observation 7284 only six days later, I derive an ACIS-I/HRC-I count rate factor upper limit of about 0.8. This value is larger than 0.5 and therefore does not allow a SSS classification. However, the HRC-I hardness ratios $\log(S/M) = -0.13 \pm 0.33$ and $\log(M/H) = 0.37 \pm 0.48$ are indicating a soft spectrum. Therefore, I classify the source as a candidate SSS based on *Chandra* HRC-I data.

M31N 2006-06b

The optical nova candidate was discovered independently by Ries & Riffeser (2006) and Hornoch[3] on 2006-06-06. Both authors report evidence pointing towards a slowly rising nova. An X-ray counterpart was detected in the first 2008/9 observation. Nothing was found at this position in the 2007/8

[3] see http://www.cfa.harvard.edu/iau/CBAT_M31.html#2006-06b

campaign, with an upper limit of $L_x < 1.6 \times 10^{36}$ erg s^{-1} in XMM-Newton observation 0505720601 (see Table 4.2). The source was visible in XMM-Newton and *Chandra* data until the end of the 2008/9 campaign with an average luminosity $L_x = (3.6 \pm 0.3) \times 10^{36}$ erg s^{-1} in *Chandra* data. The source luminosity was increasing significantly during the time span of the monitoring. The turn-on time given in Table 4.3 is estimated as the midpoint between the observations 0505720601 and 9825.

I fitted the XMM-Newton EPIC PN spectrum of the nova counterpart with an absorbed blackbody model with best-fit parameters $kT = 37^{+17}_{-15}$ eV and $N_{\rm H} = (0.5^{+0.9}_{-0.2}) \times 10^{21}$ cm^{-2}. The resulting confidence contours for absorption column density and blackbody temperature are shown in Fig. 4.14. This source can clearly be classified as a SSS.

M31N 2006-09c

The optical nova was discovered independently by Itagaki[4] and Quimby (2006a) on 2006-09-18. Shafter et al. (2006) classified it as a Fe II nova. A faint ($L_x \lesssim 4.0 \times 10^{36}$ erg s^{-1}) X-ray counterpart was detected in the second *Chandra* observation of 2007/8 (see Table 4.2). However, the preceding *Chandra* observation only provided an upper limit that was larger than the detection luminosity. Therefore, it is not known if the source was already active on a similar level during this observation. From the upper limits measured in 2006/7, I deduced that the source was not detected 140 days after optical outburst with an upper limit of $L_x < 0.9 \times 10^{36}$ erg s^{-1}. The turn-on time given in Table 4.3 is estimated as the midpoint between day 140 and the first *Chandra* observation of the 2007/8 campaign. Similarly, due to the faintness of the source it was not clear if the non-detections in the last two XMM-Newton observations of 2007/8 correspond to the X-ray turn off of the source. For Table 4.3 I therefore estimated the actual turn off of the source to have occurred in between the last 2007/8 and the first 2008/9 observation of XMM-Newton.

The combined XMM-Newton EPIC PN spectra of the X-ray counterpart can be fitted with an absorbed blackbody model with best-fit parameters $kT = 74^{+20}_{-24}$ eV and $N_{\rm H} = (0.2^{+0.8}_{-0.2}) \times 10^{21}$ cm^{-2}, which classify this source as a SSS. Confidence contours for absorption column density and blackbody temperature are shown in Fig. 4.15.

M31N 2007-02b

The optical nova was discovered by Hornoch[5] on 2007-02-03. It was spectroscopically confirmed by Pietsch et al. (2007a) and Shafter[6] who classified it as hybrid nova and Fe II nova respectively.

An X-ray counterpart was detected in the third XMM-Newton observation of 2007/8 (see Table 4.2). However, the source was right on the edge of the XMM-Newton field of view in this observation and its position was not covered in the first two 2007/8 observations due to the changing roll angle during the monitoring. The large distance of the nova from the M 31 centre might also have been the reason for its non-detection by *Chandra* in 2007/8 and 2008/9. This is because the *Chandra* PSF strongly degrades towards high off-axis angles, an effect which decreases the detection sensitivity significantly. I therefore assume that the source was active from the third 2007/8 observation until at least the last 2008/9 observation of XMM-Newton. The source luminosity significantly increased from one campaign to the next (see Table 4.2).

The XMM-Newton EPIC PN spectra of 2007/8 and 2008/9 could be fitted with absorbed black body models, the parameters of which were in agreement within the errors. I therefore performed

[4] see http://www.cfa.harvard.edu/iau/CBAT_M31.html#2006-09c
[5] see http://www.cfa.harvard.edu/iau/CBAT_M31.html#2007-02b
[6] see http://mintaka.sdsu.edu/faculty/shafter/extragalactic_novae/HET/

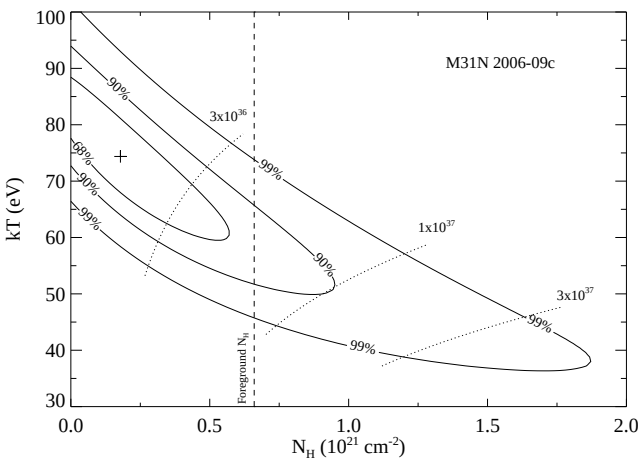

Figure 4.15: Same as Fig. 4.5 for M31N 2006-09c in 2007/8.

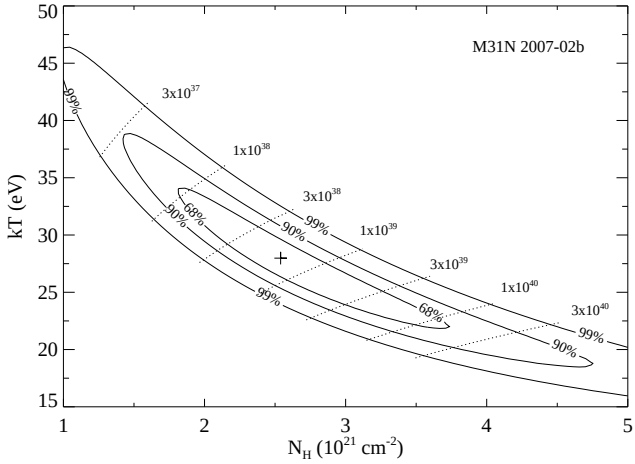

Figure 4.16: Same as Fig. 4.5 for M31N 2007-02b in 2007/8 and 2008/9.

a simultaneous modelling of both spectra which resulted in best-fit parameters $kT = (28 \pm 10)$ eV and $N_{\rm H} = (2.5^{+1.8}_{-1.1}) \times 10^{21}$ cm^{-2}, classifying this source as a SSS. Confidence contours for absorption column density and blackbody temperature are shown in Fig. 4.16.

M31N 2007-06b

This object was the first nova to be found in a M 31 GC (Shafter & Quimby 2007) and is examined in detail in Chap. 5 (see also Henze et al. 2009d).

M31N 2007-10b

The optical nova was discovered by Burwitz et al. (2007b) on 2007-10-13.26 UT. The start of the nova outburst was determined with an accuracy of less than a day from a non-detection on 2007-10-12.40 UT (Burwitz et al. 2007b). Based on optical spectra, Rau et al. (2007) classified the object as a He/N nova. They further reported an expansion velocity of (1450 ± 100) km s^{-1} and noted that this value is atypically low for He/N novae.

A bright ($L_x \sim 3 \times 10^{37}$ erg s^{-1}) X-ray counterpart was already present in the first *Chandra* observation of 2007/8. The luminosity of this source declined quickly (see Table 4.2 and Fig. 4.22). The nova exhibited a short SSS state with a duration of less than 100 days. The XMM-Newton EPIC PN spectrum therefore only contained few counts. It can be best fitted with an absorbed blackbody model with $kT = 66^{+34}_{-24}$ eV and $N_{\rm H} = (0.9^{+1.5}_{-0.8}) \times 10^{21}$ cm^{-2}, classifying this source as a SSS. Confidence contours for absorption column density and blackbody temperature are shown in Fig. 4.17.

M31N 2007-11a

The optical nova was discovered by Pietsch et al. (2007e) on 2007-11-02.28 UT. From the Super-LOTIS monitoring an optical light curve was derived which is shown in Fig. 4.18. The outburst date of M31N 2007-11a is well-constrained from the first detection on Modified Julian Day (MJD) 54406.2 and a non-detection on the night before (MJD = 54405.3). Therefore, I estimate MJD = 54405.75 for the actual outburst, with an error of ±0.45 days. The horizontal error bars in Fig. 4.18 represent this uncertainty for the days after the nova outburst.

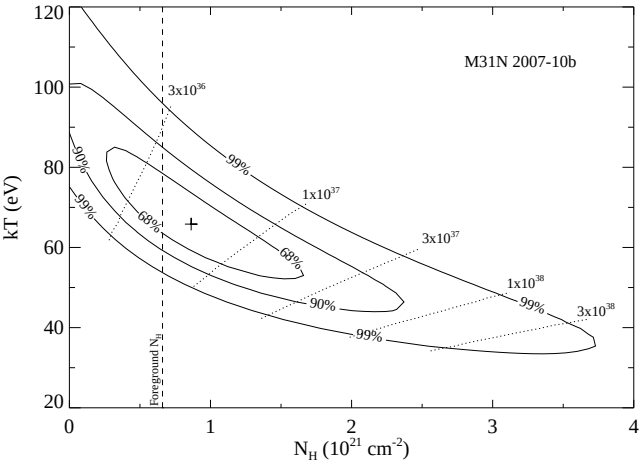

Figure 4.17: Same as Fig. 4.5 for M31N 2007-10b in 2007/8.

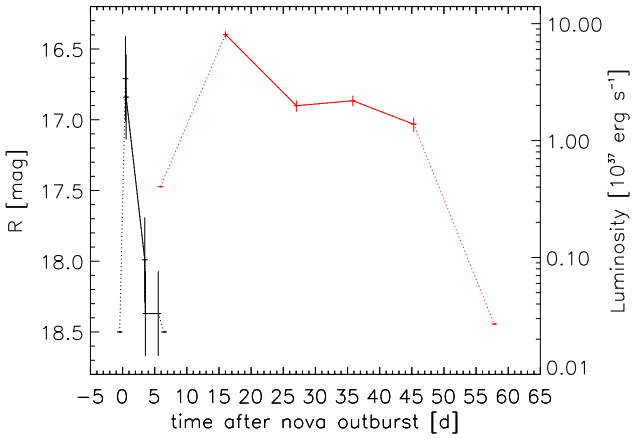

Figure 4.18: Optical (black symbols and left y-axis) and X-ray (red symbols and right y-axis) light curve of M31N 2007-11a. Detections are marked by crosses, the sizes of which correspond to the errors in magnitude/luminosity and time after outburst (MJD = 54405.75). Upper limits are represented by horizontal bars that show the uncertainty in time after outburst. Detections are connected with solid lines, upper limits to detections by dotted lines.

A bright ($L_X = 6.6 \pm 0.4 \times 10^{37}$ erg s^{-1}) X-ray counterpart was found 16 days after the optical outburst in *Chandra* data of the 2007/8 campaign (see Table 4.2). Nothing was detected at the same position 10 days earlier. Therefore, the turn-on of the X-ray counterpart is strongly confined and it is estimated here as the midpoint between these two observations. The luminosity of the source declined rapidly during the three subsequent *Chandra* observations and it was not detected any more (upper limit of $L_X < 1.1 \times 10^{36}$ erg s^{-1}) in the first XMM-Newton observation of 2007/8, 57 days after the optical outburst (see Table 4.2). The turn-off time of the source is estimated as the midpoint between this upper limit and the last *Chandra* detection.

Like the optical light curve, the evolution of the X-ray luminosity was remarkably well sampled for M31N 2007-11a. Both light curves are displayed in Fig. 4.18 and indicate that the nova was developing very fast. The X-ray state of M31N 2007-11a lasted only 29 . . . 52 days.

There is no detailed spectral information about the X-ray source, because of the very limited energy resolution of the HRC detector. Also, observations with the *Swift* XRT from 2007 Nov 24 to Dec 2 (ObsIDs 031028001 to 031028008, see Table 2.4) and with *Chandra* ACIS-I on 2007 Nov 27 (ObsID 8187, see Table 2.3) were not deep enough to help with the spectral classification. There is also no UV detection with the *Swift* UVOT or the XMM-Newton OM. However, I derived the following HRC-I hardness ratios for the ObsID 8527 detection: S/M = -0.10 ± 0.15, M/H = 0.09 ± 0.15. This is indicating a very soft spectrum.

From the well sampled optical light curve I found a rate of decline of ~ 0.6 mag/d. Extrapolating the magnitude to the day before the first observation (MJD = 54405.3) leads to an estimated maximum magnitude of $m_R \sim 16.1$, which implies an absolute magnitude at maximum of $M_R \sim -8.4 \pm 0.4$ at the distance of M 31. Within the uncertainties, this value matches the maximum magnitude versus

rate of decline (MMRD) relationship obtained by Della Valle & Livio (1995). Assuming that the strength of a nova outburst (for a given temperature of the WD and accretion rate) depends most strongly on the mass of the WD (see e.g. Livio 1992; Della Valle & Livio 1995; Della Valle 2002, and references therein), one can estimate WD masses from optical nova light curves. However, Livio (1992) mentions that great caution should be exercised when applying his maximum magnitude vs. WD mass relation to individual novae, since there are weaker dependences of the nova luminosity on the magnetic field of the WD and the enrichment of the envelope by heavy elements, which are neglected in his formula. Using our optical light curve, we compute that M31N 2007-11a likely originated from a WD with $M_{WD} \sim 0.9 \ldots 1.15\ M_{\odot}$. This is consistent with the results derived from the X-ray data given in Table 4.3.

Novae with short SSS phases are likely to be RNe. To check for the possibility that M31N 2007-11a is an RN, I looked for historical novae with positions close to M31N 2007-11a. In the compiled on-line nova catalogue of PHS2007 [7] there are two historical novae within a radius of $\sim 20''$ around M31N 2007-11a. Sharov et al. (2000) found a nova (M31N 1998-07n) at a distance of about 15″, and Hubble (1929) reported a nova (M31N 1920-10a) at a distance of about 20″ to M31N 2007-11a. The J2000 coordinates of M31N 1920-10a were taken from the Combined General Catalogue of Variable Stars (Samus et al. 2004). From the finding chart given by Sharov et al. (2000), nova M31N 1998-07n and M31N 2007-11a do not seem to be identical. This agrees with the position accuracy of 0.″5 given by Sharov et al. (2000). For M31N 1920-10a no finding chart exists and the nova positions given by Hubble (1929) have a minimum accuracy of 0.′1. The actual unknown position accuracy of historical novae leaves open the (small) possibility that both novae in fact originated on the same WD. A relatively large position error for a historical nova could be possible, since e.g. the re-analysis of photographic plates by Henze et al. (2008e) gives several examples for historical novae with position errors of $\sim 20''$ or more. Clarification of this point could only come from re-examination of the original photographic plates used in the work of Hubble (1929).

M31N 2007-12b

The optical nova was discovered independently by Lee et al. (2007) and Nishiyama & Kabashima[8] on 2007-12-09.53 UT. The time of the optical outburst is constrained to better than a day from a non-detection on 2007-12-08.57 UT. From the optical light curve of the nova, as observed with the Super-LOTIS telescope, a fast decay time of $t_2 = 8$ days is estimated. The nova was classified as He/N-type by Shafter (2007b), who described the optical spectrum as displaying strong and broad (FWHM H$\alpha \sim 4500$ km s^{-1}) Balmer emission lines. (Bode et al. 2009) report on Hubble Space Telescope (HST) observations of the pre-outburst location of M31N 2007-12b that resulted in the detection of a positionally coincident stellar source with similar magnitude and colour as the Galactic RN RS Oph in quiescence. They proposed this object as the first nova progenitor system identified in M 31.

In X-rays, a very bright ($L_x \sim 2.4 \times 10^{38}$ erg s^{-1}) counterpart was found 30 days after the optical outburst in XMM-Newton data of the 2007/8 campaign (see Table 4.2). Nothing was detected at the same position ten days earlier. The turn-on time of the SSS is estimated as the midpoint between these two observations. The source stayed bright, with varying luminosities, until the end of February 2008. It was no longer detected in a *Swift* observation on 2008-05-13 (see Table 2.4 and also Bode et al. 2009). The turn-off is estimated as the midpoint between this upper limit and the last XMM-

[7] http://www.mpe.mpg.de/~m31novae/opt/m31/index.php
[8] see http://www.cfa.harvard.edu/iau/CBAT_M31.html#2007-12b

Newton detection in February 2008.

I fitted the XMM-Newton EPIC spectrum of the X-ray counterpart of M31N 2007-12b with an absorbed black body model with a maximum temperature (in ObsID 0505720501) of $kT = (81 \pm 2)$ eV and an absorption of $N_{\rm H} = (1.8 \pm 0.2) \times 10^{21}$ cm^{-2}. This classifies the source as a SSS. Confidence contours for absorption column density and blackbody temperature are shown in Fig. 4.19.

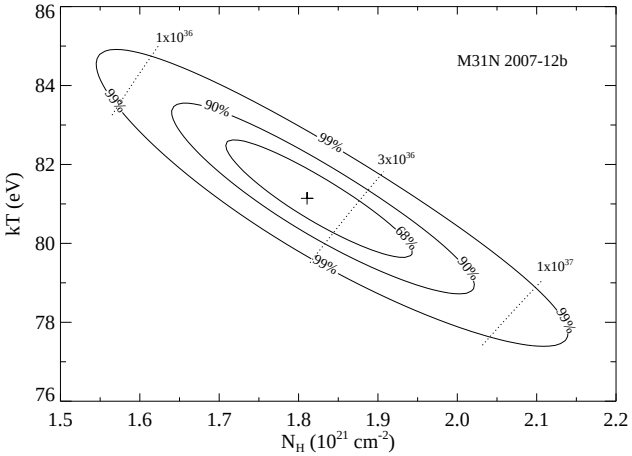

Figure 4.19: Same as Fig. 4.5 for M31N 2007-12b in observation 0505720501.

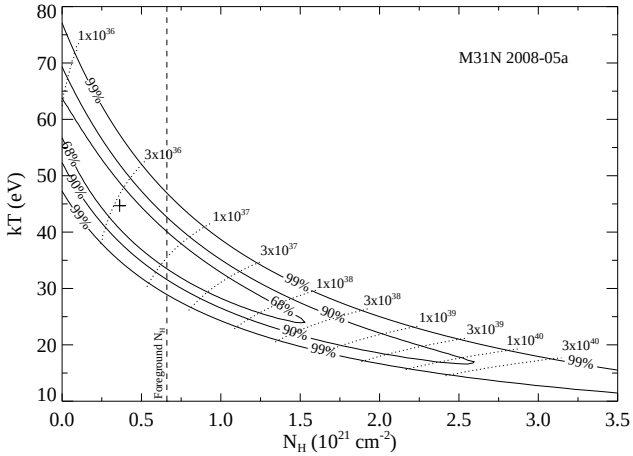

Figure 4.20: Same as Fig. 4.5 for M31N 2008-05a in 2008/9.

The analysis of the short term X-ray light curves of M31N 2007-12b revealed a significant periodicity with a duration of about 1100 s (see also Pietsch 2010). This period was measured consistently, within the errors, for all four XMM-Newton observations where the nova was detected (see Table 4.2). I show the power spectra for these observations, generated using the FTOOLS FFT algorithm `powspec`, in Fig. 4.21 in the panels on the right.

To search for residual non-periodic variability in the observations I overplot in Fig. 4.21 the data combined in 1110 s bins. Observations 0505720301, 0505720401, and 0505720501 clearly show dips starting at JD = 2450000.0 + (4473.4475, 4483.6717, 4493.0769), respectively. There is no significant hardness ratio variation accompanied with these dips.

M31N 2007-12d

The optical nova was discovered independently by Henze et al. (2007a) and Nishiyama & Kabashima[9] on 2007-12-17.58 UT. The accuracy of the time of the nova outburst is about 0.4 days, based on a non-detection on 2007-12-17.19 UT (Burwitz et al. 2008a; Henze et al. 2007a). From our optical data obtained following the discovery (see Appendix C) I estimated a very fast decline of the optical light curve ($t_2 \sim 4$ days). The object was classified as a He/N nova by Shafter (2007a), who reported strong and broad Balmer lines with a FWHM for Hα of about 5500 km s^{-1}. This line width implies a high ejection velocity of the nova envelope of about 2750 km s^{-1}. Together with the fast decline of the optical light curve this points towards a rapidly evolving nova.

A faint X-ray counterpart ($L_x = (2.8 \pm 0.8) \times 10^{36}$ erg s^{-1}) was visible in only one XMM-Newton observation about 22 days after outburst (see Table 4.2). Unfortunately, there are too few source counts to perform a spectral fit for this source. However, I could classify it as a SSS based on the hardness ratio criterion described in Chap.2.2.

[9] see http://www.cfa.harvard.edu/iau/CBAT_M31.html#2007-12d

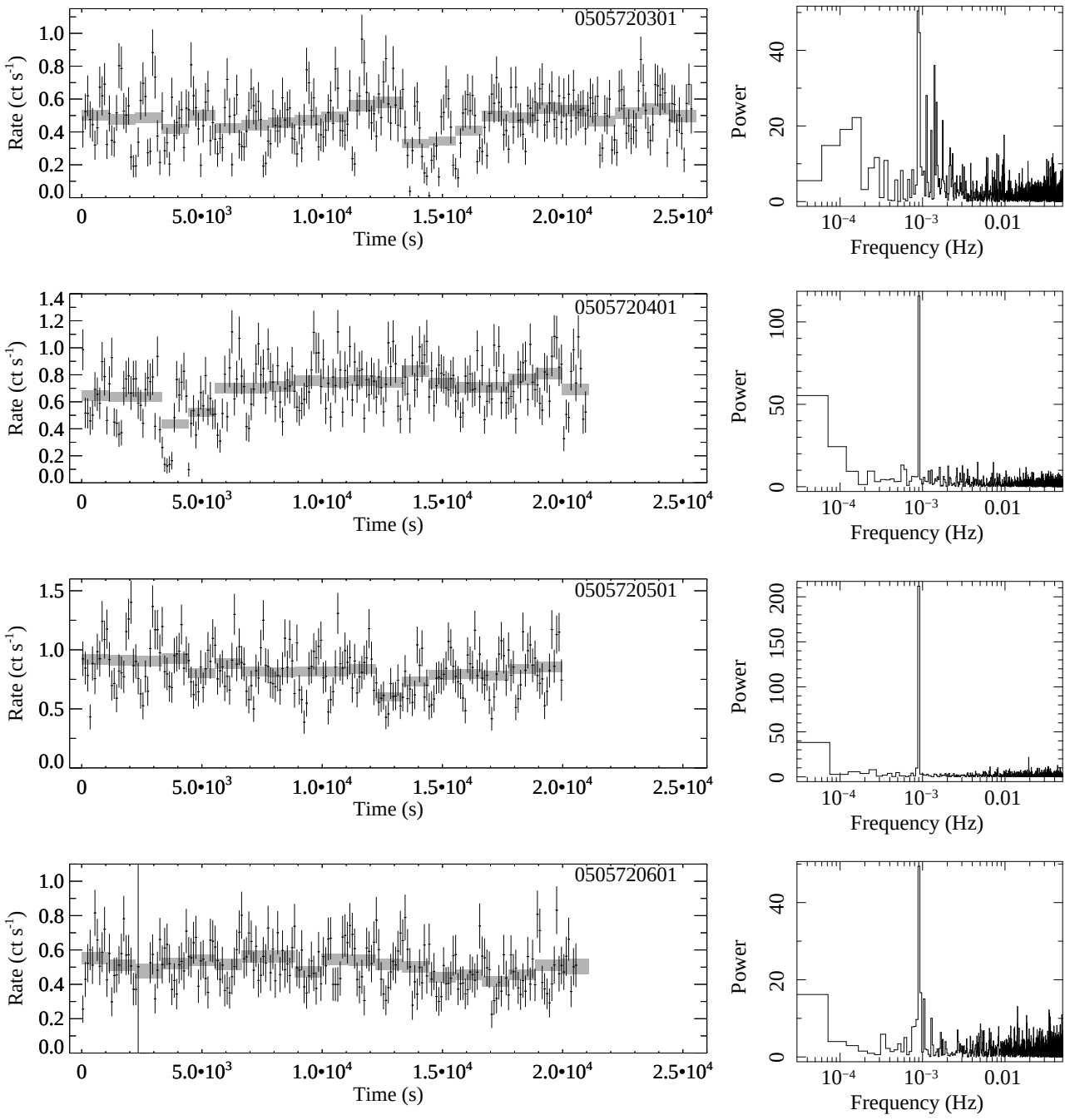

Figure 4.21: left: XMM-Newton EPIC PN background corrected light curves (0.15–1 keV) of M31N 2007-12b for observations 0505720301, 0505720401, 0505720501 and 0505720601 integrated over 100 s (data points with error bars) and 1110 s (shaded, size indicates 1σ error). Time zero corresponds to JD 245 0000.0 + (4473.2933, 4483.6332, 4492.9356, and 4509.2042), respectively (solar system barycentre corrected). **right:** XMM-Newton EPIC PN power spectra (0.15–1 keV) of M31N 2007-12b for the same observations.

Nothing was found at the position of M31N 2007-12d in X-ray data on day 12 and 32 after outburst with upper limits of $L_x \lesssim 1.5 \times 10^{36}$ erg s^{-1}. This indicates that the nova exhibited an extremely short SSS state of less than 20 days, supporting the interpretation of a very fast nova suggested by its optical properties. The speed of the nova evolution is remarkable, because it makes M31N 2007-12d not only the fastest SSS in M 31 (see Table 4.3), but more so, the fastest of *all* novae known so far, for which SSS emission was found. Its SSS duration is considerably shorter than those of the M 31 novae M31N 2007-11a and M31N 2007-12b (see Table 4.2) as well as those of the Galactic RNe RS Oph (about 60 days, Osborne et al. 2006a) and even U Sco (about 28 days Schaefer et al. 2010; Schlegel et al. 2010). For all of these nova systems it was discussed that they might contain a massive WD (Kahabka et al. 1999; Hachisu et al. 2007; Henze et al. 2009f; Pietsch 2010). The SSS duration of nova V2491 Cyg could be of comparable length, but its turn-on time is longer (about 35 days, Page et al. 2010). In fact, so far V2491 Cyg and the two RNe mentioned above are the only Galactic novae with a short SSS phase of less than 100 days. Note, that V2491 Cyg is discussed as a candidate RN in Page et al. (2010). Implications on the possible connection of RNe with M31N 2007-12d and other fast novae in our sample are discussed in Chap. 6.5.

M31N 2008-05a

The optical nova was discovered by Nishiyama & Kabashima[10] on 2008-05-15 and confirmed by Henze et al. (2008i) using Hα observations. Immler et al. (2008) reported *Swift* UVOT detections of the source on 2008-05-26. An X-ray counterpart became visible in the 2008/9 campaign and its light curve (see Table 4.2) indicates significant variability by a factor of three or more. The turn-on time of the source was estimated as the midpoint between observations 9826 and 9827. The object was still detected at the end of the 2008/9 campaign, therefore I can only give a lower limit for its X-ray turn-off (see Table 4.3).

The XMM-Newton EPIC spectrum of the source can be fitted by an absorbed black body model with best-fit parameters $kT = 45^{+25}_{-28}$ eV and $N_{\rm H} = (0.4^{+1.8}_{-0.4}) \times 10^{21}$ cm^{-2}, classifying this source as a SSS. Note, that the formal best-fit $N_{\rm H}$ is smaller than the Galactic foreground absorption of $\sim 6.7 \times 10^{20}$ cm^{-2} (but still compatible with it within the errors). Confidence contours for absorption column density and blackbody temperature are shown in Fig. 4.20.

M31N 2008-05b

The optical nova was discovered by Nishiyama & Kabashima[11] on 2008-05-23. It was confirmed as a nova by Henze et al. (2008i), using Hα observations, and Immler et al. (2008) reported *Swift* UVOT detections on 2008-05-27.

A faint X-ray counterpart was detected in four consecutive *Chandra* HRC-I observations 190 – 209 days after the outburst (see Table 4.2). The source was not detected in the first two *Chandra* observations, nor in the last two observations of the 2008/9 campaign. I estimated the turn-on (turn-off) time as the midpoint between observations 9826 and 9827 (10838 and 0551690201). There was no significant variability during the duration of the X-ray visibility.

[10] see http://www.cfa.harvard.edu/iau/CBAT_M31.html#2008-05a
[11] see http://www.cfa.harvard.edu/iau/CBAT_M31.html#2008-05b

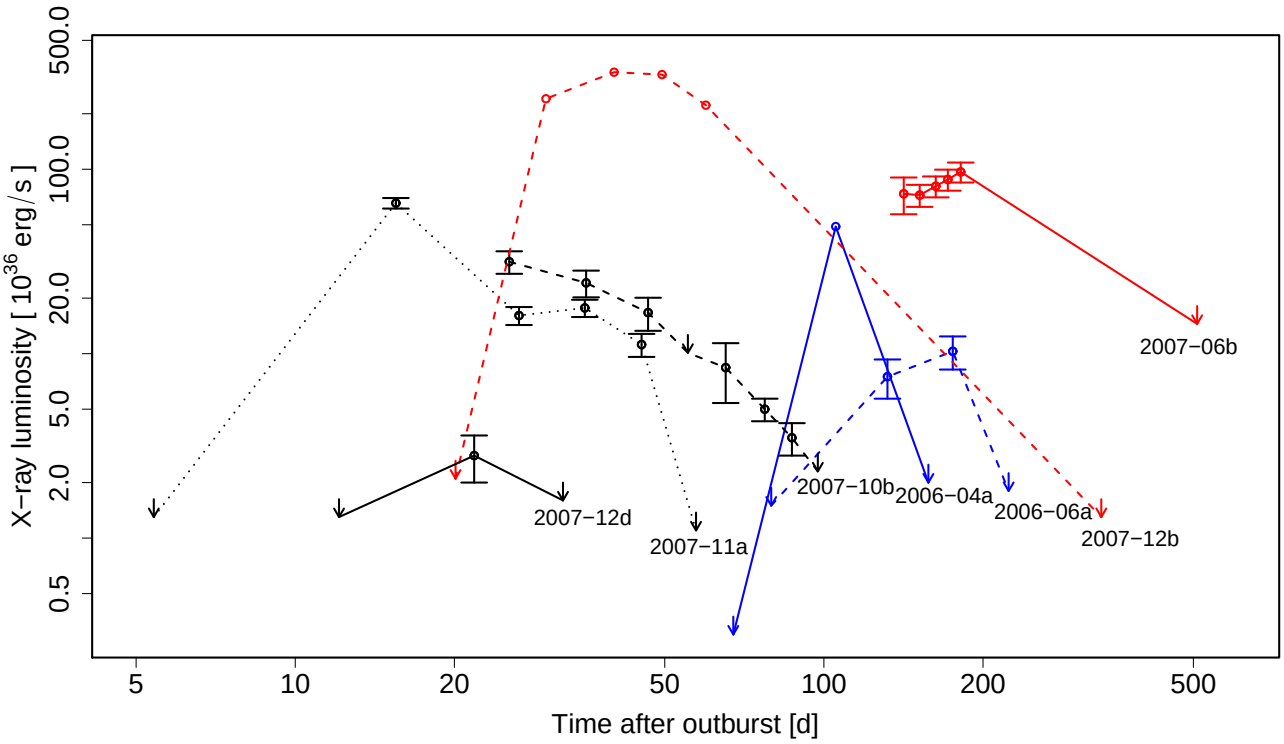

Figure 4.22: X-ray light curves for all novae detected in 2007/8 and 2008/9 with short SSS turn-on times. Detections are indicated as open circles with error bars and upper limits as down pointing arrows. For novae M31N 2007-12b and M31 2006-04a the error bars are smaller than the size of the symbols. All measurements for an individual nova are connected by lines, the style and colour of which differentiates between the novae.

M31N 2008-06a

The optical nova was discovered by Henze et al. (2008c) on 2008-06-14. An optical re-brightening of the object was observed on 2008-09-01 by Valcheva et al. (2008) (see also Ovcharov et al. 2009). Henze et al. (2008i) confirmed the object as a nova on the basis of Hα observations.

A faint X-ray counterpart only was detected after 257 days in the very last observation of the 2008/9 campaign (see Table 4.2).

4.3 The complete sample of M 31 novae with X-ray counterpart

I compiled a catalogue that includes all optical novae with an X-ray counterpart in M 31 detected so far in observations prior to March 2009. This catalogue contains 60 objects and is mainly based (~ 85%) on the results of the three monitoring campaigns for M 31 novae presented here and on the analysis of archival M 31 X-ray data reported in PFF2005 and PHS2007. I searched the available literature and included further X-ray detections, corrections and measurements of M 31 novae reported by the following authors: Smirnova et al. (2006), Pietsch et al. (2007f), Voss et al. (2008), Orio & Nelson (2008), Nelson et al. (2008a), and Stiele et al. (2010).

In Fig. 4.23 I show the number of X-ray counterparts of M 31 novae found per year (black histogram) between 1982 and the end of the 2008/9 campaign in February 2009. The green histogram gives the yearly number of optical nova candidates discovered between 1982 and May 2010.

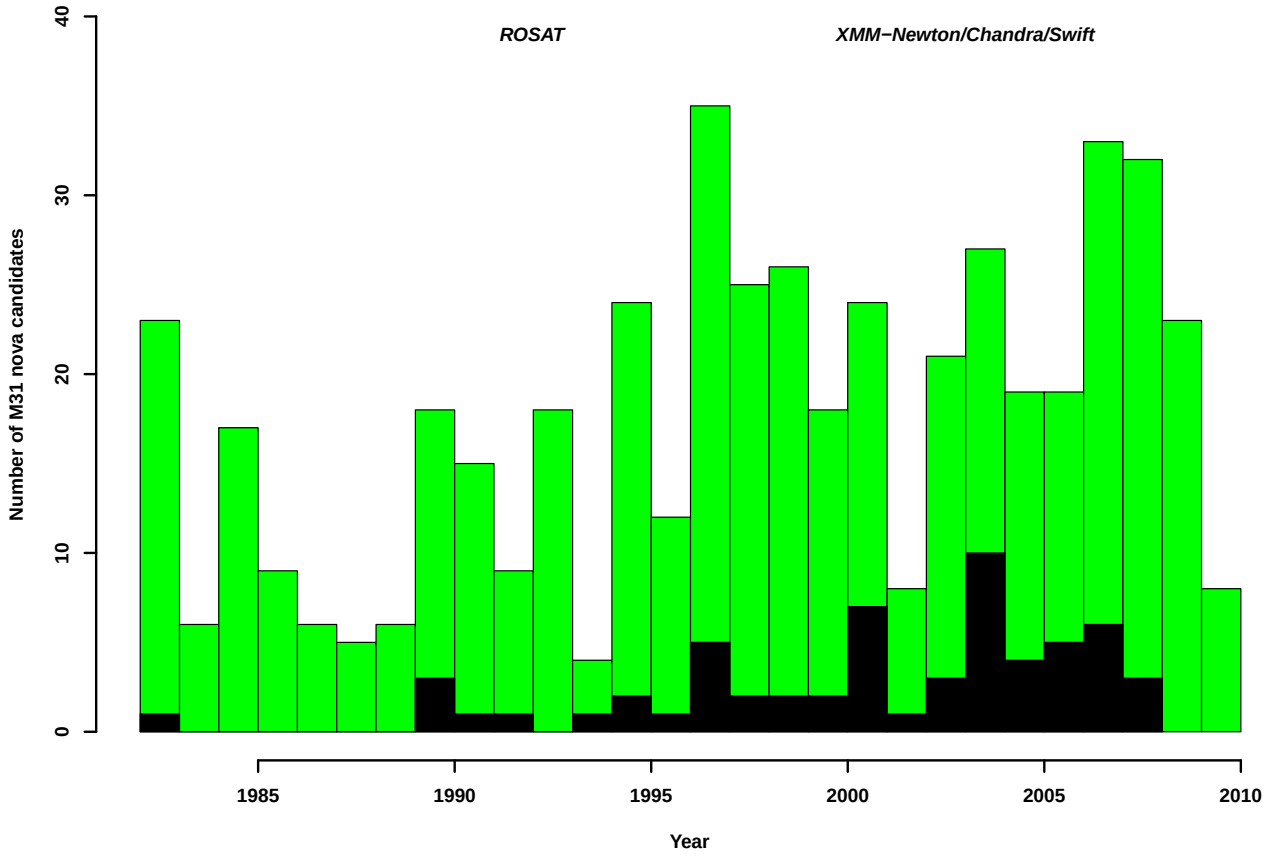

Figure 4.23: Histogram of optical novae in M 31 found per year between 1982 and May 2010 (**green**). In **black** there are the number of novae shown from the respective year that were found as SSSs later with ROSAT, XMM-Newton, *Chandra* or *Swift* .

I did not include five apparent X-ray nova counterparts from a recent census of SSSs in M 31 (Orio et al. 2010), because I cannot confirm them in our data. These sources are the suggested X-ray counterparts of the novae M31N 2004-09b, M31N 2007-08b, M31N 2007-11c, M31N 2008-02a and M31N 2008-06c (table 3 in Orio et al. 2010). In the cases of M31N 2007-11c and M31N 2008-06c the positions of the optical novae are relatively close to known X-ray sources in the field (sources 388 and 405 from Pietsch et al. 2005b, respectively), which might have been mis-identified as nova counterparts.

The catalogue is presented in Table 4.3 and contains the following information: (a) for the optical nova: the name, date of outburst detection, maximum observed magnitude in a certain filter (which is not necessarily the peak magnitude of the nova), t_2 decay time in the R band, classification as belonging to the old/young stellar population, spectroscopic nova type in the classification scheme of Williams (1992), and expansion velocity of the ejected envelope as measured from the earliest optical spectrum (half of the FWHM of the Hα line); (b) for the X-ray counterpart: the turn-on and turn-off times, a flag for SSS classification, the X-ray luminosity, and the blackbody temperature as inferred from the X-ray spectrum; (c) derived parameters: the ejected and burned masses as computed according to Chap. 6.4; (d) references. Note, that not all parameter values are known for all objects. A statistical analysis of Table 4.3 will be given in Chap. 6.

Table 4.3: Catalogue of X-ray detected optical novae in M 31.

Optical measurements						X-ray measurements					Derived parameters		References
Name M31N	Outburst[a] (JD)	Brightness[b] (mag Filter)	t_{2R} [c] (d)	Old/[d] Young	Type[e]	v_{exp} [f] (km s^{-1})	Turn on (d)	Turn off (d)	SSS?[g]	L_X^h (10^{36} erg s^{-1})	kT_{BB}^i (eV)	Ejected mass (10^{-5} $M_\odot$)	Burned mass (10^{-6} $M_\odot$)	o(ptical)[j] and x(-ray)[k]
1982-09b	2445225.01	16.7(Hα)		O		278	2874	4317		8.7 ± 2.4		40.9	7.21	o1;x1
1990-09a	2448151.94	15.7(Hα)		Y		1031	156 ± 156	501 ± 188		12.1 ± 1.9		$1.66^{+8.35}_{-1.66}$	0.84 ± 0.31	o2,3;x4,1
1990-09g	2448161.50	18.4(Hα)		O		1043	152 ± 152	842 ± 538		63.0 ± 4.0		$1.61^{+8.09}_{-1.61}$	1.41 ± 0.9	o3;x1
1990-12a	2448235.50	16.0(Hα)		O		662	417 ± 188	955 ± 188		43.0 ± 5.3		$4.89^{+17.26}_{-3.96}$	1.6 ± 0.31	o3;x1,5
1991-01b	2448280.50	16.4(Hα)		Y		696	373 ± 188	810 ± 100		88.0 ± 10.0		$4.33^{+15.91}_{-3.58}$	1.35 ± 0.17	o3;x1
1992-11b	2448935.58	16.4(Hα)		O	Fe II	790	282 ± 282	763 ± 186		13.1 ± 4.0		$3.18^{+17.18}_{-3.18}$	1.27 ± 0.31	o3;x1
1994-09a	2449622.50	17.6(R)		O		294	2529 ± 62	3121 ± 463		1.6 ± 0.2		$35.53^{+91.39}_{-25.54}$	5.21 ± 0.77	o4;x1
1995-09b	2449963.50	15.6(Hα)		O		356	1653 ± 81	3656 ± 273		16.1 ± 3.6		$22.26^{+56.13}_{-15.89}$	6.11 ± 0.46	o5;x1
1995-11c	2450048.34	16.3(Hα)		O		505	762 ± 725	3609 ± 236		13.8 ± 3.3		$9.5^{+55.69}_{-9.35}$	6.03 ± 0.39	o3,6;x1
1996-08b	2450307.50	16.1(Hα)		O		340	1831 ± 49	> 4560	spec	2.0 ± 0.3	21^{+8}_{-13}	$24.91^{+61.46}_{-17.69}$	> 7.62	o3;x1
1997-06c	2450617.50	15.6(Hα)		O		580	559 ± 559	1244 ± 326		10.6 ± 3.2		$6.75^{+39.54}_{-6.75}$	2.08 ± 0.54	o3,5;x1
1997-08b	2450661.50	16.5(Hα)		Y		366	1556 ± 34	2052 ± 463		0.7 ± 0.2		$20.82^{+49.81}_{-14.66}$	3.43 ± 0.77	o3,5;x1
1997-09a	2450718.50	16.6(B)	10.0	Y						9.6 ± 2.9				o7;x1
1997-10c	2450723.51	16.6(B)	7.9	O		447	997	1090 ± 93	spec	59.0	41^{+27}_{-21}	12.76	1.82 ± 0.16	o7;x6
1997-11a	2450753.55	18.0(R)		O		325	2027 ± 566	> 4025		4.4 ± 0.7		$27.85^{+99.18}_{-21.94}$	> 6.72	o3;x2
1998-06a	2450970.50	16.2(Hα)		O		441	1028 ± 92	1773 ± 463		1.7 ± 0.3		$13.2^{+33.19}_{-9.41}$	2.96 ± 0.77	o5;x1
1998-07d	2451019.50	15.9(Hα)		O		451	979 ± 92	1345 ± 74		80.0 ± 15.0		$12.51^{+31.46}_{-8.92}$	2.25 ± 0.12	o5;x1
1999-08d	2451400.61	18.3(i')	87.2	Y		710	357 ± 357	753 ± 35		1.2 ± 0.4		$4.12^{+22.9}_{-4.12}$	1.26 ± 0.06	o8,9;x7
1999-10a	2451454.70	17.5(W)		O		403	1256 ± 496	2203 ± 234	spec	21.2 ± 1.6	34 ± 4	$16.45^{+62.91}_{-13.38}$	3.68 ± 0.39	o10;x2
2000-07a	2451753.00	16.8(R)	22.4	O		1013	162 ± 8	1904 ± 236	spec	13.4 ± 0.7	33 ± 5	$1.73^{+3.1}_{-1.11}$	3.18 ± 0.39	o8,9;x1
2000-08a	2451719.62	18.6(R)		O		795	278 ± 75	1061 ± 567		16.8 ± 9.7		$3.13^{+8.47}_{-2.31}$	1.77 ± 0.95	o11;x1
2001-01a	2451929.32	17.1(R)		O		328	1387	2426 ± 109		2.6 ± 0.6		27.28	4.05 ± 0.18	o12;x3
2001-07a	2452094.56	18.7(R)		Y		1584	60 ± 60	153 ± 34		5.3 ± 2.0		$0.58^{+2.6}_{-0.58}$	0.26 ± 0.06	o12;x1
2001-08d	2452150.60	16.7(R)	11.8	O		1720	50 ± 13	593 ± 463		0.7 ± 0.1		$0.47^{+0.99}_{-0.32}$	0.99 ± 0.77	o12;x1
2001-10a	2452186.41	17.0(R)	39.3	O	Fe II	430	1089 ± 70	> 2702	spec	39.0 ± 8.0	14^{+4}_{-7}	$14.06^{+34.27}_{-9.94}$	> 4.51	o9,13;x2

Table 4.3: continued.

Optical measurements							X-ray measurements					Derived parameters		Comments
Name M31N	Outburst[a] (JD)	Brightness[b] (mag Filter)	t_{2R} [c] (d)	Old/[d] Young	Type[e]	v_{exp} [f] (km s^{-1})	Turn on (d)	Turn off (d)	SSS?[g]	L_X^h (10^{36} erg s^{-1})	kT_{BB}^i (eV)	Ejected mass (10^{-5} $M_\odot$)	Burned mass (10^{-6} $M_\odot$)	o(ptical)[j] and x(-ray)[k]
2001-10b	2452191.48	15.6(i')	15.8	Y		894	214 ± 214			6.7 ± 2.2		$2.35^{+12.28}_{-2.35}$		o8,9;x7
2001-10f	2452196.26	16.6(B)	12.0	Y		1704	51 ± 34	550 ± 460	spec	37.0 ± 1.7	48 ± 11	$0.48^{+1.62}_{-0.42}$	0.92 ± 0.77	o14,15;x1,2
2001-11a	2452226.21	17.1(B)	8.0	Y		1675	53			2018.4 ± 246.6		0.51		o15;x8
2002-01b	2452282.31	16.8(R)	8.0	O		**1500**	77 ± 69	534 ± 390		27.5 ± 12.0		$0.76^{+3.26}_{-0.73}$	0.89 ± 0.65	o17,18;x1
2003-08c	2452878.50	17.9(R)		O		**450**	1419 ± 126	> 2010		5.5 ± 1.1		$18.82^{+49.43}_{-13.58}$	> 3.36	o19,20;x14
2003-11a	2452948.47	16.9(R)	22.0	O		739	327 ± 70	709 ± 235		27.6 ± 1.8		$3.74^{+9.62}_{-2.7}$	1.18 ± 0.39	o21,12;x2
2003-11b	2452973.37	17.4(R)	42.2	O		766	302 ± 70	684 ± 235		10.4 ± 1.3		$3.43^{+8.93}_{-2.49}$	1.14 ± 0.39	o12;x2
2004-01b	2453006.24	18.4(R)		O		361	1609 ± 163	> 1882		6.7 ± 1.5		$21.61^{+58.84}_{-15.75}$	> 3.14	o12;x14
2004-05b	2453143.56	17.2(R)	49.7	O		896	213 ± 11	> 1745	spec	45.8 ± 5.4	30^{+6}_{-5}	$2.34^{+4.39}_{-1.52}$	> 2.92	o22,11;x2
2004-06a	2453164.54	17.2(R)	19.7	O		1539	64 ± 23	218 ± 16	spec	62.1 ± 9.0	71 ± 9	$0.62^{+1.54}_{-0.46}$	0.36 ± 0.03	o22,11;x2
2004-06c	2453181.52	17.1(R)	10.9	O		1294	94 ± 70	476 ± 234		33.9 ± 2.0		$0.96^{+3.7}_{-0.86}$	0.8 ± 0.39	o22,11;x2
2004-08a	2453220.47	17.4(R)		O		1752	48 ± 16	77 ± 13	spec	51.9 ± 8.2	80 ± 16	$0.45^{+1.04}_{-0.32}$	0.13 ± 0.02	o22,11;x2
2004-08c	2453239.54	18.7(R)	50.3	O		1661	54 ± 54	144 ± 16		9.3 ± 1.0		$0.52^{+2.29}_{-0.52}$	0.24 ± 0.03	o12;x2
2004-11f	2453311.82	17.9(R)	28.4	O		2794	17 ± 17	45 ± 10		353.3 ± 6.2		$0.14^{+0.56}_{-0.14}$	0.08 ± 0.02	o12;x2
2004-11b	2453315.35	16.6(R)	32.0	O	Fe II	**1250**	68 ± 16	343 ± 235		16.2 ± 1.6		$0.67^{+1.41}_{-0.45}$	0.57 ± 0.39	o22,11;x2
2004-11g	2453315.35	18.0(R)	28.4	O		2872	16 ± 16	343 ± 235		82.1 ± 3.0		$0.14^{+0.52}_{-0.14}$	0.57 ± 0.39	o22;x2
2004-11e	2453339.30	17.6(R)	34.6	Y		1822	44 ± 16	319 ± 235		35.9 ± 4.0		$0.41^{+0.97}_{-0.3}$	0.53 ± 0.39	o22,11;x2
2005-01b	2453389.58	16.3(W)		Y		808	268 ± 268	804 ± 269	spec	10.0	45	$3.01^{+16.15}_{-3.01}$	1.34 ± 0.45	o23;x6
2005-01c	2453399.59	16.1(W)		Y		715	352 ± 352		spec	120.0	40 ± 1	$4.06^{+22.51}_{-4.06}$		o23;x6
2005-02a	2453420.27	17.7(W)		O		855	236 ± 236	872 ± 121	spec	56.0 ± 5.0	38^{+6}_{-8}	$2.62^{+13.83}_{-2.62}$	1.46 ± 0.2	o24;x3
2005-09b	2453614.73	16.5(W)		Y	Fe II	**2200**	150 ± 150	494 ± 195	spec	25.0	60	$1.59^{+7.96}_{-1.59}$	0.83 ± 0.33	o25,26;x9,6
2006-04a	2453851.77	15.9(R)	16.0	O		1347	86 ± 19	132 ± 27	spec	51.0 ± 2.0	54^{+9}_{-10}	$0.86^{+1.85}_{-0.59}$	0.22 ± 0.05	o27,28;x3
2006-06a	2453877.60	17.6(R)		O	Fe II	**850**	106 ± 26	200 ± 25		10.0 ± 2.0		$1.08^{+2.48}_{-0.76}$	0.33 ± 0.04	o29,26;x3
2006-06b	2453869.57	18.5(R)		O		502	772 ± 138	> 1019	spec	11.0 ± 2.0	37^{+17}_{-15}	$9.63^{+26.53}_{-7.07}$	> 1.7	o30,11;x14
2006-09c	2453996.64	17.0(R)	14.0	Y	Fe II	**570**	275 ± 138	327 ± 164	spec	2.8 ± 0.8	74^{+20}_{-24}	$3.09^{+10.92}_{-2.54}$	0.55 ± 0.27	o31,32;x14

Table 4.3: continued.

Optical measurements							X-ray measurements					Derived parameters		Comments
Name M31N	Outburst[a] (JD)	Brightness[b] (mag Filter)	t_{2R} [c] (d)	Old/[d] Young	Type[e]	v_{exp} [f] (km s^{-1})	Turn on (d)	Turn off (d)	SSS?[g]	L_X^h (10^{36} erg s^{-1})	kT_{BB}^i (eV)	Ejected mass (10^{-5} $M_\odot$)	Burned mass (10^{-6} $M_\odot$)	o(ptical)[j] and x(-ray)[k]
2006-11a	2454064.17	16.0(R)	22.0	Y	Fe II	1059	147 ± 41	208 ± 21	spec	19.0	65 ± 25	$1.55^{+3.9}_{-1.12}$	0.35 ± 0.04	o33,34;x10,11
2007-02b	2454135.30	16.7(R)	37.0	Y	Fe II	**800**	175 ± 175	> 732	spec	18.0 ± 5.0	28^{+11}_{-10}	$1.88^{+9.61}_{-1.88}$	> 1.22	o35,36;x14
2007-06b	2454270.40	17.3(W)	18.0	O	He/N	**1500**	87 ± 54	452 ± 57	spec	97.0 ± 12.0	48^{+2}_{-3}	$0.87^{+2.99}_{-0.74}$	0.76 ± 0.1	o37;x12,14
2007-10b	2454386.75	17.8(R)	3.0	Y	He/N	**1450**	13 ± 13	92 ± 5	spec	32.0 ± 4.0	66^{+34}_{-24}	$0.11^{+0.4}_{-0.11}$	0.15 ± 0.01	o38,39;x14
2007-11a	2454406.78	16.7(R)	4.0	O		3399	11 ± 5	52 ± 7		66.0 ± 4.0		$0.09^{+0.19}_{-0.07}$	0.09 ± 0.01	o40;x0,14
2007-12b	2454444.03	17.0(R)	8.0	Y	He/N	**2250**	25 ± 5	115 ± 55	spec	339.0 ± 4.0	81 ± 2	$0.22^{+0.38}_{-0.14}$	0.19 ± 0.09	o41,42;x13,14
2007-12d	2454452.07	17.2(R)	4.0	O	He/N	**2750**	17 ± 5	27 ± 5		2.8 ± 0.8		$0.14^{+0.27}_{-0.1}$	0.05 ± 0.01	o43,44;x14
2008-05a	2454601.29	16.4(R)	25.0	O		939	192 ± 5	> 278	spec	11.0 ± 2.0	45^{+25}_{-28}	$2.08^{+3.68}_{-1.33}$	> 0.46	o45,11;x14
2008-05b	2454609.26	16.0(W)		O		957	184 ± 6	204 ± 5		4.9 ± 1.3		$1.99^{+3.53}_{-1.27}$	0.34 ± 0.01	o45,11;x14
2008-06a	2454631.96	17.7(R)		O		831	252 ± 5	> 252		3.2 ± 1.3		$2.81^{+5.12}_{-1.81}$	> 0.42	o46;x14

Notes: [a]: Julian day of optical nova outburst; [b]: maximum observed magnitude, "W" indicates unfiltered magnitude; [c]: time in days the nova R magnitude needs to drop 2 mag below peak magnitude (see Payne-Gaposchkin 1964); [d]: positional association with the old (bulge) and young (disk) stellar populations of M 31 (see Chap. 6.6) ; [e]: spectral type of optical nova according to the classification scheme of Williams (1992); [f]: outflow velocity of the ejected envelope, values in *italic* are measured from optical spectra, all other values were computed from the SSS turn-on time using Eq. 6.4; [g]: indicates if the source was classified as a SSS using XMM-Newton spectra (spec), XMM-Newton hardness ratios (HR), *Chandra* HRC-I/ACIS-I hardness ratios (HR1), *Chandra* HRC-I hardness ratios (HR2), or a ROSAT observation (ROSAT) in the case of M31N 1990-09a; [h]: unabsorbed luminosity in 0.2–1.0 keV band in units of 10^{36} erg s^{-1} during observed maximum X-ray brightness assuming a 50 eV blackbody spectrum with Galactic foreground absorption; [i]: maximum blackbody temperature from spectral fits; [j]: optical references: o1: Ciardullo et al. (1987), o2: Nedialkov et al. (2002), o3: Shafter & Irby (2001), o4: Ansari et al. (2004), o5: Rector et al. (1999), o6: Henze et al. (2008e), o7: Sharov & Alksnis (1998), o8: Darnley et al. (2004), o9: Darnley et al. (2006), o10: Filippenko et al. (1999), o11: CBAT M 31 nova web page (http://www.cfa.harvard.edu/iau/CBAT_M31.html), o12: MPE M 31 nova catalogue (http://www.mpe.mpg.de/~m31novae/opt/m31/index.php), o13: Filippenko & Chornock (2001), o14: Smirnova & Alksnis (2006), o15: Alksnis et al. (2008), o16: Smirnova et al. (2006), o17: Fiaschi et al. (2002), o18: Filippenko & Chornock (2002), o19: Fiaschi et al. (2003), o20: di Mille et al. (2003), o21: Hornoch (2003), o22: PHS2007 , o23: D. Bishops extragalactic nova web page (http://www.supernovae.net/sn2005/novae.html), o24: Dimai & Manzini (2005), o25: Quimby et al. (2005), o26: Pietsch et al. (2006a), o27: Pietsch et al. (2006b), o28: Baernbantner & Riffeser (2006), o29: Lang et al. (2006), o30: Ries & Riffeser (2006), o31: Quimby (2006a), o32: Shafter et al. (2006), o33: K. Hornoch (2010, priv. comm.), o34: A. Shafter's web page of nova spectra (http://mintaka.sdsu.edu/faculty/shafter/extragalactic_novae/HET/index.html), o35: Burwitz et al. (2010, in prep.), o36: Pietsch et al. (2007a), o37: Shafter & Quimby (2007), o38: Burwitz et al. (2007b), o39: Rau et al. (2007), o40: Pietsch et al. (2007e), o41: Bode et al. (2009), o42: Shafter (2007b), o43: Henze et al. (2007a), o44: Shafter (2007a), o45: Henze et al. (2008i), o46: Henze et al. (2008c); [k]: X-ray references: x1: PFF2005 , x2: PHS2007 , x3: this work (2006/7), x4: Nedialkov et al. (2002), x5: Pietsch et al. (2006c), x6: Stiele et al. (2010), x7: Nelson et al. (2008a), x8: Smirnova et al. (2006), x9: Orio & Nelson (2008) (wrongly named 2005-09c there), x10: Pietsch et al. (2007f), x11: Voss et al. (2008), x12: Henze et al. (2009d), x13: Pietsch et al. (2010, in prep.), x14: this work (2007/8 and 2008/9).

4.4 Upper limits for non-detected novae

From the 14 SSS nova counterparts found by PHS2007, ten were no longer detected in the 2006/7 monitoring. Upper limits for the X-ray luminosity of these objects are given in Table 4.4. Therefore, it was possible to estimate a SSS turn-off time for these novae. Upper limits for undetected novae with optical outburst from May 2005 – March 2007, October 2006 – February 2008 and October 2007 – February 2009 are listed in Tables 4.5, 4.6 and 4.7 for the 2006/7, 2007/8 and 2008/9 campaigns, respectively. The non-detections strongly constrain the turn-on and turn-off time for a possible SSS state of these novae. I assumed that nova M31N 2006-12d, which was reported by Hornoch (see http://www.cfa.harvard.edu/iau/CBAT_M31.html#2007-12d), was actually caused by a re-brightening of nova M31N 2006-11b because the positions of both novae, as given by the discoverers, coincide within 0.″4.

Table 4.4: Upper limits for non-detected M 31 CN from PHS2007.

Optical nova candidate			X-ray measurements			
Name M31N	RA (h:m:s)[a] Dec (d:m:s)[a]	MJD[b] (d)	Observation[c] ID	Δt[d] (d)	L_X^e (10^{36} erg s^{-1})	Comment
1995-09b	0:42:43.10	49963.0	mrg1 (HRC-I)	3928.3	< 1.1	close to the
	41:16:04.1		mrg1 (EPIC)	3955.6	< 37.1	M 31 centre
1995-11c	0:42:59.35	50047.8	mrg1 (HRC-I)	3843.5	< 0.2	
	41:16:43.1		mrg1 (EPIC)	3870.9	< 0.1	
1999-10a	0:42:49.70	51454.2	mrg1 (HRC-I)	2437.0	< 1.0	
	41:16:32.0		mrg1 (EPIC)	2464.4	< 5.2	
2000-07a	0:42:43.97	51752.5	mrg1 (HRC-I)	2138.8	< 0.2	
	41:17:55.5		mrg1 (EPIC)	2166.1	< 0.1	
2003-11a	0:42:53.78	52948.0	mrg1 (HRC-I)	943.3	< 0.3	
	41:18:46.2		mrg1 (EPIC)	970.6	< 8.6	
2003-11b	0:43:00.76	52972.8	mrg1 (HRC-I)	918.5	< 0.2	
	41:11:26.9		mrg1 (EPIC)	945.9	< 0.1	
2004-06c	0:42:49.02	53181.0	mrg1 (HRC-I)	710.3	< 0.4	
	41:19:17.8		mrg1 (EPIC)	737.6	< 0.4	
2004-11b	0:43:07.45	53314.8	mrg1 (HRC-I)	576.5	< 0.2	
	41:18:04.6		mrg1 (EPIC)	603.9	< 0.2	
2004-11g	0:42:52.48	53314.8	mrg1 (HRC-I)	576.5	< 0.3	
	41:18:00.2		mrg1 (EPIC)	603.9	< 0.3	
2004-11e	0:43:31.85	53338.8	mrg1 (HRC-I)	552.5	< 1.5	
	41:09:42.6		mrg1 (EPIC)	579.9	< 0.2	

Notes: [a]: RA, Dec are given in J2000.0; [b]: Modified Julian Date; MJD = JD - 2 400 000.5; [c]: mrg1/2/3 (HRC-I/EPIC) indicates merged data of all HRC-I/EPIC observations during 2006/7, 2007/8 or 2008/9; [d]: Time after observed start of optical outburst; [e]: unabsorbed 3σ upper limits in 0.2–10.0 keV band assuming a 50 eV blackbody spectrum with Galactic foreground absorption.

Table 4.5: Upper limits for M 31 CNe with outburst from about one year before the start of the 2006/7 campaign until its end.

Optical nova candidate			X-ray measurements			
Name M31N	RA (h:m:s)[a] Dec (d:m:s)[a]	MJD[b] (d)	Observation[c] ID	Δt^d (d)	L_X^e (10^{36} erg s^{-1})	Comment[f]
2005-05a	0:42:54.84	53506.0	mrg1 (HRC-I)	385.3	< 0.5	
	41:16:51.5		mrg1 (EPIC)	412.6	< 0.2	
2005-05b	0:42:47.15	53532.2	mrg1 (HRC-I)	359.0	< 0.2	near source
	41:15:35.7		mrg1 (EPIC)	386.4	< 37.6	[PFH2005] 338
2005-06a	0:42:28.42	53539.2	mrg1 (HRC-I)	352.0	< 1.9	
	41:16:50.9		mrg1 (EPIC)	379.4	< 0.3	
2005-06c	0:42:31.39	53544.2	mrg1 (HRC-I)	347.0	< 3.4	near source
	41:16:20.7		mrg1 (EPIC)	374.4	< 28.5	[PFH2005] 275
2005-07a	0:42:50.79	53581.0	mrg1 (HRC-I)	310.3	< 0.2	
	41:20:39.8		mrg1 (EPIC)	337.6	< 0.3	
2005-09a	0:42:52.23	53626.0	mrg1 (HRC-I)	265.3	< 0.8	
	41:19:59.4		mrg1 (EPIC)	292.6	< 0.1	
2005-09d	0:42:42.11	53635.0	mrg1 (HRC-I)	256.3	< 0.1	
	41:14:01.2		mrg1 (EPIC)	283.6	< 0.1	
2005-10b	0:42:42.11	53659.8	mrg1 (HRC-I)	231.5	< 0.9	
	41:18:00.3		mrg1 (EPIC)	258.9	< 0.1	
2006-02a	0:42:50.68	53768.8	mrg1 (HRC-I)	122.5	< 0.3	near source
	41:15:49.9		mrg1 (EPIC)	149.9	< 41.7	[PFH2005] 352
2006-05a	0:43:13.94	53863.0	mrg1 (HRC-I)	28.3	< 1.8	
	41:20:05.6		mrg1 (EPIC)	55.6	< 1.0	
2006-06b	0:42:32.77	53869.0	mrg1 (HRC-I)	22.3	< 1.6	
	41:16:49.2		mrg1 (EPIC)	49.6	< 0.1	
2006-09a	0:42:33.16	53981.5	7284 (HRC-I)	27.4	< 2.3	
	41:10:06.8		7285 (HRC-I)	70.8	< 4.0	
			0405320701 (EPIC)	119.1	< 0.2	
			0405320801 (EPIC)	135.0	< 0.7	
			0405320901 (EPIC)	154.7	< 0.3	
			7286 (HRC-I)	189.1	< 2.4	
2006-09b	0:42:41.45	53993.0	7284 (HRC-I)	15.9	< 1.0	
	41:14:44.6		7285 (HRC-I)	59.3	< 0.5	
			0405320701 (EPIC)	107.6	< 9.7	
			0405320801 (EPIC)	123.5	< 8.1	
			0405320901 (EPIC)	143.2	< 7.4	
			7286 (HRC-I)	177.6	< 2.3	

Table 4.5: continued.

Optical nova candidate			X-ray measurements			
Name M31N	RA (h:m:s)[a] Dec (d:m:s)[a]	MJD[b] (d)	Observation[c] ID	Δt^d (d)	L_X^e (10^{36} erg s^{-1})	Comment[f]
2006-09c	0:42:42.38	53996.2	7284 (HRC-I)	12.6	< 2.9	
	41:08:45.5		7285 (HRC-I)	56.0	< 1.5	
			0405320701 (EPIC)	104.4	< 2.4	
			0405320801 (EPIC)	120.2	< 0.6	
			0405320901 (EPIC)	139.9	< 0.9	
			7286 (HRC-I)	174.4	< 3.1	
2006-11b	0:42:44.05	54058.0	0405320701 (EPIC)	42.6	< 8.8	later
	41:15:02.2		0405320801 (EPIC)	58.5	< 5.3	re-brightening
			0405320901 (EPIC)	78.2	< 4.9	(named
			7286 (HRC-I)	112.6	< 0.7	M31N 2006-12d)
2006-11a*	0:42:56.81	54063.8	405320701 (EPIC)	36.9	< 0.6	found as
	41:06:18.4		0405320801 (EPIC)	52.7	< 0.4	SSS later
			0405320901 (EPIC)	72.4	< 0.5	
			7286 (HRC-I)	106.9	< 12.3	far off-axis
2006-12a	0:42:21.09	54085.0	0405320701 (EPIC)	15.6	< 2.7	
	41:13:45.3		0405320801 (EPIC)	31.5	< 1.4	
			0405320901 (EPIC)	51.2	< 6.9	
			7286 (HRC-I)	85.6	< 4.8	
2006-12b	0:42:11.14	54092.8	0405320701 (EPIC)	7.9	< 0.3	
	41:07:43.8		0405320801 (EPIC)	23.7	< 1.0	
			0405320901 (EPIC)	43.4	< 0.5	
			7286 (HRC-I)	77.9	< 2.9	
2006-12c	0:42:43.27	54093.8	0405320701 (EPIC)	6.9	< 0.5	
	41:17:48.1		0405320801 (EPIC)	22.7	< 0.6	
			0405320901 (EPIC)	42.4	< 0.5	
			7286 (HRC-I)	76.9	< 0.3	
2007-01a	0:42:51.13	54114.8	0405320801 (EPIC)	1.7	< 5.6	
	41:14:33.1		0405320901 (EPIC)	21.4	< 6.1	
			7286 (HRC-I)	55.9	< 0.9	
2007-02c	0:42:39.96	54140.8	7286 (HRC-I)	29.9	< 1.7	
	41:17:21.9					
2007-03a	0:42:53.60	54163.8	7286 (HRC-I)	6.9	< 2.5	
	41:12:09.8					

Notes: [a–e]: As for Table 4.4; [f]: Names of nearby sources from the catalogue of Pietsch et al. (2005b) ; *: M31N 2006-11a was found as a SSS in *Swift* observations on 2007-06-01 (188 d after outburst; Voss et al. 2008)

Table 4.6: Upper limits for M 31 CNe with outburst from about one year before the start of the 2007/8 monitoring until its end.

Optical nova candidate			X-ray measurements			
Name M31N	RA (h:m:s)[a] Dec (d:m:s)[a]	MJD[b] (d)	Observation[c] ID	Δt[d] (d)	L_X^e (10^{36} erg s^{-1})	Comment[f]
2006-10a	0:41:43.23	54030.8	mrg2 (HRC-I)	380.9	< 6.2	
	41:11:45.9		mrg2 (EPIC)	432.8	< 2.6	
2006-11b	0:42:44.05	54058.0	mrg2 (HRC-I)	353.6	< 0.4	re-brightened
	41:15:02.2		mrg2 (EPIC)	405.6	< 7.3	(M31N 2006-12d)
2006-11a	0:42:56.81	54063.8	mrg2 (HRC-I)	347.9	< 2.8	
	41:06:18.4		mrg2 (EPIC)	399.8	< 0.1	
2006-11c	0:41:33.23	54069.8	mrg2 (HRC-I)	341.9	< 11.3	far off-axis;
	41:10:12.3					not in EPIC
						field of view
2006-12a	0:42:21.09	54085.0	mrg2 (HRC-I)	326.6	< 0.9	
	41:13:45.3		mrg2 (EPIC)	378.6	< 0.9	
2006-12b	0:42:11.14	54092.8	mrg2 (HRC-I)	318.9	< 6.4	
	41:07:43.8		mrg2 (EPIC)	370.8	< 0.1	
2006-12c	0:42:43.27	54093.8	mrg2 (HRC-I)	317.9	< 0.6	
	41:17:48.1		mrg2 (EPIC)	369.8	< 0.5	
2007-01a	0:42:51.13	54114.8	mrg2 (HRC-I)	296.9	< 0.8	
	41:14:33.1		mrg2 (EPIC)	348.8	< 1.8	
2007-02c	0:42:39.96	54140.8	mrg2 (HRC-I)	270.9	< 0.2	
	41:17:21.9		mrg2 (EPIC)	322.8	< 1.4	
2007-03a	0:42:53.60	54163.8	mrg2 (HRC-I)	247.9	< 2.5	
	41:12:09.8		mrg2 (EPIC)	299.8	< 2.5	
2007-05a	0:43:02.61	54238.0	mrg2 (HRC-I)	173.6	< 0.5	
	41:14:41.4		mrg2 (EPIC)	225.6	< 0.8	
2007-06a	0:41:58.40	54265.0	mrg2 (HRC-I)	146.6	< 0.8	
	41:14:10.9		mrg2 (EPIC)	198.6	< 0.1	
2007-07a	0:43:04.05	54286.0	mrg2 (HRC-I)	125.6	< 0.3	
	41:17:08.3		mrg2 (EPIC)	177.6	< 0.2	
2007-07b	0:42:45.89	54289.0	mrg2 (HRC-I)	122.6	< 0.5	
	41:18:04.2		mrg2 (EPIC)	174.6	< 0.4	

Table 4.6: continued.

Optical nova candidate			X-ray measurements			
Name M31N	RA (h:m:s)[a] Dec (d:m:s)[a]	MJD[b] (d)	Observation[c] ID	Δt[d] (d)	$L_{\rm X}^{e}$ (10^{36} erg s^{-1})	Comment[f]
2007-07c	0:43:03.29	54300.0	mrg2 (HRC-I)	111.6	< 0.3	
	41:14:52.9		mrg2 (EPIC)	163.6	< 1.2	
2007-07d	0:42:59.49	54305.0	mrg2 (HRC-I)	106.6	< 0.5	
	41:15:06.5		mrg2 (EPIC)	158.6	< 1.3	
2007-07e	0:42:43.29	54306.5	mrg2 (HRC-I)	105.1	< 1.0	
	41:17:44.1		mrg2 (EPIC)	157.1	< 0.9	
2007-08e	0:42:44.70	54333.0	mrg2 (HRC-I)	78.6	< 0.8	close to
	41:16:36.2		mrg2 (EPIC)	130.6	< 28.8	M 31 centre
2007-08c	0:42:29.40	54342.0	mrg2 (HRC-I)	69.6	< 0.8	
	41:18:24.8		mrg2 (EPIC)	121.6	< 0.4	
2007-10a	0:42:55.95	54379.0	mrg2 (HRC-I)	32.6	< 9.9	far off-axis;
	41:03:22.0					not in EPIC
						field of view
2007-11c	0:43:04.14	54416.0	8527 (HRC-I)	5.8	< 3.8	
	41:15:54.3		8528 (HRC-I)	16.8	< 2.0	
			8529 (HRC-I)	25.6	< 3.1	
			8530 (HRC-I)	35.5	< 3.8	
			505720 (EPIC)	47.6	< 1.9	
2008-01a	0:42:58.54	54485.2	505720501 (EPIC)	7.7	< 2.2	
	41:14:44.1		505720601 (EPIC)	18.0	< 1.4	

Notes: As for Table 4.5.

Table 4.7: Upper limits for M 31 CNe with outburst from about one year before the start of the 2008/9 monitoring until its end.

Optical nova candidate			X-ray measurements			
Name M31N	RA (h:m:s)[a] Dec (d:m:s)[a]	MJD[b] (d)	Observation[c] ID	Δt[d] (d)	$L_{\rm X}^{e}$ (10^{36} erg s^{-1})	Comment[f]
2007-10a	0:42:55.95 41:03:22.0	54379.0	mrg3 (HRC-I)	399.3	< 17.0	far off-axis; not in EPIC field of view
2007-11c	0:43:04.14 41:15:54.3	54416.0	mrg3 (HRC-I)	362.3	< 0.5	
			mrg3 (EPIC)	414.1	< 2.3	
2008-01a	0:42:58.54 41:14:44.1	54485.2	mrg3 (HRC-I)	293.1	< 0.6	
			mrg3 (EPIC)	344.9	< 0.6	
2008-02a	0:42:30.38 41:09:53.8	54503.2	mrg3 (HRC-I)	275.1	< 0.9	
			mrg3 (EPIC)	326.9	< 1.0	
2008-03b	0:42:34.21 41:16:44.4	54527.8	mrg3 (HRC-I)	250.6	< 0.6	
			mrg3 (EPIC)	302.4	< 1.3	
2008-05c	0:43:12.08 41:19:15.8	54612.5	mrg3 (HRC-I)	165.8	< 2.2	
			mrg3 (EPIC)	217.6	< 0.4	
2008-07a	0:42:34.42 41:18:15.7	54619.0	mrg3 (HRC-I)	159.3	< 0.6	
			mrg3 (EPIC)	211.1	< 0.1	
2008-06b	0:42:27.81 41:14:48.2	54643.0	mrg3 (HRC-I)	135.3	< 0.8	
			mrg3 (EPIC)	187.1	< 0.4	
2008-06c	0:43:08.30 41:18:38.0	54645.0	mrg3 (HRC-I)	133.3	< 1.7	
			mrg3 (EPIC)	185.1	< 0.3	
2008-07b	0:43:27.28 41:10:03.3	54669.2	mrg3 (HRC-I)	109.1	< 4.0	
			mrg3 (EPIC)	160.9	< 0.6	
2008-08a	0:42:44.99 41:17:07.7	54688.0	mrg3 (HRC-I)	90.3	< 1.7	
			mrg3 (EPIC)	142.1	< 3.0	
2008-08b	0:42:52.38 41:16:12.9	54688.0	mrg3 (HRC-I)	90.3	< 1.5	
			mrg3 (EPIC)	142.1	< 5.4	

Table 4.7: continued.

Optical nova candidate			X-ray measurements			
Name M31N	RA (h:m:s)[a] Dec (d:m:s)[a]	MJD[b] (d)	Observation[c] ID	Δt^d (d)	L_X^e (10^{36} erg s^{-1})	Comment[f]
2008-08c	0:42:40.51 41:26:18.0	54706.2	mrg3 (HRC-I)	72.1	< 1.8	
			mrg3 (EPIC)	123.9	< 0.3	
2008-09a	0:41:46.72 41:07:52.1	54722.2	mrg3 (HRC-I)	56.1	< 13.5	far off-axis
			mrg3 (EPIC)	107.9	< 0.9	
2008-09c	0:42:51.42 41:01:54.0	54724.2	mrg3 (HRC-I)	54.1	< 18.1	far off-axis; not in EPIC field of view
2008-10b	0:43:02.42 41:14:09.9	54745.0	mrg3 (HRC-I)	33.3	< 2.5	
			mrg3 (EPIC)	85.1	< 0.6	
2008-10c	0:42:48.50 41:13:49.8	54759.0	mrg3 (HRC-I)	19.3	< 0.8	
			mrg3 (EPIC)	71.1	< 0.1	
2008-11d	0:42:57.30 41:15:41.1	54795.0	9827 (HRC-I)	3.2	< 1.1	
			9828 (HRC-I)	12.4	< 1.2	
			9829 (HRC-I)	23.0	< 1.2	
			10838 (HRC-I)	23.5	< 1.3	
			mrg3 (EPIC)	35.1	< 1.1	
			10683 (HRC-I)	83.9	< 2.7	
			10684 (HRC-I)	93.2	< 2.1	
2008-12b	0:43:04.85 41:17:51.6	54829.8	551690201 (EPIC)	0.4	< 1.9	near source [PFH2005] 386
			551690301 (EPIC)	10.5	< 3.0	
			551690401 (EPIC)	17.1	< 4.8	
			551690501 (EPIC)	28.6	< 6.3	
			551690601 (EPIC)	36.8	< 3.4	
			10683 (HRC-I)	49.1	< 0.6	
			10684 (HRC-I)	58.4	< 0.6	
2009-02b	0:42:27.77 41:13:42.4	54882.2	10684 (HRC-I)	5.9	< 1.9	

Notes: As for Table 4.5.

4.5 Non-nova supersoft X-ray sources detected in the monitoring

I also searched the XMM-Newton monitoring data for SSSs which do not have nova counterparts. This search was based on the hardness-ratio criterion described in Chap. 2.2. I found four additional SSSs that are not associated with optical novae. Three of these objects were detected in observations before our monitoring and have already been reported as SSSs in the literature. They are visible in all three campaigns. The forth sources is a new X-ray transient which was detected in the 2006/7 campaign. The light curves of these objects are given in Table 4.8 and their positions are shown in Fig. 4.1. In the following I describe briefly the properties of these sources in our observations. I refer to the known SSSs by their names in the catalogue of time variable X-ray sources by Stiele et al. (2008). The new SSSs is designated CXOM31 J004228.3+411449.

Object XMMM31 J004252.5+411541 is a bright and persistent SSS (see Table 4.8) that was discovered with the *Einstein Observatory* (source 69 in Trinchieri & Fabbiano 1991). It was extensively discussed by Trudolyubov & Priedhorsky (2008), who reported X-ray pulsations with a period of about 217.7 s. They discussed the source as a magnetic WD that is steadily accreting and burning hydrogen. During our monitoring, the source was always detected with high luminosities ($L_x > 10^{38}$ erg s^{-1}). Its light curve was variable by a factor of about two at most between individual observations (see Table 4.8). This source is most likely a classical SSS, similar to the objects found in the Magellanic Clouds.

Object XMMM31 J004318.8+412017 was discovered in early *Chandra* observations (Kaaret 2002; Kong et al. 2002b). Williams et al. (2006) included it in their catalogue of transient X-ray sources in M 31 (named r3-8 after Kong et al. 2002b) and discussed it as a Galactic foreground polar based on its soft spectrum. During our monitoring, the source showed burst-like variability with luminosity increase by more than a factor of ten (see Table 4.8). Four earlier outbursts of the source were reported by Williams et al. (2006).

Object XMMM31 J004318.7+411804 was reported as a previously unknown variable SSS by Stiele et al. (2008). They reported a maximum luminosity of $L_x = 3.3{\times}10^{36}$ erg s^{-1} and classified the source as a candidate SSS. The object is detected in less than half of our monitoring observations (see Table 4.8). Its luminosity is only a few 10^{36} erg s^{-1} in most detections with the exception of two *Chandra* observations where it reaches $\sim 10^{37}$ erg s^{-1}.

Object CXOM31 J004228.3+411449 exhibits strong variability. It is only detected in the first two observations of the 2006/7 campaign and its luminosity dropped in the 27 days from *Chandra* observation 7283 to XMM-Newton observation 0405320501 by a factor of about 40, to $1.1{\pm}0.1{\times}10^{37}$ erg s^{-1}. However, it is not detected ten days earlier in the archival *Chandra* ACIS-I observation 7137 (see Table 2.2) with an upper limit luminosity of $8.7{\times}10^{37}$ erg s^{-1}, which is well below the luminosity measured for observation 7283. The *Chandra* HRC-I position of the source is RA = 00:42:28.31 and Dec = +41:14:48.6 (J2000). The only nearby X-ray source in the literature is 2XMMi J004227.8+411454 from the XMM-Newton 2nd Incremental Source Catalogue (2XMMi, XMM-SSC 2008) at a distance of $7\farcs4$. It was detected as a faint object ($L_x = 2.5 \pm 0.9{\times}10^{36}$ erg s^{-1}, detection likelihood 8.5) in XMM-Newton observation 0202230401 on 2004-07-19.07 UT. I re-analysed the data of this observation and cannot confirm this object. This is likely to be due to the improved screening procedures I applied (see Chap. 2.2) in comparison to the standard reduction chain used for the 2XMMi catalogue (Watson et al. 2009).

I classify CXOM31 J004228.3+411449 therefore as a new source in M 31. There is no bright optical object near this position in the Local Group Galaxies Survey catalogue (LGGS; Massey et al. 2006). No nova was reported within the error box of the source. The strong variability of CXOM31 J004228.3+411449 could indicate a very soft black hole transient, a transient SSS (similar

Table 4.8: Non-nova SSSs detected during the monitoring.

Name[a] XMMM31	RA (h:m:s)[b] Dec (d:m:s)[a]	Observation ID	MJD[c] (d)	$L_{\rm X}^{d}$ (10^{36} erg s^{-1})	Comment[e]
J004252.5+411541	00:42:52.5	7283 (HRC-I)	53891.3	102.4 ± 4.9	217.7 s
	41:15:40.1	405320501 (EPIC)	53918.6	222.9 ± 3.7	period (1)
		405320601 (EPIC)	53956.5	194.9 ± 3.5	
		7284 (HRC-I)	54008.9	211.1 ± 8.0	
		7285 (HRC-I)	54052.3	245.9 ± 9.7	
		405320701 (EPIC)	54100.6	215.9 ± 3.4	
		405320801 (EPIC)	54116.5	201.9 ± 3.6	
		405320901 (EPIC)	54136.2	227.0 ± 3.4	
		7286 (HRC-I)	54170.6	182.8 ± 8.7	
		8526 (HRC-I)	54411.6	267.1 ± 9.6	
		8527 (HRC-I)	54421.8	294.4 ± 10.2	
		8528 (HRC-I)	54432.8	361.7 ± 14.1	
		8529 (HRC-I)	54441.6	217.8 ± 11.3	
		8530 (HRC-I)	54451.5	248.7 ± 11.6	
		505720201 (EPIC)	54463.6	203.1 ± 2.3	
		505720301 (EPIC)	54473.3	228.1 ± 2.5	
		505720401 (EPIC)	54483.6	178.1 ± 2.6	
		505720501 (EPIC)	54492.9	215.7 ± 3.5	
		505720601 (EPIC)	54503.2	247.8 ± 3.1	
		9825 (HRC-I)	54778.3	156.1 ± 7.3	
		9826 (HRC-I)	54787.1	232.3 ± 9.0	
		9827 (HRC-I)	54798.2	362.2 ± 14.2	
		9828 (HRC-I)	54807.4	301.6 ± 12.8	
		9829 (HRC-I)	54818.0	261.5 ± 16.7	
		10838 (HRC-I)	54818.5	303.5 ± 18.0	
		551690201 (EPIC)	54830.1	244.5 ± 3.0	
		551690301 (EPIC)	54840.3	189.7 ± 2.6	
		551690401 (EPIC)	54846.9	224.2 ± 4.6	
		551690501 (EPIC)	54858.3	230.6 ± 3.1	
		551690601 (EPIC)	54866.6	176.0 ± 3.2	
		10683 (HRC-I)	54878.9	255.7 ± 10.8	
		10684 (HRC-I)	54888.2	224.2 ± 10.0	

to the SSSs in the Magellanic Clouds), or a SSS counterpart of an undetected nova. In the latter case, the fast evolution of the X-ray light curve might imply a scenario similar to M31N 2006-04a, with an optical nova outburst within one hundred days before the first detection of the SSS (from March to June 2006) and a short SSS phase.

To summarise, in the three monitoring campaigns I found in total 21 X-ray nova counterparts. Fifteen of these sources have been classified as SSSs. Comparing this number to the four non-nova SSSs presented here confirms the finding of PFF2005 that optical novae are the major class of SSSs in the central part of M 31.

Table 4.8: continued.

Name[a]	RA (h:m:s)[b] Dec (d:m:s)[a]	Observation ID	MJD[c] (d)	$L_{\rm X}^{d}$ (10^{36} erg s^{-1})	Comment[e]
J004318.8+412017	00:43:18.8	7283 (HRC-I)	53891.3	< 7.1	foreground
	41:20:16.1	405320501 (EPIC)	53918.6	< 1.6	polar(?) (2)
		405320601 (EPIC)	53956.5	< 5.3	
		7284 (HRC-I)	54008.9	42.6 ± 6.5	
		7285 (HRC-I)	54052.3	< 15.2	
		405320701 (EPIC)	54100.6	14.8 ± 1.2	
		405320801 (EPIC)	54116.5	22.3 ± 2.4	
		405320901 (EPIC)	54136.2	< 3.5	
		7286 (HRC-I)	54170.6	< 3.7	
		8526 (HRC-I)	54411.6	< 5.9	
		8527 (HRC-I)	54421.8	< 11.0	
		8528 (HRC-I)	54432.8	< 1.6	
		8529 (HRC-I)	54441.6	< 1.5	
		8530 (HRC-I)	54451.5	10.2 ± 2.6	
		505720201 (EPIC)	54463.6	9.4 ± 0.9	
		505720301 (EPIC)	54473.3	4.6 ± 0.6	
		505720401 (EPIC)	54483.6	< 3.8	
		505720501 (EPIC)	54492.9	5.3 ± 0.9	
		505720601 (EPIC)	54503.2	1.1 ± 0.4	
		9825 (HRC-I)	54778.3	20.5 ± 5.4	
		9826 (HRC-I)	54787.1	14.5 ± 4.2	
		9827 (HRC-I)	54798.2	< 2.7	
		9828 (HRC-I)	54807.4	< 1.6	
		9829 (HRC-I)	54818.0	< 7.2	
		10838 (HRC-I)	54818.5	< 10.8	
		551690201 (EPIC)	54830.1	3.0 ± 0.6	
		551690301 (EPIC)	54840.3	2.5 ± 0.7	
		551690401 (EPIC)	54846.9	< 3.3	
		551690501 (EPIC)	54858.3	< 1.9	
		551690601 (EPIC)	54866.6	< 2.4	
		10683 (HRC-I)	54878.9	< 7.7	
		10684 (HRC-I)	54888.2	< 3.5	

Table 4.8: continued.

Name[a]	RA (h:m:s)[b] Dec (d:m:s)[a]	Observation ID	MJD[c] (d)	L_X^d (10^{36} erg s^{-1})	Comment[e]
XMMM31 J004318.7+411804	00:43:18.7	7283 (HRC-I)	53891.3	< 5.4	
	41:18:05.2	405320501 (EPIC)	53918.6	2.3 ± 0.6	
		405320601 (EPIC)	53956.5	< 3.4	
		7284 (HRC-I)	54008.9	< 4.7	
		7285 (HRC-I)	54052.3	< 10.8	
		405320701 (EPIC)	54100.6	< 2.6	
		405320801 (EPIC)	54116.5	< 2.2	
		405320901 (EPIC)	54136.2	< 3.5	
		7286 (HRC-I)	54170.6	< 2.3	
		8526 (HRC-I)	54411.6	< 6.5	
		8527 (HRC-I)	54421.8	< 3.3	
		8528 (HRC-I)	54432.8	< 9.0	
		8529 (HRC-I)	54441.6	< 8.6	
		8530 (HRC-I)	54451.5	< 6.1	
		505720201 (EPIC)	54463.6	1.1 ± 0.4	
		505720301 (EPIC)	54473.3	0.9 ± 0.3	
		505720401 (EPIC)	54483.6	0.6 ± 0.3	
		505720501 (EPIC)	54492.9	< 6.9	
		505720601 (EPIC)	54503.2	1.7 ± 0.5	
		9825 (HRC-I)	54778.3	9.7 ± 3.3	
		9826 (HRC-I)	54787.1	< 8.1	
		9827 (HRC-I)	54798.2	< 4.3	
		9828 (HRC-I)	54807.4	< 4.3	
		9829 (HRC-I)	54818.0	< 10.1	
		10838 (HRC-I)	54818.5	9.5 ± 3.3	
		551690201 (EPIC)	54830.1	2.4 ± 0.6	
		551690301 (EPIC)	54840.3	1.9 ± 0.5	
		551690401 (EPIC)	54846.9	< 3.2	
		551690501 (EPIC)	54858.3	4.8 ± 1.9	
		551690601 (EPIC)	54866.6	< 2.1	
		10683 (HRC-I)	54878.9	< 7.2	
		10684 (HRC-I)	54888.2	< 2.8	
CXOM31 J004228.3+411949	00:42:28.3	7283 (HRC-I)	53891.3	422.8 ± 14.3	new source
	41:14:48.5	405320501 (EPIC)	53918.6	11.0 ± 1.0	
		405320601 (EPIC)	53956.5	< 0.4	
		7284 (HRC-I)	54008.9	< 2.3	
		7285 (HRC-I)	54052.3	< 0.4	
		405320701 (EPIC)	54100.6	< 1.0	
		405320801 (EPIC)	54116.5	< 0.7	
		405320901 (EPIC)	54136.2	< 0.8	
		7286 (HRC-I)	54170.6	< 3.8	

Notes: [a]: Source name from the catalogue of Stiele et al. (2008); [b]: RA, Dec are given in J2000.0; [c]: Modified Julian Date MJD = JD - 2 400 000.5; [d]: unabsorbed luminosity in 0.2–10.0 keV band assuming a 50 eV blackbody spectrum with Galactic foreground absorption, luminosity errors are 1σ, upper limits are 3σ; [e]: (1): Trudolyubov & Priedhorsky (2008), (2): Williams et al. (2006).

Chapter 5

Highlight: First SSSs in M 31 globular clusters

This chapter describes the first two SSSs that were found in the M 31 GC system (see also Henze et al. 2009d). Both objects were transient X-ray sources. They were discovered in the 2007/8 monitoring campaign with *Chandra* and observed subsequently with XMM-Newton and *Swift*. Whereas one source could be identified with the very first nova found in a M 31 GC, no optical nova counterpart could be found for the second SSS. I discuss the impact of this finding on the nova rate within M 31 GCs.

5.1 Supersoft source in Bol 111

In the first *Chandra* observation of the 2007/8 monitoring campaign, starting on 2007-11-07.64 UT (ObsID 8526), there was a new source (hereafter SS1) detected at the very edge of the HRC-I field of view (see also Pietsch et al. 2007b). SS1 remained active during the following *Chandra* monitoring observations (ObsIDs 8527-30) in 2007 November and December. I followed the light curve of SS1 with *Swift* ToO observations (ObsIDs 00031017001-12, 2007 November - 2008 January) and also found the source to be still visible in the XMM-Newton M 31 large survey observations 0511380201 and 0511380601, in January and February 2008. In Table 5.1 I present details on all observations. Due to the location of SS1 near the edge of the *Chandra* HRC-I field of view during all observations (see Fig. 5.2 for the location of the *Chandra* field and the source), I used the XMM-Newton observations to perform precise astrometry. The offset-corrected XMM-Newton position of the source was determined to be RA = 00:42:33.21, Dec = +41:00:26.1 (J2000) with a 3σ error of $1\farcs6$, including the uncertainty of the offset correction. These coordinates coincide (distance = $0\farcs5$), within the errors, with the position of the M 31 GC Bol 111 (Galleti et al. 2004, 00:42:33.16, +41:00:26.1). Therefore, I assumed that SS1 is situated within the globular cluster. Note, that no X-ray source was previously known in this GC. See Fig. 5.3 for a visualisation of the agreement of optical (DSS POSS-II Red) and X-ray positions.

Table 5.1: X-ray observations of SS1 in Bol 111.

Telescope/Instrument[a]	ObsID	Exp. time[b] [ks]	Date[c] [UT]	Offset[d] [d]	Count Rate[e] [ct s^{-1}]	$L_{0.2-1.0}$ [e] [erg s^{-1}]
XMM-Newton EPIC PN	0505760201	49.2	2007-07-22.55	33	$< 1.1 \times 10^{-3}$	$<1.4 \times 10^{36}$
Chandra HRC-I	8526	18.7	2007-11-07.64	141	$> (1.9 \pm 0.4) \times 10^{-2}$	$>(5.3 \pm 1.1) \times 10^{38}$
Chandra HRC-I	8527	20.0	2007-11-17.76	151	$(2.5 \pm 0.2) \times 10^{-2}$	$(7.0 \pm 0.7) \times 10^{38}$
Chandra HRC-I	8528	20.0	2007-11-28.79	162	$(2.2 \pm 0.2) \times 10^{-2}$	$(6.0 \pm 0.6) \times 10^{38}$
Chandra HRC-I	8529	18.9	2007-12-07.57	171	$(2.8 \pm 0.3) \times 10^{-2}$	$(7.7 \pm 0.7) \times 10^{38}$
Chandra HRC-I	8530	19.9	2007-12-17.49	181	$(2.5 \pm 0.3) \times 10^{-2}$	$(7.1 \pm 0.7) \times 10^{38}$
Swift XRT	00031017001/2	7.1	2007-11-18.40	152	$(1.2 \pm 0.2) \times 10^{-2}$	$(11.6 \pm 1.4) \times 10^{38}$
Swift XRT	00031017003	3.0	2007-11-13.02	177	$(0.8 \pm 0.2) \times 10^{-2}$	$(8.1 \pm 1.9) \times 10^{38}$
Swift XRT	00031017004	3.0	2007-12-14.02	178	$(1.1 \pm 0.2) \times 10^{-2}$	$(10.6 \pm 2.2) \times 10^{38}$
Swift XRT	00031017005	3.2	2007-12-15.03	179	$(1.1 \pm 0.2) \times 10^{-2}$	$(11.1 \pm 2.1) \times 10^{38}$
Swift XRT	00031017006	2.2	2007-12-20.25	184	$(1.1 \pm 0.3) \times 10^{-2}$	$(11.1 \pm 2.6) \times 10^{38}$
Swift XRT	00031017007	2.1	2007-12-22.39	186	$(0.5 \pm 0.2) \times 10^{-2}$	$(5.1 \pm 1.9) \times 10^{38}$
Swift XRT	00031017008	2.3	2007-12-24.33	188	$(0.9 \pm 0.2) \times 10^{-2}$	$(9.1 \pm 2.4) \times 10^{38}$
Swift XRT	00031017009	2.3	2007-12-30.15	194	$(1.0 \pm 0.2) \times 10^{-2}$	$(10.0 \pm 2.4) \times 10^{38}$
Swift XRT	00031017010	2.0	2008-01-03.44	198	$(1.2 \pm 0.3) \times 10^{-2}$	$(12.2 \pm 2.8) \times 10^{38}$
Swift XRT	00031017011	1.9	2008-01-06.25	201	$(0.4 \pm 0.3) \times 10^{-2}$	$(4.0 \pm 2.8) \times 10^{38}$
Swift XRT	00031017012	1.7	2008-01-10.00	205	$(1.1 \pm 0.3) \times 10^{-2}$	$(11.1 \pm 1.3) \times 10^{38}$
XMM-Newton EPIC PN	0511380201	23.0	2008-01-05.99	200	$(8.2 \pm 0.2) \times 10^{-2}$	$(10.6 \pm 0.2) \times 10^{38}$
XMM-Newton EPIC PN	0511380601	24.0	2008-02-09.31	235	$(7.5 \pm 0.2) \times 10^{-2}$	$(12.2 \pm 0.4) \times 10^{38}$
Swift XRT	00037718001	4.8	2008-05-26.29	342	$(0.5 \pm 0.1) \times 10^{-2}$	$(4.6 \pm 1.3) \times 10^{38}$
XMM-Newton EPIC PN	0560180101	17.4	2008-07-18.26	395	$(3.0 \pm 0.2) \times 10^{-2}$	$(8.9 \pm 0.5) \times 10^{38}$

Notes: [a]: Telescope and instrument used for observation; [b]: Dead time corrected exposure time of the observation; [c]: Start date of the observation; [d]: Time in days after the discovery of nova M31N 2007-06b in the optical (Shafter & Quimby 2007) on 2007 June 19.38 (JD = 2454271); [e]: Source count rates, X-ray luminosities (unabsorbed, blackbody fit, 0.2 - 1.0 keV) and upper limits were estimated according to Chap. 5.1. For *Chandra* ObsID 8526 the source is right on the detector edge, therefore I give lower luminosity limits.

Table 5.2: X-ray observations of SS2 in Bol 194

Telescope/Instrument[a]	ObsID	Exp. time[b] [ks]	Date[c] [UT]	Offset[d] [d]	Count Rate[e] [ct s^{-1}]	Luminosity[e] [erg s^{-1}]
XMM-Newton EPIC PN	0505760201	49.2	2007-07-22.55	0	$< 2.9 \times 10^{-3}$	$< 1.6 \times 10^{36}$
Chandra ACIS-S	8186	5.0	2007-11-03.18	104	2.1×10^{-2}	3.4×10^{37}
Chandra HRC-I	8526	18.7	2007-11-07.64	108	$(3.6 \pm 0.3) \times 10^{-2}$	$(8.4 \pm 0.6) \times 10^{37}$
Chandra HRC-I	8527	20.0	2007-11-18.76	118	$(3.0 \pm 0.3) \times 10^{-2}$	$(7.0 \pm 0.6) \times 10^{37}$
Swift XRT	00031027001	7.3	2007-11-24.34	125	$(8.0 \pm 1.2) \times 10^{-3}$	$(6.4 \pm 1.0) \times 10^{37}$
Chandra ACIS-S	8187	5.0	2007-11-27.16	128	$< 6 \times 10^{-4}$	$< 9.7 \times 10^{35}$
Swift XRT	00031027002/3	4.7	2007-12-02.64	133	$(3.2 \pm 1.0) \times 10^{-3}$	$(3.9 \pm 1.2) \times 10^{37}$
Swift XRT	00031027004	3.9	2007-12-16.77	147	$< 3.2 \times 10^{-3}$	$< 3.9 \times 10^{37}$
Swift XRT	00031027005	4.0	2007-12-30.02	160	$< 2.0 \times 10^{-3}$	$< 2.4 \times 10^{37}$
XMM-Newton EPIC PN	0511380201	22.8	2008-01-05.99	167	$< 5.1 \times 10^{-3}$	$< 3.5 \times 10^{36}$

Notes: [a]: Telescope and instrument used for observation. ACIS-S count rates are from Galache et al. (2007); [b]: Dead time corrected exposure time of the observation; [c]: Start date of the observation; [d]: Time in days after the last X-ray non-detection of SS2 on 2007 July 22.55 (JD = 2454304); [e]: Source count rates, X-ray luminosities (unabsorbed, blackbody fit, 0.2 - 1.0 keV) and upper limits were estimated according to Chap. 5.2.

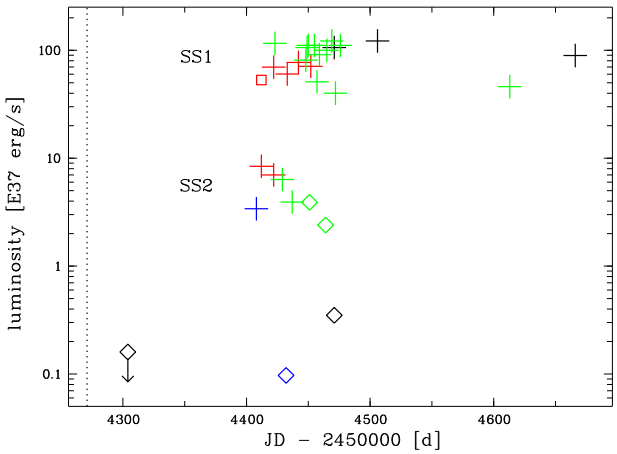

Figure 5.1: X-ray light curves of SS1 and SS2 (0.2-1.0 keV) obtained from XMM-Newton (**black**), *Chandra* HRC-I (**red**), *Chandra* ACIS-S (**blue**), and *Swift* XRT (**green**) (see also Tables 5.1,5.2). The upper limit for SS1 is indicated by a **down-pointing arrow**, the upper limits for SS2 are marked by **open lozenges**. An **open square** indicates the lower limit luminosity for SS1 in *Chandra* ObsID 8526. **Crosses** symbolise luminosities of detections. The (statistical) errors are mostly smaller than the size of the symbols. The vertical dotted line indicates the day of the first detection of nova M31N 2007-06b in the optical (Shafter & Quimby 2007).

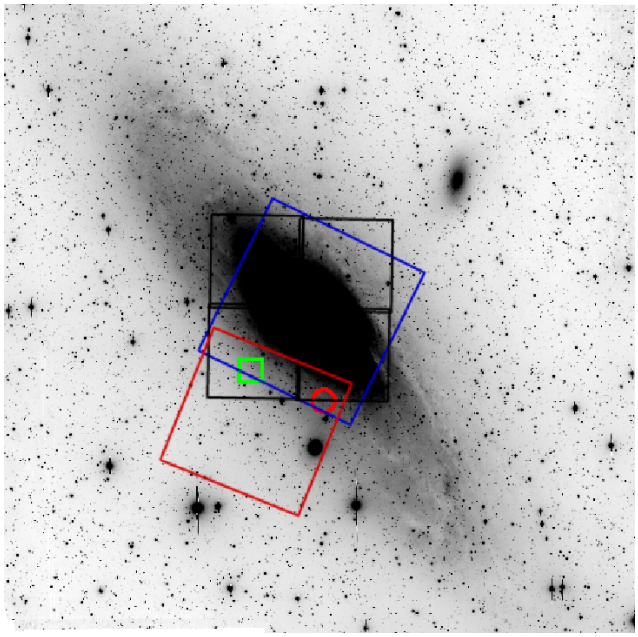

Figure 5.2: ROTSE-III M 31 central field (see Chap. 5.2.1). Overlaid are the four Super-LOTIS fields (black squares), the *Chandra* HRC-I field for ObsID 8527 (big blue square) and the XMM-Newton field for ObsID 0511380201 (big red square). Indicated are the position of Bol 111 (red circle) and Bol 194 (green square).

To perform spectral analysis of SS1 I used XMM-Newton observations obtained on 2008-01-05.99 UT and 2008-02-09.31 UT (ObsIDs 0511380201 and 0511380601). I extracted the EPIC PN spectra of SS1 from both observations and fitted them simultaneously in order to increase statistics.

I fitted the spectra using an absorbed blackbody model. Temperature and foreground $N_{\rm H}$ were both assumed to be the same during the two observations and only the respective normalisations were allowed to vary independently from each other. The relative stability of the spectral parameters is confirmed by a XMM-Newton observation on 2008-07-18.26 UT (160 days later than 051138601), from which I extracted a spectrum of SS1 that can be fitted by a model with similar parameters (see below). The blackbody model yields an acceptable $\chi^2_r = 1.39$ for the best fit values of kT = 48^{+2}_{-3} eV and $N_{\rm H} = 2.3 \pm 0.1 \times 10^{21}$ cm^{-2}. This fit is shown in Fig. 5.4 and the associated contour plot is given in Fig. 5.5. I computed the unabsorbed EPIC PN X-ray luminosities, in the range 0.2 – 1.0 keV, from the best fit model. Based on the best fit values I created in XSPEC fake spectra (command `fakeit`) to infer the energy conversion factors (ecf) for the *Swift* XRT (ecf$_{XRT}$) and the *Chandra* HRC-I (ecf$_{HRC-I}$). The ecf values are given in Table 5.3 and were used to convert the *Swift* XRT and *Chandra* HRC-I count rates to unabsorbed luminosities. All luminosities assume a distance to M 31 of 780 kpc (Holland 1998; Stanek & Garnavich 1998) and are presented in Table 5.1. Note, that for the first detection of SS1 in the *Chandra* HRC-I observation 8526 only a lower limit for the luminosity could be derived, due to the location of the source on the edge of the detector. The blackbody fit parameters and derived values are given in Table 5.3.

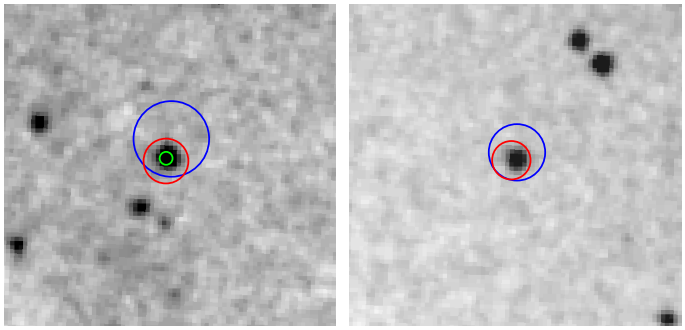

(a) Bol 111 (b) Bol 194

Figure 5.3: X-ray position error circles for SS1 and SS2 as described in Chap. 5.1 and Chap. 5.2 with respect to Bol 111 and Bol 194. **Blue/big**: *Chandra* HRC-I, **red/medium**: *Swift* XRT, **green/small**: XMM-Newton PN. Underlying optical image: $5' \times 5'$ DSS POSS-II Red.

The unabsorbed X-ray luminosities inferred from the blackbody fit are in the order of 10^{39} erg s^{-1}, and therefore significantly exceed the Eddington luminosity of a hydrogen rich atmosphere of a WD: $L_{\mathrm{Edd}} = 1.3 \times 10^{38} \left(\frac{M}{M_{\odot}}\right)$ erg s^{-1}. The fact that blackbody fits to SSS spectra produce in general too high values of N_{H} and too low temperatures, and therefore too high luminosities, is well known (see e.g. Greiner et al. 1991; Kahabka & van den Heuvel 1997, and references therein), thus the values given in Table 5.1 define upper limits on the actual luminosity of SS1.

Blackbody fits are very simple approximations for SSS emission of novae that allow to compare parameters like effective temperature for different novae. However, as mentioned in Chap. 1.1, these fits are physically not realistic. Therefore, I tested fitting the low-resolution spectra with WD atmosphere models, that are based on physically more realistic assumptions. I used a grid of synthetic ionizing spectra for hot compact stars from NLTE model atmospheres computed by Rauch (2003). These NLTE models are plane-parallel, in hydrostatic and radiative equilibrium and contain all elements from H to Ca (Rauch 1997). The models were computed using the Tübingen Model-Atmosphere Package (TMAP, Rauch & Deetjen 2003). Elemental abundances are fixed to either galactic halo ([X][1] = [Y] = 0, [Z] = -1) or solar ([X] = [Y] = [Z] = 0) ratios. The grids of model atmosphere fluxes, as well as FITS tables which can be used in XSPEC, are available on-line[2]. The XSPEC tables contain temperatures and fluxes (binned to 0.1 Å intervals) for fixed surface gravity and elemental abundances. In our case, the available grid parameter space was restricted to models with $\log g = 9.0$, since only these tables include temperatures high enough to fit our spectra. This restriction clearly limits the significance of our best fits, since models with different surface gravity may have provided equally good fits with different parameters. Also note, that the assumptions of plane parallel and static are not physically realistic for a nova atmosphere. Furthermore, the spectral analysis is limited by the low energy resolution of the EPIC PN spectra, which are, due to the faintness of the source, the only available spectra with sufficient signal to noise ratio. Great caution should therefore be applied when interpreting the results of these test fits.

I fitted the EPIC PN spectra with both halo and solar abundance ratios. Galactic halo abundances are more representative of the metallicity of the M 31 GCs (Barmby & Huchra 2000). Figure 5.6 gives the fit for halo abundances and shows that the atmosphere model fits the spectrum well only up to an energy of about 600 eV (χ^2 dof^{-1} = 1.01) but predicts too high flux at energies above, which

[1] []: log(abundance/solar abundance)
[2] http://astro.uni-tuebingen.de/~rauch/

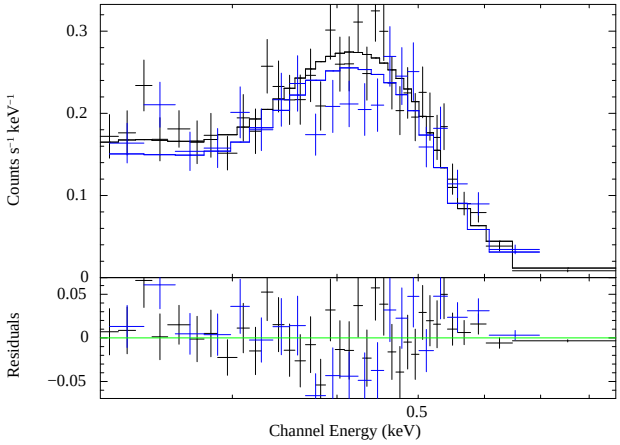

Figure 5.4: XMM-Newton EPIC PN spectra of SS1 (**crosses**) from observations 0511380201 (**black**) and 0511380601 (**blue**) fitted with an absorbed blackbody (**solid lines**).

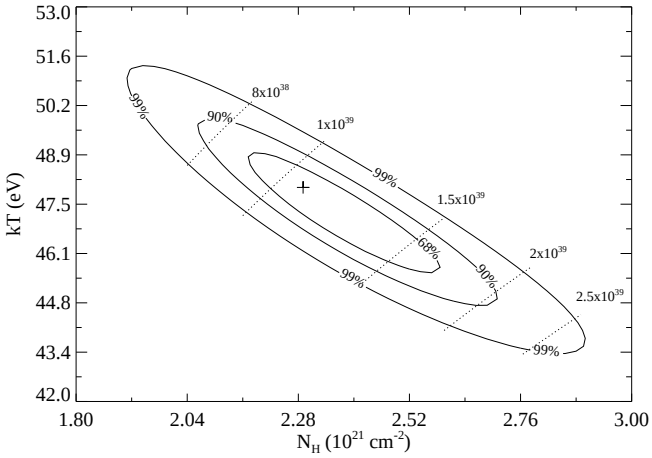

Figure 5.5: Column density ($N_{\rm H}$) - temperature (kT) contours inferred from the blackbody fit to the XMM-Newton EPIC PN spectra of SS1 (see Fig. 5.4). Normalisation has been adjusted. Indicated are the formal best fit parameters (**cross**) and the lines of constant X-ray luminosity (0.2-1.0 keV, **dotted lines**).

is clearly indicated by the residuals. This is true for solar and halo abundances. However, this is no surprise since recent detailed X-ray spectroscopy of the SSS phase of Galactic novae showed that these spectra are complex (see e.g. Ness et al. 2007b, who reported nova spectra obtained with the XMM-Newton RGS and the *Chandra* LETGS). Spectral models currently available may be not suitable for a correct fitting of SSS spectra of novae, especially with respect to the elemental abundances of a hot post-nova atmosphere.

In Table 5.3 I compare the parameters of the WD atmosphere model fits (fitted to the 0.2 – 0.6 keV range) to the parameters of the blackbody fit described above. I give unabsorbed X-ray luminosities (L_x), that were computed for the range 0.2 – 1.0 keV in XSPEC, and bolometric luminosities (L_{bol}) as well as WD radii (R), inferred from the bolometric luminosities. The bolometric luminosity for the blackbody fit was directly computed from the normalisation of the spectra in XSPEC. For the WD atmosphere model I used an absorbed blackbody fit with the same temperature and foreground $N_{\rm H}$ to compute bolometric luminosity and WD radius. These values overestimate the actual luminosity and radius and are therefore upper limits. Energy conversion factors (ecf) for the *Swift* XRT (ecf$_{XRT}$) and the *Chandra* HRC-I (ecf$_{HRC-I}$) detectors were again computed in XSPEC, using fake spectra as for the blackbody fit, and are listed in Table 5.3 together with the ecf for the XMM-Newton EPIC PN (ecf$_{PN}$).

The comparison of the fits shows that the WD atmosphere models give physically more plausible results. The high value of $N_{\rm H}$ which was required for the blackbody fit (three times the foreground absorption) is significantly reduced to a value which is just slightly above the foreground level of $N_{\rm H} = 0.7\times 10^{21}$ cm^{-2}. As a consequence, the super-Eddington luminosity derived from the blackbody fits is reduced to more realistic values for the atmosphere models. The connection of $N_{\rm H}$ and effective temperature can be seen in the confidence contours shown in Fig. 5.5. The effective temperature for the WD atmosphere is higher than the blackbody temperature and is revealing the hot photosphere. Still, one has to be cautious interpreting these models, because the elemental abundances are fixed and

Table 5.3: Comparison of SS1 spectral best fit parameters and derived parameters for blackbody and WD atmosphere models with halo and solar abundances.

Model (energy range [keV])	Blackbody (0.2 – 0.8)	WD halo (0.2 – 0.6)	WD solar (0.2 – 0.6)
kT (eV)	48^{+2}_{-3}	61 ± 1	70 ± 1
$N_{\rm H}$ (10^{21} cm^{-2})	2.3 ± 0.1	1.0 ± 0.2	1.0 ± 0.2
χ^2_r	1.39	1.01	1.06
dof	53	44	48
L_x (10^{38} erg s^{-1})	10.6 ± 0.2	1.00 ± 0.02	0.88 ± 0.02
L_{bol} (10^{38} erg s^{-1})	$28.7^{+0.2}_{-0.1}$	2.7 ± 0.1	1.5 ± 0.1
R (10^9 cm)	$7.0^{+1.6}_{-0.7}$	1.21 ± 0.07	0.70 ± 0.04
ecf$_{PN}$ (ct cm^2 erg^{-1})	5.0×10^9	5.5×10^{10}	6.1×10^{10}
ecf$_{HRC-I}$ (ct cm^2 erg^{-1})	2.6×10^9	3.2×10^{10}	3.7×10^{10}
ecf$_{XRT}$ (ct cm^2 erg^{-1})	7.4×10^8	8.7×10^9	9.9×10^9

Notes: Luminosities and WD radii refer to the XMM-Newton observation 0511380201. The unabsorbed X-ray luminosity L_x is for the 0.2 - 1.0 keV range. Bolometric luminosities and WD radii for the WD atmosphere model are upper limits (see Sec. 5.1 for details).

may be not realistic to describe abundances in a burning WD atmosphere. However, the consideration of model substructures, like absorption edges, already causes a reduction of the $N_{\rm H}$ necessary to adjust the model to the spectra. Truly physical models for supersoft emission from novae are strongly needed and should be validated using high resolution spectra obtained with current and future missions.

I checked *Swift* (ObsID 00037718001, starting at 2008-05-26.29 UT) and XMM-Newton (ToO 0560180101, starting at 2008-07-18.26 UT) data and found that SS1 was still visible in both observations (see also Table 5.1 for details). Preliminary data analysis was published in Pietsch et al. (2008b,c). For *Swift* I used the blackbody fit described above and in Table 5.3 to convert the XRT count rate to unabsorbed luminosity. For XMM-Newton I extracted an EPIC PN spectrum of SS1 as described above for the two earlier XMM-Newton observations. The spectrum can be fitted with an blackbody fit with best fit values of kT = (43 ± 8) eV and $N_{\rm H} = 2.2^{+1.0}_{-0.7} \times 10^{21}$ cm^{-2} ($\chi^2_r = 1.52$). These parameters are consistent with the blackbody fit described above and result in an unabsorbed X-ray luminosity (range of 0.2 - 1.0 keV) of $(8.9 \pm 0.5) \times 10^{38}$ erg s^{-1}. Both observations show that the X-ray luminosity of SS1 is slowly declining.

Supersoft spectra like the one of SS1 are typical for counterparts to optical novae and indicate that after the outburst there is hydrogen burning going on in the remaining envelope of the WD (see Pietsch et al. 2005a, and references therein). Therefore, I identify the supersoft X-ray transient in the globular cluster Bol 111 with the nova M31N 2007-06b reported by Shafter & Quimby (2007). This optical nova was first detected on 2007 June 19.38 and was detected in X-rays the first time 141 days later on 2007 November 07.64. SS1 was not visible on 2007 July 22.55, which is 33 days after the first detection in the optical (see Table 5.1).

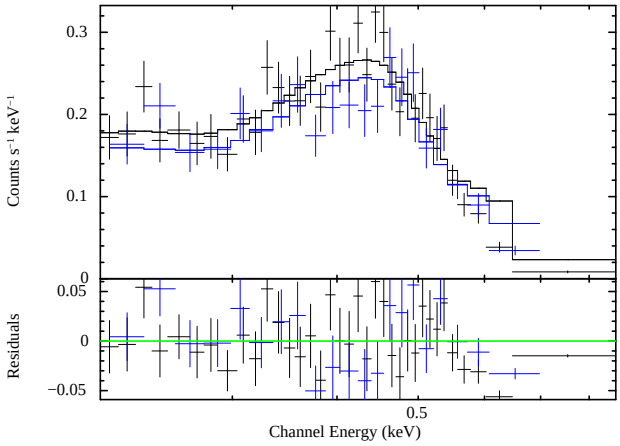

Figure 5.6: XMM-Newton EPIC PN spectra of SS1 from observations 0511380201 (**black**) and 0511380601 (**blue**) fitted with an WD atmosphere model with galactic halo abundances (**solid lines**).

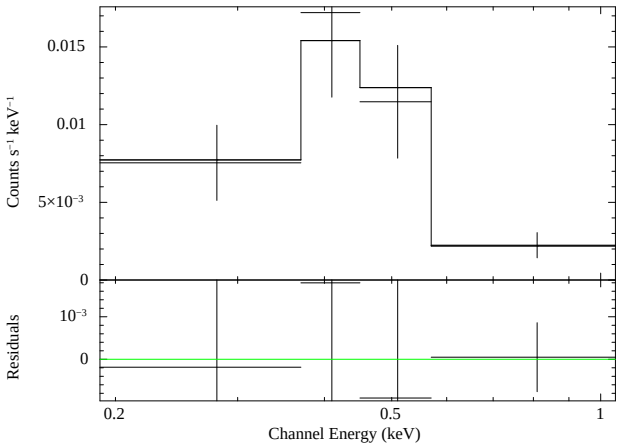

Figure 5.7: *Swift* XRT spectrum of SS2 in Bol 194 from observation 00031027001 (7.3 ks exposure time) fitted with an absorbed blackbody fit (**solid line**).

5.2 Supersoft source in Bol 194

A second supersoft source (SS2) was detected in the same *Chandra* HRC-I observation as SS1 (ObsID 8526) as a new, bright X-ray transient (Haberl et al. 2007a). In the following observation (ObsID 8527) SS2 was again detected with similar brightness close to the edge of the HRC-I field of view (see Fig. 5.2). For the remaining three *Chandra* observations of the monitoring campaign the position of SS2 was outside the field of view due to the changing roll angle of the observations. Therefore, I used *Swift* XRT ToO follow up observations (starting with ObsID 00031027001) to constrain the spectrum of SS2 and follow the X-ray light curve. The X-ray luminosities given in Table 5.2 show that this source faded much faster than SS1. Therefore, no XMM-Newton observations of SS2 are available and I could use the XMM-Newton data only to compute upper limits. Since SS2 also has a large off-axis position in the HRC-I field, I used the *Swift* observation 00031027001 to compute the position of the source. I found the following coordinates: RA = 00:43:45.3, Dec = +41:06:08.15 (J2000). With a 1σ position error of $4\farcs6$ and a distance of $1\farcs1$ to the GC Bol 194 (Galleti et al. 2004, 00:42:45.20, +41:06:08.3) these coordinates are in good agreement with the position of Bol 194. See Fig. 5.3 for a comparison of optical (DSS POSS-II Red) and X-ray positions.

The *Swift* XRT spectrum of SS2 (ObsID 00031027001) only shows photons with energies below 750 eV (see Fig. 5.7). Therefore, I classified this source as a SSS. Since there are not many spectral counts for this source, I used Cash statistics for spectral modelling. The best spectral fit is an absorbed blackbody with best fit values of kT = 74^{+32}_{-23} eV and $N_{\rm H} = \left(1.0^{+1.6}_{-0.9}\right) \times 10^{21}$ cm^{-2}. The best fit parameters differ from the preliminary data analysis published in Haberl et al. (2007b), where a different abundance table in XSPEC (angr; Anders & Grevesse 1989) and χ^2 statistics were used. Using the best fit values I computed the X-ray luminosity of SS2 to be $(6.4 \pm 1.0) \times 10^{37}$ erg s^{-1}, the bolometric luminosity to be $10^{+7}_{-4} \times 10^{37}$ erg s^{-1} and therefore the radius of the WD to be $5^{+11}_{-3} \times 10^{8}$ cm. Unfortunately, the low count *Swift* XRT spectrum does not provide enough degrees of freedom to test the WD atmosphere model that I fitted to the XMM-Newton EPIC PN spectra of SS1.

After the discovery of SS2, Galache et al. (2007) reported that they found the source to be present in a 5 ks *Chandra* ACIS-S observation taken on 2007-11-03.18 UT, which is four days earlier than the first *Chandra* HRC-I detection. They confirmed the classification of SS2 as a SSS and further report that the source is not visible any more in a 5 ks *Chandra* ACIS-S observation on 2007-11-27.16 UT (~ 24 days after the previous ACIS observation) with an 95% confidence upper limit of $\sim 6 \times 10^{-4}$ ct s^{-1}. Note, that this observation was taken just three days after our Swift observation on 2007-11-24.34 UT. Additional *Swift* XRT observations by Kong & Di Stefano (2007) showed a re-brightening of the source on 2007-12-02.64. However, the source faded quickly again and was not found in follow-up *Swift* observations and in the XMM-Newton monitoring data.

I re-analysed the *Swift* and *Chandra* HRC-I data, computed upper limits for the XMM-Newton observations and present all available data on SS2 in Table 5.2. I took the count rates for detections and upper limits from Kong & Di Stefano (2007) to compute luminosities in XSPEC using my spectral model. For the *Swift* observations 00031027004/5 I give 95% confidence upper limits on the SS2 luminosity. These values are comparable to actual luminosities obtained for earlier *Swift* observations, an effect which is due to longer effective source exposure times for the earlier observations. X-ray luminosities for the three instruments were computed using XSPEC and the blackbody fit inferred from the *Swift* spectrum.

Analogous to SS1 and its connection to M31N 2007-06b in Bol 111, the supersoft spectrum and the transient light curve could indicate that SS2 is the X-ray counterpart of a recent optical nova in the GC Bol 194. The following section describes the optical data analysis and the constraints that I can put on a possible nova counterpart in Bol 194.

5.2.1 Search for an optical nova counterpart

As there was no optical nova reported in Bol 194 I searched the recent optical data available to me for indications of a nova outburst in the GC. Note, that the constant background light from the GC makes it difficult to detect nova outbursts. However, difference imaging is a successful method in this context and was used to analyse a big part of the optical data set. In the following I describe the observational set-up and the analysis of the optical data.

Optical observations

The majority of the optical data on Bol 194 was obtained in the context of the Texas Supernova Search (TSS; Quimby 2006b). The TSS employed the 0.45-m ROTSE-IIIb telescope at the McDonald observatory in Texas, and the data presented here are supplemented by its twin, the ROTSE-IIId telescope, which is located at the Turkish National Observatory at Bakirlitepe, Turkey. The ROTSE-III system is described in Akerlof et al. (2003). The $1\overset{\circ}{.}85 \times 1\overset{\circ}{.}85$ field of view covered by the unfiltered 2k×2k Marconi CCD encompasses practically all of M 31's light in a single exposure (see Fig. 5.2), and additional overlapping fields to the north-east and south-west add to the haul. Beginning in November 2004, these 3 fields were imaged several times nightly as weather and season allowed.

The second largest data set consists of optical monitoring data obtained with Super-LOTIS (see Chap. 2.1.3). The south-east Super-LOTIS field covers Bol 194 and the astrometric and photometric 1σ accuracies for this particular object (~ 16.8 mag) are $0\overset{''}{.}11$ and 0.06 mag, respectively.

Additionally, in this research the optical data set is supplemented by archival data from K. Hornoch obtained at telescopes in Lelekovice (Newtonian focus of 350/1658 mm telescope, CCD camera G2CCD-1600, Kron-Cousins R filter, 1.12″/pixel, FOV 28.7′x19.1′) and Ondřejov (primary focus of 650/2342 mm telescope, CCD camera G2CCD-3200, Kron-Cousins R filter, 1.20″/pixel, FOV

21.8′x14.7′). Standard reduction procedures for raw CCD images were applied (dark and bias subtraction and flat-field correction) using SIMS[3] and Munipack[4] programs. Reduced images of the same series were co-added to improve the S/N ratio (total exposure time varied from 600s up to 1800s). The gradient of the galaxy background of co-added images was flattened by the spatial median filter using SIMS. These processed images were used for aperture photometry, carried out in GAIA[5]. Relative photometry was done using brighter field stars which were calibrated using standard Landolt fields. The 1σ measurement uncertainties were low (~ 0.03 mag), thanks to the long exposure times, the brightness of Bol 194, and its location far from the high surface brightness levels found near the center of M 31.

Optical data analysis

I searched the optical data of Bol 194 obtained by the monitoring programs described above for a significant optical excess that could indicate a nova outburst in the GC. The significance for the Super-LOTIS data and for Hornoch's data is defined by applying a 3σ clipping to the light curves of Bol 194 and judging every two neighboured data points that lie outside the final $\pm 3\sigma$ range as possible indications of a nova outburst.

For the ROTSE-III data, the PSF-matched image subtraction code developed by the Supernova Cosmology Project (Perlmutter et al. 1999) was used to search for residual light from an optical nova. With this method the outburst of nova M31N 2007-06b in Bol 111 was detected (Shafter & Quimby 2007). First, a deep reference image was constructed by co-adding 100 ROTSE-IIIb images obtained between December 2004 and June 2006. Then, this image was convolved to match the PSF of each ROTSE-III image, subtracted off this template light, and searched for any point sources coincident with Bol 194. It was attempted to measure any residuals at this location with the DAOPHOT PSF-fitting routines (Stetson 1987; ported to IDL by Landsman 1989).

These procedures did not lead to the discovery of an optical nova counterpart of SS2 in Bol 194. However, the optical monitoring data of the M 31 bulge region allowed me to put strong constraints on the outburst date of any nova that may have occurred in Bol 194. Figure 5.8 includes all optical data of Bol 194 from November 2004 until 2007-11-08, which is 5 days after the first detection of SS2 in X-rays on 2007-11-03. I show the minimum detectable magnitude of a possible optical nova occurring in Bol 194 during this period.

To calculate the limiting magnitudes of the ROTSE-III observations, the noise on the subtracted frames was measured in annuli centred on the location of Bol 194. The limits reported here correspond to the flux required of a point source to be detected at the 4σ level. The magnitude scale was calibrated against the USNO-B1.0 R2 measurements (Monet et al. 2003).

In contrast to this procedure, the limiting magnitude for the Super-LOTIS data and for Hornoch's data is computed as follows. At the distance of M 31 the light of a nova in a GC would blend with the light of the GC itself. Therefore, we have to take into account the intrinsic magnitude of the cluster (~ 16.8 mag in the Super-LOTIS data) and compute the resulting magnitude using

$$R_t = -2.5\, log_{10}(10^{-0.4\,R_{gc}} + 10^{-0.4\,R_n}),$$

with R_t, R_{gc}, and R_n being the total magnitude, the magnitude of the GC, and the magnitude of the nova, respectively. Thus, for the Super-LOTIS data and for Hornoch's data, the minimum detectable

[3] http://ccd.mii.cz/
[4] http://munipack.astronomy.cz/
[5] http://www.starlink.rl.ac.uk/gaia

magnitude R_L of a nova is defined as the magnitude that leads to a significantly brighter R_t. The significance criterion used here is:

$$R_t < R_{gc} - 3\sigma_{R_{gc}},$$

with $3\sigma_{R_{gc}}$ being the 3σ photometric standard error for Bol 194 (~ 0.16 mag for the Super-LOTIS data reduction and ~ 0.09 mag for Hornoch's data). These measurement errors are mean values derived from our light curves of Bol 194. Since I used a 3σ clipping method to search for a nova outburst in Bol 194, I assume that the mean photometric errors given for both instruments would correspond to the final 3σ range in the case of a nova outburst-modified light curve. Therefore, I compute R_L as follows:

$$R_L = -2.5\, log_{10}(10^{-0.4\,(R_{gc}-3\sigma_{R_{gc}})} - 10^{-0.4\,R_{gc}}).$$

In order to judge the time coverage of the optical data set, I simulated the outburst of novae with different peak magnitudes and t_2 times in Bol 194 on any day between 2004 October and 2007 November and checked whether we would have detected the outburst according to the limiting magnitudes, or not. I simulated novae with peak magnitudes of 15.5, 16.0, 16.9, 18.0, 18.5 and 19.0 mag in the R band and t_2 times of 6, 15, 29, 63, 102 and 164 days, respectively. The peak magnitude of nova M31N 2007-06b in Bol 111 as given in Shafter & Quimby (2007) is 16.9 mag. To compute the t_2 time, I used the maximum magnitude versus rate of decline (MMRD) relationship given by Della Valle & Livio (1995), for $t_2 \leq 50$ d:

$$M_{V,max} = -7.92 - 0.81 \arctan\left(\frac{1.32 - \log t_2}{0.23}\right),$$

and by Cohen (1988), for $t_2 > 50$ d:

$$M_{V,max} = 2.41 \log t_2 - 10.70.$$

I used this combination of the two different MMRDs according to Shafter (1997) in order to compensate for the breakdown of the MMRD from Della Valle & Livio (1995) at large values of t_2. Both MMRDs give the relation of the t_2 time of a nova to its maximum magnitude in the V band. The colour relation for novae at maximum light is $(B-V)_0 = 0.23 \pm 0.06$ (van den Bergh & Younger 1987). This fact implies for novae at maximum light a spectral type close to F0 and therefore a $(V-R)_0 \sim 0.30$ (see e.g. Allen 1976) which I used to match both MMRDs to the R band data.

For the simulations I used a M 31 extinction free distance modulus of $\mu_0 = 24.38$ mag (Freedman et al. 2001). I applied a reddening towards M 31 of $E(B-V) = 0.062$ (Schlegel et al. 1998) and a foreground extinction in the R band of $A_R^f = 0.17$ mag, obtained via the NASA Extragalactic Database (NED). I estimated the internal absorption of M 31 to be $A_R^i \sim 0.11$ mag, using $A_{pg}^i \sim 0.20$ mag (Capaccioli et al. 1989) and assuming that $A_{pg} \sim A_B$.

The results of these simulations are shown in the bottom panel of Fig. 5.8, with the upper parts of the curves indicating the periods over which each simulated nova would have been detected. The figure visualises the fact that the optical monitoring is efficient in the sense that the only periods in which we would not have been able to detect novae were the periods when M 31 was not observable due to its annual visibility. These periods, computed for a nova with parameters of M31N 2007-06b, and the estimated constraints on the delay time between optical outburst and detection in X-rays are shown in Table 5.4. Note also, that a bright nova (peak luminosity = 15.5 mag) would have been missed more likely than a fainter nova. This is due to the faster decline of luminosity for the brighter novae and good detection limits of our observations down to ~ 19 mag.

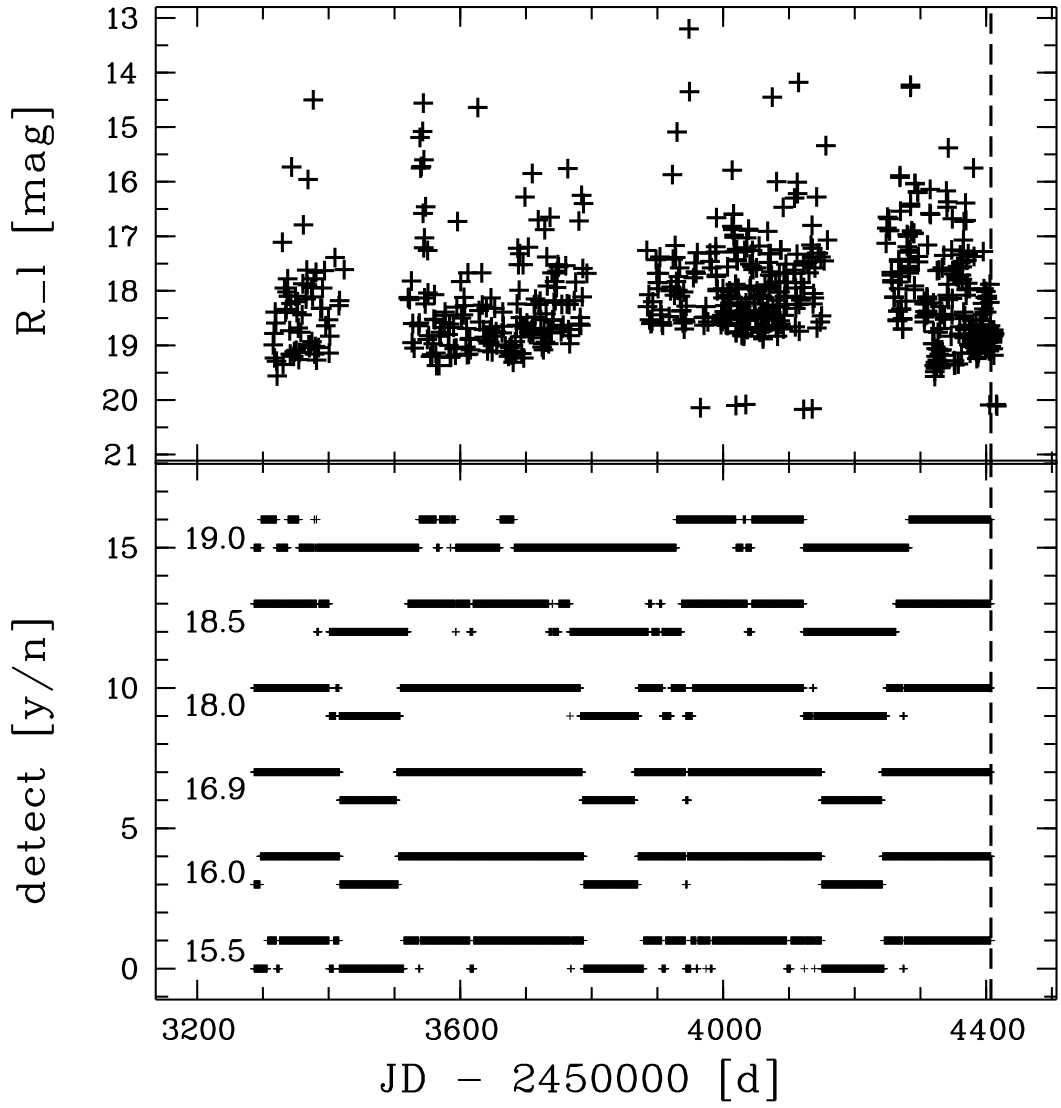

Figure 5.8: Top: Limiting magnitudes of all optical data since 2004 November. **Bottom**: simulated detection (upper points) or non detection (lower points) for novae with indicated peak magnitudes. In both panels the vertical dashed line shows the date of the first detection of SS2 in X-rays.

Table 5.4: Optical constraints on a nova in Bol 194

Date1 [UT][a]	Date2 [UT][a]	RJD1 [d][b]	RJD2 [d][b]	Delay [d][c]
2005-02-15	2005-05-12	3417	3503	990 - 904
2006-02-19	2006-05-09	3786	3865	621 - 542
2007-02-18	2007-05-20	4150	4241	257 - 166

Notes: [a]: Start date (date1) and end date (date2) of the non-detection periods
[b]: The same as in [a] but in RJD = JD - 2 450 000
[c]: Periods of possible delay time between nova outburst and first detection in X-rays

5.3 Discussion

5.3.1 Globular cluster nova rate - the optical point of view

The statistics of novae in GCs of other galaxies is still poor. Tomaney et al. (1992) conducted a search in Hα of over 200 M 31 GCs for nova eruptions and found nothing over an effective survey time of one year. This results in an upper limit for the M 31 GC nova rate of 0.005 novae yr^{-1} GC^{-1}. Another search for novae in 54 M 31 GCs was done by Ciardullo et al. (1990b) based on the M 31 Hα survey data of Ciardullo et al. (1987, 1990a). Over a mean effective survey time of approximately two years no indications for a nova outburst in one of the GCs was found. From one nova found in a GC of the giant elliptical galaxy M 87 Shara et al. (2004) derive a rate of 0.004 novae yr^{-1} GC^{-1} for the whole system of 1057 known M 87 GCs (4.2 novae yr^{-1}).

There are about 500 GCs known that belong to M 31 (482 confirmed GCs, according to the Revised Bologna Catalogue[6] (V.3.5, March 2008; Galleti et al. 2004, 2005, 2006, 2007)). This corresponds approximately to a stellar mass of about 5 $\times 10^9$ M$_\odot$. Given a rate of 2.2 novae yr^{-1} (10^{10} M$_\odot$)$^{-1}$, which is observed in old systems like elliptical galaxies (data derived from Table 3 of Della Valle et al. (1994) and Equation (1) of Mannucci et al. (2005)), one derives a rate of about 1.1 novae yr^{-1} for the M 31 GC system, which corresponds to about 0.002 novae yr^{-1} GC^{-1}. This figure is comparable (within a factor of 2) with the observed rate (0.004) of the M 87 GC system obtained by Shara et al. (2004) and suggests that the discovery of only one nova in the M 31 GC system (Shafter & Quimby 2007) over about a century of observations may be the result of a strong observational bias (see Shafter & Quimby 2007).

5.3.2 Globular cluster nova rate - the X-ray point of view

While the detection of CNe in GC in the optical is strongly hampered by the light from the GC itself, the detection of supersoft emission from a hydrogen-burning post-nova atmosphere is not affected by this. However, the presence of other X-ray sources in a GC, such as LMXBs, may create a similar problem for the detection of a SSS in that GC. In the following, I discuss the impact of our results on the rate of novae for the M 31 GCs.

If we assume that both SS1 and SS2 are post-novae and assume the duration of the SSS phase to be of the order of 1 yr then we find a nova rate of 0.015 novae yr^{-1} GC^{-1} for the $\sim$ 130 GCs from Galleti et al. (2007) in the field of view of our *Chandra* HRC-I observations (see also Fig. 5.2 for the *Chandra* field). The duration of the SSS phase of novae is a critical parameter for a correct estimate of the nova rate. Although there are some novae known to have much longer SSS phases than 1 yr (see e.g. Ögelman et al. 1993, and Table 4.3), it is likely (see PHS2007) that novae with short SSS phases were just not found in the past due to selection effects. Also note, that the SSS phase of SS2 lasted only $\lesssim$ 4 months and therefore the assumed duration of 1 yr may still be a quite conservative estimate.

The nova rate computed using the X-ray data on the SSSs is about a factor 10 larger (after assuming the duration of the SSS phase to be 1 yr) than the nova rate estimated by assuming that GCs produce novae with a rate comparable to the old stellar populations in Ellipticals. The match between the rates in X-ray and in optical is obtained for a duration of the SSS phase of about a decade. Such long times have been observed indeed (see Table 4.3), but they do not seem to be the rule (see PHS2007).

[6] http://www.bo.astro.it/M31/

The results based on the small size of our sample of GC SSSs are clearly dominated by Poissonian statistics. In this case, the discovery of two GC novae would still be consistent with a nova rate of ~ 0.002 novae yr^{-1} GC^{-1} (95% confidence level) and ~ 0.004 novae yr^{-1} GC^{-1} (99.87% confidence level), respectively. Both values are below the upper limit of 0.005 novae yr^{-1} GC^{-1} estimated by Tomaney et al. (1992) from optical observations.

Furthermore, I want to emphasize the fact that not all optical novae in the Galaxy and in M 31 were detected as SSSs. Novae with supersoft X-ray emission are a subset, with yet unknown size, of the whole nova population. The nova rates deduced from X-ray observations are therefore lower limits on the actual nova rates.

5.3.3 Implications on the nova rate in M 31 globular clusters

The nova rate in the M 31 GC system may be larger by about one order of magnitude than expected in old stellar systems like giant ellipticals. This fact implies the existence of some other (dynamical) mechanism which acts inside the GCs and is capable to raise the fraction of CN systems naturally produced by stellar evolution. It is well known that LMXBs are highly overabundant in GCs, with respect to the rest of a galaxy (see e.g. Fan et al. 2005, and references therein). This is explained by dynamical effects like tidal captures of low-mass main-sequence stars by neutron stars (see also Clark 1975; Fabian et al. 1975). One would expect similar effects for WDs (Hut & Verbunt 1983), but although large numbers of cataclysmic variables (CVs) have been found in Galactic GCs, the number of novae detected in GCs is still small (see Shara et al. 2004, and references therein).

Further, I note that novae with short SSS states seem to be an important contributor to the SSS population of galaxies (see also PHS2007). XMM-Newton observations of M 31 in the past (Stiele et al. 2008; Pietsch et al. 2005b; Trudolyubov & Priedhorsky 2004) did not detect SSS with positions that agree with GC positions. This might in part be due to the fact that the individual observations of these monitorings were separated by half a year or more. The discoveries of SS1 and SS2 are the first results of a new monitoring strategy, that uses XMM-Newton and *Chandra* observations that are separated just by 10 days. Future observations that follow this strategy may increase the statistics for SSS in M 31 GCs. If future surveys of M 31 will be able to find between six to eight new GC novae per year, the existence of a nova rate excess, of the size reported above, will be proven at 95% and 99.87% confidence level, respectively.

Finally, given the possible link between SSS and type Ia supernovae (SNe-Ia) (e.g. Della Valle & Livio 1994; Di Stefano & Rappaport 1994) if a high rate for SSS in GCs will be confirmed by future surveys, it may not be inconceivable to expect detection of SNe-Ia in GC systems around giant ellipticals or bulge dominated galaxies.

Chapter 6

Discussion of the sample of M 31 novae with X-ray counterpart

In this chapter I discuss the results presented in Chap. 4. First, individual novae that showed a short-term variable light curve (Chap. 6.1) or a particularly long SSS state (Chap. 6.2) are discussed. After that, in Chap. 6.3 I present correlations between various nova parameters that I found in a statistical analysis of Table 4.3 and include a note of caution about the physical interpretation of these correlations. I further describe how I computed the derived nova parameters in Table 4.3 (Chap. 6.4) and present a simulation targeting the duration of the SSS state in novae and the completeness of the X-ray monitoring (Chap. 6.5). In Chap. 6.6 I discuss nova populations studies and how my results from the X-ray monitoring point towards two different nova populations. Finally, I describe an asymmetry in the geometrical distribution of SSS counterparts of M 31 novae in Chap. 6.7.

6.1 Short-term variable supersoft X-ray light curves of novae

6.1.1 M31N 2006-04a

The EPIC PN light curve of M31N 2006-04a (see Fig. 4.12) points towards a (1.6 ± 0.3) h period. Previously, there were only three other SSSs known in M 31 for which light curves indicated periodic variability. This small sample consists of the transient SSS XMMU J004319.4+411758 (865.5 s period; Osborne et al. 2001), the persistent supersoft source XMMU J004252.5+411540 (217.7 s; Trudolyubov & Priedhorsky 2008), and the SSS counterpart of the CN M31N 2007-12b (1100 s; Pietsch 2010, see below). In M 31, M31N 2006-04a therefore is only the second nova to show a periodically variable X-ray flux at all and the only known SSS with a period longer than one hour.

Also in the Galaxy only six novae with periodic X-ray variability are known, namely V1494 Aql (2500 s; Drake et al. 2003), RS Oph (35 s; Osborne et al. 2006b), V4743 Sgr (several periods, e.g. 6.7 h and ~ 1300 s; Leibowitz et al. 2006; Dobrotka & Ness 2010), V5116 Sgr (2.97 h; Sala et al. 2008), CSS 081007:030559+054715 (1.77 d; Osborne et al. 2009) and KT Eri (35 s; Beardmore et al. 2010).

The typical orbital periods of CVs range between one and ten hours (Ritter & Kolb 2003). CNe show similar orbital periods (Warner 2002). The pulsation periods of WDs in CNe are typically shorter than 1 hour (see e.g. Drake et al. 2003, 2500 s pulsation period in nova V1494 Aql). Therefore, the X-ray variability of M31N 2006-04a might reveal the orbital period of the binary system. Alternatively, the observed variability could also be caused by an eclipsing accretion disk (see e.g. Sala et al. 2010) or might point towards the influence of strong magnetic fields in a similar way

to what is known for thermonuclear bursts on neutron stars (Strohmayer & Bildsten 2006; Watts & Strohmayer 2006).

6.1.2 M31N 2007-12b

The SSS counterpart of nova M31N 2007-12b showed pulsations at a period of 1110 s that stayed constant over 30 days (see Fig. 4.21) during the four XMM-Newton observations where it was detected (see Table 4.2). These pulsations most certainly represent the rotation period of the WD in the system. Rotation periods with similar values have been reported for many CVs and specifically for intermediate polar (IP) systems that had a nova outburst (see e.g. Warner 2002). The 1110 s modulation is the first definite rotational period of a WD found in a M 31 optical nova system. As in other CVs containing a magnetic WD the modulation most likely is caused by brighter spots on the photosphere due to asymmetric fuel coverage because of magnetic channelling during accretion.

Furthermore, there are dips present in the X-ray light curves of M31N 2007-12b (see Fig. 4.21), which may have been caused by occulting material in the binary system and therefore reflect the orbital period of the system. There is a dip in three out of four observations but never more than one. Therefore, the orbital period should be close to the duration of the individual observations. The possible orbital period can be determined as follows: The time differences between the start time of the dips in observations 0505720301 and 0505720401 as well as 0505720401 and 0505720501 (see Table 4.2) are 10.2242(128) d and 9.4052(128) d, respectively. These differences must be multiples of the orbital period. Also, the difference between these differences (0.8190(256) d) has to be a multiple n of the period. These conditions can be fulfilled for $n = 2$ and $n = 4$, suggesting periods of 0.4095 d and 0.2047 d (9.828 h and 4.914 h), respectively. Shorter periods are not allowed as they would have led to a second dip within observation 0505720401.

The proposed orbital periods of 4.9 h or even 9.8 h are on the long side of – but well within – the distribution of orbital periods of classical Galactic novae (see e.g. Diaz & Bruch 1997). Based on the proposed rotation period of 1110 s and the differing binary period, M31N 2007-12b can be classified as an IP system. Therefore, M31N 2007-12b can be added as the first extragalactic IP candidate identified with an optical nova to the list of Galactic nova IPs and IP candidates (Warner 2002)[1].

6.2 Novae with long supersoft X-ray source states

6.2.1 Two recurrent novae with a very long supersoft X-ray source phase?

Two novae are still observed as SSSs more than ten years after the optical outburst: M31N 1996-08b (12.5 y) and M31N 1997-11a (11.0 y). Interestingly, both novae were classified as RN candidates by Shafter & Irby (2001) and discussed as RNe in PHS2007. If these two novae would turn out to be actual RNe, this would present a serious challenge to the models of X-ray emission in novae, because RNe are believed to contain a massive WD, which should lead to a very short SSS phase (Sala & Hernanz 2005; Tuchman & Truran 1998).

However, to search for RN candidates Shafter & Irby (2001) looked for positional coincidences between novae they discovered and novae from the literature, using a relatively large error box of $15'' \times 12''$ size (with the long side orientated along the major axis of M 31). They consequently stress to have applied "relatively loose selection criteria" and that therefore "these novae are recurrent nova *candidates*". I found large distances of both novae to their assumed recurrent counterparts of $9\farcs9$

[1] for an up-to-date catalogue of IPs and IP candidates see http://asd.gsfc.nasa.gov/Koji.Mukai/iphome/catalog/alpha.html

for M31N 1996-08b to M31N 1925-01a (Hubble 1929, his nova 41) and 7.″8 for M31N 1997-11a to M31N 1982-09a (Ciardullo et al. 1987, their nova 1). This led me to the tentative conclusion that neither of the two novae is a RN. In the case of M31N 1996-08b, also the low effective temperature of $kT = (22^{+31}_{-15})$ points towards a low mass WD (see e.g. Sala & Hernanz 2005), rather than a RN. Note however that for both novae none of the proposed historic nova counterparts has a published finding chart. Clarification about the nature of these novae can therefore only come from a re-examination of the original data, because historical novae can have relatively large positional errors (see e.g. Henze et al. 2008e).

There is of course the possibility that both novae actually are RNe and that their last optical outbursts had been missed. But while on one hand this scenario would shorten the SSS durations considerably, on the other hand it would also result in extremely short recurrence times, implying massive WDs. There are two consequences of this scenario: (a) a massive WD should lead to an even shorter SSS phase of less than a year (see e.g. Hachisu & Kato 2006), and (b) earlier nova outbursts, following the same recurrence time scale, would far more likely have been detected in the past. None of these consequences agrees with the observational facts for both objects.

6.2.2 Six novae with long supersoft X-ray source states

In the monitoring I detected six X-ray counterparts of optical novae that were still active for about five to twelve years after the optical outburst. These novae are M31N 1996-08b, M31N 1997-11a, M31N 2001-10a, M31N 2004-05b (all described in Chap. 4.1), M31N 2003-08c and M31N 2004-01b (see Chap. 4.2). They are all still visible at the end of the 2008/9 monitoring for 12.5, 11.0, 7.4, 4.8, 5.5 and 5.2 years after the optical outburst, respectively (see Tables 4.1 and 4.2). Additionally, there is the possibility that faint SSSs like XMMM31 J004318.7+411804 (see Chap. 4.5 and Table 4.8), which shows a light curve similar to that of M31N 2003-08c and was already detected in 2002 with XMM-Newton (Stiele et al. 2008), might be novae with a long SSS phase for which the optical outburst had been missed due to gaps in the optical monitoring.

Novae M31N 2003-08c and M31N 2004-01b are relatively faint sources ($L_x \sim 5{\times}10^{36}$ erg s^{-1}) that were detected for the first time in the 2007/8 and 2008/9 campaign, respectively. Both sources show variability by at least a factor of two (see Table 4.2) but there is no indication of a decline in luminosity over time. All of the remaining four novae were already detected by PHS2007 and were also present in the 2006/7 campaign. Of these four SSSs only M31N 1997-11a shows a declining light curve over the course of the three monitoring campaigns described in this work. The X-ray luminosity of the other three nova counterparts exhibits on average no significant change from 2007 to 2009.

For four of the novae (M31N 1997-11a, M31N 2004-05b, M31N 2003-08c and M31N 2004-01b) I found significant variability in their X-ray light curves on short time scales. The luminosity of M31N 1997-11a increased by about a factor of two from *Chandra* observation 8528 to 8529 and returned to its previous state in observation 8530. For M31N 2004-05b I noticed a similar phenomenon between observations 8526, 8527 and 8528 (see Table 4.1). The observations are separated by about ten days (see Table 2.1). The variability of M31N 2003-08c is difficult to constrain, because the source is only slightly above the detection limit in most cases. The luminosity of nova M31N 2004-01b increased significantly towards the end of the 2008/9 campaign.

There are two scenarios in which the long SSS duration of these six novae can be explained. The first scenario assumes that the novae occured on low-mass WDs, for which long post-nova SSS phases are expected (see e.g. Hachisu & Kato 2006). For the duration of the H-burning, the bolomet-

ric luminosity of the nova should be constant while the photospheric surface shrinks and the effective temperature increases (see e.g. Gallagher & Starrfield 1976; Hernanz 2005; Bode 2010). The slowly declining X-ray count rate of M31N 1997-11a therefore could be due to a change in effective temperature (compare the energy conversion factors in Table 2.5).

In this context, it is noteworthy that Shen et al. (2009) recently reported that for novae on He-core WDs with masses below 0.5 $M_{\odot}$ the SSS phases can last for centuries or longer. These objects are expected to have low effective temperatures of $\sim$ 20 eV and low X-ray luminosities. Shen et al. (2009) further note that CVs with He-core WDs have not yet been unambiguously discovered and that their post-nova SSS phase could be the easiest way to find them.

The second scenario assumes re-established hydrogen accretion in the binary system to prolong the nuclear burning on the WD surface that was initiated by the nova outburst. Such a setting was discussed by Ness et al. (2008) for the Galactic nova V723 Cas which has the longest SSS phase known so far (more than 14 years in 2009; Schaefer & Collazzi 2010). In this hierarchy, M31N 1996-08b is the current runner-up followed by M31N 1997-11a and the Galactic nova GQ Mus (SSS turn-off after 10 years; Schaefer & Collazzi 2010; Shanley et al. 1995). For V723 Cas, Ness et al. (2008) reported an X-ray count rate variability within a factor of two of the mean, the physical reason of which is unclear.

A prolonged SSS phase caused by magnetically channelled, irradiation enhanced accretion onto a WD from its nearby companion star was also discussed recently by Schaefer & Collazzi (2010) for their new ”V1500 Cyg stars“ subclass of Galactic novae. Unfortunately, the low X-ray and optical luminosities of the M 31 novae discussed here do not allow to test them for other characteristics of these subclass as short orbital periods, highly magnetised WDs and the behaviour of their quiescence magnitudes.

The scenarios discussed above underline the potential of M 31 novae with long SSS states for important progress in the understanding of nova physics. Future monitoring observations of the M 31 central region would prove very useful in following the X-ray luminosity evolution of these novae and might allow further interpretation in favour of one scenario or the other.

6.3 Correlations between nova parameters

The nova SSS catalogue compiled in Table 4.3 was used to search for statistical correlations between the various X-ray and optical observables. Here I present correlations that I found between the following parameters: turn-on time ($t_{\rm on}$), turn-off time ($t_{\rm off}$), effective blackbody temperature kT (all X-ray), t_2 decay time and expansion velocity of the ejected envelope (both optical). The correlations are shown in Figs. 6.1 – 6.5. To model the visible trends I used a least-square fit with a power law, the results of which are given Eqs. 6.1 – 6.4.

I assume that the WD mass is the physical parameter predominantly responsible for the various correlations. Also in optical studies the WD mass was found to be the dominant parameter (see e.g. Livio 1992; Della Valle & Livio 1995; Della Valle 2002, and references therein). However, theoretical nova models show a more complicated picture (see e.g. Sala & Hernanz 2005; Hachisu & Kato 2006) and I include a note of caution about the physical interpretation of the correlations.

While a detailed interpretation of the observed correlations is beyond the scope of this work I believe that my analysis revealed certain trends between different nova parameters that might be used as input for future theoretical models. In the following, I describe the correlations that I found.

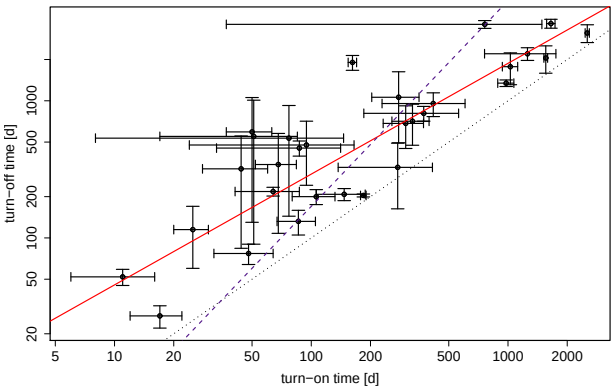

Figure 6.1: Double logarithmic plot of turn-on time versus turn-off time (both in days after outburst) including error bars. The solid red line represents the best fit from a weighted regression. The dashed purple line shows the $t_{\rm off}$ vs $t_{\rm on}$ relation of Hachisu & Kato (2010). The dotted black line indicates the limiting case of $t_{\rm off} = t_{\rm on}$.

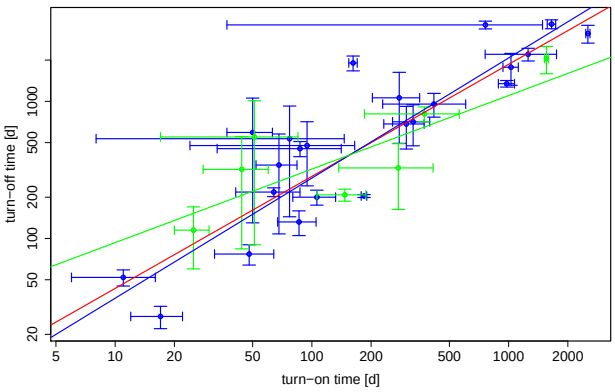

Figure 6.2: Same as Fig. 6.1, here with different colours of symbols and best-fit lines for old novae (associated with bulge stellar population; **blue**) and young novae (disk population; **green**). The red line still shows the overall best fit.

6.3.1 Supersoft X-ray source turn-on time vs turn-off time

I plot the two X-ray time scales $t_{\rm on}$ vs $t_{\rm off}$ in Fig. 6.1. There is a trend correlating increasing turn-on times with increasing turn-off times. Note, that because of the definition of both times it is not possible that $t_{\rm off} \leq t_{\rm on}$. The limiting case of $t_{\rm off} = t_{\rm on}$ is shown as a dotted black line in Fig. 6.1. However, the correlation that I found is much more specific than $t_{\rm off} > t_{\rm on}$ and can be fitted with a powerlaw model. This model is shown as the solid red line in Fig. 6.1 and defined by the following relation (both time scales in units of days after outburst):

$$t_{\rm off} = 10^{(0.9\pm0.2)} \cdot t_{\rm on}{}^{(0.8\pm0.1)} \quad . \tag{6.1}$$

This dependence is significantly less steep than the relation between $t_{\rm on}$ and $t_{\rm off}$ inferred from a prediction formula of the SSS phase of novae recently published by Hachisu & Kato (2010). From their equations 25 and 26 one can derive that $t_{\rm off} \propto t_{\rm on}^{1.5}$. This relation is shown as the dashed purple line in Fig. 6.1.

Separate modelling of novae from young and old stellar populations (see Chap. 6.6) indicates a difference in the model slope (see Fig. 6.2). The slope for old novae is 0.88 ± 0.10 (blue line in Fig. 6.2) and for young novae 0.54 ± 0.18 (green line in Fig. 6.2). However, this difference is significant only on the 1σ level and an analysis of covariance does not show a significant impact of the type of population on the model. Since this result is strongly influenced by the small number of young novae, a larger sample is needed to study the difference further.

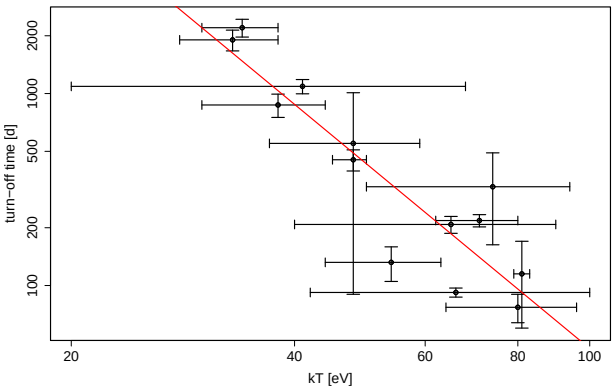

Figure 6.3: Double logarithmic plot of effective blackbody temperature (kT) in eV versus turn-off time in days after outburst including error bars. The red line represents the best fit from a weighted regression.

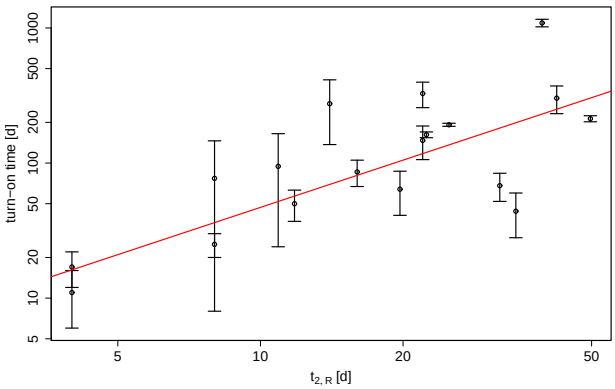

Figure 6.4: Double logarithmic plot of optical decay time $t_{2,R}$ versus turn-on time (both in units of days after outburst) including error bars. The red line represents the best fit from a weighted regression.

6.3.2 Effective blackbody temperature vs X-ray time scales

I plot the effective blackbody temperature kT vs the SSS turn-off time $t_{\rm off}$ in Fig. 6.3. The figure shows an anti-correlation of these two X-ray parameters. I fitted this trend with a powerlaw, which is represented by the solid red line in Fig. 6.3. The fit indicates the following relation, where the turn-off time is given in units of days after outburst and the effective temperature in units of eV:

$$t_{\rm off} = 10^{(8.1\pm0.8)} \cdot kT^{(-3.2\pm0.5)} \quad . \tag{6.2}$$

In order to interpret this relation physically, I make use of a result from theoretical models which states that higher effective temperatures indicate a larger WD mass (see e.g. figure 7 in Sala & Hernanz 2005). It is therefore tempting to speculate that Eq. 6.2 represents a relation between WD mass and turn-off time. This relation might be similar to the one shown in figure 9(a) of Hachisu & Kato (2006), where they plot the WD mass versus the time when hydrogen-burning ends (which is generally agreed on to correspond to the SSS turn-off time). One caveat in establishing such a relation is that figure 7 in Sala & Hernanz (2005) is given for the *maximum* effective temperature which might not be the same as the blackbody kT derived from the observations for two main reasons. Firstly, blackbody fits to supersoft spectra are not physically correct representations of an evolving WD atmosphere and are generally known to underestimate the source temperature (see Chap. 1). Secondly, the monitoring observations might not detect the SSS at its maximum temperature. However, the trend visible in Fig. 6.3 shows that a simple blackbody parametrisation seems capable of at least distinguishing between high temperature and low temperature SSSs. Furthermore, figures 10 and 11 in Sala & Hernanz (2005) show that novae evolve quickly through the low kT phase in their SSS state and spend most of the time close to their maximum effective temperature. I repeated the regression for old novae and young novae separately (see Chap. 6.6) but did not find significant differences.

6.3.3 Optical decay time vs supersoft X-ray source turn-on time

I plot the time of optical decay by two magnitudes in the R band ($t_{2,R}$) vs the SSS turn-on time in Fig. 6.4. There is only sufficient data from optical R band light curves to perform a statistical analysis. The plot indicates a trend that is positively correlating the two parameters. I modelled this correlation with a powerlaw, which is indicated as a red line in Fig. 6.4. The model gives the following relation:

$$t_{\rm on} = 10^{(0.5\pm0.3)} \cdot t_{2,R}^{\ (1.2\pm0.2)} \quad . \tag{6.3}$$

Both time scales are in units of days after nova outburst. I therefore obtained a roughly linear relation between the two important time scales in optical and X-rays. However, the scatter of the data points in Fig. 6.4 is relatively large and a few data points lie significantly off the powerlaw model. This behaviour might indicate a more complex relation between the two time scales that should be further examined in future studies using a larger nova sample.

Note, that from their theoretical models, which were based on observations of Galactic novae, Hachisu & Kato (2010) recently derived a relation between t_2 and the turn-on time which is also linear but much steeper (their equation 30 combined with 29). This discrepancy might be due to the fact that Hachisu & Kato (2010) used decay times in the emission line free optical y band, whereas my results depend on R band light curves. The continuum flux of a nova in this band is contaminated by the Hα emission line, which is the most prominent characteristic of a nova spectrum. Observers have used the fact that novae are visible longer in Hα than in broad band filters since the work of Ciardullo et al. (1983).

6.3.4 Optical expansion velocity vs supersoft X-ray source turn-on time

I plot the expansion velocity of the ejected envelope ($v_{\rm exp}$), as measured from the Hα line of the optical spectrum, vs the SSS turn-on time ($t_{\rm on}$) in Fig. 6.5. This diagram includes all novae for which $v_{\rm exp}$ is known and $t_{\rm on}$ had been measured accurately enough. It shows an anti-correlation between both parameters.

Before I modelled this trend I excluded two novae, which are colour coded in Fig. 6.5: M31N 2003-08c (blue) and M31N 2007-10b (red). M31N 2003-08c has a luminosity close to our detection limit and is only found in half of the *Chandra* observations during 2007/8 and 2008/9 (see Table 4.2). Because of its faintness, the turn-on time of the source is difficult to determine. M31N 2007-10b seems to be a peculiar nova, since already Rau et al. (2007) noted the atypically low expansion velocity (for He/N novae) of 1450 ± 100 km s^{-1}.

The powerlaw model that describes the correlation between the remaining data points is indicated by a red line in Fig. 6.5 and described by the following relation:

$$t_{\rm on} = 10^{(7.1\pm0.8)} \cdot v_{\rm exp}^{\ (-1.7\pm0.2)} \tag{6.4}$$

The turn-on time is given in units of days after nova outburst and the expansion velocity in units of km s^{-1}. This model is based only on a few objects for which both quantities are known. Nevertheless, the scatter is small and the correlation is strong, with a Pearson correlation coefficient of -0.96 and a non-correlation p-value of 0.0008. Note, that the uncertainty ranges of the expansion velocity are not available in the literature for all novae shown in Fig. 6.5 except of M31N 2006-09c (570 ± 45 km s^{-1}; Hatzidimitriou 2010, priv. comm.) and M31N 2007-10b (1450 ± 100 km s^{-1}; Rau et al. 2007).

Another caveat is that the expansion velocities of novae are known to be time dependent. Hatzidimitriou et al. (2007) found for the optical nova M31N 2005-09c (no SSS counterpart known) a decline

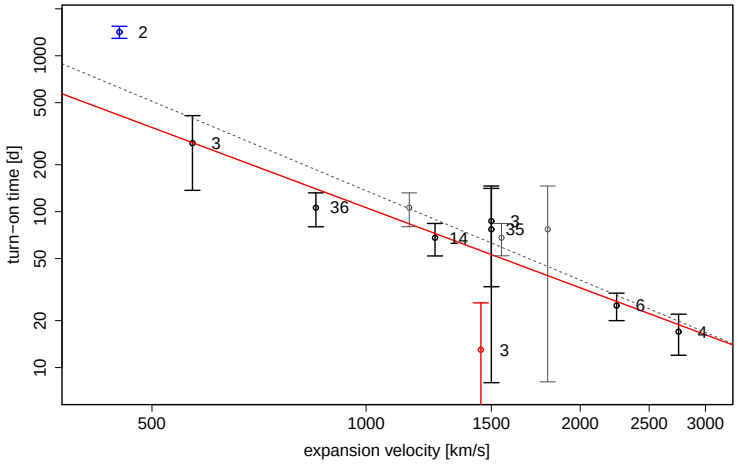

Figure 6.5: Double logarithmic plot of expansion velocity in km s^{-1} versus turn-on time in days after outburst including error bars. Annotations refer to the time in days after outburst the optical spectrum was obtained. The red line indicates the best fit from a weighted regression. The red data point represents the atypical nova M31N 2007-10b. The blue data point is nova M31N 2003-08c for which the actual turn-on time is difficult to determine. The grey symbols visualise a generic shift of the expansion velocity by +300 km s^{-1} for those novae for which spectra were taken more than ten days after outburst. The grey, dashed line shows the best fit after the shift.

in Hα FWHM of about 200 km s^{-1} within six days. However, there is no explicit relation between expansion velocity and time after nova outburst known so far. For four of the seven novae that I used to derive Eq. 6.4 the optical spectrum was taken within the first six days after outburst (see annotations in Fig. 6.5). Assuming a decline in expansion velocity over time, correcting for the delay in the remaining three novae, with a generic shift of +300 km s^{-1}, would decrease the (negative) slope of the best fit, since these data points would move towards higher expansion velocities. This effect is visualised by the grey symbols and best fit line in Fig. 6.5.

The implications of the trend visible in Fig. 6.5 are intuitively clear: larger expansion velocities should result in shorter turn-on times of the SSS, because the ejected envelope becomes optically thin earlier. Equation 6.4 quantifies this correlation. It connects the two parameters needed to compute ejected masses (see Table 4.3) and could allow to estimate these masses with higher accuracy (see Chap. 6.4). Furthermore, it could allow the estimation of the SSS turn-on time from the optical spectrum and therefore it could be an important tool for planning X-ray observations of optical novae.

6.3.5 Physical interpretations - a note of caution

At this point, a general note of caution is in order: Theoretical models emphasise that the properties of a nova outburst are not only influenced by the mass of the WD, but also by its chemical composition (mainly the hydrogen content of the envelope, see e.g. Sala & Hernanz 2005; Hachisu & Kato

2006). This additional dependence is not accounted for in any of the simple power-law relationships presented here. However, according to the theoretical models the impact of the chemical composition on the observed parameters appears to be considerably weaker than the influence of the WD mass: see e.q. figure 9 in Hachisu & Kato (2006) and figure 7 in Sala & Hernanz (2005). In particular, the effect of the chemical composition on kT in figure 7 of Sala & Hernanz (2005) (WD mass versus maximum effective temperature) seems to be in the same range ($\sim$ 15 eV) as the scatter and the error bars for kT in my Fig. 6.3 (effective blackbody temperature versus turn-on time). Therefore, there is the possibility that most of the impact from parameters other than the WD mass on the correlations found in this work is still within the range of the (still relatively large) error bars. As to which extend the varying hydrogen content itself could be causing the observed scatter in the correlations might be an interesting question for further studies.

6.4 Derived nova parameters

In addition to the observed parameters of the optical nova and the X-ray counterpart, the nova catalogue (see Table 4.3) also contains the derived parameters ejected mass and burned mass.

The mass ejected in a nova outburst can be estimated from the turn-on time of the SSS and from the expansion velocity of the ejected material. The decrease in the optical thickness of the expanding ejecta is responsible for the rise in the X-ray light curve of the post-outburst novae, as shown for V1974 Cyg (Shore et al. 1996; Krautter et al. 1996). Following Della Valle et al. (2002), I assumed the volume of the nova shell, expanding at constant velocity v, to be $V \sim 4\pi \times \mathrm{v}^3 \times t^3 \times f$, where the fill factor f is a dimensionless parameter describing the thickness of the shell. I chose $f = 0.2$, which incorporates the increase of the thickness of the envelope due to thermal motions inside the gas (see Della Valle et al. 2002, and references therein). Under this assumption, the column density of hydrogen evolves with time as

$$N_H(\mathrm{cm}^{-2}) = M_{\mathrm{ej,H}}/(\frac{4}{3}\pi \cdot m_H \cdot v_{\mathrm{exp}}^2 \cdot t^2 \cdot f') \quad , \tag{6.5}$$

where $m_H = 1.673 \times 10^{-24}$ g is the mass of the hydrogen atom and $f' \sim 2.4$ (for $f = 0.2$) a geometric correction factor. Note that PHS2007 used a slightly different approach to compute ejected masses. I further assumed that the SSS turns on at $t = t_{\mathrm{on}}$ when the absorbing hydrogen column density decreases to $\sim 10^{21}$ cm^{-2}. The newly found correlation between SSS turn-on time and expansion velocity given in Eq. 6.4 allowed me to eliminate the expansion velocity from this relation. I could therefore compute the ejected mass solely from the SSS turn-on time. This allowed more accurate mass and error range estimates for the vast majority of novae without an optical spectrum. Although Eq. 6.4 is only based on a few objects, it yields an improvement compared to earlier work, where ejected masses had to be computed using a "typical" expansion velocity with unknown errors (see e.g. PHS2007). Ejected hydrogen masses and error ranges in Table 4.3 were computed as follows, with $a = 10^{8.4\pm0.2}$ being a correlation coefficient derived from inserting Eq. 6.4 into Eq. 6.5 for $t = t_{\mathrm{on}}$:

$$M_{\mathrm{ej,H}} = N_H \cdot \frac{4}{3}\pi \cdot m_H \cdot f' \cdot a \cdot {t_{\mathrm{on}}}^{(1.1\pm0.1)} \quad . \tag{6.6}$$

This equation was also used for novae with known expansion velocities. Because of the tight correlation seen in Fig. 6.5, for these novae there are no big differences between computed and measured expansion velocity.

The turn-off time of the SSS phase allowed me to estimate the amount of hydrogen-rich material burned on the WD surface:

$$M_{\rm burn,H} = (L_{\rm bol} \cdot t_{\rm off})/(X_H \epsilon) \quad . \tag{6.7}$$

Here, $L_{\rm bol}$ is the bolometric luminosity, $t_{\rm off}$ the SSS turn-off time, X_H the hydrogen fraction of the burned material, and $\epsilon = 5.98 \times 10^{18}$ erg g^{-1} (Sala & Hernanz 2005). Following PHS2007, I assumed a bolometric luminosity of $3 \times 10^4 L_\odot$ and a hydrogen mass fraction $X_H = 0.5$. Note that in Eq. 6.7 I use the SSS turn-off time and *not* the duration of the SSS phase (i.e. $t_{\rm off} - t_{\rm on}$), as it was done in PHS2007. The reason for this is that the steady nuclear burning phase already starts before the turn-on of the SSS, a time which is dependent on the ejected mass. But hydrogen burning is powering the nova since the outburst and later settles to be stable after the inner layers of the envelope returned to hydrostatic equilibrium (Sala & Hernanz 2005). The onset of stable burning is not well defined theoretically but hydrogen clearly is already burned before the SSS becomes visible. Therefore, the turn-off time of the SSS provides a better base to estimate the hydrogen mass burned on the WD surface.

The hydrogen mass fraction of a nova is rarely determined observationally and the uncertainties associated with the above assumed value are not established. From theoretical models by Sala & Hernanz (2005) one sees that e.g. for a high degree (75%) of mixing of the accreted envelope with the degenerate core (which results in $X_H = 0.18$) the stable hydrogen-burning phase is expected to last less than two months, even for a relatively small WD mass of $0.9\,M_\odot$. Therefore, the chemical abundances of a nova strongly affect the intrinsic duration of the SSS phase and $X_H \sim 0.3$ would have been a more appropriate choice for fast and bright novae. However, overall $X_H = 0.5$ can be considered as a reasonable assumption.

I decided to use a constant bolometric luminosity to compute the burned masses, because the luminosities obtained from spectral fits are partly unphysically high and possess huge errors that would dominate the resulting mass estimates. This approach allowed me to concentrate on the more robustly determined source parameters. However, bolometric luminosities of novae are expected to be close to the Eddington limit. Sala & Hernanz (2005) determine in their model a plateau luminosity in the range of 2–6 $\times 10^4$ $L_\odot$, which includes my generic assumption and can very well serve as its error range.

Despite the uncertainties, the burned masses presented in Table 4.3 are within the range expected from models of stable envelopes with steady hydrogen burning (Sala & Hernanz 2005; Tuchman & Truran 1998). In general, the burned masses are about one order of magnitude smaller than the ejected masses, which for most novae are within the values predicted from hydrodynamical models of nova outbursts (José & Hernanz 1998). The exceptions are novae M31N 1995-09b, M31N 1996-08b, and M31N 1997-11a, for which I estimated very large burned masses. Above, I rejected the interpretation that the latter two objects might be recurrent novae. Moreover, that neither nova has yet reached the end of its SSS phase points towards a burning envelope with a high mass and/or a large hydrogen fraction. Because a high envelope mass points towards a low WD mass, the WD masses in these nova systems might be below the mass range used by Sala & Hernanz (2005) ($> 0.9\,M_\odot$) and by José & Hernanz (1998) ($> 0.8\,M_\odot$) in their models. However, without information on the degree of mixing of the accreted material with the degenerate core, we cannot draw conclusions on the actual long-term evolution of the WD mass. Note, that in the scenario of sustained H-burning through re-established accretion (see Chap. 6.2.2) the burned masses computed for novae with long SSS states only constitute upper limits on the actual hydrogen mass left on the WD after the outburst.

6.5 Novae with short supersoft X-ray source states and the completeness of the X-ray monitoring

In previous studies it had been noticed that only a minor fraction of novae in M 31 were actually observed as SSSs. While PHS2007 detected SSS emission from 11 out of 32 novae within about a year after optical outburst, in 2006/7 only 2 out of 25 novae were found in X-rays over a comparable time span. For the ten-day monitorings the corresponding numbers were 6 out of 28 (2007/8) and 3 out of 23 (2008/9) novae, respectively.

Based on current theoretical models, all novae are expected to display a SSS phase (see e.g. Hachisu & Kato 2010). Therefore, the cause of the low percentage of actual detections remained an open question. It could be (a) due to the inevitably incomplete observational coverage, or (b) due to some inadequacy (or incompleteness) of the theoretical models.

Using the nova SSSs catalogue (see Table 4.3) I could test scenario (a) for the first time. This study strongly benefited from the large number of optical novae found in M 31 over the last 15 years and from the large number of archival and monitoring X-ray observations covering the M 31 central area.

The main steps of my approach were the following: I took the observed mass distribution of WDs in novae as known from theoretical work, converted it into a distribution of SSS turn-on times, "convolved" it with the observational coverage and compared the expected number of detections to the actual observed number of SSS novae using a Monte Carlo Markov Chain (MCMC) method. The entire procedure is explained in detail in the following paragraphs and the results are discussed.

My starting point was the observed mass function of WDs in CNe which I computed based on Truran & Livio (1986). This approach assumes a Salpeter IMF $\Phi(M) \propto M^{-2.35}$ (Salpeter 1955) for the WD progenitors and computes the nova recurrence frequency as $\nu_{\rm rec} \propto M_{\rm WD}/R^4_{\rm WD}$ based on the critical envelope mass needed to trigger the nova explosion (for more details see Truran & Livio 1986). The intrinsic mass distribution of WDs has its strongest peak at low masses around $0.6\,M_\odot$ (see e.g. Catalán et al. 2008, and references therein). However, the WD mass dependence of the recurrence frequency leads to a much higher *observed* frequency of high mass WDs in CNe (see also Ritter et al. 1991).

In order to translate the expected observed WD mass distribution into an expected observed distribution of SSS turn-on times I used the theoretical models of Hachisu & Kato (2006). These authors computed SSS turn-on and turn-off times for different WD masses and chemical compositions based on a free-free emission model. I used their model values for CO WDs and $X_H = 0.45$ (their table 4; $t_{\rm wind}$ corresponds to $t_{\rm on}$) because it is closest to my assumptions in this work. Moreover, figure 9 in Hachisu & Kato (2006) shows that the impact of choosing different WD chemical parameters is not huge and thus would not introduce significant errors to my analysis. The values between the grid points in their model were interpolated using a polynomial function. In Fig. 6.6 I show the resulting expected observed distribution of SSS turn-on times, which is clearly dominated by fast SSSs.

My method is based on all optical novae discovered in M 31 from 1995 until February 2009, the end of the 2008/9 campaign. From this data set I selected all novae in the field of view of the XMM-Newton/*Chandra* M 31 centre monitoring. To account for the fact that XMM-Newton observations suffer from source confusion in the innermost arcminute around the M 31 centre, I exclude novae from this region. The resulting sample consists of 206 objects. Using a Monte Carlo method I randomly selected SSS turn-on times for a certain fraction x of these novae based on the expected turn-on distribution described above. To compute the associated SSS turn-off times I used the correlation found in the catalogue sample (see Eq. 6.1). This resulted in a certain time span of SSS visibility for

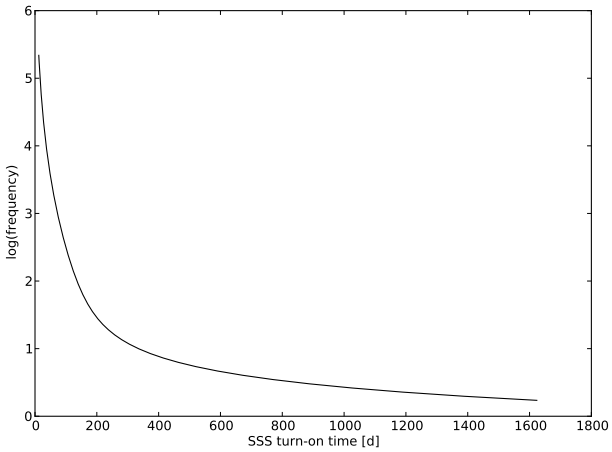

Figure 6.6: Expected logarithmic frequency of SSS turn-on times in CNe based on Truran & Livio (1986) and Hachisu & Kato (2006)

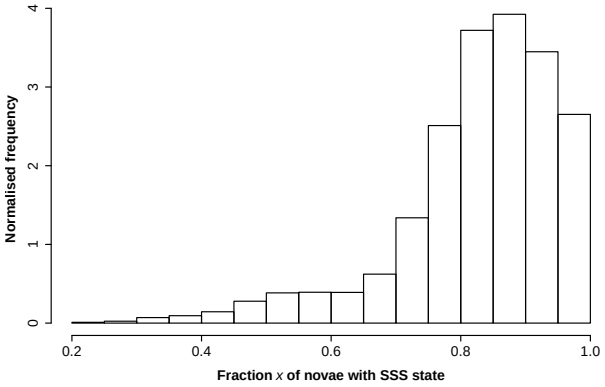

Figure 6.7: Result from a MCMC simulation based on the intrinsic distribution of SSS turn-on times for novae in M 31. Shown is the frequency distribution of the intrinsic fraction x of novae with SSS emission which would be needed to cause the detections in our observation campaigns.

the selected fraction of novae. The fraction x was the free parameter to be optimised by the MCMC, thereby allowing me to test the scenario (a) outlined above.

I now made use of the large number of M 31 centre observations to estimate discovery rates for the simulated SSSs. These observations include the three monitoring campaigns this dissertation is based on (see Table 2.1) and the archival XMM-Newton and *Chandra* HRC-I observations analysed by PHS2007 (their tables 2 and 3) and PFF2005. From PFF2005, I only used the XMM-Newton centre observations (c1 - c4 in table 1 of Pietsch et al. 2005b) and the long *Chandra* observations 1912 and 1575. The other observations analysed by PFF2005 were either not pointed at the M 31 centre or had only a short exposure time, and are therefore not useful for this simulation. In total, there are 48 individual observations covering 8.7 years.

In the context of the simulation, the SSS counterpart of a nova is defined as detected if there is at least one observation between SSS turn-on time and turn-off time. This somewhat ideal assumption is nonetheless justified by the fact that SSS counterparts of novae are expected to have a bolometric luminosity close to the Eddington limit of the WD (Hernanz 2005), which is between $6{\times}10^{37}$ erg s^{-1} and $2{\times}10^{38}$ erg s^{-1} for WD masses between 0.5 and 1.4 solar masses. If we assume that most of that luminosity is emitted in the soft X-ray band and take into account a typical observational sensitivities of a few 10^{36} erg s^{-1} (see e.g. Table 4.7), the actual detection efficiency for the monitoring observations should be close to 100%.

Using the MCMC, SSS turn-on and turn-off times were determined for all novae and the number of sources with detected SSS phase was measured for each of the five campaigns separately. These predicted numbers were then compared to the actual number of novae detected as SSSs in PFF2005 (10), PHS2007 (14), 2006/7 (8), 2007/8 (11) and 2008/9 (9) for the epoch and spatial region selected above. The deviations between prediction and observation were summed up quadratically to create an error for the estimate. The Markov chain is governed by a Metropolis algorithm (Metropolis et al. 1953) that seeks to minimise this error by modifying the fraction x of novae that gets turn-on times assigned to. The random walk nature of the MCMC allowed me to find the fraction associated

with the minimum error and to sample the parameter space around it.

I show the result of the simulation in Fig. 6.7, where the frequency distribution of the SSS fraction x is plotted. This graph shows that the observational findings are consistent with the assumption that all novae exhibit a SSS stage and that the incomplete observational coverage is the reason for the detection of only a part of them. This result further highlights the importance of novae with high mass WDs and very short SSS turn-on times, which was first found by PHS2007. According to my simulations the intrinsic observed WD mass function strongly favours novae with short SSS states which are expected to account for the majority of the observed sources.

Indeed, I have already found seven novae with fast SSS turn-on times in the 2006/7 and 2007/8 campaigns. Their light curves are shown in Fig. 4.22. A particularly interesting object from this sample is M31N 2007-12d. This nova showed a very short SSS phase and was only detected as a faint source in one observation (see Table 4.2). An object like this would have been very likely missed with a sparser sampling. Even in the ten day monitoring of 2007/8 it is very close to the detection limit. Therefore, M31N 2007-12d might indicate the lower limit of SSS durations that can be found with the monitoring strategy applied for 2007/8 and 2008/9.

6.6 Nova population study

The existence of two different nova populations, associated with the bulge and disk of a spiral galaxy, was first postulated based on optical data of Galactic novae (Duerbeck 1990; Della Valle et al. 1992; Della Valle & Livio 1998). Slow Fe II novae were found to be located preferably in the bulge, whereas the faster He/N novae (see Williams 1992, for the spectral classification) mostly belong to the disk. This suggests an association of fast (slow) novae with the overall young (old) stellar population in the disk (bulge). The size and spatial coverage of the new nova catalogue, presented in Table 4.3, for the first time allowed me to investigate the X-ray properties of novae belonging to these two populations in M 31.

My approach was two-fold. First, I used geometric parameters to distinguish between bulge (old population) and disk (young population) and examined the differences in the distributions of the individual nova parameters for both subsets. Second, I used the X-ray parameters of all novae to divide them into two groups of novae with massive or less massive WDs and tested their geometric distributions. While the first method assumes the existence of two different nova populations, as suggested from optical data, the second method is independent of this assumption. By comparing both approaches, I hoped to correct for selection biases that either of them might introduce. However, in both approaches I applied a geometric criterion and have to be aware that because of the high inclination of M 31 (77.5°; see e.g. Beaton et al. 2007) a significant number of novae occurring in the disk will be projected onto the bulge.

For the first approach, in order to assign a nova to one of the two populations I used an entirely geometrical criterion. I followed the work of Beaton et al. (2007), who analysed NIR images of M 31, and defined the projected M 31 bulge as an ellipse with a semimajor axis of 700″, an ellipticity of 0.5, and a position angle of $\sim 50°$. The boundary between the bulge and disk regions is marked by a grey ellipse in Fig. 6.8. In the context of this approach, old novae are defined as situated within this boundary and young novae lie outside of it. In Fig. 6.8 I show the positions of X-ray detected old novae as white and young novae as black crosses, respectively. Note, that I classified nova M31N 2007-06b as a “old nova”, the position of which is indicated by the only white cross outside the grey ellipse in Fig. 6.8. As a nova in a M 31 globular cluster (see Chap. 5), it belongs to a stellar population similar to the one dominating in the bulge.

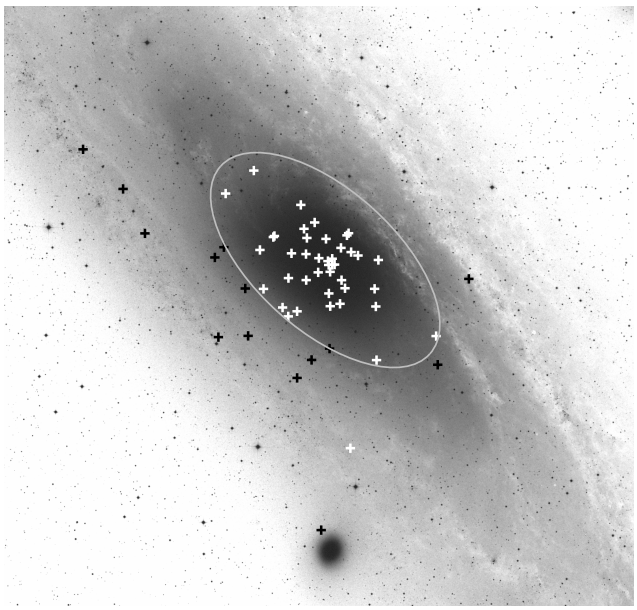

Figure 6.8: Location of the M 31 old (white) and young novae (black) overlaid on a DSS2-R image. The grey ellipse marks the boundary between the M 31 bulge and the disk that was used in this work. See Chap. 6.6 for an explanation of the classification. Only four of the 60 nova SSSs from Table 4.3 are outside this image.

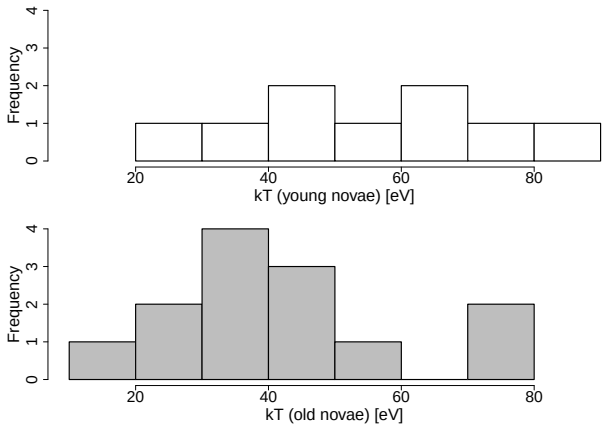

Figure 6.9: Distribution of effective blackbody temperature kT for young novae (white/upper panel) and old novae (grey/lower panel), respectively.

I checked the observed distributions of the X-ray parameters given in Table 4.3 for dependencies on the classification as old or young nova. I found significant differences only for the blackbody temperature kT. In Fig. 6.9 I show the individual kT distributions for young and old novae, respectively. Both distributions are compatible with a Gaussian distribution on the 1σ level (Kolmogorov-Smirnov (KS) test), but have different mean values of 42 eV (old) and 56 eV (young). I performed a two sample t-test which gives a p-value of ~ 0.08 for 20 degrees of freedom, resulting in a $\sim 92\%$ probability that the two distributions are different. An F test shows that both variances are equal on the 1σ level (p-value = 0.88) and that the t-test is therefore justified. However, the samples of both old and young novae with measured temperatures (13 and 9) are small. Indeed, statistical power calculations show that if the measured difference in kT between the samples actually is 14 eV we would need at least 24 novae in each group to see a difference on the 95% confidence level (with a power of 0.8).

In order to examine the extend to which the result obtained above depends on my selection of the boundary between bulge and disk, I tested the method outlined above for different bulge extensions. In Fig. 6.10 I display the results depending on the semi-major axis of the bulge region. For this computation, I took into account the effect of changing ellipticity in the NIR isophotes of M 31 (see Beaton et al. 2007, their figure 3). The figure shows the t-test p-values for the kT distributions of the respective groups of old and young novae. We can see that only for $200'' \ldots 300''$ and $\sim 700''$ "bulges" there really is a significant difference on the 90% level.

In the second approach, I corrected the nova coordinates for the inclination of M 31 and computed M 31-centric distances for all objects. Of course, the effect of projection of disk novae onto the bulge must also be kept in mind here. The X-ray parameter measured for most novae is the turn-on time.

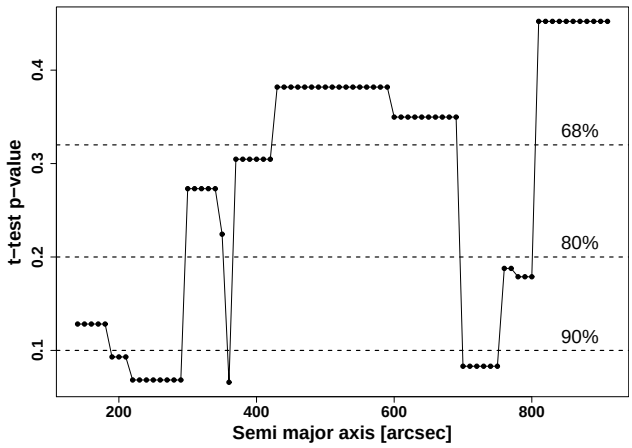

Figure 6.10: Two sample t-test p-values for the *kT* distributions of old and young novae. The abscissa gives the semi-major axis of the "bulge" region with is defined to contain the old novae. The solid line connects the solid circles of the data points for better readability. Dashed lines show three acceptance levels for the t-test.

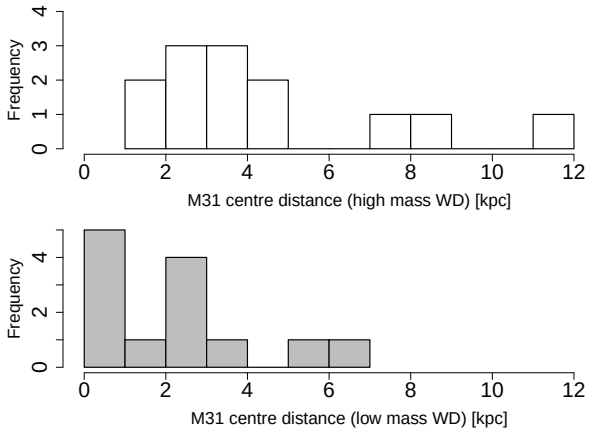

Figure 6.11: Distribution of inclination corrected M 31-centric distances for novae with high mass (upper panel, white) and low mass (lower panel, grey) WDs. Distances are given in kpc, assuming a distance to M 31 of 780 kpc and are not corrected for projection effects.

Similar to Chap. 6.5, I used the connection between the WD mass and the turn-on time inferred from Hachisu & Kato (2006) to distinguish between high and low mass WDs. I defined high mass WDs as $M_{WD} \gtrsim 1.2\ M_{\odot}$, which corresponds to $t_{\rm on} \lesssim 100$d, and low mass WDs as $M_{WD} \lesssim 0.7\ M_{\odot}$, corresponding to $t_{\rm on} \gtrsim 500$d. With this selection I sampled both the high end of the WD mass distribution, which dominates the observed mass distribution of WDs in nova systems, and the region around the peak of the observed mass distribution of single WDs at $\sim 0.6\ M_{\odot}$ (see Chap. 6.5). Again, I only used novae where the turn-on time is determined accurately enough. In Fig. 6.11 I give the distributions of the distance from the M 31 centre for both groups. It shows that novae with low mass WDs seem to be more concentrated towards the centre of the galaxy than those with high mass WDs. A KS two-sample test shows that both distributions are significantly different on the 95% level (p-value of 0.044).

It is clear that these results have to be interpreted carefully, both because of the relatively small size of the sample of SSS novae and because of projection effects. Despite these caveats my two approaches used *two different* geometric criteria as well as *two different* X-ray parameters and reached similar results. Both approaches gave a first hint that in the X-ray regime there are also two distinct populations of novae that can be associated with the different stellar environments of bulge and disk. Further observations are needed, in particular of the relatively neglected M 31 disk, in order to examine if my results can be verified.

6.7 Asymmetric distribution of novae in X-rays

Another observational result that I derived from Fig. 6.8 is that there appears to be an asymmetry in the spatial distribution of nova SSSs with respect to the major axis of M 31. There were more objects found on the (far) south-east side of M 31 than on the (near) north-west side. No such asymmetry was found in the spatial distribution with respect to the minor axis (north-east vs south-west). In Fig. 6.12

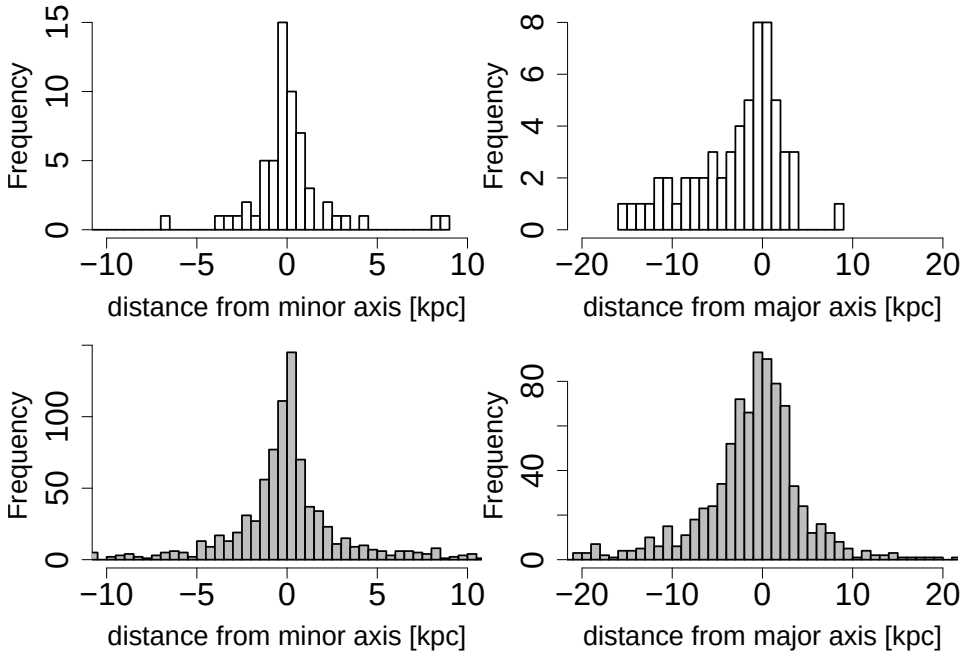

Figure 6.12: Distributions of inclination corrected nova positions with respect to the minor axis (left) and the major axis (right) of M 31 for all known optical novae (lower panels, grey) and for novae with detected SSS counterpart (upper panels, white). Coordinate units are kpc, assuming a distance to M 31 of 780 kpc, and are not corrected for projection effects. Negative major axis distances correspond to positions in the south-east (near) part of M 31.

I plot both distributions in the upper panels and compare them in the lower panels to the equivalent distributions for all known optical novae in M 31. The overall distributions appear symmetric with respect to both axes. I carried out KS tests that confirm the visual impression. The hypothesis, that the distribution of nova SSS positions is symmetric with respect to the major axis (upper right panel in Fig. 6.12) is rejected on the 99% confidence level. On the other hand, the symmetry of the nova SSSs positions with respect to the minor axis (upper left panel in Fig. 6.12) is confirmed on the 85% level. Projection effects might influence this result slightly, but cannot explain the asymmetry.

The cause of this asymmetry might be the fact that the north-west side of the galaxy is largely seen through the gas and dust in the spiral arms of M 31 (see Walterbos & Kennicutt 1988). Bogdán & Gilfanov (2008) found a similar asymmetry for the diffuse soft X-ray emission of the M 31 bulge. Based on a microlensing survey, An et al. (2004) found that also in the optical "all the variable star distributions are asymmetric in the sense that the far side (or south-east) is brighter or has more detected objects than the near side (or north-west)". They concluded that extinction within M 31 is the reason for this behaviour. For the entire optical nova sample, we see a slight asymmetry with respect to the major axis (lower right panel in Fig. 6.12). The median of the distribution is shifted to the south-east (negative values in Fig. 6.12) by about 0.5 kpc. However, this effect is significantly weaker than the asymmetry of the nova SSSs distribution.

Therefore, I assume that extinction within M 31 is the main reason for the observed asymmetry in nova SSS positions with respect to the major axis of M 31. Currently, the number of known nova SSSs is not sufficient to allow a quantitative estimate of the influence of the nova position in M 31 on the SSS detection probability. Note, that such a relation, once it is derived, would be useful to implement in the simulation method described in Chap. 6.5.

Chapter 7

Summary and conclusions

In this dissertation I have presented results from a dedicated monitoring campaign for SSS emission of optical novae in the central region of M 31. This galaxy was observed with the X-ray satellites XMM-Newton and *Chandra* in three monitoring campaigns that covered the time spans June 2006 – March 2007, November 2007 – February 2008 and November 2008 – February 2009. Additionally, I made use of archival data obtained with XMM-Newton, *Chandra* and *Swift* .

The X-ray survey was complemented by an optical monitoring campaign carried out with several small telescopes. The reduction and analysis of the optical data constituted an important part of my work. The optical monitoring led to the discovery of 25 optical novae from October 2007 till August 2010.

In total, I detected 21 X-ray counterparts of novae in the observations of the X-ray monitoring. Only four of these novae were found in earlier studies. These results increased the sample of known novae with X-ray emission by almost 50%. Several interesting individual objects were found in this work, the most remarkable of which were the first two SSSs in M 31 GCs and the first two novae with a periodically variable X-ray light curve in M 31.

I detected seven novae with a very fast turn-on of the SSS state. This confirmed the claim made in earlier studies by PHS2007 that novae with short SSS states are a major contributor to the overall population. Based on the WD mass function in novae predicted by theoretical models I carried out simulations to determine the expected fraction of novae with a SSS state. Results of these simulations showed that a population of novae dominated by fast SSSs is in agreement with the detected fraction of novae in our X-ray monitoring.

Six novae showed long SSS phases and were still active 12.5, 11.0, 7.4, 5.5, 5.2, and 4.8 years after the optical outburst. I discuss whether these long SSS phases might be caused by a low-mass WD or indicate burning sustained by re-established accretion onto the WD. While the first scenario might have implications on the search for He-core WDs, the latter scenario was recently proposed for a number of novae in our Galaxy.

During the three monitoring campaigns I found only four SSSs that do not have a known optical counterpart, compared to 16 out of the 21 nova counterparts that I could classify as SSSs. This result strongly supports the statement of PFF2005 that novae are the major class of SSSs in the central region of M 31.

Based on the results from this work and previous, partly archival studies I compiled a catalogue of novae with SSS state in M 31. This catalogue contains 60 sources in total. For most of them several optical and X-ray parameters are known. I used this catalogue to search for statistical correlations between these properties. Relationships were found between the parameters turn-on time, turn-off time, effective blackbody temperature kT (all X-ray), t_2 decay time and expansion velocity of the

ejected envelope (both optical). I discussed possible physical implications of these correlation and noted that a larger sample is needed to improve the simple powerlaw models I used to describe them.

I derived the values for the masses that were ejected and burned during the nova process, based on theoretical models, and included them in the catalogue. Furthermore, I analysed the geometric distribution of nova SSSs in M 31 for different ranges of X-ray parameters. Thereby, a first hint was found that in the X-ray regime there might be two populations of novae that are associated with different stellar environments. A similar interpretation of optical data has been the subject of discussion for almost two decades. Additionally, I detected an asymmetry in the spatial distribution of SSS nova counterparts with respect to the major axis of M 31, that might be caused by extinction within the galaxy.

Finally, I would like to emphasize that the effort of a regular monitoring of M 31 dedicated to novae has led to the point where, for the first time, a sample of nova SSSs exists that is becoming large enough to study it with statistical methods. The trends that I derived from this sample in this dissertation might help to gain deeper insight into the physics of the nova process. A study of nova SSSs as a population as I present it here can only be performed with the M 31 population. Therefore, it is important to continue the regular monitoring of this galaxy in order to examine if these first results can be confirmed with an increased sample of supersoft X-ray counterparts of optical novae in M 31.

Appendix A

Discoveries of X-ray transients in M 31

A further science goal of the X-ray monitoring with XMM-Newton and *Chandra* was the discovery of new X-ray transients in the M 31 central region that were not connected with optical novae. Here I present the first highlights from this analysis. In addition to the two SSS transients *CXOM31 J004228.3+411449* (see Chap. 4.5) and *SS2 in Bol 194* (see Chap. 5.2) six new X-ray sources and seven new outbursts of recurrent sources were detected in the monitoring data as well as in publicly available *Swift* data. All transients were announced by our group in ATels between October 2007 and August 2010. The sources are summarised in Table A.1 and described in detail in this chapter.

Table A.1: New and recurrent X-ray transients found between October 2007 and August 2010.

Name	New/ rec.	Outburst [UT]	Comments
CXOM31 J004217.0+411508	rec.	2007-11-07.63	rec. time ~ 1.2 y
XMMU J004245.9+411036	new	2008-05-26.30	
XMMU J004241.2+411821	new	2008-05-26.70	
[PFH2005] 430	rec.	2008-07-18.26	
[PFH2005] 329	rec.	2008-07-18.26	
SWIFT J004420.1+413702	new(?)	2008-05-28.11	possible ROSAT counterpart
SWIFT J004320.5+411528	new	2008-08-21.31	light curve in Table A.2
XMMM31 J004224.5+412401	rec.	2008-10-15.15	second observed outburst
XMMM31 J004205.8+411329	rec.	2008-10-21.63	
SWIFT J004159.3+410539	new	2009-10-22.60	bright
RX J0043.2+4127	rec.	2009-11-07.23	in GC Bol 163
CXOM31 J004253.1+411422	new	2009-12-17.89	brightest M 31 transient

CXOM31 J004217.0+411508

A new outburst of the recurrent X-ray transient CXOM31 J004217.0+411508 (r3-46) was discovered in the *Chandra* observations 8526 and 8527 (November 2007; see Table 2.1) of the 2007/8 campaign (Henze et al. 2007b). I measured count rates of (12.6 ± 0.8) $\times 10^{-3}$ ct s^{-1} and (9.9 ± 0.8) $\times 10^{-3}$

ct s^{-1}, respectively, which correspond to luminosities (0.2–10 keV) of 1.9 $\times 10^{37}$ erg s^{-1} and 1.5 $\times 10^{37}$ erg s^{-1} (assuming an absorbed power-law model with photon index = 1.7 and $N_{\rm H}$ = 6.6$\times$ 10^{20} cm^{-2} at a distance of 780 kpc). The object is identified as a hard X-ray source in the 4.6 ks *Swift* XRT observation 00031028002 (starting on 2007-11-24.21 UT; see Table 2.4). I derived a count rate of (4.8 ± 1.1) $\times 10^{-3}$ ct s^{-1} corresponding to a luminosity of 1.6 $\times 10^{37}$ erg s^{-1}, for the same spectral parameters as above. This is consistent with the *Chandra* luminosities.

This transient was first reported by Kong et al. (2002a). Williams et al. (2006) included it in their catalogue of transient X-ray sources in M 31 and gave as time of the first outburst 2000-08-18 with a peak luminosity of 3.67 $\times 10^{37}$ erg s^{-1}. The X-ray light curve till mid 2002 indicates a second, but not so bright outburst on 2001-10-31 (0.9$\times 10^{37}$ erg s^{-1}, see also Kaaret 2002). In the *Chandra* archive, there are two additional outbursts that have not been reported before: ACIS-I, ObsID 4681, 2004-01-31, 2.7 $\times 10^{37}$ erg s^{-1} and ACIS-I, ObsID 7137, 2006-05-26, 0.7 $\times 10^{37}$ erg s^{-1}; assuming the same spectral parameters.

The time lags between the detected outbursts indicate a recurrence time of about 1.2 years. There is no X-ray coverage at the expected times of earlier outburst in 2003 and 2005. However, further outbursts with similar luminosities were found by our group in the *Chandra* observations 10683 and 10684 (February 2009; see Table 2.1) of the 2008/9 campaign and in a 4.4 ks *Swift* XRT observation (ObsID 00035336022) starting on 2010-07-09.95 UT (Pietsch et al. 2010b). Transients with similar recurrence times have been identified as neutron star systems (e.g. Aql X-1) or black hole systems (e.g. 4U 1630-472) in the Galaxy.

XMMU J004245.9+411036

This source was detected as a new X-ray transient at RA = 00:42:45.97, Dec = +41:10:36.6 (J2000; 1σ position error 0.″6 mainly determined by the systematic error) in the XMM-Newton ToO observation 0560180101 (starting on 2008-07-18.26 UT, see Pietsch et al. 2008b). This observation was requested by our group to follow up the light curve of nova M31N 2007-12b. The 0.5–5.0 keV EPIC PN spectrum of XMMU J004245.9+411036 was fitted by a power law model with best fit parameters $N_{\rm H}$ = 1.9$\times$ 10^{21} cm^{-2} and photon index = 2.4. The unabsorbed luminosity in this band was 4.2$\times 10^{37}$ erg s^{-1}. This source is most likely a low-mass X-ray binary. Furthermore, it was already detected in *Swift* observation 37718001, starting on 2008-05-26.30 UT (Pietsch et al. 2008c), and was still active in the *Swift* observations 00031255001, starting on 2008-08-21.31 UT (Pietsch et al. 2008a), and 00031255010, starting on 2008-10-21.63 UT (Henze et al. 2008j).

XMMU J004241.2+411821

This source was detected in the aforementioned XMM-Newton observation 0560180101 as a new transient at RA = 00:42:41.27, Dec = +41:18:21.5 (J2000) with 1σ position error of 1.″0 (Pietsch et al. 2008b). Its EPIC PN count rate was 2.4$\times 10^{-2}$ ct s^{-1}, which corresponds to an unabsorbed luminosity (0.5–5 keV) of 6.2$\times 10^{36}$ erg s^{-1} (assuming an absorbed power law model with photon index 1.7 and galactic foreground absorption of $N_{\rm H}$ = 6.6$\times$ 10^{20} cm^{-2}). The luminosity presents a lower limit as the source spectrum shows a strong soft component. This source is most likely a low-mass X-ray binary. Our group later found an earlier detection of the source in *Swift* observation 00037719001 starting on 2008-05-26.70 UT (Pietsch et al. 2008c). XMMU J004241.2+411821 was not detected any more in the *Swift* observation 00031255001, starting on 2008-08-21.31 UT (Pietsch et al. 2008a). However, the luminosity upper limit is compatible to the brightness of the source measured with XMM-Newton.

[PFH2005] 430

Another outburst of the recurrent supersoft transient [PFH2005] 430 = r3-8 (see e.g. Pietsch et al. 2005b; Williams et al. 2006) was detected in the XMM-Newton observation 0560180101 (Pietsch et al. 2008b). The position of the source close to CCD gaps in both cameras and at the position of the missing CCD in MOS1 prevented a more detailed analysis. However, a lower limit for the EPIC PN count rate was estimated to 1.9×10^{-2} ct s^{-1}. The object only showed photons below 750 eV in EPIC PN and MOS2, thus confirming its SSS nature. [PFH2005] 430 seems to be a classical transient SSS as identified as a class in ROSAT observations of the Magellanic Clouds (Trümper et al. 1991).

[PFH2005] 329

Another outburst of the hard recurrent transient [PFH2005] 329 = r2-16 (see e.g. Pietsch et al. 2005b; Williams et al. 2006) was detected in the aforementioned XMM-Newton observation 0560180101 (Pietsch et al. 2008b). The EPIC PN count rate of 8.1×10^{-2} ct s^{-1} corresponds to an unabsorbed luminosity (0.5–5 keV) of 2.1×10^{37} erg s^{-1} (assuming an absorbed power law model with photon index 1.7 and galactic foreground absorption of $N_{\rm H} = 6.6\times 10^{20}$ cm^{-2}). This source is most likely a low-mass X-ray binary.

SWIFT J004420.1+413702

This source was detected as a new X-ray transient at RA = 00:44:20.12, Dec = +41:37:02.1 (J2000; 1σ position error 4.″5) in the *Swift* XRT observation 37721001 starting on 2008-05-28.11 UT (Pietsch et al. 2008c). This observation was part of a series of pre-planned *Swift* observations that mapped M 31 with XRT integration times of up to 5 ks from 2008 May 25 to July 26 (PI: S. Immler).

In seven observation intervals spread over 17 hours (total exposure time 4.38 ks) 50 ± 7 counts were detected in the 0.5–5 keV band (90% PSF). This corresponds to a unabsorbed luminosity (0.5–5 keV) of 3.3×10^{37} erg s^{-1} (assuming an absorbed power law model with photon index 1.7 and galactic foreground absorption of $N_{\rm H} = 6.6\times 10^{20}$ cm^{-2}). No source was found at this position in the XMM-Newton survey (Pietsch et al. 2005b) or in the second ROSAT PSPC survey of M 31 (Supper et al. 2001). However, the first ROSAT PSPC survey (Supper et al. 1997), WGACAT[1] (White et al. 2000) and the ROSAT HRI 1RXH catalogue[2] contain sources consistent in position that clearly indicate variability. In an outburst in January 1992 the source reached similar brightness as during the *Swift* observation. Optical and IR images show a red star-like object within 3″ of the X-ray position with 14.6 and 12.8 mag in R and K in the UCAC2 and NOMAD Catalogues, respectively (Zacharias et al. 2003, 2005). This object seems to be in the Galactic foreground and may not be related to the X-ray source.

SWIFT J004320.5+411528

This source was detected as a new X-ray transient at RA = 00:43:20.56, Dec = +41:15:28.8 (J2000; 1σ position error 3.″7) in the *Swift* XRT observation 00031255001 starting on 2008-08-21.31 UT (Pietsch et al. 2008a). In five observation intervals spread over seven hours (effective exposure 5.8 ks) 411 ± 21 counts were detected in the 0.5–5 keV band (90% PSF). The *Swift* XRT spectrum was best fitted with a absorbed disk-blackbody model with an $N_{\rm H} = (1.1 \pm 0.8) \times 10^{21}$ cm^{-2} and an inner disk

[1] http://wgacat.gsfc.nasa.gov/wgacat/wgacat.html
[2] http://www.xray.mpe.mpg.de/rosat/rra/roshri/

temperature of (0.55 ± 0.08) keV. The unabsorbed luminosity of the source corresponds to 1.8×10^{38} erg s^{-1} (0.5–5 keV) for a M 31 distance of 780 kpc. These parameters are consistent with a neutron star low-mass X-ray binary. However, a black hole as compact object can not be excluded.

The transient is not detected in simultaneous *Swift* UVOT uvw1 and uvw2 filter observations (3σ upper limit of 20.3 and 20.6 mag, respectively). The images and catalogue of the Local Galaxy Group Survey (LGGS Massey et al. 2006) show no counterpart brighter than V = 20.8 mag within the 3σ position error radius. No source is detected about one month earlier in the XMM-Newton observation 0560180101 (see above) with an EPIC PN upper limit for the unabsorbed luminosity of 1.4×10^{35} erg s^{-1} (0.5–5 keV), assuming a spectrum as above.

After exhibiting irregular variability for three weeks after discovery, SWIFT J004320.5+411528 showed a declining luminosity in subsequent *Swift* observations over a time span of four weeks. The light curve is given in Table A.2.

Table A.2: *Swift* XRT detections of the X-ray transient SWIFT J004320.5+411528.

ObsID	Date [UT]	Count rate [10^{-2} ct s^{-1}]
31255001	2008-08-21.31	8.9 ± 0.4
31255002	2008-08-28.68	13.2 ± 0.8
31255003	2008-09-04.23	11.6 ± 0.8
31255004	2008-09-06.59	9.8 ± 0.5
31255005	2008-09-11.48	11.0 ± 0.5
31255006	2008-09-25.51	7.4 ± 0.5
31255008	2008-10-14.74	6.3 ± 0.6
31255009	2008-10-15.15	5.5 ± 0.5
31255010	2008-10-21.63	5.2 ± 0.4

XMMM31 J004224.5+412401

A new outburst of the X-ray transient XMMM31 J004224.5+412401 = VG2007 233 (Voss & Gilfanov 2007; Stiele et al. 2008) was detected with 12 ± 4 counts (corrected for exposure and vignetting) in the 2.5 ks *Swift* XRT observation 00031255009, starting on 2008-10-15.15 UT (Henze et al. 2008j). The count rate corresponds to an unabsorbed luminosity of $(1.9 \pm 0.4)\times10^{37}$ erg s^{-1}, assuming an absorbed power law with $N_{\rm H} = 6.6\times 10^{20}$ cm^{-2} and photon index of 1.7, for a M 31 distance of 780 kpc. The transient was still visible, with a similar luminosity (26 ± 6 counts in 6.0 ks), in a *Swift* XRT observation starting on 2008-10-21.63 UT (ObsID 00031255010), but was not detected (3σ upper limit of 1.4×10^{37} erg s^{-1}) in observation 00031255006 (4.7 ks), starting on 2008-09-25.51. XMMM31 J004224.5+412401 was previously detected in a XMM-Newton observation starting on 2004-07-16.69 (ObsID 0202230201) and was classified as a X-ray binary candidate according to its time variability. The source was not known before as a recurrent transient.

XMMM31 J004205.8+411329

A new outburst of the recurrent transient XMMM31 J004205.8+411329 = r3-125 (Williams et al. 2004; Stiele et al. 2008) was detected with 62 ± 9 counts (corrected for exposure and vignetting)

in the 6.0 ks *Swift* observation 00031255010, starting on 2008-10-21.63 UT (Henze et al. 2008j). This corresponds to an unabsorbed luminosity of $(4.5 \pm 0.7)\times10^{37}$ erg s^{-1}, assuming an absorbed power law with $N_{\rm H} = 6.6\times 10^{20}$ cm^{-2} and photon index of 1.7, for a M 31 distance of 780 kpc. The transient was not detected during the *Swift* observations 00031255006 (starting on 2008-09-25.51 UT) and 00031255009 (starting on 2008-10-15.15 UT) with 3σ upper limits of 4.3×10^{-3} ct s^{-1} (1.6×10^{37} erg s^{-1}) and 8.4×10^{-3} ct s^{-1} (3.1×10^{37} erg s^{-1}), respectively. The source was also not detected during the XMM-Newton observation 0560180101 (see above) with an EPIC PN upper limit for the unabsorbed luminosity of 8.4×10^{35} erg s^{-1} (0.5–5 keV), assuming a spectrum as above.

SWIFT J004159.3+410539

This source was detected as a new bright X-ray transient at RA = 00:41:59.3, Dec = +41:05:39 (J2000; uncertainty 3.″7) in the 7.0 ks *Swift* observation 00031518002, starting on 2009-10-22.60 UT (Haberl et al. 2009). The object was located near the edge of the field of view of the XRT. Its X-ray spectrum was modelled by an absorbed powerlaw with $N_{\rm H} = 1.4\times 10^{21}$ cm^{-2} and a photon index of 1.9. The unabsorbed 0.2–10.0 keV luminosity was estimated to 4.6×10^{38} erg s^{-1} (assuming a distance of 780 kpc). The X-ray light curve showed variations by a factor of about 3 on time scales of about 20 min, but no significant period was found.

SWIFT J004159.3+410539 was also detected in the *Chandra* HRC-I observation 10882, starting on 2009 Nov 07.227 UT (Pietsch et al. 2009c). Assuming the spectral model described above, an unabsorbed luminosity (0.2–10 keV) of 5.5×10^{38} erg s^{-1} was derived. The HRC-I X-ray light curve showed similar variability as in the *Swift* observation. Again, no significant period could be found.

RX J0043.2+4127

A new outburst of the recurrent X-ray transient RX J0043.2+4127 = CXO J004317.8+412745 in the M 31 GC Bol 163 (see Trudolyubov & Priedhorsky 2004) was detected in a 19.1 ks *Chandra* HRC-I observation (ObsID 10882) starting on 2009-11-07.23 UT (Pietsch et al. 2009c). The source showed a count rate of $(6.5 \pm 0.3)\times10^{-2}$ ct s^{-1} which corresponds to an unabsorbed luminosity (0.2–10 keV) of 1.6×10^{38} erg s^{-1}. This assumes an absorbed power-law model with photon index = 1.54 and $N_{\rm H} = 1.1\times 10^{21}$ cm^{-2}, as given by Trudolyubov & Priedhorsky (2004), and a distance of 780 kpc. The transient was listed in the catalogue of Supper et al. (2001). Trudolyubov & Priedhorsky (2004) reported an earlier *Chandra* detection on 2001-02-18 and an analysis of ROSAT data that revealed several outbursts.

CXOM31 J004253.1+411422

This source was discovered as a very bright new X-ray transient in the 19 ks *Chandra* HRC-I observation 10886, which started on 2009-12-17.89 UT (Henze et al. 2009b). The transient was detected with a count rate of 3.28 ± 0.04 ct s^{-1} (corrected for exposure and vignetting), making it by far the brightest object in the field of view. The source position was RA = 00:42:53.15, Dec = +41:14:22.9 (J2000), using the catalogue of Kaaret (2002) as an astrometric reference.

Furthermore, the source was serendipitously in the field of view of the 4.4 ks *Swift* observation 00031518013, which started on 2009-12-22.04 UT. It was still the brightest source in the field of view, with a count rate of about 0.7 ct s^{-1}. The X-ray spectrum was modelled (reduced $\chi^2 = 0.9$, 89 d.o.f.) with an absorbed disk blackbody model with $N_{\rm H} = (6.6 \pm 2.6)\times 10^{20}$ cm^{-2}, consistent with the Galactic foreground absorption, and an inner disk temperature of (1.15 ± 0.08) keV. This model

gives an unabsorbed 0.2–10.0 keV luminosity of $(1.7 \pm 0.1)\times10^{39}$ erg s^{-1} (assuming a distance of 780 kpc). Applying the spectral model to the *Chandra* HRC-I count rate, I derived an unabsorbed 0.2–10.0 luminosity of $(4.6 \pm 0.1)\times10^{39}$ erg s^{-1}. The spectral parameters and the very large X-ray luminosity indicate a black hole X-ray transient. This makes the source a good candidate for the first ultraluminous X-ray source found in M 31.

CXOM31 J004253.1+411421 was the brightest transient ever detected in M 31 so far. The drop in luminosity by more than a factor of 2.5 in the four days between the *Chandra* and the *Swift* observation showed that the transient was rapidly variable. The source was not detected in a *Chandra* HRC-I observation on 2009-12-08.94 (ObsID 10885) with a 3σ upper limit luminosity of 2.1×10^{36} erg s^{-1}. No emission is detected in a 1.5 ks UVOT exposure during the *Swift* observation (3σ limiting magnitude of 20.1 mag in the uvw2 filter).

Appendix B

The curious case of the quasar Sharov 21

This chapter briefly describes new insights on the nature of the object Sharov 21 (= J004457+4123; Meusinger et al. 2010), with special emphasis on my contributions to this work. The designation "Sharov 21 " that is used here and by Meusinger et al. (2010) follows the terminology of Sharov et al. (1998), who included the object as "nova 21" in their catalogue.

During my work on the search for novae in archival photographic plate data of the Tautenburg observatory Schmidt telescope (see Henze et al. 2008e), Sharov 21 emerged as a possible nova candidate with its outburst in the year 1992. Eventually, I rejected the interpretation of the object as a nova because of the atypically slow rise of the "outburst" and the existence of a very faint persistent object at the same position in reference images of the Digitized Sky Survey[1]. However, I decided that the object was interesting and that it merited further study. In the literature I found the following information:

Sharov 21 was first discovered as a nova candidate in M 31 by Nedialkov et al. (1996). It was discussed as a "remarkable nova in M 31" by Sharov et al. (1998) on the grounds that its optical light curve was highly unusual for a nova. The brightness of the object was nearly constant at $R \sim 20.5$ mag from 1969 through 1991, showed an outburst by ~ 3 magnitudes in 1992 and returned to the pre-outburst level one or two years later. According to Sharov et al. (1998), Sharov 21 was not detected before 1969 and therefore must have been considerably fainter than $R = 20.5$ mag. Such a slow rise in brightness over decades before the outburst would be very peculiar for a nova. Furthermore, a possible X-ray counterpart of Sharov 21 was found by PFF2005 in archival ROSAT and XMM-Newton data. They identified Sharov 21 with the source [PFH2005] 601 of their catalogue of XMM-Newton EPIC X-ray sources (Pietsch et al. 2005b) and with the hard ROSAT source [SHL2001] 306 from the catalogue of Supper et al. (2001). Based on the hardness of the X-ray source and the peculiar optical light curve, PFF2005 noted that Sharov 21 "may not be a nova at all".

In order to infer the true nature of Sharov 21, our group requested on my initiative optical spectroscopy of the object. The spectroscopy was carried out with the Double Imaging Spectrograph (DIS) on the 3.5 m telescope at Apache Point Observatory (APO) in New Mexico, USA, in November 2007. The spectrum revealed that Sharov 21 is in fact a quasar with redshift $z \sim 2.1$ behind the disk of M 31. This finding was even more of a surprise, as the optical spectrum was that of a typical type 1 quasar, for which an optical variability as found for Sharov 21 is highly unusual (see Meusinger et al. 2010). To study further the properties of this peculiar object, Meusinger et al. (2010) created a broad band spectrum from literature data of different wavelength regimes and collected and re-analysed an extensive set of archival data in order to construct a long term light curve.

[1] available at http://stdatu.stsci.edu/cgi-bin/dss_form

The broad band spectrum consisted of publicly available data obtained in various wavelength with different telescopes: radio (Very Large Array radio telescope; VLA), near and far ultraviolet (Galaxy Evolution Explorer; GALEX), near infrared (2MASS catalogue) and X-ray (XMM-Newton, ROSAT). I re-analysed the archival X-ray data, with special emphasis on the ROSAT data which was taken shortly after the optical "outburst". For this task, I familiarised myself with ROSAT data reduction procedures in ESO MIDAS within the EXSAS context. The following two paragraphs describe the results of this analysis and are slightly altered from what I contributed to the Meusinger et al. (2010) paper.

For computing fluxes from instrument dependent count rates, I used an absorbed power-law model with a generic photon index of 1.7 (see also Pietsch et al. 2005b). I adopted a foreground extinction of $E(B-V) = 0.20$ mag, derived form the optical data, which translates to a $N_{\rm H} = 1.1\times 10^{21}$ cm^{-2} following Predehl & Schmitt (1995). Based on this spectral model, I used the source count rates given by Pietsch et al. (2005b) for [PFH2005] 601 in the XMM-Newton observation 0151580401 (obtained at 2003-02-06) to estimate an unabsorbed flux of $(5.8 \pm 1.9)\times 10^{-14}$ erg s^{-1} cm^{-2} in the (0.2-10.0) keV band and a monochromatic flux $F_\nu = (4.5 \pm 1.5) \times 10^{-9}$ Jy at $\nu = 1.71017$ Hz.

The ROSAT data of the Sharov 21 field[2] consists of twelve observations with the Position Sensitive Proportional Counter (PSPC) and 3 observations with the High Resolution Imager (HRI). I performed source detection around the position of Sharov 21 on the original event files and computed count rates and 3σ upper limits for all observations. There is just one 3σ detection of an X-ray source in the data set, identical with [SHL2001] 306, which is supplemented by upper limits for the rest of the observations. The flux estimated from the detection is consistent, within the errors, with the XMM-Newton data. Although the ROSAT observations were performed during the decline of the optical "outburst" (around JD = 2449000) no significant X-ray variability is detected. Note however, that the only ROSAT detection is a very faint off-axis PSPC detection and due to the large positional error circle of this instrument it is not possible to assume a doubtless correlation with [PFH2005] 601. Including data from all wavelength regimes mentioned above, the broad band spectrum turned out to be very similar to that of normal, radio-quite type 1 quasars. This confirmed the first impression based on the optical spectrum.

To study the variability of Sharov 21, Meusinger et al. (2010) compiled a long-term light curve consisting of more than 1100 single observations from 15 telescopes. Altogether, these observations covered more than a century (1900–2009). While the early data provided mostly upper limits, there were detections at 221 epochs from 1948 to 2009, with a relatively good time coverage after 1961. The light curve showed that the 1992 "outburst" was an unique event and Sharov 21 spent most of the time (98%) in a ground state around $B = 20.5$ mag. In this ground state, the variability of Sharov 21 did not differ significantly from that of other radio-quiet quasars of comparable redshift and luminosity. The 1992 "outburst", observed mainly in the optical B band, was interpreted as a UV-flare in the rest-system of the quasar. During the flare, the UV flux of Sharov 21 increased by a factor ~ 20. Such a strong flare is a very rare and unusual event for a radio-quite high-redshift quasar. Meusinger et al. (2010) discussed two possible scenarios in which the event could be explained.

The first scenario discussed the flare being a microlensing event in which a star in M 31 acted as a gravity lens for the background quasar. In this case, the quasar would not be intrinsically variable. The lens would have had to be a low-mass binary star, in order to explain a weak but clearly indicated asymmetry of the flare. However, while such a scenario is possible, the probability for a magnification as strong as in Sharov 21 is very low.

The second scenario is a tidal disruption event (TDE) of a star by the gravitational forces of the

[2] available at http://www.xray.mpe.mpg.de/cgi-bin/rosat/seq-browser

supermassive black hole of the quasar. This case is supported by the total energy in the outburst, the shape of the light curve, and the time scale of the event. However, TDEs have only been found so far in non-AGN galaxies and it is unclear how the presence of massive accretion disk, necessary to maintain the quasar activity, would influence the tidal disruption.

While the work of Meusinger et al. (2010) marked an important step in understanding the variability of the peculiar quasar Sharov 21, further efforts in completing the light curve and modelling the possible physical processes are necessary.

Appendix C

Optical light curves from the M 31 centre monitoring

Here I show the optical light curves of novae that were detected in the M 31 centre monitoring described in Chap. 2.1.3. I plot the *R* band magnitude of the nova (including 1σ error bars), calibrated with the M 31 catalogue of the LGGS (Massey et al. 2006), against the time in days after the optical outburst. Dotted lines connect the detected brightnesses for better readability. Labels within the figure give the name of the nova and the telescope involved in the observations (see Chap. 2.1.3), while the label of the abscissa gives the JD of the optical outburst.

For some of the light curves, the smooth decline after the maximum magnitude is interupted by significant variability (compare also Chap. 1.1.2). Furthermore, for four bright novae with good observational coverage I was able to estimate their t_2 times from the light curves presented here: M31N 2007-12d: $\sim$ 4 d (see also Table 4.3), M31N 2008-05c: $\sim$ 20 d, M31N 2009-11d: $\sim$ 16 d, M31N 2010-01a: $\sim$ 10 d.

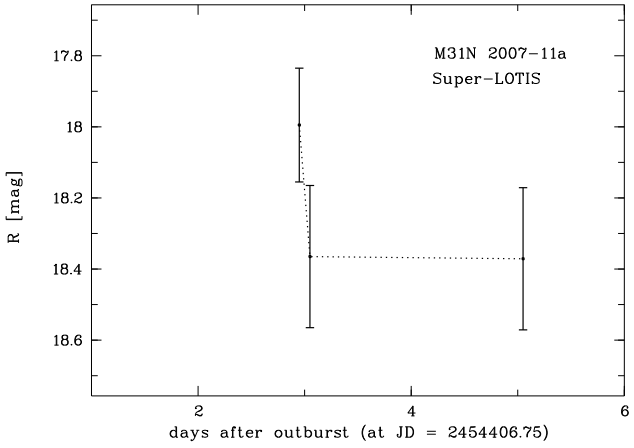

Figure C.1: Nova M31N 2007-11a (Super-LOTIS).

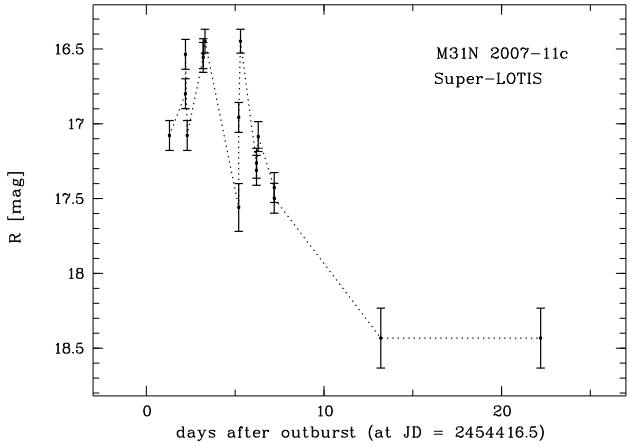

Figure C.2: Nova M31N 2007-11c (Super-LOTIS).

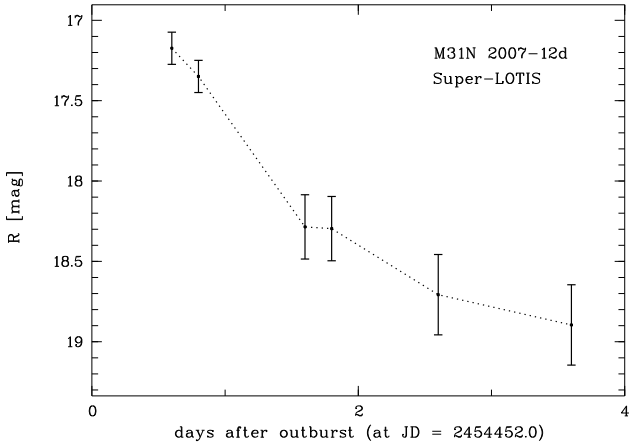

Figure C.3: Nova M31N 2007-12d (Super-LOTIS).

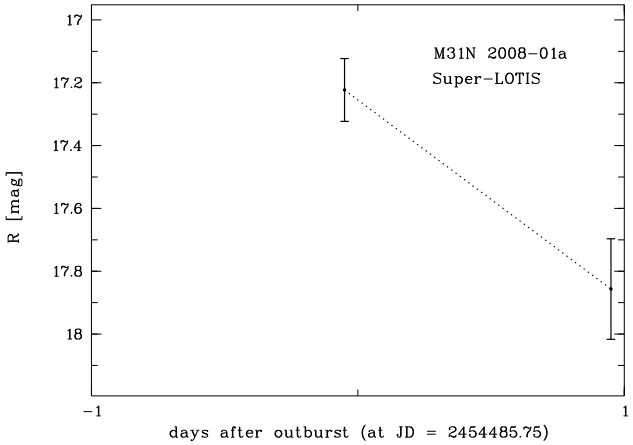

Figure C.4: Nova M31N 2008-01a (Super-LOTIS).

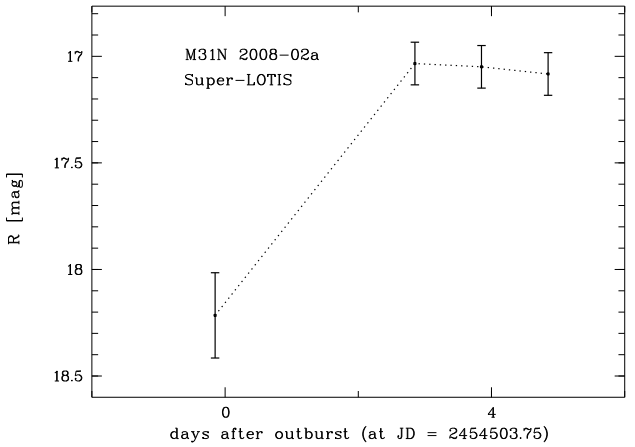

Figure C.5: Nova M31N 2008-02a (Super-LOTIS).

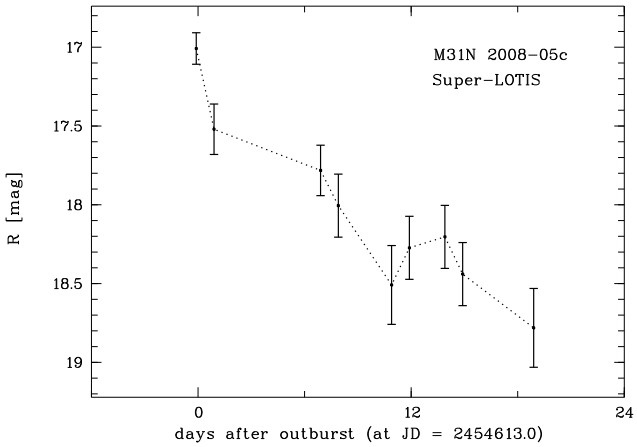

Figure C.6: Nova M31N 2008-05c (Super-LOTIS).

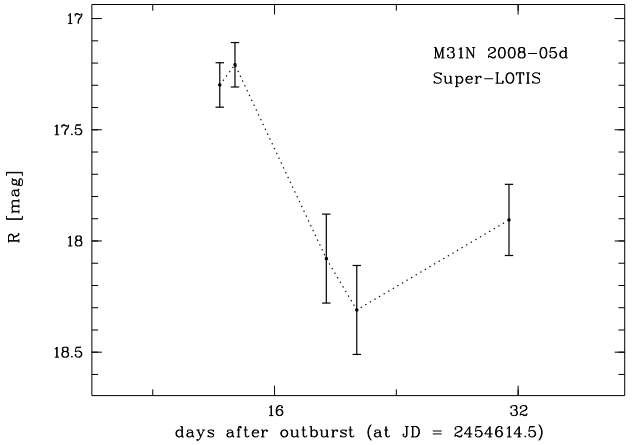

Figure C.7: Nova M31N 2008-05d (Super-LOTIS).

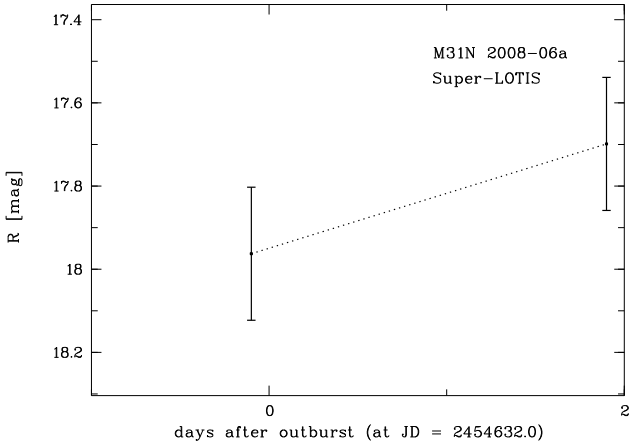

Figure C.8: Nova M31N 2008-06a (Super-LOTIS).

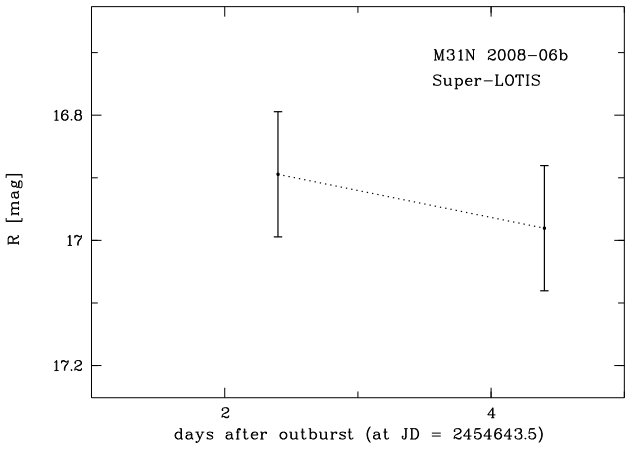

Figure C.9: Nova M31N 2008-06b (Super-LOTIS).

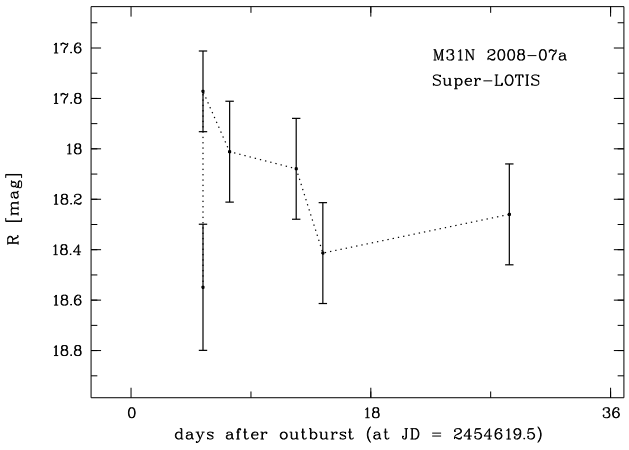

Figure C.10: Nova M31N 2008-07a (Super-LOTIS).

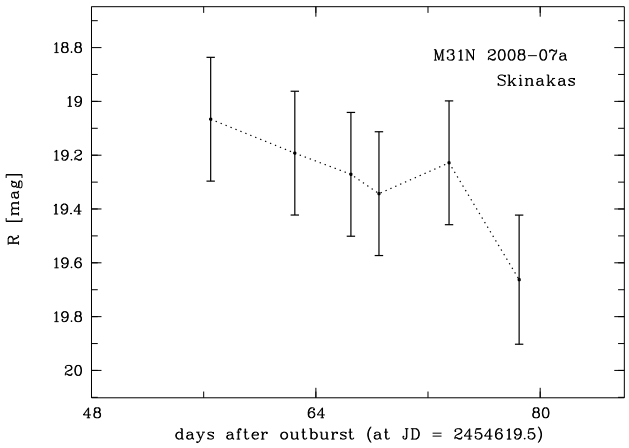

Figure C.11: Nova M31N 2008-07a (Skinakas).

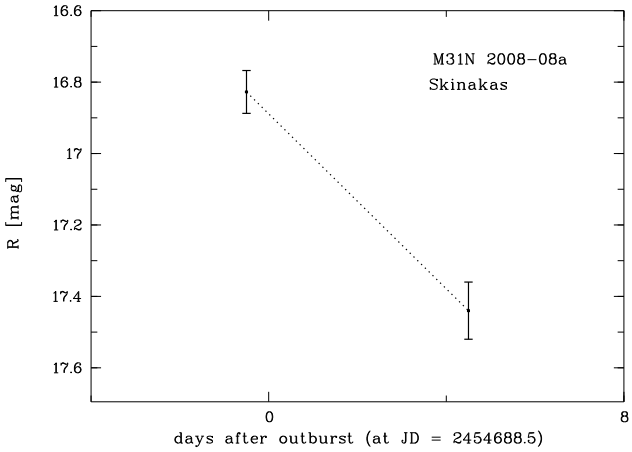

Figure C.12: Nova M31N 2008-08a (Skinakas).

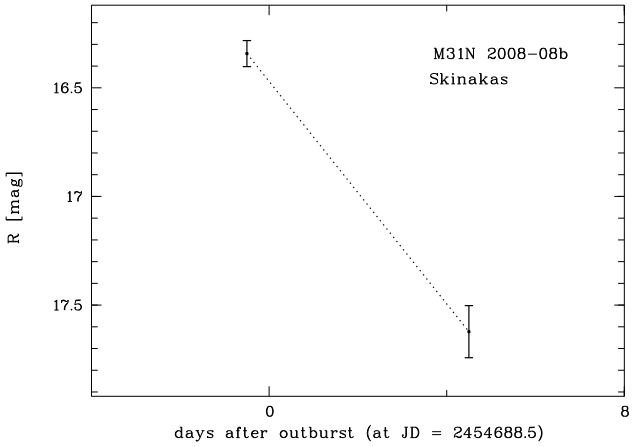

Figure C.13: Nova M31N 2008-08b (Skinakas).

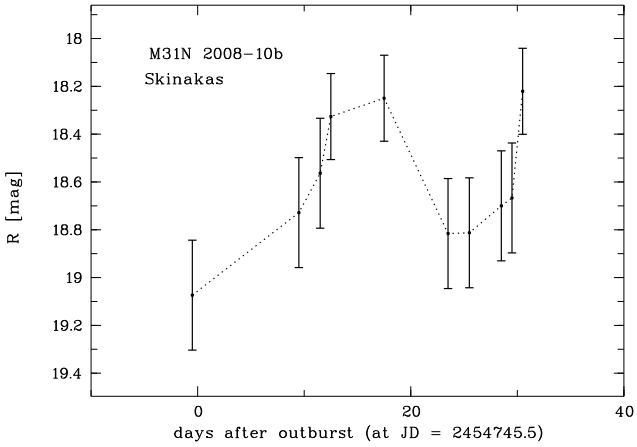

Figure C.14: Nova M31N 2008-10b (Skinakas).

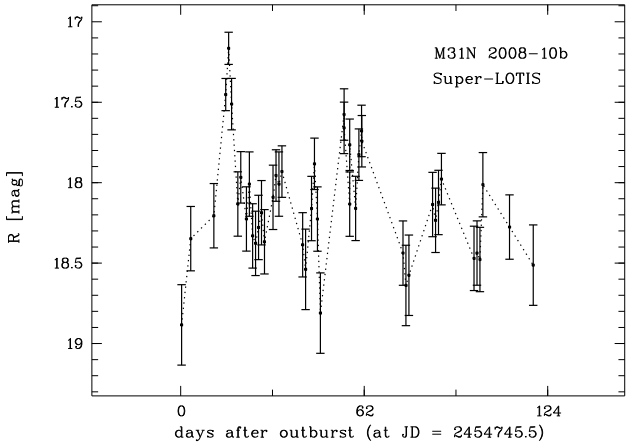

Figure C.15: Nova M31N 2008-10b (Super-LOTIS).

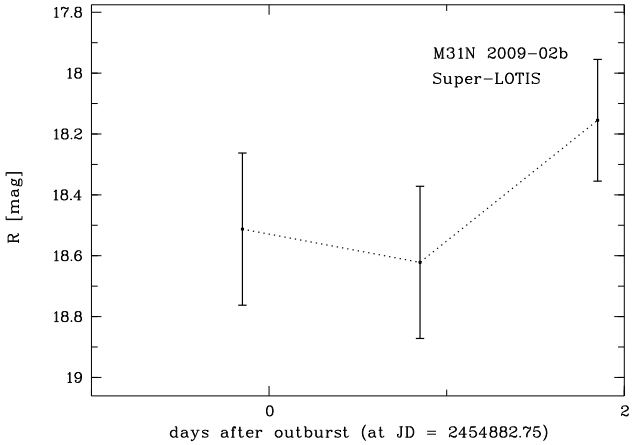

Figure C.16: Nova M31N 2009-02b (Super-LOTIS).

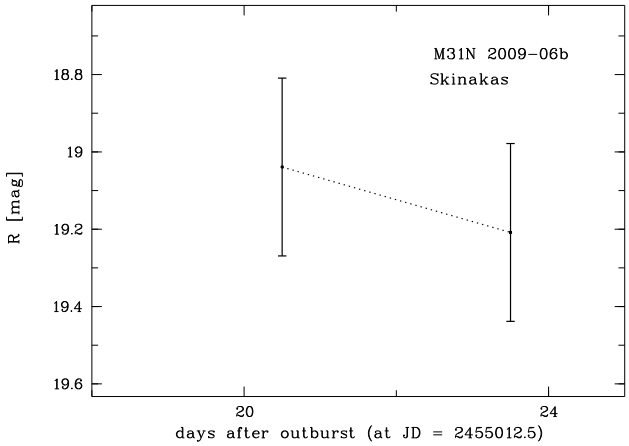

Figure C.17: Nova M31N 2009-06b (Skinakas).

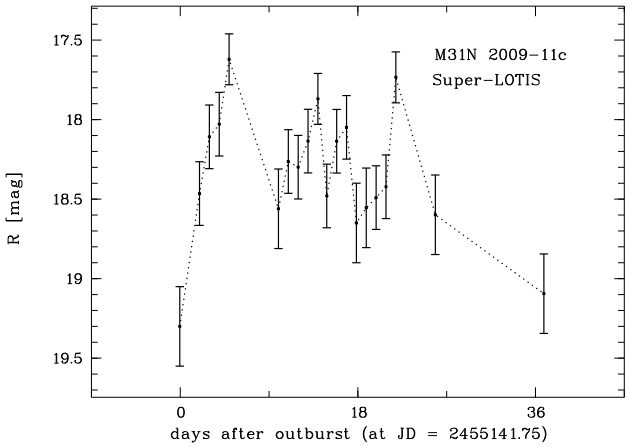

Figure C.18: Nova M31N 2009-11c (Super-LOTIS).

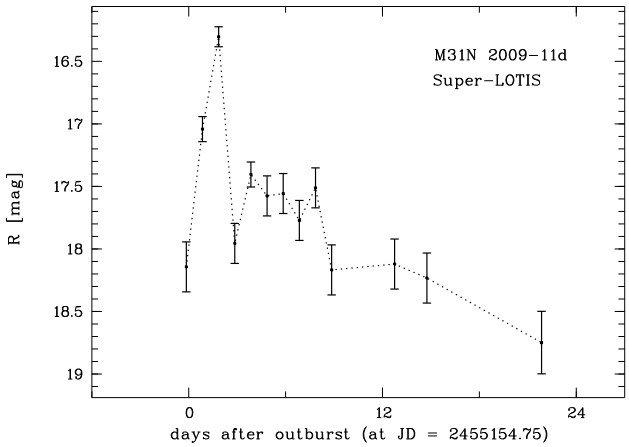

Figure C.19: Nova M31N 2009-11d (Super-LOTIS).

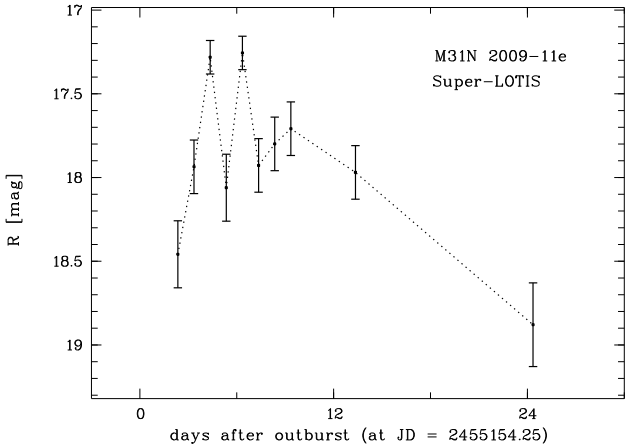

Figure C.20: Nova M31N 2009-11e (Super-LOTIS).

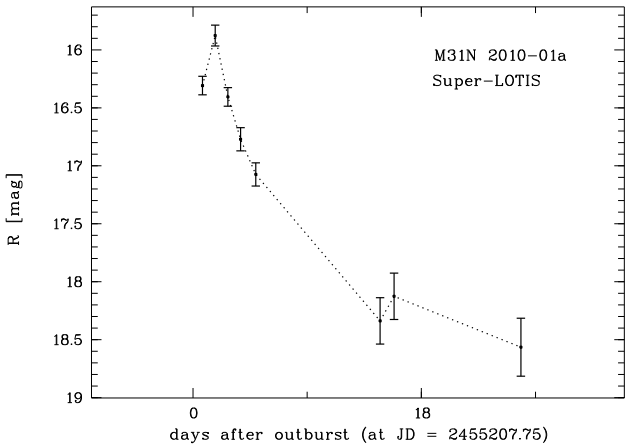

Figure C.21: Nova M31N 2010-01a (Super-LOTIS).

Bibliography

Akerlof, C. W., Kehoe, R. L., McKay, T. A., et al. 2003, PASP, 115, 132

Alksnis, A., Smirnova, O., & Zharova, A. V. 2008, Astronomy Letters, 34, 563

Allen, C. W. 1976, Astrophysical Quantities (Astrophysical Quantities, London: Athlone (3rd edition), 1976)

An, J. H., Evans, N. W., Hewett, P., et al. 2004, MNRAS, 351, 1071

Anders, E. & Grevesse, N. 1989, Geochim. Cosmochim. Acta, 53, 197

Ansari, R., Aurière, M., Baillon, P., et al. 2004, A&A, 421, 509

Aschenbach, B., Briel, U. G., Haberl, F., et al. 2000, in Society of Photo-Optical Instrumentation Engineers (SPIE) Conference Series, Vol. 4012, Society of Photo-Optical Instrumentation Engineers (SPIE) Conference Series, ed. J. E. Truemper & B. Aschenbach, 731–739

Baernbantner, O. & Riffeser, A. 2006, The Astronomer's Telegram, 808, 1

Balucinska-Church, M. & McCammon, D. 1992, ApJ, 400, 699

Barmby, P. & Huchra, J. P. 2000, ApJ, 531, L29

Barsukova, E., Sholukhova, O., Valeev, A., et al. 2008, The Astronomer's Telegram, 1773, 1

Barthelmy, S. D., Barbier, L. M., Cummings, J. R., et al. 2005, Space Sci. Rev., 120, 143

Beardmore, A. P., Balman, S., Osborne, J. P., et al. 2010, The Astronomer's Telegram, 2423, 1

Beaton, R. L., Majewski, S. R., Guhathakurta, P., et al. 2007, ApJ, 658, L91

Bertin, E. & Arnouts, S. 1996, A&AS, 117, 393

Blackburn, J. K. 1995, in Astronomical Society of the Pacific Conference Series, Vol. 77, Astronomical Data Analysis Software and Systems IV, ed. R. A. Shaw, H. E. Payne, & J. J. E. Hayes, 367–+

Bode, M. F. 2010, Astronomische Nachrichten, 331, 160

Bode, M. F., Darnley, M. J., Shafter, A. W., et al. 2009, ApJ, 705, 1056

Bode, M. F. & Evans, A. 2008, Classical Novae, ed. Bode, M. F. & Evans, A.

Bogdán, Á. & Gilfanov, M. 2008, MNRAS, 388, 56

Brinkman, B. C., Gunsing, T., Kaastra, J. S., et al. 2000, in Society of Photo-Optical Instrumentation Engineers (SPIE) Conference Series, Vol. 4012, Society of Photo-Optical Instrumentation Engineers (SPIE) Conference Series, ed. J. E. Truemper & B. Aschenbach, 81–90

Burrows, D. N., Hill, J. E., Nousek, J. A., et al. 2005, Space Sci. Rev., 120, 165

Burwitz, V., Henze, M., Pietsch, W., et al. 2008a, The Astronomer's Telegram, 1364, 1

Burwitz, V., Pietsch, W., Cikota, M., Henze, S., & Violat-Bordonau, F. 2008b, The Astronomer's Telegram, 1591, 1

Burwitz, V., Pietsch, W., Henze, M., et al. 2010a, The Astronomer's Telegram, 2697, 1

Burwitz, V., Pietsch, W., Henze, M., et al. 2007a, The Astronomer's Telegram, 1275, 1

Burwitz, V., Pietsch, W., Henze, M., et al. 2010b, The Astronomer's Telegram, 2383, 1

Burwitz, V., Pietsch, W., Updike, A., et al. 2007b, The Astronomer's Telegram, 1238, 1

Canizares, C. R., Davis, J. E., Dewey, D., et al. 2005, PASP, 117, 1144

Capaccioli, M., Della Valle, M., Rosino, L., & D'Onofrio, M. 1989, AJ, 97, 1622

Catalán, S., Isern, J., García-Berro, E., & Ribas, I. 2008, MNRAS, 387, 1693

Ciardullo, R., Ford, H., & Jacoby, G. 1983, ApJ, 272, 92

Ciardullo, R., Ford, H. C., Neill, J. D., Jacoby, G. H., & Shafter, A. W. 1987, ApJ, 318, 520

Ciardullo, R., Shafter, A. W., Ford, H. C., et al. 1990a, ApJ, 356, 472

Ciardullo, R., Tamblyn, P., & Phillips, A. C. 1990b, PASP, 102, 1113

Ciroi, S., Mille, F. D., Rafanelli, P., & Temporin, S. 2007, The Astronomer's Telegram, 1292, 1

Clark, G. W. 1975, ApJ, 199, L143

Cohen, J. G. 1988, in Astronomical Society of the Pacific Conference Series, Vol. 4, The Extragalactic Distance Scale, ed. S. van den Bergh & C. J. Pritchet, 114–127

Cruddace, R. G., Hasinger, G. R., & Schmitt, J. H. 1988, in European Southern Observatory Conference and Workshop Proceedings, Vol. 28, European Southern Observatory Conference and Workshop Proceedings, ed. F. Murtagh & A. Heck, 177–182

Cutri, R. M., Skrutskie, M. F., van Dyk, S., et al. 2003, 2MASS All Sky Catalog of point sources.

Darnley, M. J., Bode, M. F., Kerins, E., et al. 2006, MNRAS, 369, 257

Darnley, M. J., Bode, M. F., Kerins, E., et al. 2004, MNRAS, 353, 571

Della Valle, M. 2002, in American Institute of Physics Conference Series, Vol. 637, Classical Nova Explosions, ed. M. Hernanz & J. José, 443–456

Della Valle, M., Bianchini, A., Livio, M., & Orio, M. 1992, A&A, 266, 232

Della Valle, M. & Livio, M. 1994, ApJ, 423, L31

Della Valle, M. & Livio, M. 1995, ApJ, 452, 704

Della Valle, M. & Livio, M. 1996, ApJ, 473, 240

Della Valle, M. & Livio, M. 1998, ApJ, 506, 818

Della Valle, M., Pasquini, L., Daou, D., & Williams, R. E. 2002, A&A, 390, 155

Della Valle, M., Rosino, L., Bianchini, A., & Livio, M. 1994, A&A, 287, 403

den Herder, J. W., Brinkman, A. C., Kahn, S. M., et al. 2001, A&A, 365, L7

di Mille, F., Ciroi, S., Botte, V., & Boschetti, C. S. 2003, IAU Circ., 8231, 4

Di Mille, F., Ciroi, S., Orio, M., et al. 2008a, The Astronomer's Telegram, 1818, 1

Di Mille, F., Ciroi, S., Orio, M., et al. 2008b, The Astronomer's Telegram, 1703, 1

Di Stefano, R. & Rappaport, S. 1994, ApJ, 423, 274

Diaz, M. P. & Bruch, A. 1997, A&A, 322, 807

Dimai, A. & Manzini, F. 2005, The Astronomer's Telegram, 421, 1

Dobrotka, A. & Ness, J. 2010, MNRAS, 685

Dotani, T., Asai, K., & Greiner, J. 1999, PASJ, 51, 519

Drake, J. J., Wagner, R. M., Starrfield, S., et al. 2003, ApJ, 584, 448

Duerbeck, H. W. 1990, in Lecture Notes in Physics, Berlin Springer Verlag, Vol. 369, IAU Colloq. 122: Physics of Classical Novae, ed. A. Cassatella & R. Viotti, 34–+

Edmonds, P. D., Kahabka, P., & Heinke, C. O. 2004, ApJ, 611, 413

Elvis, M., Civano, F., Vignali, C., et al. 2009, ApJS, 184, 158

Fabian, A. C., Pringle, J. E., & Rees, M. J. 1975, MNRAS, 172, 15P

Fabrika, S., Sholukhova, O., Valeev, A., Hornoch, K., & Pietsch, W. 2009, The Astronomer's Telegram, 2240, 1

Fan, Z., Ma, J., Zhou, X., et al. 2005, PASP, 117, 1236

Fiaschi, M., Di Mille, F., Cariolato, R., Swift, B., & Li, W. D. 2002, IAU Circ., 7794, 1

Fiaschi, M., Tiveron, D., & Cardullo, A. 2003, IAU Circ., 8226, 2

Filippenko, A. V. & Chornock, R. 2001, IAU Circ., 7738, 3

Filippenko, A. V. & Chornock, R. 2002, IAU Circ., 7825, 3

Filippenko, A. V., Chornock, R. T., Coil, A. L., Leonard, D. C., & Li, W. D. 1999, IAU Circ., 7272, 2

Freedman, W. L., Madore, B. F., Gibson, B. K., et al. 2001, ApJ, 553, 47

Fruscione, A., McDowell, J. C., Allen, G. E., et al. 2006, in Society of Photo-Optical Instrumentation Engineers (SPIE) Conference Series, Vol. 6270, Society of Photo-Optical Instrumentation Engineers (SPIE) Conference Series

Gabriel, C., Denby, M., Fyfe, D. J., et al. 2004, in Astronomical Society of the Pacific Conference Series, Vol. 314, Astronomical Data Analysis Software and Systems (ADASS) XIII, ed. F. Ochsenbein, M. G. Allen, & D. Egret, 759–+

Gal-Yam, A. & Quimby, R. 2007, The Astronomer's Telegram, 1236, 1

Galache, J. L., Garcia, M. R., Torres, M. A. P., et al. 2007, The Astronomer's Telegram, 1328, 1

Gallagher, J. S. & Starrfield, S. 1976, MNRAS, 176, 53

Galleti, S., Bellazzini, M., Federici, L., Buzzoni, A., & Fusi Pecci, F. 2007, A&A, 471, 127

Galleti, S., Bellazzini, M., Federici, L., & Fusi Pecci, F. 2005, A&A, 436, 535

Galleti, S., Federici, L., Bellazzini, M., Buzzoni, A., & Fusi Pecci, F. 2006, A&A, 456, 985

Galleti, S., Federici, L., Bellazzini, M., Fusi Pecci, F., & Macrina, S. 2004, A&A, 416, 917

Garmire, G. P., Bautz, M. W., Ford, P. G., Nousek, J. A., & Ricker, Jr., G. R. 2003, in Society of Photo-Optical Instrumentation Engineers (SPIE) Conference Series, Vol. 4851, Society of Photo-Optical Instrumentation Engineers (SPIE) Conference Series, ed. J. E. Truemper & H. D. Tananbaum, 28–44

Gehrels, N., Chincarini, G., Giommi, P., et al. 2004, ApJ, 611, 1005

Greiner, J., Hasinger, G., & Kahabka, P. 1991, A&A, 246, L17

Haberl, F., Henze, M., & Pietsch, W. 2007a, The Astronomer's Telegram, 1296, 1

Haberl, F., Henze, M., Pietsch, W., & Orio, M. 2009, The Astronomer's Telegram, 2262, 1

Haberl, F., Pietsch, W., & Henze, M. 2007b, The Astronomer's Telegram, 1306, 1

Hachisu, I. & Kato, M. 2006, ApJS, 167, 59

Hachisu, I. & Kato, M. 2010, ApJ, 709, 680

Hachisu, I., Kato, M., & Luna, G. J. M. 2007, ApJ, 659, L153

Hatano, K., Branch, D., Fisher, A., & Starrfield, S. 1997, ApJ, 487, L45

Hatzidimitriou, D., Reig, P., Manousakis, A., et al. 2007, A&A, 464, 1075

Henze, M., Burwitz, V., Pietsch, W., et al. 2008a, The Astronomer's Telegram, 1654, 1

Henze, M., Burwitz, V., Pietsch, W., et al. 2010a, The Astronomer's Telegram, 2727, 1

Henze, M., Burwitz, V., Pietsch, W., et al. 2007a, The Astronomer's Telegram, 1336, 1

Henze, M., Burwitz, V., Pietsch, W., et al. 2008b, The Astronomer's Telegram, 1546, 1

Henze, M., Burwitz, V., Pietsch, W., et al. 2008c, The Astronomer's Telegram, 1580, 1

Henze, M., Burwitz, V., Pietsch, W., et al. 2008d, The Astronomer's Telegram, 1567, 1

Henze, M., Kaduk, F., Burwitz, V., et al. 2009a, The Astronomer's Telegram, 2165, 1

Henze, M., Meusinger, H., & Pietsch, W. 2008e, A&A, 477, 67

Henze, M., Pietsch, W., Burwitz, V., et al. 2008f, The Astronomer's Telegram, 1790, 1

Henze, M., Pietsch, W., Burwitz, V., et al. 2008g, The Astronomer's Telegram, 1609, 1

Henze, M., Pietsch, W., Burwitz, V., et al. 2008h, The Astronomer's Telegram, 1380, 1

Henze, M., Pietsch, W., Burwitz, V., et al. 2008i, The Astronomer's Telegram, 1602, 1

Henze, M., Pietsch, W., Greiner, J., & Burwitz, V. 2008j, The Astronomer's Telegram, 1806, 1

Henze, M., Pietsch, W., & Haberl, F. 2007b, The Astronomer's Telegram, 1307, 1

Henze, M., Pietsch, W., & Haberl, F. 2010b, The Astronomer's Telegram, 2787, 1

Henze, M., Pietsch, W., Haberl, F., & Greiner, J. 2009b, The Astronomer's Telegram, 2356, 1

Henze, M., Pietsch, W., Haberl, F., et al. 2010c, A&A, 523, A89+

Henze, M., Pietsch, W., Haberl, F., et al. 2010d, ArXiv e-prints

Henze, M., Pietsch, W., Haberl, F., & Orio, M. 2009c, The Astronomer's Telegram, 2274, 1

Henze, M., Pietsch, W., Haberl, F., et al. 2009d, A&A, 500, 769

Henze, M., Pietsch, W., Podigachoski, P., et al. 2009e, The Astronomer's Telegram, 2286, 1

Henze, M., Pietsch, W., Sala, G., et al. 2009f, A&A, 498, L13

Hernanz, M. 2005, in Astronomical Society of the Pacific Conference Series, Vol. 330, The Astrophysics of Cataclysmic Variables and Related Objects, ed. J.-M. Hameury & J.-P. Lasota, 265

Hertz, P. & Grindlay, J. E. 1983, ApJ, 267, L83

Holland, S. 1998, AJ, 115, 1916

Hornoch, K. 2003, IAU Circ., 8248, 2

Hornoch, K. & Pejcha, O. 2009, Central Bureau Electronic Telegrams, 2061, 5

Hornoch, K., Pejcha, O., Kusnirak, P., & Pietsch, W. 2009a, Central Bureau Electronic Telegrams, 2058, 3

Hornoch, K., Pejcha, O., Zasche, P., & Kusnirak, P. 2009b, Central Bureau Electronic Telegrams, 2057, 3

Hornoch, K., Prieto, J., Khan, R., et al. 2010, Central Bureau Electronic Telegrams, 2127, 1

Hubble, E. P. 1929, ApJ, 69, 103

Hut, P. & Verbunt, F. 1983, Nature, 301, 587

Iben, Jr., I. & Tutukov, A. V. 1984, ApJS, 54, 335

Immler, S., Pietsch, W., Kruse, W., et al. 2008, The Astronomer's Telegram, 1673, 1

Jansen, F., Lumb, D., Altieri, B., et al. 2001, A&A, 365, L1

José, J. & Hernanz, M. 1998, ApJ, 494, 680

Kaaret, P. 2002, ApJ, 578, 114

Kahabka, P., Hartmann, H. W., Parmar, A. N., & Negueruela, I. 1999, A&A, 347, L43

Kahabka, P. & van den Heuvel, E. P. J. 1997, ARA&A, 35, 69

Kato, M. 2010, Astronomische Nachrichten, 331, 140

Kong, A. K. H. & Di Stefano, R. 2007, The Astronomer's Telegram, 1334, 1

Kong, A. K. H., Garcia, M. R., Primini, F. A., & Murray, S. S. 2002a, ApJ, 580, L125

Kong, A. K. H., Garcia, M. R., Primini, F. A., et al. 2002b, ApJ, 577, 738

Krautter, J. 2002, in American Institute of Physics Conference Series, Vol. 637, Classical Nova Explosions, ed. M. Hernanz & J. José, 345

Krautter, J. 2008, in Astronomical Society of the Pacific Conference Series, Vol. 401, Astronomical Society of the Pacific Conference Series, ed. A. Evans, M. F. Bode, T. J. O'Brien, & M. J. Darnley, 139–+

Krautter, J., Ögelman, H., Starrfield, S., Wichmann, R., & Pfeffermann, E. 1996, ApJ, 456, 788

Landsman, W. B. 1989, BAAS, 21, 784

Lang, F., Lerchster, M., & Fliri, J. 2006, The Astronomer's Telegram, 821, 1

Lee, C.-H., Ries, C., Riffeser, A., & Seitz, S. 2007, The Astronomer's Telegram, 1324, 1

Leibowitz, E., Orio, M., Gonzalez-Riestra, R., et al. 2006, MNRAS, 371, 424

Livio, M. 1992, ApJ, 393, 516

Mannucci, F., Della Valle, M., Panagia, N., et al. 2005, A&A, 433, 807

Mason, K. O., Breeveld, A., Much, R., et al. 2001, A&A, 365, L36

Massey, P., Olsen, K. A. G., Hodge, P. W., et al. 2006, AJ, 131, 2478

Metropolis, N., Rosenbluth, A. W., Rosenbluth, M. N., Teller, A. H., & Teller, E. 1953, J. Chem. Phys., 21, 1087

Meusinger, H., Henze, M., Birkle, K., et al. 2010, A&A, 512, A1+

Monet, D. G., Levine, S. E., Canzian, B., et al. 2003, AJ, 125, 984

Murray, S. S., Austin, G. K., Chappell, J. H., et al. 2000, in Society of Photo-Optical Instrumentation Engineers (SPIE) Conference Series, Vol. 4012, Society of Photo-Optical Instrumentation Engineers (SPIE) Conference Series, ed. J. E. Truemper & B. Aschenbach, 68–80

Nedialkov, P., Orio, M., Birkle, K., et al. 2002, A&A, 389, 439

Nedialkov, P. L., Tikhonov, N. A., Kurtev, R. G., & Ivanov, G. R. 1996, Information Bulletin on Variable Stars, 4411, 1

Nelson, T., Liu, J. F., di Stefano, R., et al. 2008a, The Astronomer's Telegram, 1672, 1

Nelson, T., Orio, M., Cassinelli, J. P., et al. 2008b, ApJ, 673, 1067

Ness, J., Schwarz, G., Starrfield, S., et al. 2008, AJ, 135, 1328

Ness, J., Schwarz, G. J., Retter, A., et al. 2007a, ApJ, 663, 505

Ness, J.-U., Starrfield, S., Beardmore, A. P., et al. 2007b, ApJ, 665, 1334

Nomoto, K. 1982, ApJ, 253, 798

Ögelman, H., Orio, M., Krautter, J., & Starrfield, S. 1993, Nature, 361, 331

Orio, M., Covington, J., & Ögelman, H. 2001, A&A, 373, 542

Orio, M. & Nelson, T. 2008, The Astronomer's Telegram, 1390, 1

Orio, M., Nelson, T., Bianchini, A., Di Mille, F., & Harbeck, D. 2010, ApJ, 717, 739

Osborne, J., Page, K., Beardmore, A., et al. 2006a, The Astronomer's Telegram, 838, 1

Osborne, J., Page, K., Goad, A. B. M., et al. 2006b, The Astronomer's Telegram, 770, 1

Osborne, J. P., Beardmore, A. P., Page, K. L., et al. 2009, The Astronomer's Telegram, 1942, 1

Osborne, J. P., Borozdin, K. N., Trudolyubov, S. P., et al. 2001, A&A, 378, 800

Ovcharov, E., Valcheva, A., Kostov, A., et al. 2009, The Astronomer's Telegram, 1927, 1

Page, K. L., Osborne, J. P., Evans, P. A., et al. 2010, MNRAS, 401, 121

Payne-Gaposchkin, C. 1964, The galactic novae (New York: Dover Publication, 1964)

Perlmutter, S., Aldering, G., Goldhaber, G., et al. 1999, ApJ, 517, 565

Petz, A., Hauschildt, P. H., Ness, J., & Starrfield, S. 2005, A&A, 431, 321

Pietsch, W. 2010, Astronomische Nachrichten, 331, 187

Pietsch, W., Burwitz, V., Greiner, J., et al. 2007a, The Astronomer's Telegram, 1009, 1

Pietsch, W., Burwitz, V., Greiner, J., et al. 2007b, The Astronomer's Telegram, 1294, 1

Pietsch, W., Burwitz, V., Greiner, J., Henze, M., & Stiele, H. 2008a, The Astronomer's Telegram, 1674, 1

Pietsch, W., Burwitz, V., Greiner, J., et al. 2006a, The Astronomer's Telegram, 850, 1

Pietsch, W., Burwitz, V., Henze, M., Morales, N., & Nomen, J. 2007c, The Astronomer's Telegram, 1329, 1

Pietsch, W., Burwitz, V., Rodriguez, J., & Garcia, A. 2006b, The Astronomer's Telegram, 805, 1

Pietsch, W., Burwitz, V., Stoss, R., et al. 2007d, The Astronomer's Telegram, 1230, 1

Pietsch, W., Burwitz, V., Updike, A., et al. 2007e, The Astronomer's Telegram, 1257, 1

Pietsch, W., Fliri, J., Freyberg, M. J., et al. 2005a, A&A, 442, 879 [PFF2005]

Pietsch, W., Fliri, J., Freyberg, M. J., et al. 2006c, A&A, 454, 773

Pietsch, W., Freyberg, M., & Haberl, F. 2005b, A&A, 434, 483

Pietsch, W., Freyberg, M., Haberl, F., Henze, M., & Stiele, H. 2008b, The Astronomer's Telegram, 1647, 1

Pietsch, W., Freyberg, M., Henze, M., Stiele, H., & Immler, S. 2008c, The Astronomer's Telegram, 1671, 1

Pietsch, W., Greiner, J., Haberl, F., & Sala, G. 2007f, The Astronomer's Telegram, 1116, 1

Pietsch, W., Haberl, F., Sala, G., et al. 2007g, A&A, 465, 375 [PHS2007]

Pietsch, W. & Henze, M. 2010, The Astronomer's Telegram, 2435, 1

Pietsch, W., Henze, M., Burwitz, V., et al. 2010a, The Astronomer's Telegram, 2713, 1

Pietsch, W., Henze, M., Burwitz, V., et al. 2009a, The Astronomer's Telegram, 2105, 1

Pietsch, W., Henze, M., Burwitz, V., et al. 2009b, The Astronomer's Telegram, 1935, 1

Pietsch, W., Henze, M., & Haberl, F. 2009c, The Astronomer's Telegram, 2287, 1

Pietsch, W., Henze, M., & Haberl, F. 2010b, The Astronomer's Telegram, 2730, 1

Pietsch, W., Kaduk, F., Henze, M., et al. 2009d, The Astronomer's Telegram, 2147, 1

Pietsch, W., Podigachoski, P., Haberl, F., et al. 2009e, The Astronomer's Telegram, 2308, 1

Podigachoski, P., Henze, M., Pietsch, W., et al. 2009a, The Astronomer's Telegram, 2234, 1

Podigachoski, P., Pietsch, W., Henze, M., et al. 2009b, The Astronomer's Telegram, 2285, 1

Podigachoski, P., Pietsch, W., Henze, M., et al. 2009c, The Astronomer's Telegram, 2304, 1

Predehl, P. & Schmitt, J. H. M. M. 1995, A&A, 293, 889

Quimby, R. 2006a, The Astronomer's Telegram, 887, 1

Quimby, R. 2006b, PhD Thesis, University of Texas, United States

Quimby, R., Mondol, P., Hoeflich, P., Wheeler, J. C., & Gerardy, C. 2005, The Astronomer's Telegram, 600, 1

Rau, A., Burwitz, V., Cenko, S. B., et al. 2007, The Astronomer's Telegram, 1242, 1

Rau, A. & Cenko, S. B. 2007, The Astronomer's Telegram, 1331, 1

Rau, A., Kasliwal, M. M., & Burwitz, V. 2008, The Astronomer's Telegram, 1568, 1

Rauch, T. 1997, A&A, 320, 237

Rauch, T. 2003, A&A, 403, 709

Rauch, T. & Deetjen, J. L. 2003, in Astronomical Society of the Pacific Conference Series, Vol. 288, Stellar Atmosphere Modeling, ed. I. Hubeny, D. Mihalas, & K. Werner, 103–+

Rector, T. A., Jacoby, G. H., Corbett, D. L., Denham, M., & RBSE Nova Search Team. 1999, in American Astronomical Society Meeting Abstracts, Vol. 195, American Astronomical Society Meeting Abstracts, 36.08

Reig, P., Primak, N., Akras, S., et al. 2008, The Astronomer's Telegram, 1612, 1

Ries, C. & Riffeser, A. 2006, The Astronomer's Telegram, 829, 1

Riffeser, A., Fliri, J., Gössl, C. A., et al. 2001, A&A, 379, 362

Ritter, H. & Kolb, U. 2003, A&A, 404, 301

Ritter, H., Politano, M., Livio, M., & Webbink, R. F. 1991, ApJ, 376, 177

Roming, P. W. A., Kennedy, T. E., Mason, K. O., et al. 2005, Space Sci. Rev., 120, 95

Sala, G. & Hernanz, M. 2005, A&A, 439, 1061

Sala, G., Hernanz, M., Ferri, C., & Greiner, J. 2008, ApJ, 675, L93

Sala, G., Hernanz, M., Ferri, C., & Greiner, J. 2010, Astronomische Nachrichten, 331, 201

Salpeter, E. E. 1955, ApJ, 121, 161

Samus, N. N., Durlevich, O. V., & et al. 2004, VizieR Online Data Catalog, 2250, 0

Schaefer, B. E. & Collazzi, A. C. 2010, AJ, 139, 1831

Schaefer, B. E., Pagnotta, A., Osborne, J. P., et al. 2010, The Astronomer's Telegram, 2477, 1

Schlegel, D. J., Finkbeiner, D. P., & Davis, M. 1998, ApJ, 500, 525

Schlegel, E. M., Schaefer, B., Pagnotta, A., et al. 2010, The Astronomer's Telegram, 2430, 1

Shafter, A. W. 1997, ApJ, 487, 226

Shafter, A. W. 2007a, The Astronomer's Telegram, 1341, 1

Shafter, A. W. 2007b, The Astronomer's Telegram, 1332, 1

Shafter, A. W., Coelho, E. A., Misselt, K. A., et al. 2006, The Astronomer's Telegram, 923, 1

Shafter, A. W. & Irby, B. K. 2001, ApJ, 563, 749

Shafter, A. W. & Quimby, R. M. 2007, ApJ, 671, L121

Shanley, L., Ogelman, H., Gallagher, J. S., Orio, M., & Krautter, J. 1995, ApJ, 438, L95

Shara, M. M., Zurek, D. R., Baltz, E. A., Lauer, T. R., & Silk, J. 2004, ApJ, 605, L117

Sharov, A. S. 1993, Astronomy Letters, 19, 7

Sharov, A. S. & Alksnis, A. 1998, Astronomy Letters, 24, 641

Sharov, A. S., Alksnis, A., Nedialkov, P. L., et al. 1998, Astronomy Letters, 24, 445

Sharov, A. S., Alksnis, A., Zharova, A. V., & Shokin, Y. A. 2000, Astronomy Letters, 26, 433

Shen, K. J., Idan, I., & Bildsten, L. 2009, ApJ, 705, 693

Shore, S. N., Starrfield, S., & Sonneborn, G. 1996, ApJ, 463, L21

Smirnova, O. & Alksnis, A. 2006, Informational Bulletin on Variable Stars, 5720, 1

Smirnova, O., Alksnis, A., & Zharova, A. V. 2006, Informational Bulletin on Variable Stars, 5737, 1

Stanek, K. Z. & Garnavich, P. M. 1998, ApJ, 503, L131

Stark, A. A., Gammie, C. F., Wilson, R. W., et al. 1992, ApJS, 79, 77

Starrfield, S. 1989, in Classical Novae, 39

Starrfield, S., Sparks, W. M., & Truran, J. W. 1974, ApJS, 28, 247

Stetson, P. B. 1987, PASP, 99, 191

Stiele, H., Pietsch, W., Haberl, F., et al. 2010, Astronomische Nachrichten, 331, 212

Stiele, H., Pietsch, W., Haberl, F., & Freyberg, M. 2008, A&A, 480, 599

Strohmayer, T. & Bildsten, L. 2006, New views of thermonuclear bursts, ed. Lewin, W. H. G. & van der Klis, M., 113–156

Strope, R. J., Schaefer, B. E., & Henden, A. A. 2010, AJ, 140, 34

Strüder, L., Briel, U., Dennerl, K., et al. 2001, A&A, 365, L18

Supper, R., Hasinger, G., Lewin, W. H. G., et al. 2001, A&A, 373, 63

Supper, R., Hasinger, G., Pietsch, W., et al. 1997, A&A, 317, 328

Tomaney, A., Crotts, A., & Shafter, A. 1992, in Bulletin of the American Astronomical Society, Vol. 24, Bulletin of the American Astronomical Society, 1237

Tomaney, A. B. & Shafter, A. W. 1992, ApJS, 81, 683

Trinchieri, G. & Fabbiano, G. 1991, ApJ, 382, 82

Trudolyubov, S. & Priedhorsky, W. 2004, ApJ, 616, 821

Trudolyubov, S. P. & Priedhorsky, W. C. 2008, ApJ, 676, 1218

Trümper, J., Hasinger, G., Aschenbach, B., Braeuninger, H., & Briel, U. G. 1991, Nature, 349, 579

Truran, J. W. & Livio, M. 1986, ApJ, 308, 721

Tuchman, Y. & Truran, J. W. 1998, ApJ, 503, 381

Turner, M. J. L., Abbey, A., Arnaud, M., et al. 2001, A&A, 365, L27

Valcheva, A., Ovcharov, E., Latev, G., et al. 2008, The Astronomer's Telegram, 1687, 1

Valeev, A., Barsukova, E., Sholukhova, O., et al. 2009, The Astronomer's Telegram, 2208, 1

van den Bergh, S. & Younger, P. F. 1987, A&AS, 70, 125

van den Heuvel, E. P. J., Bhattacharya, D., Nomoto, K., & Rappaport, S. A. 1992, A&A, 262, 97

van Rossum, D. R. & Ness, J. 2010, Astronomische Nachrichten, 331, 175

Verbunt, F., Bunk, W., Hasinger, G., & Johnston, H. M. 1995, A&A, 300, 732

Voss, R. & Gilfanov, M. 2007, A&A, 468, 49

Voss, R., Pietsch, W., Haberl, F., et al. 2008, A&A, 489, 707

Walterbos, R. A. M. & Kennicutt, Jr., R. C. 1988, A&A, 198, 61

Warner, B. 1995, Cataclysmic variable stars (Cambridge Astrophysics Series, Cambridge, New York: Cambridge University Press, 1995)

Warner, B. 2002, in American Institute of Physics Conference Series, Vol. 637, Classical Nova Explosions, ed. M. Hernanz & J. José, 3–15

Watson, M. G., Schröder, A. C., Fyfe, D., et al. 2009, A&A, 493, 339

Watts, A. L. & Strohmayer, T. E. 2006, MNRAS, 373, 769

Webbink, R. F. 1984, ApJ, 277, 355

Weisskopf, M. C., Brinkman, B., Canizares, C., et al. 2002, PASP, 114, 1

Whelan, J. & Iben, Jr., I. 1973, ApJ, 186, 1007

White, N. E., Giommi, P., & Angelini, L. 2000, VizieR Online Data Catalog, 9031, 0

Williams, B. F., Garcia, M. R., Kong, A. K. H., et al. 2004, ApJ, 609, 735

Williams, B. F., Naik, S., Garcia, M. R., & Callanan, P. J. 2006, ApJ, 643, 356

Williams, G. G., Milne, P. A., Park, H. S., et al. 2008, in American Institute of Physics Conference Series, Vol. 1000, American Institute of Physics Conference Series, 535

Williams, R. E. 1992, AJ, 104, 725

Wilms, J., Allen, A., & McCray, R. 2000, ApJ, 542, 914

Wolter, H. 1952, Annalen der Physik, 445, 94

Yaron, O., Prialnik, D., Shara, M. M., & Kovetz, A. 2005, ApJ, 623, 398

Zacharias, N., Monet, D. G., Levine, S. E., et al. 2005, VizieR Online Data Catalog, 1297, 0

Zacharias, N., Urban, S. E., Zacharias, M. I., et al. 2003, VizieR Online Data Catalog, 1289, 0

Acknowledgements

Finally, it is a great pleasure to express my gratitude to everybody who contributed to the success of this dissertation.

First of all, I would like to thank Prof. Dr. Günther Hasinger for giving me the great opportunity to work in the High-Energy group at the Max-Planck-Institut für extraterrestrische Physik and to participate at several conferences and workshops.

Special thanks go to my supervisor Dr. Wolfgang Pietsch, who was always there to discuss my problems, breakthroughs and how to turn the first into the latter.

I would like to thank my colleagues in the High-Energy group for their support and open doors. Especially, Frank Haberl for sharing his expertise on X-ray spectra, Hermann Brunner for help with the XMMSAS *Chandra* tools, and Vadim Burwitz for insights on optical telescopes in particular and on the world of professional astronomy in general.

Many thanks go to my collaborators Margarita Hernanz, Gloria Sala, Massimo Della Valle, Despina Hatzidimitriou, Arne Rau, Dieter Hartmann, Robert Quimby, Kamil Hornoch, Jochen Greiner, Michael Freyberg, Helmut Meusinger, Jürgen Fliri, Holger Stiele, Marina Orio and Albert Kong for their constructive criticism and to the optical observers Grant Williams, Peter Milne, Alexios Liakos, Natalia Primak and Agnieszka Slowikowska for providing the data for our nova discoveries. I am particularly grateful to the observers Fujio Kabashima, Koichi Nishiyama and Takeshi Urata for doing me the honour of naming the minor planet 6642 “Henze”.

I thank Felix Kaduk for his help in compiling the first version of the nova catalogue.

Additional thanks go to the system administrators Harald Baumgartner and Joachim Paul for their astonishing ability to solve countless software problems and to recover data that seemed lost forever all within 15 minutes after my call for help.

I wish to thank my office mates, my friends at the International Max-Planck School for Astrophysics, and the MPE/MPA/IPP football team for helping me to acclimatise in Munich at the beginning of my PhD and for just the right amount of distraction over the following three years.

More gratitute than I could express goes to my girlfriend Laura for being her and being mine.

Last but surely not least, I want to thank my parents Astrid and Jost Henze for their support, help and motivation throughout my PhD and my entire life. Without them, this dissertation would not exist for more than one reason.

This work is based in part on observations with XMM-Newton, an ESA Science Mission with instruments and contributions directly funded by ESA Member States and NASA. The XMM-Newton project is supported by the Bundesministerium für Wirtschaft und Technologie / Deutsches Zentrum für Luft- und Raumfahrt (BMWI/DLR FKZ 50 OX 0001) and the Max-Planck Society. I would like to thank the *Swift* team for the scheduling of the ToO observations. This research has made use of the NASA/IPAC Extragalactic Database (NED) which is operated by the Jet Propulsion Laboratory, California Institute of Technology, under contract with the National Aeronautics and Space Administration. This study made use of the Digitized Sky Surveys which were produced at the Space Telescope Science Institute under U.S. Government grant NAG W-2166. M. H. acknowledges support from the BMWI/DLR, FKZ 50 OR 0405.